The electrostatic effect on particle trajectories and particle deposition in horizontal and vertical wind tunnels

Haeve, M.G.N.

Award date:
2021

Department of Applied Physics
Master Thesis

The Electrostatic Effect on Particle Trajectories and Particle Deposition in Horizontal and Vertical Wind Tunnels

Mitchel Haeve 0943888

Supervisors:
dr. ir. Paul Blom
dr. ir. Job Beckers

University of Eindhoven.
March 1, 2021

Abstract

Contamination on wafers can cause big problems and costs the semiconductor industry millions of dollars each year. Contamination landing on the wafer can disrupt the lithography process and cause faulty chips. The purpose of this study is to examine the utilization of electrostatic fields as a high potential solution for contamination control. These electric fields will be applied in a horizontal and vertical wind tunnel to examine if the deposition of particles on the wafer decreases because of these fields. Different kinds of particles (glass, copper and polyamide seeding particles) were dropped through different kinds of inlets (metal, plastic and glass) to examine the triboelectric effect that causes charging. The different charging properties of the particles also means that these particles behave differently in electric fields. Two positions for an electric field were used: a potential present on the walls of the setup and a potential present on the wafer. Particles deviation in trajectory was measured using a particle counter and plotter to visualise the differences compared to a calibration or reference measurement.

Both insulating and conductive particles (glass and copper particles) deviated in the horizontal wind tunnel. Potentials of -3 kV on plates and -2 kV potentials on a wafer showed significant changes in trajectory of the particles in the horizontal wind tunnel. In line with the theory, this can increase or decrease deposition according to the polarity of the field and the charge on the particle.

In the vertical wind tunnel, insulating particles only showed significant deviation in experiments where no flow was present. The glass particles in these experiments had a charge of 36 e for a 5 μm particle. The particles which possess charge can be attracted away from the center of the wafer, where most contamination occurs according to the FEM simulations. For copper, no significant deviations in the vertical wind tunnel could be found.

If the electric field increases deposition of particles, it is best to neutralize it. An ionizer has showed potential to neutralize surfaces quicker than charge decay does. In the wind tunnel however, the distances and flow were not sufficient to show significant effects.

These findings could be used as a foundation for further investigation on how electric fields can help prevent contamination. Neutralizing the correct materials with ions could stop the particles from being attracted to the wafer. On the other hand, plates which cause electric fields could be used to catch charged contamination in vortexes where the flow of the AWH is disturbed and not flowing at the full 0.4 m/s.

Contents

1 Introduction

1.1 From wafer to chip, what is the importance?

Almost all computer and smartphone devices use chips which are extremely small. Current chips are in the order of 7 nanometers (the node of the transistor) and use all 3 dimensions to function properly. The making of these chips is an incredibly complicated process and a lot of other papers have already focused on the many stages of the fabrication process. A full overview of this fabrication process can be found in appendix C.1. Chapter C.1 in the appendix will provide the reader with more knowledge about the complications of making chips in the size of nanometers, and it will also provide a background on the wafers which are used, the techniques used to make chips and the transistor design.

The importance of making a functioning chip is embedded in our society everywhere. The mission statement of ASML visualises this well: "Without it, there would be no smartphones, internet or modern aviation to connect us, wherever and whoever we are. There would be no satellites to better understand our planet, and none of the medical technology that helps to diagnose and treat disease" [1]. To increase this capacity, it is important to keep innovating this technology. Innovation will lead to 3rd world countries also being able to afford this technology, and it will increase the benefits that come with technology even more. Two things can be done to make this innovation happen at a faster rate: produce chips faster or reduce the size needed for chips. Both processes are happening simultaneously. More wafers enter the machine every minute. The wafers used in these production processes are flat silicon disks, the foundation of a chip. Secondly, more precise processing is done each year. The size of the node of a transistor has shrunk from 32 nm to 7 nm in the last ten years, and current goals are set for the 5 nm range.

With every technological improvement, there are challenges. One of the challenges faced in the industry today is the generation of particles which become airborne. These particles can be in the order of nanometers or micrometers. Once these particles land on the wafer, they are called contaminants. One can understand that if these contaminants land on such a delicate device during the fabrication process, it will result in defects or short circuits. This will slow down the amount of chips being produced which will result in losses for the company. Especially since the process uses lithography (more information can be found in appendix chapter C.1), it is vulnerable to particles depositing on front-side of the wafer. This thesis will focus on the prevention of these contaminants using electrostatic forces. First, let us take a look at what contamination actually is and how it can cause a problem in chapter 1.2.

1.2 Contamination classification and sources

This chapter will focus on the understanding of this contamination. What are the classifications, behavior and sources of these contaminants? Probable sources and deposition in the AWH will be discussed in the appendix in chapter M.

Let us start at the beginning. There are many kinds of contamination which can be found, and they can be subdivided into five categories [2]:

1. classification by detection method
2. classification by material
3. classification by force of adhesion
4. classification by size
5. classification by yield and reliability

In this research, a classification on both size and force of adhesion will be made. A more thorough explanation for this choice can be found in appendix C.2.

There are several places where particles can cause a problem. The main three places which are of an influence to the photo-lithography regarding contamination are the front-side of the wafer, the back-side of the wafer and the mask used for lithography. Since the masks are also in the order of nm, a small contaminant might

result in a big area of the chip not being treated, thus causing defects. For a wafer the most important area to protect is the front-side. Particles that have a diameter equal to half the feature size (the size at which the processing occurs and thus are the smallest in length) can already have a detrimental effect on the function of a chip. These particles cause distortions in the lithographic process, such as local masking or etching defects, which will eventually result in open or short circuits. The back-side of the wafer is less important and might not have a direct effect on the lithography, but it is still worth mentioning what the effects and problems are that arise when contaminant attach themselves to the backside of the wafer. One of these problems can be that particles which deposit on the back-side of the wafer become airborne again when the wafer is moved. These particles can then attach themselves to the front-side of a newly processed wafer. Another possibility is that the particles deposition causes deformation of the wafer. This usually happens when the wafer is placed on a chuck. A chuck uses a suction force to hold the wafer in place. A particle between the chuck and the wafer can cause the wafer to deform, creating so called hot spots during the lithography process. Another impact that contamination might have on the back-side of the wafer is that certain elements can diffuse into the silicon bulk of the wafer (especially metallic contamination). This can also cause the chip to malfunction. A final note here, metallic contamination and the diffusion of metals into the silicon is a large problem area as well. Metallic particles can change the oxidation rates and increase etch rates. To keep the research focused and manageable, only the front-side of the wafer will be investigated.

Finally, it is good to know where these contaminants are coming from. There are a lot of ways contaminants can be introduced into the system, such as rinsing or drying residues. Let us pick the most likely sources of contaminants, those which become airborne contamination or aerosols. An example of such a contamination source is the handling of the wafer. First, wafer handling is a contact required operation, meaning that due to wear, particles can be released. Furthermore, if one wafer is severely contaminated, the contact can spread this contamination to new wafers which are processed later. The most important things to pay attention to are applying a constant force and adjusting the surface which picks the wafer up to have the right morphology. It must be said that these are not the only forms of airborne contaminated particles. Filters with some form of defect, humans and the moving parts inside a chamber (friction of components) can all cause contaminants to form, which is why the source of any contaminant is hard to establish if the material is not known.

So, there are a lot of possible ways to classify a particle. The most important used in this research are size and force of adhesion. Furthermore, there are three main places for a contaminant to deposit which forms a problem: the mask, the back-side of the wafer and the front-side of the wafer. The most important place to protect is the front-side of the wafer, where the lithography takes place. Another challenge is finding the source of contaminants and preventing them from happening. This will not be discussed in this report.

1.3 Atmospheric wafer handler

VDL focuses on three main subjects of the AWH, which are contamination control, dis-charge control and thermal control. This research focuses on contamination control. In contamination control, three processes play a role, namely the generation, the transport and the collection or removal of particles. First of all, one wants to stop the production of contaminated particles. Since that method is not fault-proof, it is also important to stop the transport from the particles to the wafer. This is currently done with a vertical airflow. Thirdly, if particles do attach themselves to the wafer, they should be removed. This research will mainly focus on the subcategory of transport, but one can also use the charge on the wafer to be able to lift the particles from the wafer, as will be seen in chapter 2.

In chapter 1.1 and especially appendix C.1, it was explained how the wafers, transistors and finally chips were made. This chapter also already described some of the techniques used to make these chips, such as etching, masks and lithography. However, it did not discuss yet how part of such a machine would look like and how it functions. The focus of this chapter will be on the design of the atmospheric wafer handler, the primary research goal of this thesis and part of a lithography machine.

The atmospheric wafer handler consist of 6 basic parts, as can be seen in figure 1. The three most important parts of the wafer handler are the two robot arms and the pre-aligner. They move and interact with the wafer. Their function is explained more thoroughly in appendix C.3. In the appendix, the route that the

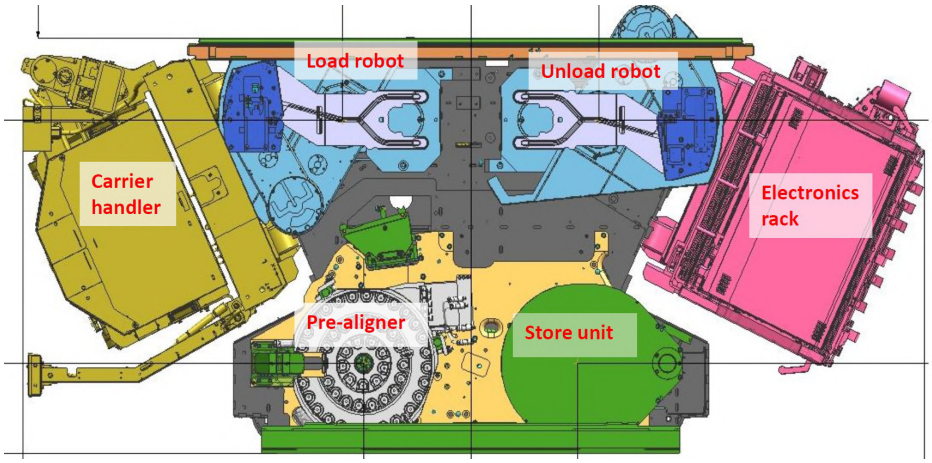

Figure 1: *The components of the atmospheric wafer handler (courtesy of VDL ETG).*

wafer travels is discussed and it will give a more detailed description of the AWH components and where the wafer goes after it has left the AWH.

For now, let us look at the current contamination control in the AWH. First and most important of all, a downward vertical flow is present of 0.4 m/s. This airflow consists of streamlines, which move around the wafer and thus prevents contamination on the wafer surface. In the AWH however, this flow is not always uniform and vortexes are created due to the geometry of the AWH. This enables contaminants to more around in the AWH. The creation of vortexes is strengthened due to the movement of the robot arms, disturbing the flow. A second challenge in the AWH is temperature control. Large fluctuations in temperature can cause unwanted forces to occur on the particles, which can increase the deposition of these particles. Finally, the main research area of this thesis, the electrostatic force which occurs in the AWH. This force will attract particles of the opposite polarity, thus increasing the deposition. However, the electrostatic force can also be used to the advantage of VDL, since particles and surfaces of the same polarity repel each other. The focus of the thesis can therefore be split into two parts: can VDL use the electrostatic force to their advantage for specific kinds of particles and if not, how can VDL neutralize the charge on the particles or the surface to take away this attracting force.

Previous literature has already shown that particles can be attracted or repelled from electric fields. This will be discussed in great detail in chapter 2. The current literature gives information about how particles can be attracted to the wafer when the wafer has a certain potential, but it does not have the exact same flow or wafer diameter as used in these experiments. These parameters can have a large effect on the deposition of the particles. Furthermore, current knowledge about triboelectric charging is not that extensive. This is why this research will also focus on the impact of materials on the charging properties of particles. These two factors will increase the knowledge of VDL on how to deal with potentials on surfaces in the current setup, and which materials will induce charging and how large this amount of charge on the particle is. This gives VDL the opportunity to look for materials which cause lower amounts of charging. Finally, literature has already pointed out how electrostatic precipitators and ionizers can help to neutralize a surface. Again, these previous studies were often executed in smaller ducts or had very high fields applied over a large surface. A simpler and smaller device in the form of an ionizer will be tested in this thesis, to enable the application of the ionizers charge neutralizing properties in the AWH.

1.4 Outline of thesis

As discussed in the previous chapter, the AWH has a lot of components, moving parts and space requirements which are not ideal to start our research. In order to simplify the situation, a wind tunnel will be used. This wind tunnel will allow us to only change one parameter at a time, therefore being able to collect results with a higher level of confidence. Since the thesis focuses on the prevention of contamination using the

electrostatic force, the main question of this research will be:

How can particle trajectories be controlled using static electric fields in horizontal and vertical wind flows?

The sub-questions of this research will thus be: how are the trajectories of microscopic particles influenced by an electric field in a uniform flow? How does the trajectory change if either the wafer, wall or particles are charged? Is there a difference between the electrostatic charging of different particle materials? Can we predict the behavior of these particles? Which flow velocity is the best to prevent contamination on the wafer and why? And can we use an electric field to our advantage to prevent contamination on the wafer? If the electric field does prove to be a disadvantage, what is a possible method to neutralize the charged areas?

First, the scope, constraints, requirements and assumptions are written down, as can be found in appendix B. The literature study will be performed in chapter 2. In this chapter, the flow and the electric properties will be analysed. Also, the forces on the particles and wafer will be analyzed. Chapter 3 will discuss how the wind tunnel looks like and functions, which particles are used and the devices used to perform the measurements. Next, chapter 4 will present simulations done before and during the measurements to provide theoretical feedback for the results. After modeling, the results will be discussed in chapters 5.1 through 5.10. First, chapters 5.1, 5.2 and 5.3 will discuss the horizontal wind tunnel with and without electric fields. This will provide us with knowledge about particle behavior and size, and these measurements are easier to validate using SEM images and the COMSOL FEM models. In chapters 5.4, 5.5 and 5.6 the vertical wind tunnel will be discussed. The advantage of this setup is that measurements can be done without a flow present, therefore gaining even better insight in the force exerted by the electric fields. Chapters 5.7 and 5.8 will try to provide a solution to unwanted fields that cause more deposition on the wafer. This is done using two methods, both with an ionizer. Finally, chapters 5.9 and 5.10 give extra context to the measurement method used throughout the study and thermal effects in the wind tunnel. After these results, the reliability of the measurements will be discussed in chapter 6, as well as any surprising result and recommendation. Finally, the research will be put in a broader perspective in chapter 7, where final recommendations will be made as well.

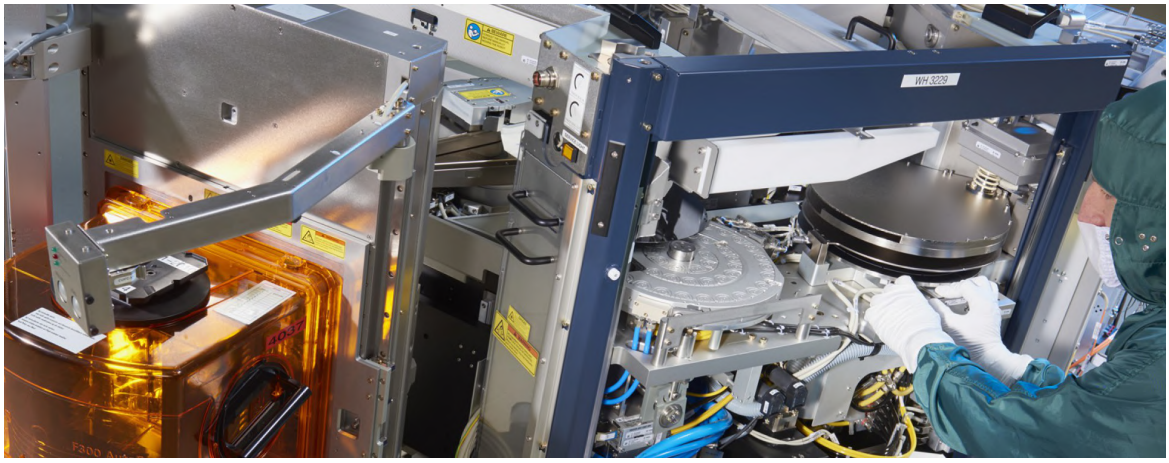

Figure 2: *A visual impression of the atmospheric wafer handler, where the silicon wafers can be seen on the store unit. The middle stage (round aluminium part in the middle of the figure) is the pre-aligner, used to get the wafer to the right temperature and align its position. (Courtesy of VDL ETG)*

2 Theory

In this research, three major parts of information are needed to investigate and understand the behavior of particles. In section 2.1 the main types of flow in the wind tunnel will be discussed. The first is laminar flow, which is predictable concerning the velocity of the stream and the boundary layer near the edge of the wind tunnel. Turbulent flow does not have these properties, and is therefore harder to predict. Also, the flow through an HEPA filter and the particle trajectory due to a flow are discussed in this chapter. The flow will help to prevent contamination due to the streamlines, and can be used in combination with other effects. Such an effect is given in chapter 2.2, which will discuss how particles behave in electric fields. Charging mechanisms will be discussed and a possible charge neutralization device, called an ionizer, will also be discussed. The electric fields can prevent contamination, but also increase it. If this is the case, a neutralization method should be used. Finally, section 2.3 will discuss all the major forces which might play a role in this setup. A distinction is made in the importance of the force depending on the size of the particle. These forces give the theoretical background to compare the results with calculations.

Next, one needs to verify these equations and predictions with a model. The analystical model will be made in Matlab and the FEM model in COMSOL. Both simulations will include certain assumptions as well. Results of these numerical estimations are presented in chapter 4 after the experimental setup has been discussed.

2.1 Flow in the wind tunnel

Since an air stream is traveling through the wind tunnel, some kind of velocity profile will develop caused by this flow. In this section, several typical characteristics of these flows and what these effects mean are discussed. Furthermore, an explanation will be provided on what kind of effects HEPA filters have on the airflow.

2.1.1 Laminar flow

A laminar flow is often given between two plates and visualised by the Navier-Stokes equation. This equation only holds for a fluid of which the viscous stresses arising from the flow are related linearly to the strain rate (also, the material must be continuum and isotropic). This can be visualised by equation $\tau_d = \mu \frac{dU}{dy}$ where τ_d is the shear stress in the stream, μ is the viscosity and U is the velocity derived in a certain direction. See figure 3 for a visualisation of this flow.

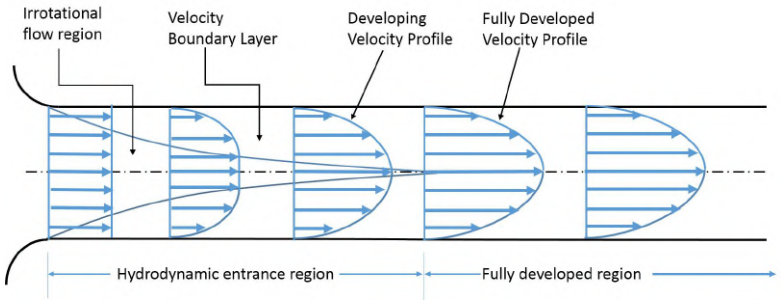

Figure 3: *A visualisation of a developing laminar flow. The velocity profile differs in the y axis, while velocity is constant on the x axis.[3]*

If the assumptions made above are correct, one can use the incompressible Navier-Stokes equation in 1 to determine the velocity profile (for slow velocities of air, namely 0.3 Mach, incompressibility holds). In vector notation:

$$\frac{\partial U}{\partial t} + (U \cdot \boldsymbol{\nabla})U = -\frac{1}{\rho}\boldsymbol{\nabla} p + \nu \boldsymbol{\nabla}^2 U + g \tag{1}$$

Where ρ is the density, p the pressure, g the gravitational constant, U the velocity profile and ν the kinematic

viscosity. Some assumptions are used to simplify the problem. The first assumption is that the flow is fully developed after it has travelled for some time in the wind tunnel, given by 2. This is called the entrance length and it is given by a fraction of the Reynolds number. What the Reynolds number indicates will be discussed later in this chapter. This relation shows that for high Reynolds numbers, long lengths are needed for a fully developed flow. However, the flow will develop reasonably well on smaller length scales.

$$L_{elaminar} = 0.06 * Re_s \tag{2}$$

Furthermore, the velocity at the walls of the wind tunnel will be zero. This assumption is called the no slip condition. These two assumptions lead to a reduced Navier-Stokes equation. The formulas given in 3 are the result of the assumptions. These equations can be solved to give a velocity profile between the two parallel plates

$$\begin{aligned} 0 &= -\frac{\partial p}{\partial x} + \mu \frac{d^2 U}{dy^2} \\ 0 &= -\frac{\partial p}{\partial y} \end{aligned} \tag{3}$$

As already shortly mentioned above, the flow on the walls of the wind tunnel can be approximated to be zero. The consequence of this assumption is that a so-called boundary layer is created. In this area, the flow is not a free stream and the effects of viscosity are significant. The boundary layer thickness is defined as the region of flow where the velocity is 99% of free stream velocity. In a laminar flow this boundary layer can be expressed as equation 4.

$$\delta \approx 5.0 \frac{x}{\sqrt{\mathrm{Re_s}}} \tag{4}$$

Where δ is the thickness of the boundary layer, x is the position along the plate and $\mathrm{Re_s}$ is the Reynolds number of the stream, given by $\mathrm{Re_s} = \frac{\rho U x}{\mu}$ where μ is the dynamic viscosity.

The Reynolds number is the ratio of inertial forces to viscous forces and it is an important dimensionless number, since it can indicate if a flow is laminar or turbulent. For low Reynolds numbers (Re$<$ 2300), the flow will be laminar. For high Reynolds numbers, the flow is turbulent (Re$>$ 4000). [4] The region in-between these two Reynolds numbers is called the transitional flow (and will be discussed in chapter 2.1.2). Important to realize in the experiment is that there are two Reynolds numbers, the stream Reynolds number $\mathrm{Re_s}$ and the particle Reynolds number $\mathrm{Re_p}$. The latter will be discussed when talking about the drag force in chapter 2.3.1, the stream Reynolds number will be discussed now. The equation $\mathrm{Re_s} = \frac{\rho U x}{\mu}$ can be rewritten if the flow is flowing through a circular pipe into the equation $\mathrm{Re} = \frac{Ud}{\nu}$ where d is the typical length scale and ν the kinematic viscosity. Since the wind tunnel that is used in this experiment is not fully radial symmetrical, one must use the hydraulic diameter d_h to calculate the typical length scale. For a rectangular duct this is given by $d_h = \frac{4ab}{2(a+b)} = \frac{2ab}{a+b}$ where a and b represent the length and the width of the opening where the stream travels through.

The second dimensionless number which is important to introduce is the Knudsen number. This number gives the ratio of the molecular mean fee path to a representative physical length scale. It is defined as $\mathrm{Kn} = \frac{\lambda}{L}$ for a Boltzmann gas at atmospheric pressure and at T=0°C, where the mean free path is in the order of 100 nm for atmospheric pressure. In the limit of very small Knudsen numbers, the flow is continuum and can be solved by the non-linear Boltzmann equation. For large Knudsen numbers, the drag is determined by other molecules hitting the object and is therefore determined by collision dynamics. [5] Finally, another important dimensionless number is the Prandtl number, which tells something about the ratio of momentum and heat dissipation through a gas. For gasses such as air, this number is in the order of 1.

2.1.2 Transitional and turbulent flow

In contradiction to laminar flow, turbulent flow does not have a nicely defined velocity profile. It does however have some characteristics which will be discussed in this chapter.

Turbulence is primarily an instability created by shear of the walls (it can also be caused by the instabilities in inflow, small forces or natural instabilities, but the shear of the walls will be the main focus). This shear is 0 at the wall, meaning that a small layer next to the wall does not experience turbulence. This is called the laminar sub layer. Somewhat farther away from the wall, the turbulence increases as there is a large gradient in the velocity profile creating shear. When moving even farther away from the wall towards the middle of the flow, the velocity profile will flatten out, thus decreasing the amount of turbulence present. The length over which the turbulence in the laminar sublayer becomes stable, is given by equation 5 [6]. The turbulent flow itself might not stabilize over any length scale.

$$L_{eturbulence} = 4.4\mathrm{Re}^{\frac{1}{6}} d_h \tag{5}$$

For a flow, the mean velocity at a given point in space will stay constant, thus giving the equations $u(t) = \overline{u}$ and $v(t) = \overline{v}$ for a system defined in the x and y axis. These averages are taken over a certain time scale, and for the time scales used in this thesis, the means will be reliable. However, turbulent flows are made up of eddies. An eddy is a swirl in the gas which reverses the current of the fluid locally, thus creating vortexes. To visualise this effect, the velocities can be changed to $u(t) = \overline{u} + u'(t)$ and $v(t) = \overline{v} + v'(t)$, where the term $u'(t)$ and $v'(t)$ are the turbulent fluctuations. [7] The intensity of the turbulence can then be given by the root mean square, $u_{\mathrm{rms}} = \sqrt{\overline{u'(t)^2}}$. This equation looks similar for $v_{\mathrm{rms}} = \sqrt{\overline{v'(t)^2}}$.

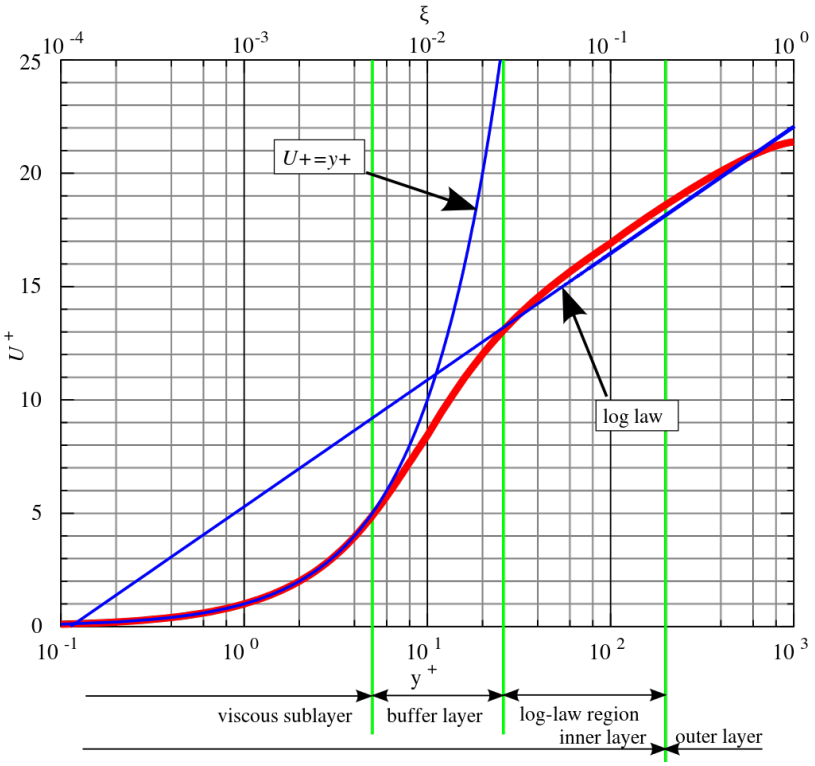

Figure 4: *The regimes of a boundary layer in a turbulent flow. In this figure, the dimensionless distance is plotted against the dimensionless velocity. Note that the bottom axis is a logarithmic scale, explaining the linear correlation in the log law layer. [8]*

This u_{rms} gives a good idea about the turbulence in the middle of the flow, but the boundary layers are not well defined here. As stated earlier, there is still a viscous sublayer (called the laminar sublayer) and an intermediate layer (called the log-law region layer, not previously mentioned) which needs be described to have a full mathematical description of the flow. The viscous sublayer is described by the wall coordinate stated in equation 6

$$y^+ = \frac{yU_\tau}{\nu} \tag{6}$$

Here y is the distance from the wall and U_τ is the friction velocity. This friction velocity can in its turn be expressed as $U_\tau = \sqrt{\frac{\tau_w}{\rho}}$ where τ_w is the shear stress of the wall. The scaling in the viscous layer is linear, until the intermediate layer is reached. For the log law layer, the velocity profile scales logarithmic, as can be seen in equation 7

$$U^+ = \frac{1}{\kappa} \ln y^+ + C^+ \tag{7}$$

Where C^+ is an arbitrary constant, κ is the Von Karman constant and U^+ is the dimensionless velocity (the velocity u parallel to the wall divided by the friction velocity U_τ). [9] [10] The viscous layer slowly transitions into the log-law intermediate layer, which is called the buffer layer. See figure 4 for a visualisation of the turbulent boundary layer and its different regimes.

2.1.3 Flow through a HEPA filter

To stop contamination in the first place, a filter must be placed in between the fan and the wafer. These are HEPA filters, where HEPA stands for High-Efficiency Particulate Air. It must capture at least 99.95% of the 0.3 μm particles in order to be classified as a HEPA filter by European standards. This filter uses particle behavior to its advantage. First, the largest particles (>1 μm) get trapped by the filter using interception or impaction. For interception to happen, the streamline needs to be close enough to the fibre of the filter for the outer radius to touch the fiber. Once it does, it will stick there because of the high Van Der Waals force. Impaction is another process where large particles have some inertia and therefore do not always follow the streamline precisely, especially when making turns around a fibre. These two processes enable the HEPA filter to catch large particles.

The smaller particles are trapped because of diffusion. The Brownian like motion of small particles (<0.1 μm) makes them zigzag because of the collisions with air molecules, which are not neglectable at this particle radius. The extra random motion raises the probability of a particle colliding with a fiber, again sticking to it.

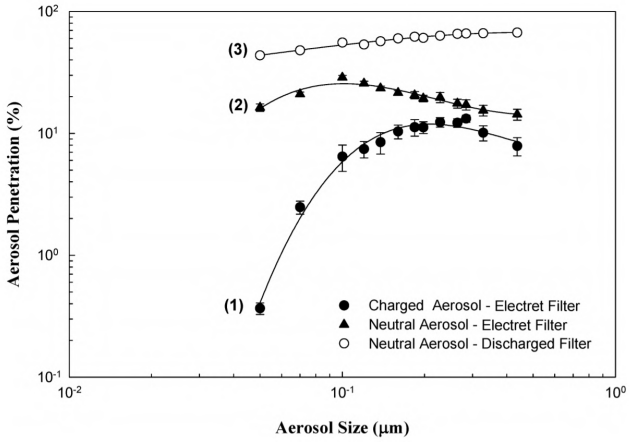

Figure 5: *The efficiency of trapping particles which are charged, uncharged or if the HEPA filter has no electrets at all. The lowest penetration rate is when particles are charged and the filter uses electrets to trap these particles [11].*

The hardest particles to capture are particles which are in between these regimes. Particles of 0.3 μm do follow the streamlines around the fibre's and are not heavy or large enough to collide easily by interception and impaction. These particles are however big enough to not show much Brownian motion, making the probability of a random collision smaller as well. HEPA filters use another clever method to capture these particles, namely electric fields. The fibres of the HEPA filters are called electrets, which are dielectric materials that have a quasi-permanent electrical charge. [12] This means that even if the 0.3 μm particle is neutral, because of the distribution of charge on the particle (if its free to move around) it is still trapped

by the electric field induced by the fibre's potential. If a particle is charged, it is even easier to capture it using the electrets. Figure 5 shows how the charge of a particle of different sizes can change the filter penetration rate [11]. The functioning of these electrets can be affected by blowing in heavily ionized air from an ionizer for example. Placing an ionizer in front of an electrets filter can increase the filters efficiency by 10 to 20 percent, which is certainly noticeable [13]. The filters used in these experiments are often only electrets. They do not have the same properties as an HEPA filter. An HEPA filter already does a better job at capturing any kind of particles, however an ionizer might provide an extra efficient interception of particles. Finally, humidity and gas flow can also influence how many particles penetrate the filter.

2.1.4 Particle trajectory due to flow

To help prevent contamination, a flow will be used. This flow will create streamlines which the particles follow, and because of the no slip condition and boundary layer, most particles will already be moved away from the wafer. To make the deviation of particles caused by the flow as effective as it can be, this chapter will focus on the research which is already available about flows over a wafer.

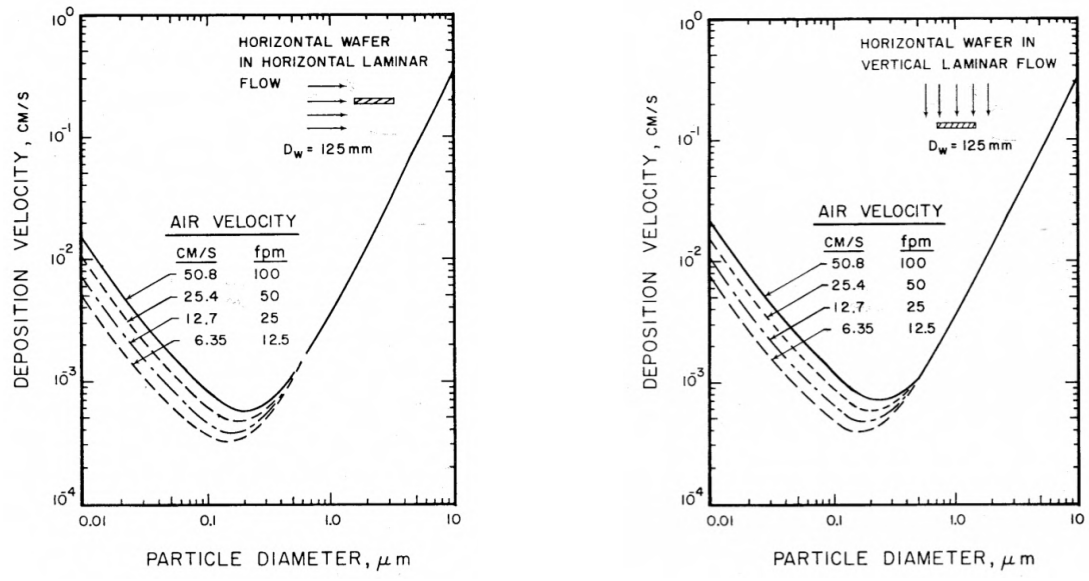

(a) Horizontal flow, horizontal wafer *(b) Vertical flow, horizontal wafer*

Figure 6: *Left) the deposition velocity in a horizontal flow setup. Right) the deposition velocity in a vertical flow setup. Both surfaces are flat plates with diameter of 12.5 mm [14].*

A horizontal air stream flowing over a horizontal surface will form a boundary layer around the wafer, causing the particles streamlines to move away from the wafer. However, streamlines are only valid for particles without any mass since larger particles do not always follow the streamlines. The larger particles will still fall even though the boundary layer is pushing them up.

As can be seen, the deposition velocity differs for different particle diameters. In figure 6a the flow is laminar and it flows over a flat plate with a diameter of 12.5 cm. For figure 6b, the flow is vertical compared to a horizontal wafer. Comparing the two figures it can be noted that the horizontal wafer is better in preventing particles from reaching the surface for all the air velocities. [14] Furthermore, increasing the diameter of the flat plate does not change the preference for a horizontal flow, although the difference is minimal. Finally, it can be seen that larger wafers are better at preventing deposition of particles relatively. Other research also states that the dimensionless shear velocity of the horizontal flow is larger than that of the vertical flow. [14]

To conclude, both flows decrease the amount of contamination that would have landed on the wafer if no flow was present. This means that the flow is one of the mechanisms used in the AWH to limit the deposition

of particles on the wafer. Increasing the flow velocity will also increase the deposition velocity, but only slightly. Larger wafers of 200 mm showed approximately the same results.

2.2 Charging and neutralization of particles

This chapter will include the prior knowledge necessary to understand how the particles charge in a system, what static charge is and how this static charge can be neutralized using an ionizer. First, chapter 2.2.1 will explain how different particles react to different electric fields and how charge is distributed over such a particle. Chapter 2.2.2 will explain the effect of electrostatic charge and how this effect is material dependent. Finally, chapter 2.2.3 will give more information about how an ionizer can be used to neutralize static charge on a surface. This will give an overview of which material is most likely to charge. Again, this can be an advantage or disadvantage, depending on the charge of the particle and the field. If it is a disadvantage, the theory of the ionizer can provide a solution.

2.2.1 Electrodynamics, dipoles and bound charge

In the experiments in this thesis, particles and electric fields are used. The electric field caused by two parallel plates is easy to calculate and determine, and will not be discussed in great detail. However, the spherical particles are made of different kinds of materials, causing them to also create electric fields, induced charges, dipoles and other effects. In this chapter, these effects will be discussed to create a better understanding of these phenomenon. [15]

First, let us discuss the potential generated by metallic particles. In these particles, charge can move freely, meaning that no electric field can exist in the material itself. The ability for electrons to move freely causes the conductor to be at an equipotential (which means that the potential is constant) in static situations. If there would be a field present inside the conductor, the abundance of free electrons would cancel the field easily. In an external field however, the ability for charge to freely flow causes an induced charge to occur in external electric fields. These charges would then be found on the surface of the conducting sphere, since there is no other place for the charge to reside. Now to calculate the surface charge or potential of a conducting sphere, a special technique must be used. This technique is called separation of variables in spherical coordinates. The derivation starts with a potential which is angle θ and radius dependent. These are the only two degrees of freedom because of azimuthal symmetry, making the ϕ coordinate abundant. This leads to a general solution for the radial component and the angular component. The radial component is fairly simple as can be seen in equation 8, but the angular component is not as seen in equation 9. In these equations, l is the separation constant and A and B are constants.

$$R(r) = Ar^l + \frac{B}{r^{l+1}} \tag{8}$$

$$\frac{d}{d\theta}\left(\sin\theta \frac{d\Theta}{d\theta}\right) = -l(l+1)\sin\theta\Theta \tag{9}$$

In the angular component equation, the solutions are Legendre polynomials given by $\Theta(\theta) = P_l(\cos\theta)$, where $P_l(x)$ is defined by Rodrigues formula $P_l(x) = \frac{1}{2^l l!}\left(\frac{d}{dx}\right)^l \left(x^2-1\right)^l$. Combining both solutions gives the general solution of the separation of variables as seen in equation 10.

$$V(r,\theta) = \sum_{l=0}^{\infty}\left(A_l r^l + \frac{B_l}{r^{l+1}}\right) P_l(\cos\theta) \tag{10}$$

This result gives a solid ground to calculate the induced charge density of a conducting sphere. If an electric field E_0 would point in the z-direction, then filling in the boundary conditions $V = 0$ when $r = R$ and $V = -E_0 r cos(\theta)$ for r»R into equation 10 gives the potential of a conducting sphere in equation 11.

$$V(r,\theta) = -E_0\left(r - \frac{R^3}{r^2}\right)\cos\theta \tag{11}$$

This result can be rewritten to the induced charge density: $\sigma(\theta) = -\epsilon_0 \frac{\partial V}{\partial r}\big|_{r=R} = \epsilon_0 E_0 \cos\theta$. In this result it can be seen that the maximum positive charge is present for the largest z coordinate of the sphere ($\theta = \frac{1}{2}\pi$) and the maximum negative charge is present on the smallest z coordinate of the sphere ($\theta = -\frac{1}{2}\pi$)

Now to simplify this situation, the conducting sphere might be visualised as a pure dipole. The pure dipole assumption can only be applied if the quadrupole moments of the dipole can be neglected, which is the case on these scales. This would mean that all positive charge and negative charge is focused in one point. Using the dipole moment $p = qd$, the electric field caused by this pure dipole can be seen in equation 12.

$$E_{\text{dip}}(r) = \frac{1}{4\pi\epsilon_0}\frac{1}{r^3}[3(p \cdot \hat{r})\hat{r} - p] \tag{12}$$

It is important to realize that this dipole can not cancel any charge. If a charge Q would reside on the surface of this conducting sphere, no dipole moment or induced charge could overcome this acquired charge.

Now for an insulating sphere the situation is different. There are no free charges that could move around cancelling the electric field inside the materials. In insulating materials, bound charges exhibit all electric behaviors. These bound charges can be seen as small dipoles which all line up, facing positive-negative-positive-negative etc. The only charge that matters then is the charge which is at the outer edge of the sphere, since here the beginning and ends of these dipole strings are present.

Zooming out from the micro scale to the macro scale, the re-positioning of these dipoles is called the polarization of an object. Polarization can also be caused by induced charge separation in a conductor, which is a different kind of polarization. What is important for the polarization to hold, is that the polarization is proportional to the electric field: $P = \epsilon_0 \chi_e E$. In this formula ϵ_0 is better known as the electric permittivity of free space. The electric permittivity is material dependent and is assumed to be a linear dielectric. Another dimensionless quantity which is often used is the relative permittivity, and it relates the permittivity of a materials with that of vacuum. The relative permittivity is given by $\epsilon_r \equiv 1 + \chi_e = \frac{\epsilon}{\epsilon_0}$. To calculate the field inside a spherical linear dielectric particle which is uncharged, separation of variables can be used. The boundary conditions are known: the charge must be conserved and there is no free charge on the surface. Assuming again that a field of E_0 points in the z direction, the potential can be calculated to be $V_{\text{in}}\ (r, \theta) = -\frac{3E_0}{\epsilon_r+2} r\cos\theta$. Integration will result in the electric field within the dielectric material, given by equation 13

$$E_{ins} = \frac{3}{\epsilon_r + 2}E_0 \tag{13}$$

As can be seen in this formula, the electric field is partly cancelled due to the bound charge. The relative permittivity decides how large or small this cancellation of the field is.

A final thing which needs to be discussed is the boundary of the two plates. On these boundaries the field fringes, meaning that electric field lines do not suddenly stop above or below the plates and a gradient thus exists. These fringing fields also have an effect on dielectric material, it pulls the dielectric material into the space between the charged plates. This is caused by the change in energy inside the capacitor. However, this phenomenon commonly happens when large fringes are felt by the material. In the case of this thesis, the dielectric particles are much smaller than the field and the rest of the environment. Therefore, this effect will be hardly noticeable on the particles when entering the field.

2.2.2 Electrostatic charging

One of the sub-focuses of this research is what effect the electrostatic charge has on the adhesion forces of particles, and how particles react in the vicinity of the wafer to this electrostatic charge. There are still many unanswered questions regarding this topic, but the basic knowledge that is available gives us enough tools to do a reasonably well analysis of this phenomenon. There are multiple ways in which a static charge can appear on a surface, namely 1) contact induced charge separation, 2) pressure induced charge separation, 3) heat induced charge separation and 4) charge induced charge separation.

This research will mainly focus on the first method of charge separation, where two materials contact each other and exchange charge. The term materials in this case can be interpreted universally. The materials

can be solids, liquids and gasses. The effect is most dominant when rubbing two solid materials together, but this in itself is a complicated process. The speed and strength of rubbing can have an effect on the charge being exchanged between the two surfaces. [16]. The effect where two materials directly exchange charges is called the triboelectric effect. This effect is larger for one material compared to the other. Furthermore, some materials prefer to be negatively charged, while others prefer a positive charge. A summary of some common materials are given in figure 7.

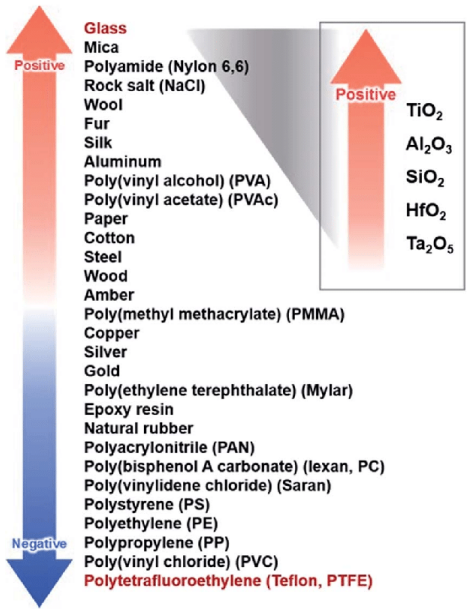

Figure 7: *The triboelectric series, where the materials at the top and bottom are the easiest to charge. The materials are sorted to visualise which materials like to be positively and negatively charged. [17]*

Static charge can occur on a lot of materials, ranging from conductors to insulators. The reason why they are in the order they are in is because of the work function of materials. [18] This work function explains how much effort it takes to remove one electron from the surface and move it to an infinite distance from the surface. The work function is dependent on the surface of the material, and even the crystal face structure on the surface. Another important property one must consider is the ability for electrons to move around. Even if the work function of a material is low (it takes a low amount of energy to charge the surface), it must be able to hold this charge at the surface. This is why statically charging a metal can be hard, since electrons are free to move around. If the electrons are easily redistributed over other larger conducting surfaces (or a bulk of particles), the acquired charge will almost be unnoticeable. Therefore, it is important to have a material floating if charge is wanted, and grounded if no charge is wanted (for conductors).

Gathering charge is easy for insulators. Charges can not freely move around, making it hard for the material to redistribute the charges. The intermediate case is a semiconducting material, which possesses a forbidden gap between the valence and conduction band. [16] Figure 8 displays how charges move around after being rubbed together. As explained, the insulator holds its charges in place while the metal will quickly exchange the charges to become neutral again at the final point of contact. A way to charge metal is by the method of charge induced charging, which can also be seen in figure 8. After the charge has been separated and the electrons have moved towards the ground, one can simply remove the ground to end up with a charged surface.

As explained before, it is important for charge to be present at the surface to be noticeable. The penetration depth of static charge has been researched and is approximately 30 nm. [19] Some insulators can be charged up to several kV in this small layer, before reaching the breakdown voltage. This is the voltage at which air becomes conductive and the material loses its charge.

Furthermore, it is important to consider how long the charge will be present on the surface. The charge

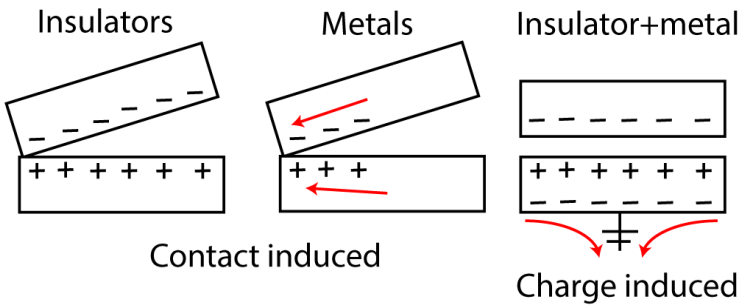

Figure 8: *A figure visualising how contact induced static charge is possible in insulators, but hard in metals. Furthermore, charge induced charge separation does work in metals.*

decay formula 14 can be used to calculate the duration. This formula can be derived using Ohm's law and equations of continuity. [20]

$$q = q_0 \mathrm{e}^{-t/\tau} \tag{14}$$

where $\tau = \varepsilon_\rho \varepsilon_\mathrm{o} \rho = \varepsilon_\rho \varepsilon_\mathrm{o} \frac{1}{\sigma}$ and q_0 is the initial charge. The formula described in 14 describes cases for good conductors and metals well, however in practice insulating materials often appear to have a hyperbolic decay rate in the beginning of the charge decay. This is because σ was taken to be constant in time, but since charging the material also takes time, the correct assumption is $\sigma(t)$. This can be derived by assuming that the material has an intrinsic material conductivity τ_m and initial perturbation charge τ_p. This results in formula 15 [21].

$$q_p(t) = \frac{q_{p0} \exp\left(-t/\tau_m\right)}{1 + \frac{\tau_m}{\tau_p}\left[1 - \exp\left(-t/\tau_m\right)\right]} \tag{15}$$

Knowing that the vacuum permittivity is $\varepsilon_0 = 8.854 * 10^{-12}$ C/Vm, one can easily derive that the resistivity of a material in air must be in the order of 10^{12} to hold the charge for at least a few minutes. This effect was briefly tested by charging a glass with a cloth and putting the glass on PVC (which is a good negative insulator) to see how the electrostatic field changed. This result can be seen in figure 81 in the appendix, where the exponential fit resembles formula 14. This means that according to this curve, the resistivity of glass would be $5 * 10^{12}$, and this fits the theory of resistivity well. [22]

So it is clear that charge does indeed decay and that this phenomenon is related to the resistivity. The question that might arise now is how this charge exactly decays. There are 3 main ways at which charge decays: 1) conduction, 2) dissipation into the air and 3) absorption of counter ions. Firstly, when grounding the insulator it was found that the free diffusion towards the ground happened exponentially. When the insulator was not grounded however, intrinsic effects play a role. In polymers such effects can be ohmic conduction, drift or diffusion. In this case, ohmic and drift effects are responsible for the internal decay, diffusion only plays a minor role. [16] Furthermore, a thicker insulating plate results in slower electrostatic decay. The dissipation into the air of static charge happens because of the humidity in the air. Tiny water droplets can pick up some of the charge on the surface and evaporate again, resulting in decay. Finally, the adsorption of counter-ions on the surface can also neutralize the surface. Since the surface is charged, these counter-ions are attracted to the surface giving them a higher probability to neutralize charge. However, in previous experiments the significance of this effect was questioned, unless the air was purposely ionized. [23]

In the atmospheric wafer handler, static charge is a problem as was mentioned before. The charge after some of the processes (such as spin drying, where a wafer is rotated at high speeds while injecting de-ionized water to clean the wafer) can lead up to -3 kV of static charge on the wafer. [24] This is well above the allowed charge on a wafer [25]. However, this experimental result does not seem to match with formula 15. Silicon is not a great insulator (only at very low temperatures) and has a resistivity of 0.1-60 ohm per meter in room temperature. This would mean that it does not hold charge for a long time, making the problem of static charge not very impact-full. However, there are three reasons why static charge might be present on the wafer. The atomic wafer handler arm needs to grab the wafer and it does this using rubber-like

cushions to not cause any damage to the wafers. This is an insulating layer, and as previously explained, one of the methods of charge decay is the drainage of charge to the ground. Silicon has a native oxide layer of approximately 2 nm, which is also insulating. [26] Secondly, since there is no contact between the wafer and the photolithography, the silicon wafer has no opportunity to drain the charge to another object. Thirdly, the normal drainage through air will also be slowed down, since lithography takes place in vacuum systems. The wafer will be carried from the vacuum systems to the AWH again, which results in the wafer being charged in the AWH as well. The problem of drainage through contact was a problem when physically rubbing two materials: as long as there is a single point of contact between the two surfaces, the charge in metals (and the electrons in the conduction band in semiconductors) are able to move towards this single point of contact, thus neutralizing the charge. [27] Another interesting phenomenon that happens in silicon wafers is that water or humidity in the air can reform the native oxide layer of silicon, causing OH groups to form in the first 40 nm of the surface. This causes charge decay as well, especially since static charge is a surface phenomenon which is dominant in the first 30 nm of the surface. [28] [19]

Not only the silicon wafer can be charged, contaminants can also be charged. This can happen when they are released, due to diffusion or due to the electric field. Charged contamination is more likely to be sucked up by the particle counter in comparison to neutral contamination when looking at the induced charge repulsion. When an insulating contaminant particle has a charge and rests on a neutral surface, there will be a charge difference. This charge difference has a negative effect on the adhesion of the particle. In other words, it is easier for the particle to be released from the surface.[29] Also, due to the Boltzmann distribution of particle charge (seen in formula 23), a lot of particle will have a slight charge at the least. Thus charged particles are likely to occur. As stated before, this can be advantageous if the wafer is neutral and the particles are charged. However in some cases, the wafer has the opposite charge of the particle, thus attracting the particle. In this case it might be wise to neutralize the contamination particle. The larger the particle, the higher the conductivity, thus the lower the resistivity. This means that small particles, which are the hardest to remove according to chapter 2.3.5, will be more likely to have a high charge decay [30]. One method to neutralize the charge on surfaces is using IPA. In an IPA solution the charge and contaminants are taken up in tiny droplets before evaporating. [31] Another method is using ions or plasma's to neutralize particles. [32]

Another method to neutralize all charge in the wind tunnel are ionizers. Ionizers can be set to release both positive and negative ions. Take for example a positively charged glass particle. The positive ions in the air will be repelled while the negative ions will be attracted to the particle. This results in a neutral glass particle. [33] An ionizer can also be used to neutralize a wafer or a surface. More information about the ionizer can be found in chapter 2.2.3.

2.2.3 Ionizer and neutralization of charge

In this chapter, the functioning of the ionizer will be discussed in physical terms and a model will be developed which can predict and explain the behavior of the ionizer. First, a look will be taken at the laws governing the functioning of the ionizer.

The ionizer works with emitter points, which have high voltages applied to them. One of the emitter points has a negative voltage, the other one has a positive voltage applied to the emitter. This voltage will create an AC or DC corona discharge [34]. There are several kinds of discharges, ranging from dark to glow to arc discharges. The regime of a corona discharge is an unstable glow discharge. Because the emitter points are small, no glow can be seen. If it were to produce any light, the critical voltage should be reached as described by peeks law, as stated in formula 16.

$$e_v = m_v g_v r_w \ln\left(\frac{S}{r}\right) \tag{16}$$

Where e_v is the critical voltage, m_v is a factor for the smoothness of the wires, S is the distance between the wires, r_w the radius of the wire and g_v is the visual critical electric field

The dark discharge regime uses electron avalanches to produce more electrons. At the start of the flow and when not yet experiencing any field, some molecules will already be charged. These charges exist because

of outside radiation or forced collisions with other molecules. When these charges enter the electric field, they will be either attracted or repelled by the field. This will primarily happen for electrons, which have a much lower mass than ions. Electrons will thus gain speed, resulting in more collisions with other uncharged molecules. These collisions produce positive ions. These ions are again repelled or attracted depending on the field. This means that one electron can exponentially charge the surrounding molecules, making ionization effective.

Since all corona discharges start with an electron avalanche, there is a difference between a positive and negative electrode. The positive electrode often has less free electrons in the vicinity of the electrode, but the electron energy is often higher. This is because the electrons near a positive electrode are concentrated close to the surface, generating a region of high potential energy. Furthermore, the positive electrode creates new electrons (named secondary electrons) which can start another avalanche using photons. Thermal energy releases these photons, which can ionize another neutral molecule. The negative electrode has more electrons but with a lower energy. Since electrons are pushed away from the negative electrode, another mechanism is needed to produce new electrons which can start an avalanche. It is primarily the photoelectric effect on the electrode which produces these ions, but the impact of positive ions on the electrode could also result in new electrons. As stated above, the electrons drift away from the electrode. When the electron encounters a molecule which is electronegative such as oxygen, it attaches itself to that molecule creating a negative ion. A final note is that a positive corona discharge often has a somewhat smaller discharge compared to the negative electrode (assuming the same geometry and voltage) because it lacks ionizing plasma in some regions. The negative corona discharge will let the electrons escape outside of the ionization region, therefore continuing the discharge further away.

When all these processes have occurred and charges are formed, they have to be forced out in order for them not to combine with the electrodes or recombine with other ions. Therefore, a flow of pressurised air is used. For the ionizer to work correctly, both the flow and the discharge must be at a correct level [35].

COMSOL is able to calculate the ions which are generated due to the corona discharges and transported by the flow. To calculate the space charge, formula 17 is used. Here the charge of the ion z_q, the ion reduced mobility, the velocity u and the space charge density ρ are all considered.

$$J = z_q \mu \rho E + \rho U \tag{17}$$

When uncharged particles or molecules pass through this space charge field, they will acquire the charge associated with that position, as will be shown later on in this chapter in figure 30a. For now it is also interesting to look at the different kinds of ionization which may be possible in an ionizer, namely: bipolar and unipolar ionization. This simply means that for unipolar ionization, only one species of ion is developed (positive or negative). This would be more efficient since it prevents recombination of charged particles and one is even more certain what kind of ions are created [36]. The advantage therefore is that if one knows the charge of the contamination or wafer (for example positive), one can quickly neutralize the surface using the opposite charge (so negative). [34] However, it is important to stop at the right time with applying these extra negative ions, otherwise the surface might become negatively charged, thus not fully neutralizing the surface. Furthermore, it has been shown that charging efficiency increases with particle or ion size. The emitter voltage also has an effect up to a certain level and even the time that has been spend in the compartment where ionization occurs can have an effect on the charging efficiency. [37] This research has also shown that indeed bipolar charging is less efficient than unipolar charging. It has also been shown that the frequency of the ionizer, the charge and the flow have an influence on the neutralization of a wafer surface [38] [39].

It is however more likely that the ionizer used in the coming experiments uses some form of bipolar ionization. It is not possible to completely switch one emitter off, meaning that the ion concentration defined by $\frac{Ion_+}{Ion_-}$ will always be a ratio and never undefined. In the coming experiments however, the ratio will be either large, small or close to 1 (so $Ion_+ > Ion_-$, $Ion_+ < Ion_-$ or $Ion_+ \approx Ion_-$). The advantage of the bipolar ionization is that the user does not need to know which sign the potential is of the particle or wafer. Say for example that a wafer is negatively charged. Applying a negative ionizer will not help. Applying a positive ionizer will help very well, but one must be careful not to treat the surface for a too long duration. When

$Ion_+ \approx Ion_-$, the negative ions will be repelled from a negative surface while the positive ions are attracted. When the surface is neutral, none of the species get attracted or repelled, and the charge of the surface will balance out. This is also shown in figure 9. Furthermore, using the fact that $Ion_+ \approx Ion_-$, one can calculate how long it takes to neutralize contamination. In formula 18 an initial charged contamination particle with n_i elementary units of charge and the n_f final charge on the contamination will be investigated. Knowing the ion mobility Z and the concentration of the ions (of either polarity) N, one can easily calculate the neutralization time for a bipolar ionizer. Formula 18 is only valid in the continuum regime where Kn«1.

$$N_t = \frac{1}{4\pi Ze} \ln\left(n_i/n_f\right) \tag{18}$$

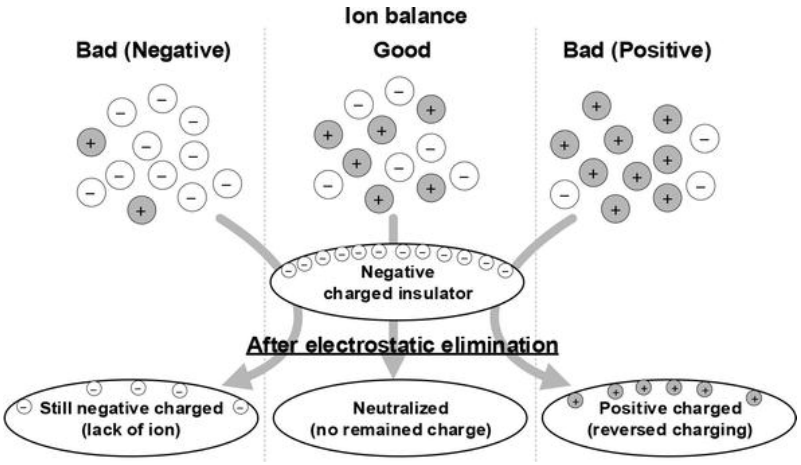

Figure 9: *The different kind of ion outputs and effects they might have on the surface [34].*

Building on previous knowledge, it is interesting to find out how these charged particles are distributed. First of all, when applying a bipolar ionizer with ratio $\frac{Ion_+}{Ion_-} = 1$, not all particles will have an exact charge of 0. The charge will be Boltzmann distributed [40] as given in formula 23, meaning that the average will be at 0 with a standard deviation to both the negative and positive polarisation.

This charge distribution shifts when different ratios of $\frac{Ion_+}{Ion_-} = 1$ are applied. The following set of equation shown in appendix 61 then holds. Notice that when $N^+\eta_{\mathrm{p}}^+ = N^-\eta_{\mathrm{p}}^-$, the Boltzmann equation from 23 holds again.

Finally, one needs to consider what is actually produced in the ionizer. Difference masses of particles can gather different amount of charges. No clear studies can be found on what effect the mass of the ion or ion species has on the neutralization properties. It is however known from studies that some species in air are easier to charge and therefore more common in the ionizer [41].

2.3 Forces on the particle

This research focuses on a range of particles, namely from 0.1 µm to 50 µm. Since there is a whole range of particles, it is also important to consider the forces they experience depending on their size. This chapter will take a closer look at the multiple forces that are important and how large their effect is. [42] This will provide background knowledge to compare the results gathered and the calculations which can be made using the formulas in this section.

2.3.1 Gravitational force and drag force

The most noticeable forces for larger particles (in the order of micrometers) is the gravitational force and the drag force. The gravitational force is given by equation 19. The last part of this equation is the buoyancy

(the force exerted against gravity by the fluid or gas).

$$F_G = m_p g = V_p(\rho_p - \rho)g \tag{19}$$

If 1) a particle is dominated by viscous forces instead of inertial forces (so $Re_p \ll 1$), 2) the flow is incompressible and 3) the particle does not encounter any other particles or walls in his trajectory, the drag force can be calculated by Stokes law. This form of the drag force can be found in equation 20 [43].

$$F_{\text{drag}} = 6\pi\mu r_p U_\infty \tag{20}$$

This equation can be rewritten for small enough particles to give the drag coefficient approximation in equation 21

$$C_d = \frac{24}{\text{Re}} \tag{21}$$

(this approximation gives reasonable results for $Re_p < 1$). [44]

An important parameter which can be derived from the drag force and the gravity is the terminal velocity. The terminal velocity is the maximum velocity the particle can obtain while being in free fall. Equating the gravitational forces with the drag forces gives the terminal velocity in equation 22. [42]. The terminal velocity equation approaches the final velocity exponential. It thus assumes a large enough time scale, being able for the tanh term in $v = \sqrt{\frac{2mg}{\rho A C_d}} \tanh\left(t\sqrt{\frac{g\rho A C_d}{2m}}\right)$ to become 1.

$$v_{ts} = \frac{g d_p^2}{18\mu}(\rho_p - \rho) \tag{22}$$

If the speed and especially the time it takes to acquire this speed is small enough, one can assume that the particle will immediately reach its terminal velocity ($t_0 = \frac{\rho_p d_p^2}{18\mu}$ for a 5 μm glass particle gives a time of 0.2 ms). This will result in a constant falling speed (no acceleration) and thus a linear trajectory.

Important to realise is that for larger particles, there is a reasonable inertia force present. This means that the particle will not travel with the same speed as the flow surrounding it. This finding is visualised in figure 10 for different diameters and densities of particles. [44] It can be seen that the density and size of the particle increase this inertia. It is therefore a possibility that large particles travel slower at the start of the wind tunnel, causing them to spend more time at that part of their trajectory.

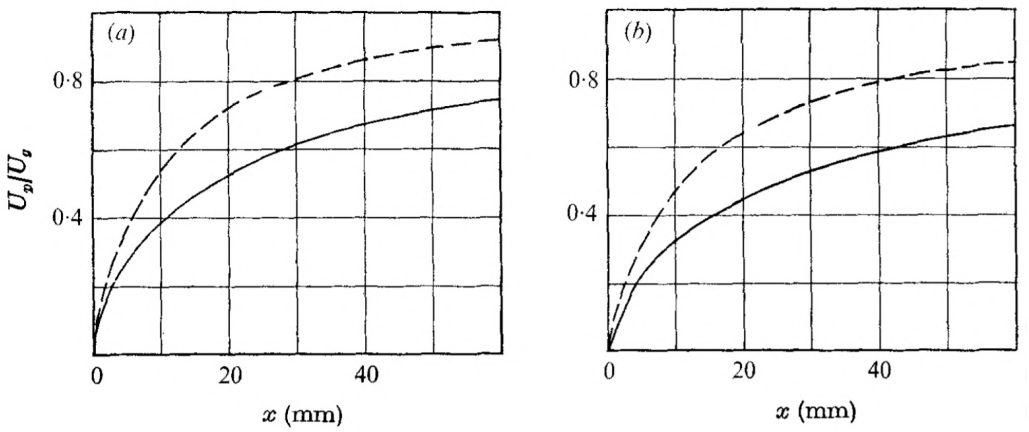

Figure 10: *Ratio of particle velocity to air velocity vs. distance. dotted line* $d_p = 50$ *μm, steady line* $d_p = 100$ *μm with (a)* $\rho_p = 870$ kg/m^3 *and (b)* $\rho_p = 1400$ kg/m^3 *[44].*

2.3.2 Electrophoresis

Electrophoresis is the motion of particles in a uniform electric field due to the particles electric surface charge. These particles are screened by a layer of ions, which exert a force opposite to the surface charge. Finally, there is an electrophoretic retardation force caused by the opposite motion of the screening ions and the surface electrons, causing a viscous stress. When an electric field is applied and the particle moves with a constant speed, the following forces are in equilibrium: $F_{res} = 0 = F_{el} + F_f + F_{ret}$. However, when the ion has just entered the field, it will experience an acceleration. Figure 11 shows the acceleration of such an ion and the forces involved.

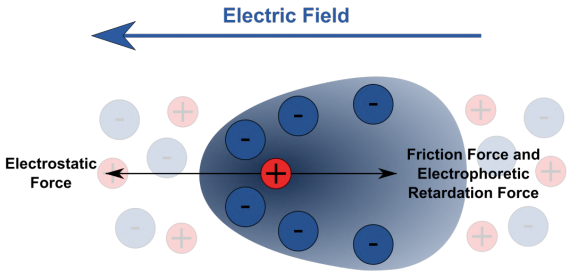

Figure 11: *The forces acting on a particle experiencing electrophoresis [45].*

Most airborne particles carry electric charge. If these particles are floating in the atmosphere and this atmosphere is bipolar, the equation which gives the fraction of electric charges n is given by the Boltzmann equilibrium. The formula is given in 23.

$$f(n) = \frac{\exp\left(-n^2e^2/dK_bT\right)}{\sum_{n=-\infty}^{\infty}\exp\left(-n^2e^2/dK_bT\right)} \tag{23}$$

If the particle is sufficiently large (>0.03 µm), then the average absolute number of charges would be given by formula 24.

$$|\bar{n}| = \sum_{n=0}^{\infty}|n|f(|n|) \tag{24}$$

The formula can be rewritten to an easy equation which includes the average number of charge and is only dependent on the diameter of the particles, namely formula 25 where d_p is given in µm. For 5 µm particles, this would give a charge of 5.2 e, where particles could get both negative and positively charged. For smaller particles, the charge gets skewed to the negative side in the Boltzmann distribution because of the difference in mobility of ions and electrons. [46] [47]

$$|\bar{n}| \simeq 2.36\sqrt{d_p}, \quad d_p \text{ in } \mu\text{m} \tag{25}$$

In the atmospheric wafer handler, two things can possess charge, the wafer and the walls of the machine itself. Since the wafer has dimensions of 30 cm [48] and the machine is even bigger, it is in good approximation to assume a uniform electric field. This is because the particles released in the machine are way smaller than the areas which can possess an electric field. It must be said that if all these walls and the wafer possess other field strengths, the fields will interact and not be uniform anymore. Therefore, an assumption will be made to make research more understandable: only one component in the atmospheric wafer handler will possess an electric charge. Let us take for example the walls of the machine to be grounded, and the wafer to have a certain charge. The wafers electric field is given by $E = \frac{V_{AB}}{d}$, and thus a force of $F = qE = \frac{qV_{AB}}{d}$ will be noticeable on the particles. This force will only be noticeable if the charge q is substantial. It does differ a lot on the setup used in previous studies, but large charges are possible according to previous research for particle sizes used in this research. [49] [50]

$$\mu_e = \frac{v}{E} \tag{26}$$

Formula 26 shows the electrophoretic mobility, and it can also be rewritten to include the zeta potential (ζ), which is the potential between the two layers (the particle and the ions surrounding it). More precisely, it represents the electrical potential at the slipping plane. This gives formula 27 where ε_r is the dielectric constant of the stream and ε_0 is the permittivity of free space.

$$\mu_e = \frac{\varepsilon_r \varepsilon_0 \zeta}{\mu} \tag{27}$$

This means that for a low Reynolds number particle and a constant speed in the direction perpendicular to the electric field, the charge can be estimated. This charge is given by 28 where X_{dis} is the deviation caused by the electric field, ΔV is the voltage difference, L_{EL} is the width of the electrically charged plates, L is the separation distance between the plates and F_C is the Cunningham slip factor. This Cunningham slip factor is given in equation 29. In equation 29 the constants A_1, A_2 and A_3 are constants which are determined for air to be 1.257, 0.4 and 0.555 respectively. [51] The maximum charge which can be present on a particle is area dependent, and given by 100 e/μm^2 [52]. A realistic charge of 5 µm spherical particles is approximately ± 30 e [53].

$$Q = \frac{3\mu\pi d_p U_0 X_{dis} L}{F_C L_{el} \Delta V} \tag{28}$$

$$F_C = 1 + \frac{2\lambda}{d_p} \cdot \left(A_1 + A_2 \cdot e^{\frac{-A_3 \cdot d_p}{\lambda}} \right) \tag{29}$$

Formula 28 gives an idea of how much charge on the particles will be present in the experiments using the deviation of the particles from the center. It is also important to discuss the maximum amount of charge that might result from the environment. This will enable us to calculate the charge on the particle due to the flow of air, without the influence of ionized air or an electric field [54] [55]. The charge developed under normal conditions (thus without an electric field), is given by equation 30. For particles smaller than 1 µm, this is the primary way of acquiring charge when freely falling. The charge given off by filtering the air by the filters is not a substantial addition to the charge [56]

$$n = \frac{d_p K_b T}{2e^2} \ln \left[1 + \frac{\pi d_p \bar{c}_i e^2 N_i t}{2kT} \right] \tag{30}$$

Where $\bar{c}_i = 2.4 \times 10^4$ cm s^{-1} is the mean thermal speed of the ions and N_i is the ion concentration. But when an electric field is present, ions will speed up, creating more collisions in the process. This effect is noticeable for particles larger than 1 µm, and the maximum saturation of the charge of these particles is given by equation 31

$$n = \left(\frac{3\varepsilon_0}{\varepsilon_0 + 2} \right) \left(\frac{E d_p^2}{4e} \right) \tag{31}$$

Some research has already been done on the effect of electric fields on airborne particles. Firstly, it is important to ground the wafer as much as possible, since airborne particles can get attracted to them, causing more contamination on the wafer. [57] Grounding the wafer is done by making the atmospheric wafer handler from conducting materials, however there is a problem. The oxide layer which is supposed to protect the wafer when being picked up is an insulator, meaning that static charge on the wafer may still remain. That static charge can form on the wafer, reach several kV and that this charge stays on the wafer for longer duration of times, is known. That this field can cause a noticeable effect on particles is also known. However, the ions the field creates can also contribute to charge on the particle. This effect is called space charge. The charge is transferred due to the ionic current (the flow of electric charge in the plasma) from the air to the particle. The ions are accelerated towards the particle and charge the ion, up until equilibrium is reached. At this point, the charges are repelled from the particle since the particle already has a high electric field itself. Another charging mechanism is diffusion. In this method, particles are charged due to the thermal energy that is possessed by the ions and this charging mechanism is therefore independent from the external electric field. [58] Both models are therefore based on solutions for the convective diffusion equation,

Diameter (μm)	Number of units of charge				
	Diffusion	$E = 20$ kV m^{-1}		$E = 200$ kV m^{-1}	
		Field	Combined	Field	Combined
0.01	0.27	0.0007	0.271	0.007	0.277
0.02	0.656	0.0028	0.659	0.028	0.684
0.05	2.03	0.02	2.05	0.17	2.17
0.1	4.65	0.07	4.72	0.69	5.3
0.5	30	2	32	17	47
1	66	7	73	69	136
2	145	28	172	278	423
3	228	63	290	625	853
5	401	174	575	1737	2138
10	862	695	1557	6948	7810
20	1844	2779	4623	27,792	29,636
40	3927	11,117	15,044	111,170	115,090
50	5006	17,370	22,375	173,700	178,700
100	10,609	69,479	80,088	694,790	705,400
200	22,415	277,920	300,330	2779,200	2801,600

Figure 12: *The difference in charge acquired from diffusion and the electric field for different contamination diameters. [47]*

although using different methods of charging. The regime at which these methods work is determined by the Knudsen number. For a Knudsen number that is «1, the continuum regime for both diffusion and electric field charging can be used. The contribution of these charge accumulation methods is shown in table 12, where the combined charge of the particles is shown as well. In this table, the formulas 31 and 30 were used to calculate the charge. For a 5 µm glass particle, the electric field charging would be around n=10 e. For diffusion charging, this number is noticeably higher. This is because the ion concentration N_i is assumed to be 10^8 ion s cm^{-3}, which might be too high for the experiments in this thesis. The combined model in the table is described by Lawless (1996) and the full derivation in the continuum regime can also be found in his paper [59]. The size of this effect will probably be small in the fields that are going to be used in these experiments, but no definite answer could be found. This is why the space charge will also be considered in the experiments as a possible cause of charge (accumulation), especially when extra ions are created on purpose (for example with an ionizer).

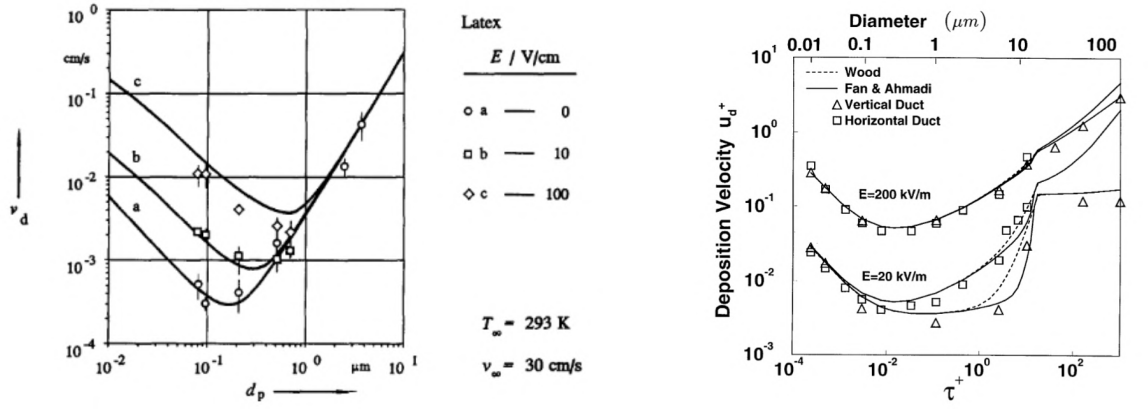

(a) *Deposition velocity vs diameter [60]* ***(b)*** *Deposition velocity vs relaxation time [47]*

Figure 13: *Left) the deposition velocity as a function of the diameter of the particle at different electric field strengths in a vertical downward flow. Right) deposition velocity plotted for a dimensionless relaxation time. Both a horizontal and vertical flow are plotted.*

Secondly, the deposition velocity (the ratio of particles hitting the surfaces compared to all the aerosols in

the air) has been researched. The main result of such research is presented in figure 13a [60] with the effect of electrophoresis (thermophoresis will be added to examine the combined effect in figure 14b). It can be seen that applying a uniform electric field has an effect on the charged airborne particles [61], since they deposit in higher amounts if the wafer is charged. Research confirms the increased deposition velocity for higher electric field on the wafer, and also states the dependency of the airflow over the wafer [62]. More information about the dimensionless deposition velocity can be found in appendix D, the electric contribution can also be plotted in dimensionless units. This is done in figure 13b, where it is visible that for large enough field, the deposition velocity of the particle is in the order of 1 u^*. Furthermore, it is again visible that the deposition velocity has increased for an increased electric field on the wafer in both a horizontal and vertical duct (the difference between these two setups is discussed in chapter 2.1.4). [47]

A way to change the charge of these particles is by first ionizing the air. Several methods exist to do this, but the most common air plasma's are air ionizers. The ionizer uses corona discharges, which generate ions in the air. These corona discharges can either neutralize the microscopic particles or charge them [40] [63]. Other ways of producing charged particles in atmospheric pressure do exist, such as direct current excitations (producing an electric arc) or microwave excitations. However, these methods are not commonly used. Another method would involve the usage of plasma's, however they will not be able to fill the entire chamber with charged particles if the pressure is atmospheric. This technique is therefore only promising in low pressure, which is why large plasma's will not be used extensively in this research. Finally, if many particles are present in the system, equilibrium of the attracted particles can be reached. This makes it important to clean the electrodes [64].

2.3.3 Thermophoresis

Increasing the temperature of the wafer or increasing the temperature difference between the wafer and the air can result in a decrease of the particle flux towards the surface [65]. This phenomenon is caused by thermophoresis. It is caused by the faster moving gas molecules that are near the wafer. The hot air that surrounds the wafer has a higher kinetic energy, and when the air collides with the colder particle, it will push it away from the wafer, which is exactly the goal of this research. [66] In the continuum limit of Kn«1 and laminar flow, the particle will experience a thermophoresis force given by equation 32 [2] [67].

$$F_{Th} = 4.5\pi \frac{\mu^2}{\rho} d_p \frac{1}{1+3Kn} \frac{\frac{C_a}{C_p} + 2.48Kn}{1 + 2\frac{C_a}{C_p} + 4.48\frac{C_a}{C_p}} \frac{\nabla T}{T} \tag{32}$$

In formula 32, C_p is the thermal coefficient of the particle and C_a the thermal coefficient of air. In a turbulent flow the expression is not defined exactly (several papers state other formulas), but in this research, the thermophoresis force in a turbulent flow will be described by formula 33 [68].

$$\eta_{tur}(\%) = 100 \times \left\{ 1 - \left[\frac{T_w + (T_e - T_w)\exp\left(-\pi DhL/\rho Q C_p\right)}{T_e} \right]^{\Pr K_{th}} \right\} \tag{33}$$

Where η is the fraction that thermophoresis contributes to the deposition velocity compared to other significant forces (such as gravity, drag and electrophoresis). Furthermore, the T_w is the wall temperature, T_e the gas temperature at the entrance, D the pipe diameter, L the pipe length, h the convective heat transfer, Q the volumetric flow rate, C_p the gas specific heat and K_{th} the thermophoretic coefficient (full formula can be found in [69]). Formula 33 assumes an ideal scenario, where the walls are heated and the circular pipe is of infinite length. These assumptions only fit the AWH partly, so one must be very careful with this formula to draw conclusions. For an estimation, this formula would be an appropriate begin.

In literature it is also visible that thermophoresis has an effect on the deposition velocity near a flat surface. Figure 14a represents such an experiment, where temperature gradients of 10 K where already enough to increase the number of particles hitting the surface by a factor of 10. In this experiment, the temperature of the air is 10 K higher than that of the wafer, so one would expect a higher deposition velocity. Again, there is no noticeable effect for particles larger than 1 µm at these temperature gradient scales.

Finally, a plot can be made of the combined effect of electrophoresis and thermophoresis, which is visualised in figure 14b. Here, the temperature gradient is always 5 K positive for the wafer, so one would expect

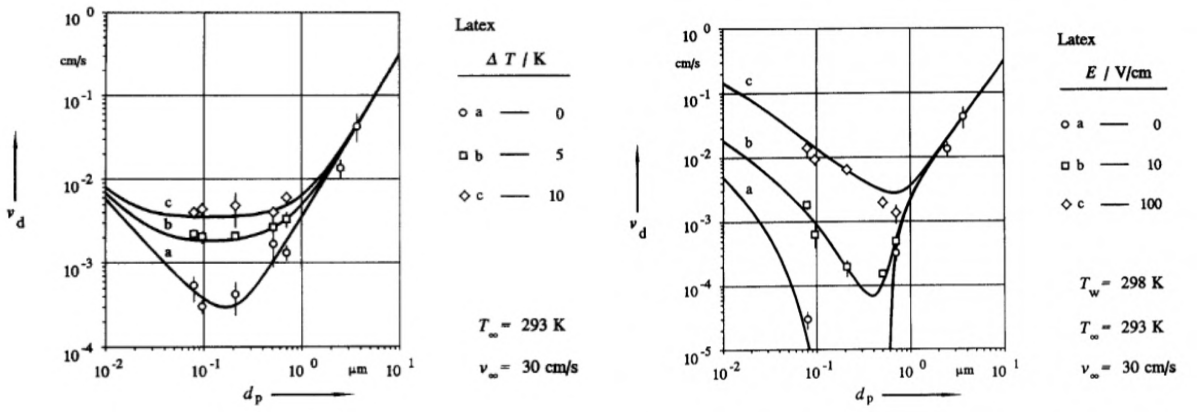

(a) Thermophoresis velocity vs diameter [60] *(b) Combined effect velocity vs diameter [60]*

Figure 14: *Left) the deposition velocity as a function of the diameter of the particle at different temperatures. Right) deposition velocity plotted when the effects of electrophoresis and thermophoresis are combined. Both with a vertical down-flow.*

the deposition velocity to decrease. This can be seen by comparing line a) of plot 14b with line a) in 14a. The line in 14a is at a 0 K gradient and in 14b the wafer is 5 K hotter, resulting in a steep decrease of particle deposition velocities, especially for particles in the range of 0.1 μm-1 μm. Again it is visible in figure 14b that an increase of charge on the wafer will cause larger deposition velocities. Since this research cares about lowering the deposition velocity instead of raising it, it would be beneficial to reverse the effect of electrophoresis. This can be done by mounting two plates with a higher potential above and below the wafer, so that the electric field is directed towards the wall of the machine.

Another phenomenon occurring in atomic wafer handlers is a temperature gradient due to heat coming from the machinery at the bottom or sides of the atomic wafer handler. Because of this convection can occur. There are two kinds of convection, free/natural and forces convection. Free convection can be seen when no forced flow is present, for example when steam rises from a hot teacup. When you start to blow to cool of your tea, you are forcing convection. Since the wafer enters the room with a ±1 K, most of the temperature effects on the wafer itself are not very noticeable. The temperature gradient which occurs between environment and the machinery of the AWH however is noticeable, as can be seen in equation 34. This coupled equation describes the velocity as a result from a heated or cooled surface. For a temperature difference of 1 K in air of a 0.5 m heated plate (parameter x), results in a maximum convective flow velocity (in the y direction) of 0.08 m/s. [70].

$$u = \frac{\partial \psi}{\partial y} = \frac{2\nu}{x} Gr_x^{1/2} f'(\eta) \qquad \psi(x,y) \equiv f(\eta) \left(4v \left(\frac{Gr_x}{4} \right)^{1/4} \right) \qquad \eta \equiv \frac{y}{x} \left(\frac{Gr_x}{4} \right)^{1/4} \tag{34}$$

The dimensionless numbers are explained in appendix E to explain formula 34 more thoroughly. Also, the Prandtl and Nusselt numbers are explained in this appendix, which are both helpful to calculate formula 34.

2.3.4 Lift forces and turbophoresis

Another force which is acting on the particles is the so-called lift force. This name is a combination term for all the forces which are caused due to the rotation of the particle or the non-uniform velocity profile. In this context, the primary forces are the Magnus and Saffman force, which will be explained in this chapter. A visualisation of these forces can be seen in figure 15

The lift due to the Magnus force is caused by the rotation of a particle as it travels. The stream follows the sphere causing a pressure difference between the top and bottom of the particle. The Magnus force has a similar looking lift coefficient compared to the drag equation as can be seen in equation 35, where C_L is the

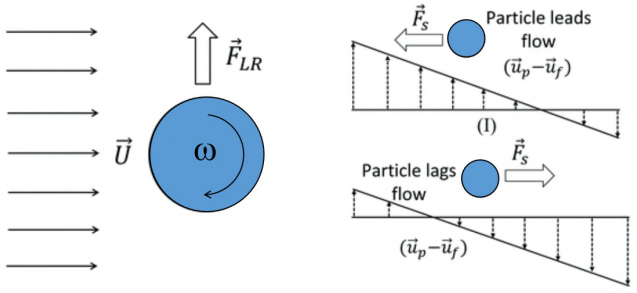

Figure 15: *Left) the rotational lift force called the Magnus force. Right) the Saffman lift force due to the velocity gradient [71].*

lift coefficient, ω is the rotational velocity and L is the lift force. For a sphere, the lift force can be equated by integrating over many cylinders using the Kutta-Joukowski theory. This result in a lift force given in equation 36.

$$C_L = \frac{2L}{\rho U^2 \pi d_p^2} \tag{35}$$

$$L = \frac{16}{3}\pi r_p^3 \omega \rho U \tag{36}$$

Solving these equations give the Magnus lift force given in formula 37

$$F_{LM} = \frac{1}{8}\pi d_p^3 \rho \vec{U} \times \omega \tag{37}$$

It must be said that research has already determined that the Magnus effect does not play a significant role in rarefied gasses under no driving force, as given by [72] [73], however this experiment will focus on atmospheric pressure with a driving force, so this force might play a minor role in this research as long as the velocity gradients are large enough.

The second lift force considered is the Saffman force, which is caused by the slip-shear motion due to the velocity profile. The particle has a tendency to go towards the center of the duct if the particle speed is slower than the speed of the stream moving around it.[74] This force is given by equation 38 [71].

$$F_{LS} = 20.3 U d_p^2 \sqrt{\frac{\gamma_g}{\nu}} \tag{38}$$

Where γ_g is the velocity gradient. These forces are in a way related with each other, since a velocity gradient will also often cause rotation of the spherical particle. The effect of these lift forces is however often smaller than 10 percent in comparison to the drag force (as can also be seen in figure 68 and calculated in chapter 2.4), meaning that they can often be neglected. These forces can however provide an explanation for small unexpected errors in measurements. [75]

Another force which is also caused by velocity gradients is turbophoresis. This force can not be incorporated in the lift forces, since it has another cause. In turbophoresis, the velocity gradients are fluctuating and assumed inhomogeneous. Particles feel this force because of the "convective flux that arises primarily as an interaction between particle inertia and the inhomogeneity of the fluid turbulence field" [76]. Homogeneous turbulence is defined as a flow where the mean velocity gradients and turbulent fluctuation statistics are independent of location in the mean field. Since the location does matter for the experiments performed in this thesis (one has larger eddies 1 cm above the wafer compared to 0.1 cm above the wafer), turbophoresis also needs to be considered in the wind tunnel. Particles experiencing turbophoresis move from a turbulent

area to a less turbulent area. Since the turbulence near the wafer is less, this could explain part of the deposition velocity of the particles. As stated in source [77]: "Very small particles (0.1 µm) complete the last part of their journey to the wall mainly by Brownian diffusion, and very large particles (50 µm) reach the wall mainly by the convective velocity imparted by turbophoresis. For intermediate-sized particles, a combination of both mechanisms is responsible." In our study, for a 5 µm particle, both mechanisms will have a contribution.

Turbopheresis is not well known in the field of flow yet and is often neglected. This can cause a problem since there are significant deviations from Fick's law of diffusion. It therefore needs to be stated as an extra term in the diffusion equation. The discussion of turbophoresis and its deviation is difficult to discuss and not fully in the scope of this thesis, but models are known as can be found (see source [78]). To see this significant deviation, figure 16 can be used as a guide. Here, τ and v are the same parameters as explained in appendix D. It can be seen in figure 16 that the effect is more than a factor of 10 for some particle diameters used in this thesis.

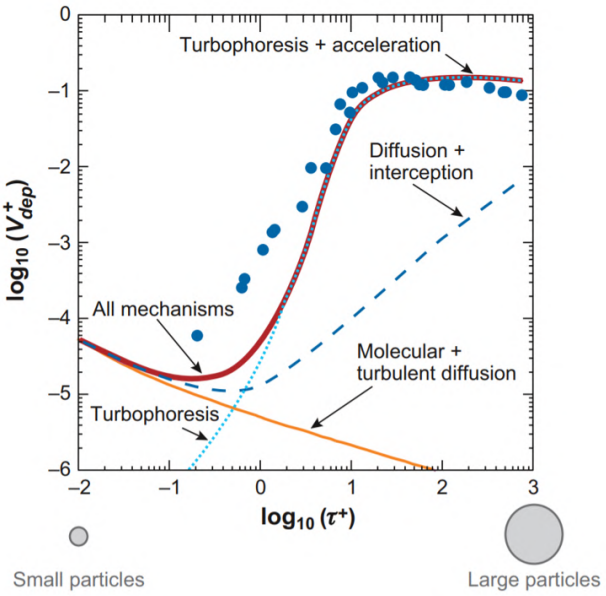

Figure 16: *The effect of turbophoresis in combination with other mechanics (red line) visualised against a classical solution of diffusion (blue striped line). The effect has been validated with experiments (blue dots) [78].*

Still, this force is difficult to include in calculations, and will therefore not be taken into account. There are a couple of reasons why this force is not taken into account. Firstly, the turbophoresis force should be constant, since the gradient of turbulence stays the same for all experiments. This thesis will primarily be about the electrical influence on the contamination, and therefore this subject is outside of the scope of this thesis. If the wafer would have been moving, this force would change and the contribution of turbophoresis would be different at different points in time, requiring to take turbophoresis into account. Secondly, turbophoresis is more difficult to model since anisotropic effects need to be taken into account. This would mean that a simple k-ϵ model would not be sufficient. Thirdly, this would also mean that eddies (even the very small ones near the wafer surface) need to be simulated to calculate the gradient, requiring a very small time step in a time dependent FEM simulation. Simulations will be run stationary (also to avoid large computation times), since the average turbulent velocity is more important than small eddies. It is however an effect which needs more research, especially near the wafer surface, where minor eddies and vortexes can make a difference.

2.3.5 Adhesion Forces

When the particle comes close to or hits the wafer, an adhesion force starts to play a role on the particle. In this chapter, the formulas that enable us to understand adhesion and common models are discussed.

Two common models are used to describe the adhesion of spherical particles on a flat surface. These are the Johnson-Kendall-Roberts (JKR) model and the Derjaguin-Muller-Toporov (DMT) model. Both models assume Hertzian contact, which means that if two surfaces contact each other, both slightly deform under the imposed load. These models were developed because the Hertz model did not give correct results at low loads. Adding adhesion to the models of JKR and DMT, did give correct results at low loads.

The JKR model applies for large compliant spheres. It is different from the Hertzian model since it assumes a larger effective contact radius. The most important parameter needed for this research is the pull-off force, which is the force required to blow or suck the particle from the wafer. The pull-off force from the JKR model is given by equation 39 where γ_E is the surface energy.

$$F_c = -3\gamma_E \pi r_p \tag{39}$$

For the DMR model, the pull-off force formula looks very similar. The DMR model is used for small stiff spheres. It assumes the same contact radius as the Hertz model, however is also assumes that there are attractive forces outside the area of contact. The pull-off force for the DMR model is given in equation 40 [79].

$$F_c = -4\gamma_E \pi r_p \tag{40}$$

These equations and models are thus opposing limits of each other regarding size and stiffness. The Tabor parameter (given by μ_T) solves the intermediate regime by equation 41

$$\begin{aligned} \mu_T &\approx \left[\frac{r_p(\Delta\gamma_E)^2}{E^{*2}z_0^3}\right]^{\frac{1}{3}} \\ \frac{1}{E^*} &= \frac{1-\nu_1^2}{E_1} + \frac{1-\nu_2^2}{E_2} \end{aligned} \tag{41}$$

where z_0 is the equilibrium separation between the two surfaces, E_1 and E_2 are the elastic moduli and ν_1 and ν_2 are the Poisson's ratios for each of the surfaces. [80]

To understand the impact of these forces, one can measure the adhesion force for different sizes of particles. This is a linear correlation for small particles below 1 µm. The force required to pull-off a silica sphere from another silica sphere, both with a diameter of 1 µm, is approximately 150 nN. [81] Other examples include a pull-off force of 20 nN for 20 nm glass and silicon particles, and these pull of forces can be calculated using the Laplace-Kelvin theory. Larger particles of 20 µm did not follow the Laplace-Kelvin theory, and had lower pull-off forces between 1200 and 7000 nN [82]. To calculate and predict the pull-off force it is important to know the surface energy of a silicon wafer. This is given by 2130 $ergs/cm^3$ (or 2.1 J/m^3) [83].

One would assume that if a particle is smaller, it has a lower contact area, so it is easier to remove smaller particles. However, this is not the case. The adhesion force for small particles is dominated by the van der Waals force and other capillary forces, which explains the scaling of r_p (and thus linear). However, the removal force of gravity scales with r_p^3 and drag forces scale with r_p^2. This means that the ratio between the adhesion force and the removal force increases with $\frac{1}{r_p}$ or even $\frac{1}{r_p^2}$, which is why it is increasingly hard to remove particles which are smaller. [24] [84]

As a final note, a lot of other factors can play a role on the adhesion of the particle on the wafer. Things such as an increased humidity can strongly increase the adhesion of the particle. Also, applying a bias of a couple of volts can be enough to strongly increase the force required to remove the particle. This behavior is, as expected by the reasons mentioned in the previous paragraph, more noticeable for smaller particles compared to larger particles. [85]

2.3.6 Brownian motion

Brownian motion is the random movement of particles in a fluid or gas due to collisions with exterior atoms. The movement is described by the diffusion coefficient and the root mean square distance, both given in equation 42

$$D = \frac{K_b T}{b} \quad \& \quad \sqrt{\langle x^2 \rangle} = \sqrt{2Dt} \tag{42}$$

Where b is the friction coefficient and K_b the Boltzmann constant. This phenomenon is important for particles with a size below 10 nm, and therefore hardly noticeable for particles larger than 1 µm. To give an example of the Brownian movement in such particles, a particle of 10 nm will travel 1 mm per second in a random direction. [86] Because the particles used in the experiments are larger than this order of magnitude, the Brownian motion of particles is not taken into account in this research. [87]

2.4 Summary of the theory

This chapter will in its turn also be split into several parts. Each theory section and force will be discussed to see the influence it has and if this influence is significant. Also, models that are going to be discussed in the theory (chapter 2) will be considered when discussing the significance of the theory. Some results were already briefly discussed in the results section. This section will provide an overview of that discussion in one chapter.

2.4.1 Flow in the wind tunnel

In all experiments, a turbulent flow was expected because of the Reynolds number, which is around 10000 for flows of 0.4 m/s in this specific wind tunnel (formula stated in chapter 2.1). Also, the entrance length would be around 5 m (formula 5). The flow is therefore not fully developed in the wind tunnel, however the largest deviations in wind speed are found in the beginning of the wind tunnel. This is caused by the HEPA filter having material in one place and no material in another place. As can be seen in the contour plots 22b, approximately 30 cm in the wind tunnel, deviation in the center of the wind tunnel are hard to find (thus creating a uniform flow). This result will be used in the models and calculations as well. Furthermore, wind measurements with smoke and a laser have confirmed the eddies and turbulence that is expected in the wind tunnel.

2.4.2 Charging and neutralization of particles

Triboelectric charging is expected to be the largest charging mechanism in the wind tunnel. The assumption will be made that the particles touching the outer diameter receive a charge, where other particles do not. Since triboelectric charging can not be calculated exactly, the triboelectric series is used to examine if different materials indeed make a difference. This series can be seen in figure 8. It is expected that the larger the difference of material in this series, the larger the charging. Also, the chapter of triboelectric charging (chapter 2.2.2) shows methods of charge induced and contact induced charging. Both mechanisms will be used in this thesis. Finally, formula 14 proposes that there is an exponential decay of static charge. This will be tested as well and the resistivity will be calculated.

When using the ionizer, the space charge which is generated becomes important. This phenomenon is already used in electrostatic precipitators, as will be shown in chapter 4.5. It is expected that the ionizer can neutralize surfaces, and maybe even particles. The ionizer uses emitter points which are charged with the opposite polarity, and this will be tested.

2.4.3 Forces on the particle

In this section, all relevant forces will be discussed. After this discussion, an overview of the relevant forces will be given in figure 17.

Gravity and drag force

Gravity and drag force are expected to be of large influence. The best way to test if the results are as hypothesized, is to do experiments in the horizontal wind tunnel. The trajectory will be modeled in figure 25b to get an idea of the distance these particles will travel. A larger particle will cover less distance in the horizontal wind tunnel and deposit in the center of the vertical wind tunnel.

Electrophoresis

As suggested in the theory, the diffusion and electric field charging mechanisms only occur in high fields (20 kV/m). The fields and ions per cubic cm are not met in the wind tunnel, and so table 12 shows a result which is too large. The same goes for formulas 30 and 31, where 1 second in the wind tunnel with given constants gives a charge of 38 e for diffusion charging and 47 e for electric field charging. For electric field charging, the maximum saturation might not be reached due to the limited time spend in the wind tunnel, so this charge might in reality be smaller.

Another result which will be tested is presented in figures 13a and 13b. Starting with the horizontal wind tunnel as visualised in figure 13b, it shows deviation even for larger particle sizes. For the vertical wind tunnel, no deviation should be found for the flows with the downward flow and micrometer sized particles.

The Boltzmann distribution does give a realistic result of the charge, namely a charge of 5 e can be present on a particle which is not charged on purpose. This charge can be one of the reasons that the particles have a small deviation already when approaching the wafer (they will not land exactly in the middle). Another result is found by equating formula 28 where the Cunningham slip factor can be neglected in this thesis ($F_C = 1.05$ for a 5 µm particle). The same result was found when equating the terminal velocity (formula 22, for a 5 µm particle 2 mm/s in no wind conditions), calculating the time present in the wind tunnel (0.5 m gives 250 s) and equating the drag force and with the electric force exerted on the particle. These calculations were done by assuming a linear trajectory and no charge accumulation. To conclude, terminal velocity is reached almost immediately. Furthermore, in order for small particles to deposit in the wind tunnel, experiments will have to take several minutes.

Thermophoresis

As could be seen in chapter 2.3.3 of the theory, thermophoresis could have an effect on small particles. Temperature changes of 5 to 10 degrees could already display this effect. In the experiments with the particles that are available, the thermophoresis force itself is expected to be too small to make particles deviate. Filling in formula 33 gave a result of 0.02 percent compared to other relevant forces such as drag, gravity and electrophoresis. However convection does play a role when heating up certain surfaces in no wind conditions. This convection can reach velocities of 0.08 m/s according to the first calculations, and therefore it is expected that without a flow present, convection can also cause particle trajectories to change.

Lift forces and turbophoresis

The lift forces as discussed in chapter 2.3.4 are of a smaller effect and therefore do not have to be taken into account. This can be seen by including lift forces in the simulation, but also by calculating formula 38. For the Saffman equation, the ratio between lift force and drag force would be 2 percent for a 5 µm particle. For other models such as Hall or Mollinger, this number can increase to 10 percent. This however would still be only a small effect compared the gravity, flow and drag. The Magnus force is even smaller, since the particles have no driving force to start or continue their spin. Because of the smaller contribution, it is hard to measure this effect without taking into account other parameters as well. The lift forces however can be a suitable explanation if the particles slightly deviate from their trajectory.

Turbophoresis does have an effect on particles, especially very close to the wafer. At this point, the turbulence gradient will be the largest. It is however a force which is hard to model and can not be taken into account in the models (also because of the computational time). The only advantage is that in all the experiments, the wafer is stationary, resulting in a constant turbophoresis force.

Adhesion forces

As stated in chapter 2.3.5, the adhesion force of the sphere with the wafer can be described by the DMR model. Taking into account the contact area of the sphere, this would result in a force of $-6.2832 * 10^{-5}$ N for the tensile load to completely remove the particle from the surface (also called the pull-off force, confirmed by [82]). The models do assume however that the contact between the bodies is elastic, and this assumption may not be fully true. It is expected that smaller particles will be harder to remove from dimension analysis. Also, the roughness of the surface can have an effect on the adhesion force, so each wafer should have its own calibration measurement.

Brownian motion

As already stated in the theory, the Brownian motion only becomes important for very small particles (<1 μm). These particles will be hardly available in the experiments which will be executed. In wind scenarios, these very small particles are likely to follow the streamlines of the flow, evading the wafer. Therefore, it is concluded that the Brownian motion of particles will be neglectable.

Conclusion of forces

For the forces present on the particles, an overview is given in figure 17. The green color displays the forces which have a large effect, the orange color displays forces which could have a significant effect when not taken into account or if the force is constant. The red color represents forces which are not significant based on the calculations above.

Forces and particles	Gravity	Drag force	Electrophoresis and triboelectric	Thermophoresis and convection	Lift forces	Turbophoresis	Brownian force	Adhesion\ roughness
Insulating particles				plates and wafers must cool to room temperature	constant and small contribution	constant, wafer is not moving	To large in future experiments	When using the same wafer, adhesion force is constant
Conducting particles			Hard to charge conducting particles	plates and wafers must cool to room temperature	constant and small contribution	constant, wafer is not moving	Only smallest particles can have an influence in future experiments	When using the same wafer, adhesion force is constant

Figure 17: *The table of forces taken into account for the AWH and the wind tunnel. Also, the forces for the corresponding particles used in the thesis are shown.*

3 Experimental setup

3.1 Overview of the setup

An overview of the wind tunnel is shown in figure 18. The wind tunnel is shown on the left (vertical) and the right (horizontal). The wind tunnel drawings are not to scale, and for more information, chapter 3.2.1 can be consulted. The horizontal wind tunnel includes three filters, one grounded plate, one charged plate and a wafer, all discussed in chapter 3.2.1. The flow velocity is checked using a velocity meter and smoke (discussed in chapter 3.2.2). It also includes an inlet, discussed in chapter 3.3.2. For the vertical wind tunnel, the extra components include an ionizer (discussed in chapter 3.5) and a laser (discussed in chapter 3.6).

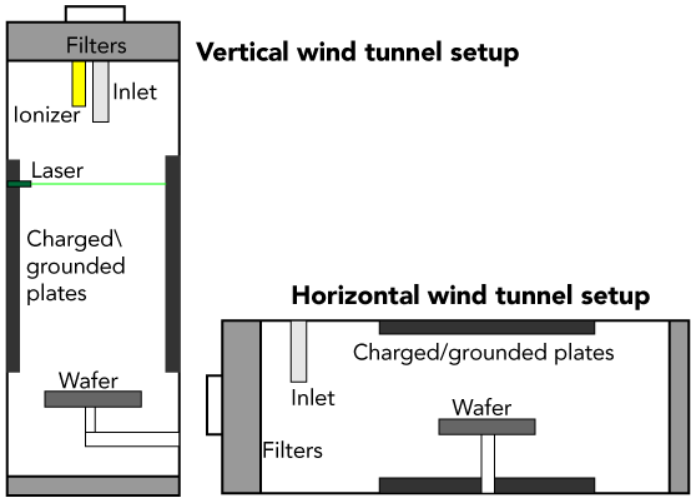

Figure 18: *Overview of wind tunnel setup, with both the vertical and horizontal wind tunnel.*

An overview of the particle setup is shown in figure 19. After the measurement is executed, the wafer is transported to the particle counter setup. Here, the particles (discussed in chapter 3.3.1) are sucked up using a particle plotter (discussed in chapter 3.3.3) which moves the particle counter (discussed in chapter 3.3.4) to the desired position. For more elaborate measurements, a SEM can be used (discussed in chapter 3.4).

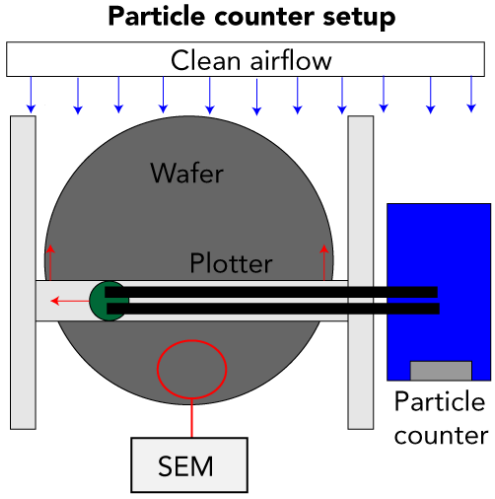

Figure 19: *Overview of the particle counter and plotter setup within a clean environment.*

3.2 Wind tunnel

As explained in chapter 2.1, the flow is the first tool in our toolkit to prevent contamination. Since the AWH discussed in chapter 1.3 has a lot of varying parameters, a wind tunnel is built. The setup of this wind tunnel and the flow will be discussed first. After that, a look will be taken at the particle counter and the calibration of the particle counter.

3.2.1 Wind tunnel setup

The experimental setup that will be used in this report is the wind tunnel, as sketched in figure 20. This wind tunnel has a width of W=0.59 cm, a length of L=2 m and a height of H=0.315 cm. This is not including the filters or the fan, which are also mounted to the wind tunnel to ensure a uniform airflow. Let us discuss the setup going from left to right as seen in figure 20. The fan is the only source in the wind tunnel which contributes to the flow of air. The fan can function up to 24 V and reach wind velocities of 0.6 m/s in the wind tunnel. The needed voltage is being generated by a power supply (Philips , which can go up to 40 V and 10 A). After this, the fan encounters a divertor. This divertor is used to split the air in four columns. These four columns signify the first stage of trying to get a uniform airflow. The dimensions of this divertor can be seen in 20. After the air has passed the divertor, it encounters the filters. The filters are H14 classed HEPA filters. They do not only make sure the air is uniform, they also stop 99,995 percent of the particles of 0.3 µm. Particles larger or smaller than 0.3 µm are stopped with an even higher percentage, since smaller particles than 0.3 µm are caught more easily due to diffusion and larger particles than 0.3 µm are stopped more easily due to inertia. The area in between the two HEPA filters results in a pressure gradient which helps to make the air flow even more uniform. The first filter is placed 7 cm after the divertor. The filter is 6.6 cm deep and has the same dimensions as the wind tunnel (so H=0.315 cm and W=0.59 cm). 13 cm after the first filter ends, the second filter is placed. The filters are all identical in dimensions. When the air leaves the second filter, it is free to develop itself over the rest of the wind tunnels length. Finally, the wind flow will encounter a third filter which helps to keep the airflow uniform all the way until the end of the wind tunnel. If this final third filter would not have been there, a lot of turbulence would be noticeable at the wind tunnels outlet. The final filter is placed after 2 m from the second filter.

Two wafers are used, a silicon wafer and a PVC wafer. Both wafers are 30 cm in diameter. When particles have travelled through the wind tunnel, they land on this wafer. The wafer is carefully positioned on a wafer stage which has a length of 30 cm (so the wafer has a full overlap with the wafer stage), The wafer stage can be easily moved through the setup so that it can be tested at multiple positions, which is true for both the horizontal and vertical wind tunnel.

The statically charged plate used in the experiments is also made of PVC, and has a length of 50 cm and width of 30 cm. This plate will be positioned parallel to a grounded plate (made of aluminium to ensure conductive properties). To check if the plate is grounded, a multimeter (of brand Fluke 179) was being used. The plates will be charged negatively using contact induced charge separation and positively using charge induced charge separation. Both mechanisms were already discussed in chapter 2.2.2. The particle inlet will also be made of different kind of materials. The materials will range from plastic, metal and glass. The (final) contact of the particle must be with this material to charge the particles. To measure the charge on the plates, an electrostatic field meter is used. This electrostatic field meter can measure the field at two positions from the charged plate (2.5 cm and 10.0 cm). The Simco FM 300 electrostatic field meter can measure both positive and negative fields. In the experiments, the electrostatic field meter will be used at several positions to see if the plates are uniformly charged within a margin of error.

3.2.2 Flow velocity measuring components

The uniformity of the wind tunnel was tested using two methods. 1) using a velocity meter from TSI (9565-P) which has an accuracy of 0.4±0.04 m/s and 2) using a smoke generator. The velocity can be measured using this device by making holes in the side of the wind tunnel and inserting the probe at different lengths in the wind tunnel. The probe of the velocity meter can be extended by 92 cm, which is enough to reach the full width of the wind tunnel. Furthermore, the probe uses a temperature sensor to determine the airflow. This temperature sensor is protected by a metal shell, which if not inserted correctly, can block the flow of

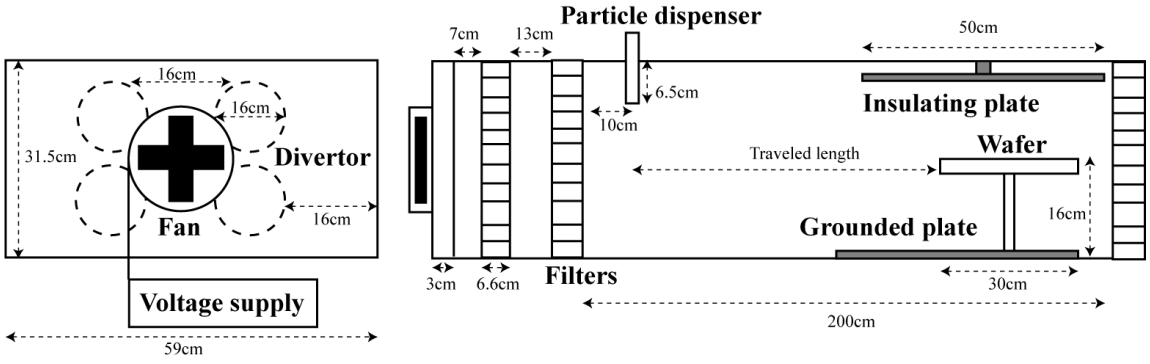

Figure 20: *The horizontal setup in greater detail, with the corresponding distances and parts of the wind tunnel.*

air. This is why the maximum readout of the velocity meter needs to be taken while turning the velocity meter around slowly.

The smoke is generated in a small compartment of water through which a constant flow of air is forced using a mist generator. This flow enters as clean air and thus exits the small compartment as a reasonably laminar flow of smoke. This smoke can be inserted at different lengths and depths into the wind tunnel by creating a hole in the top of the wind tunnel. The smoke has a starting velocity, but by inserting the smoke at the top, this velocity gradient will be perpendicular to the flow in the wind tunnel. By canceling the vertical flow from the smoke generator, one can measure the velocity of the wind tunnel. Furthermore, the smoke can be visualised using a green laser from Tacklife (SC-L07G), which produces a sheet of light that has an angle of 132.5 °. This means that if the laser is placed at the top of the wind tunnel, it will diverge and light up 135 cm at the bottom of the wind tunnel, where the brightness is the largest below the Tacklife. The smoke can be filmed with a good phone camera (in these experiments, a Samsung galaxy S10 was used) and inserted in a Matlab script to do further processing. Using both script 3 and PIVLAB (a Matlab tool), the mean velocity of the flow can be analyzed over 120 frames. As a final comment, the smoke can also be used to visualise the boundary layer by inserting the smoke right before the wafer. An example of this phenomenon is given in figure 21, where the boundary layer of the vertical setup is visualised.

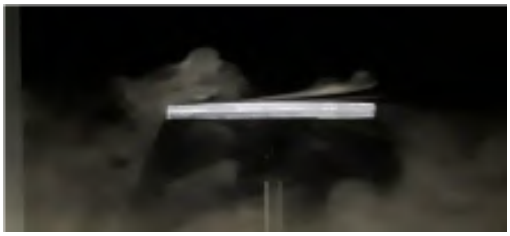

Figure 21: *Smoke in a wind tunnel visualising the boundary layer of a flat plate. The airflow is in the horizontal direction [88].*

3.2.3 Wind tunnel calibration

For our experiments in the wind tunnel, a predictable and uniform flow is needed. This flow will ensure that the deviations of particles seen later on in the thesis are actually caused by electric fields for example, and not a large deviation in the flow velocity.

To get an idea of the uniformity of the wind. the following measurement was done using the air velocity meter mentioned in chapter 3. The measurements were done at several places in the wind tunnel. 3 Slices

were made in the width W and 5 in the length L to get a good overview of the velocity contour. The 3 slices at positions W=4.5 cm, W=30 cm and W=54.5 cm are plotted in figures 22a, 22b and 22c. Each contour plot is averaged over 30 measured points with different lengths L and heights H. This means that over the three contour plots combined 90 measurements were taken (30 measurements per contour plot).

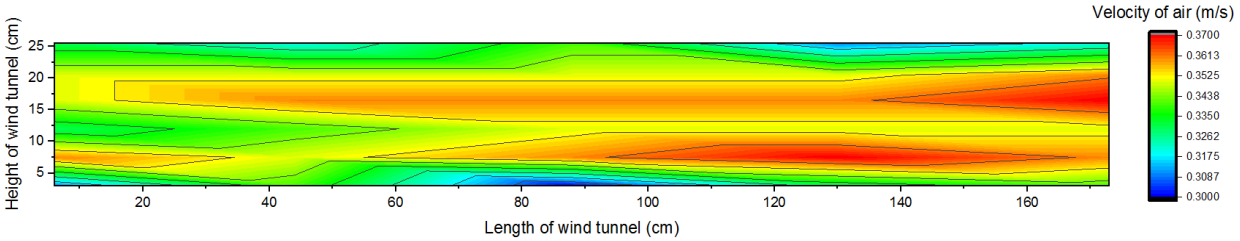

(a) Contour plot at W=4.5 cm

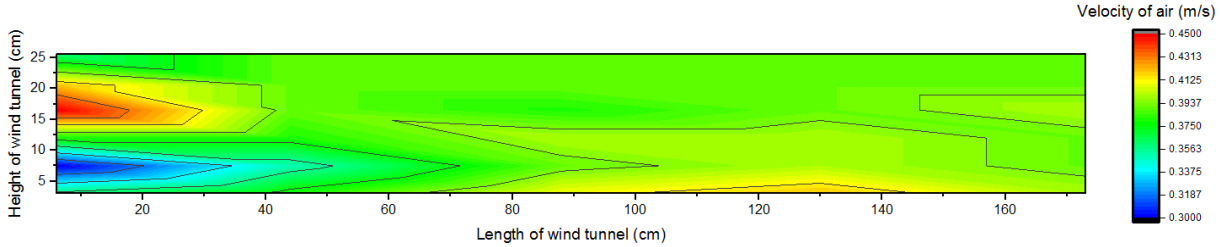

(b) Contour plot at W=30 cm

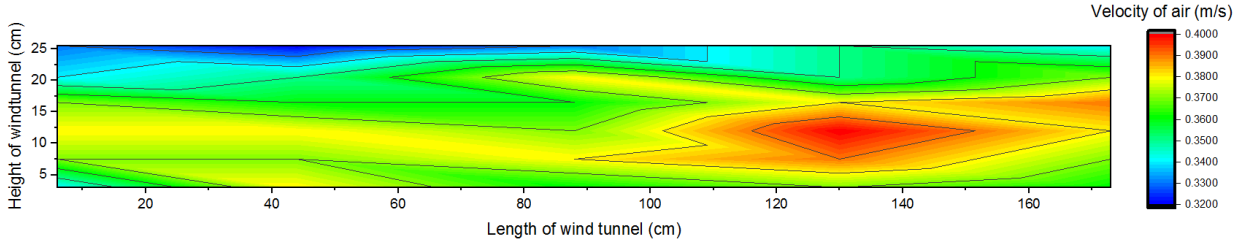

(c) Contour plot at W=54.5 cm

Figure 22: *These contour plots show the wind profile in the majority of the wind tunnel (remembering that the actual height is 31.5 cm and length 2 m). A reasonable uniform profile can be found, with somewhat slower average velocities near the walls (B=4.5 cm and B=54.5 cm) due to the boundary layer.*

These contour plots present information about the entrance length and the impact of the no-slip condition near the walls of the wind tunnel. First of all, figure 22a and 22c look quite similar as they should be. They were both taken at the same distance from a wall (only difference is that one was taken at the left side, the other at the right side of the width). It is noticeable from these images that the flow seems quite developed in the middle of the wind tunnel, but especially the top and bottom of these contour plots appear blue, which signals that the velocity of the air is slower in these regions. This is explainable. Not only is the wind dealing with the no slip condition from the left or right wall, it is also dealing with the no slip condition from the bottom or top wall. The combination of these two walls result in a corner were the velocity of the air is slower. Now, for the middle of the wind tunnel, one can see that after 30 cm, the flow is very well defined in figure 22b. The only peaks in the figure are shown right after the filter. This is because of the entrance length and the way the HEPA filters work. These filters have ducts were the wind is flowing through, meaning there is some material in one place, little material a couple of mm after that and then again some material. When holding the velocity meter close to this filter, it is important whether or not the tip of the probe is in front of the material (thus slowing down the wind velocity) or in front of the duct (thus accelerating the wind velocity). A small movement of a couple of mm with the probe can already make a

difference between fast- and slow-moving air near the filter, thus explaining these velocity differences close to the filter. It should therefore be said that both the red and blue area in figure 22b could also have been switched, if the probe would have measured a couple of mm farther in the width of the wind tunnel.

To find out if the velocity meter worked correctly, another kind of experiment was executed with smoke and a camera. These results are extensively discussed in appendix chapter F. It turns out that the velocity meter and the smoke measurements give the same results, were at the start of the wind tunnel the velocity of the smoke is slow or faster, and in the center of the wind tunnel the flow velocity is 0.4 m/s

So, both experiments (with the velocity meter and smoke measurements) have confirmed that the flow is uniform and can be well determined using the installed fan.

3.3 Particle measurement setup

This chapter will consist of 4 parts which are essential in counting the particles in the particle counter setup as seen in figure 19. First, the particles themselves will be discussed in chapter 3.3.1, after which the dispenser or inlet which drops these particles will be discusses in chapter 3.3.2. After that, the plotter moves the arm to the correct position, as explained in chapter 3.3.3. The particle counter will then collect particles. The setup will be discussed in chapter 3.3.4 and the calibration measurements (for glass) in 3.3.5. The whole particle measurement setup is installed in a fume hood, which provides a clean airflow over the wafer.

3.3.1 Particles

The glass spherical beads have a density of 2460 $\frac{kg}{m^3}$ [89]. Other particles which are used are conducting pure copper particles, which are smaller than 5 µm and are spherical. The third kind of particle that will be used are polyamide seeding particles, which have a size between 1-10 µm, a density of 1030 kg/m^3 and are described as non-spherical but round.

3.3.2 Particle dispenser

The opening of the particle dispenser is a cone (called a TT tip) like plastic (polyethylene) tube with an opening of 0.19±0.1 mm during the glass experiments. The inlet opening was increased for copper and polyamide particles, since the inlet of size 0.19 mm was not sufficiently wide. Other inlet materials include aluminium and glass. Both inlets were manually produced, but accuracy was tested by repeating measurements.

The particle dispenser experiences a shake be dropping a fixed weight from a fixed height (thus gaining the same contact velocity each time and therefore the same force which is translated to the beam), which makes the beams of the setup vibrate slightly. The vibration is kept as constant as possible for each shake. The particle dispenser is firmly tightened in the middle of the wind tunnel. Because the particle dispenser needs to be attached at different position on the wind tunnel, the shaker also has different amounts of particles leaving the particle shaker. For the horizontal wind tunnel this is 56831±4044 per 20 shakes and for the vertical setup 31413±4022 per 20 shakes, but more information about these calibration measurements will be given in the chapter 5. To make sure that the volume of the inlet does not have an influence on the number of particles released, the particle dispenser is refilled to a certain level after each experiment.

3.3.3 Particle plotter

The particle counter is attached to a Phoenix contact CMS-P1 Plotter. The arm of this device is controlled by a Matlab script, which sends DOS commands to the particle controller. The script can be found in appendix chapter P. The script ensures that the particle counter is moved in sync with the arm. The particle counter is hovering above each position for 12 seconds and it needs 197 positions before having scanned the whole wafer. After the data is gathered, it can be analyzed using a second Matlab script, found in appendix chapter P. This script plots the highest particle count as bright circles, while low particle counts are plotted in black. The excel sheet gathered from the lighthouse device can be adjusted to select a different bin of

particle sizes. For the Lighthouse Boulder counter, a different setup was used. Because of the larger (5 cm in diameter) suction head, only one axis could be taken into account while still sucking up a significant number of particles. The plotter was moved 3 mm each time to collect 100 data-points.

3.3.4 Particle counter

Several particle counters were used during the experiments. The main particle counter is a Lighthouse Solair 1100 which sucks up particles from the wafer. This suction is created by the Solair which creates a vortex to pick up the particles. The particle counter has two connections, one into the machine for the contaminated air containing particles and one out of the machine with clean air. These airflows are placed in a closed loop system (e.g. the contaminated flow from the particle suction device goes to the particle analyzer, and the clean flow flows from the particle analyzer back towards the particle suction device.) The recorded data from the particle counter can be imported to excel using the LMS XChange program from the supplier. The Solair also counts the particles, ranging for different sizes of particles. The bins which are counted are 0.1-0.15 µm, 0.15-0.2 µm, 0.2-0.25 µm, 0.25-0.3 µm, 0.3-0.5 µm, 0.5-1 µm, 1-5 µm and finally >5 µm. The particle counter never interacts with the wafer, as it is at a fixed height above the wafer. The thickness varies per wafer (the silicon wafer is 0.83mm thick and the PVC 3.4 mm thick). The height above the wafer is kept constant, and is 3mm. Between each experiment, the wafer is carefully cleaned using an IPA solution and microfiber cloths. Another particle counter which was used is the Lighthouse Solair 3100, which has a range between 0.3 µm and 10 µm. The last particle counter which was used was the Lighthouse Boulder counter, which has a range between 5 µm and 100 µm.

3.3.5 Particle counter calibration

The goal of this chapter is to find out what the error is in the particle counter. First, the number of particles on a clean wafer is being measured. This is done to see if the particle counter also measures particles on a clean wafer. Next, the wafer is measured multiple times, to see how many particles the particle counter has missed the first time. These measurements are important to know in future experiments when interpreting data.

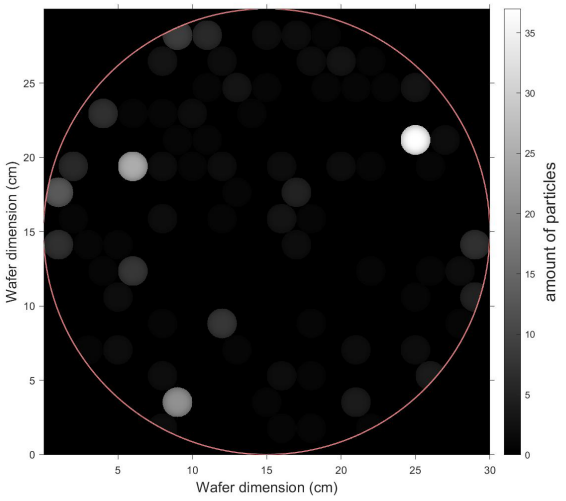

Figure 23: *Calibration measurement of the wafer for particles larger than 5 µm. Mean number of particles is 1.2 particles per position of the plotter.*

A shake of the particle dispenser contains a certain number of particles. First, one must know the number of particles that were already present on the wafer after the IPA cleaning process. This result can be seen in figure 23 for particles larger than 5 µm. The figure visualises where the largest number of particles are

present, given by the intensity of whiteness. The legend on the right of the figure gives the maximum number of particles given by one small white circle, for figure 23 this is 37 particles.

Furthermore, it is noticeable that together with the larger 5 µm particles, also smaller particles of 0.1 µm are deposited on the wafer without any shakes. The 0.1 µm particles are even seen more frequently than the >5 µm particles. This means that there is a larger correction factor for the smaller particles than the larger particles. Also, larger particles up until 100 µm can be found (for the glass particles), but these particles are present in a lower degree. In future measurements, table 1 will be subtracted from the measured sample to ensure that only the particles that are deposited on the wafer by the shakes are counted, and to compensate for the fact that it is easier for smaller particles to contaminate the wafer without any process being done to the wafer.

Particle size range (μ)	Witness	20 shakes
0.1-0.15	23217	130272
0.15-0.2	7139	92348
0.2-0.25	2563	48178
0.25-0.3	1601	44795
0.3-0.5	1021	42299
0.5-1	582	37086
1-5	435	34064
5-10	119	16982
10-25	55	12202
25-40	26	6674
40-50	13	3610
50-100	5	1065
>100	1	65

Table 1: *Table with the number of particles deposited on the entire wafer without any shakes applied to the shaker and with 20 shakes applied to shaker.*

Furthermore, to get an idea of how many particles are released during one experiment, another measurement was executed. These numbers can be seen in column 3 in table 1. It was determined from several measurements that the error in these measurements is smaller than 10 percent. This means that the particle shaker used in these experiments is consistent. This error will be taken into account when doing the error analysis in the appendix in chapter N.

As can be seen in table 1, the smallest particles are most often seen in the glass powder. However, one might ask themselves if that makes these particles also the most important particles. The answer simply stated is no. Since the triboelectric effect goes with ($\propto r_p^2$) and gravity with ($\propto r_p^3$), their do not have to be so many large particle to still dominate these effects. The large particles with charge can easily attract or repel smaller particles. Of course the drag force will also have an effect ($\propto r_p$), but this effect will work in both the vertical and horizontal direction. This confirms the following: The larger particles dominate the effects which play an essential role in this research by clumping with smaller particles, giving the smaller particles no change to escape (see chapters 5.1.3, 5.1.4 and 5.1.6) for more information on clumping). This is a shame, since the small particles would feel the largest relative effect due to the electric field. Seen in formula 28, the displacement scales with ($\propto r_p$), meaning that smaller particles would be able to change their trajectory relatively easily. More on this subject will be explained in chapter 5.5 and 5.2.

After the particle counter has treated the whole wafer, some particles are still left. To determine how many particles are left after the measurement, several measurements were executed immediately after the previous measurement was finished. After 4 measurements, SEM measurements were done to manually count the remaining particles. This resulted in a total of 15 percent of the particles being caught by the particle counter during the first measurement. It must also be noted that during these experiments it was evident that relatively more smaller particles were left compared to larger particles after the first measurement. More details can be found in appendix chapter G.

First, the error in the particle counter is no problem for the quantities of particles that are being used in future experiments. Also, approximately 15 percent of the particles are removed during the first scan of the particle plotter, and actually making contact with the wafer hardly improves the count. Finally, large particles are easier to remove than smaller particles as can be seen in experiments with several measurements. This has to be kept in mind in future experiments.

3.4 Electron microscope

The particle-particle interaction and size of particles can be investigated using an electron microscope. An electron microscope uses electrons instead of light to achieve a smaller wavelength and thus create a better resolution image, which can be as small as micrometers. The electron microscope shoots out a concentrated electron beam, which is focused using shaped magnetic fields. The focused beam hits the surface and by doing this, the surface emits secondary electrons. This technique of doing electron microscopy is called SEM. The electron microscope also has a build in EDX (Energy Dispersive X-Ray Analysis), which can identify elements. The EDX is used to investigate unknown spots on the particles and to examine the purity of the particles that were used. In this report, a certain point that needs to be examined scans the surface for 60 seconds and interpreters which element is detected using the provided software. The amount of counts in 60 seconds is often around 100000, giving the user sufficient points to draw a reliable conclusion. Using the SEM, resolutions of 1 μm are well visible and can be measured. The electron beam has an energy of 15 kV when doing these measurements.

3.5 Ionizer

An ionizer is a device which can be used to neutralize the static charge of objects. This means that if an electric field causes particles to be attracted to the surface, it might be better to have no field at all. This is where the ionizer can help.

It functions by generating ions of both polarities, which are blown towards a surface. Here, the ions which have an opposing polarity compared to the surface will neutralize each other, while ions of the same polarity of the surface will be repelled. An ionizer is thus a useful tool to control the charge in a setup. In the AWH, some parts and surfaces will be charged. If this happens to be a disadvantage, it will be helpful to be able to neutralize this surface.

In order to test the charging and neutralization of the wafer with the ionizer, it is a good idea to understand the function of the ionizer. The ionizer used in this thesis will be an AFC airflow controller from Richmond which can produce both a negative and positive ion output. When unscrewing the main box, the inside of the ionizer can be studied. The box with the labels of what each part means can be seen in figure 24. First the input power enters the ionizer where it goes through a transformer. This transformer converts the DC input voltage to an AC output voltage. One can set the frequency of the output voltage using the black round switch. Options are steady state, 1 Hz, 1.3 Hz, 2.2 Hz and 10 Hz. These frequencies are made using the resistors. Furthermore, one can also set the amount of positive and negative ionisation using the blue screw switch. Screwing the switch clockwise will increase the ion output of that certain polarity. The resistors will also take care of the level of ion output. The final high voltage output is made by the black trapeziums, which transports the high voltage towards the pressurised gun. The pressure itself is generated by a steady inflow of pressurised air. Both this pressure and the high voltage come together in the pressurised gun.

The pressurised gun works with emitter points. One emitter point for the negative high voltage, one emitter point for the positive high voltage. These emitter points work as follows: "Negative ions are produced in close proximity to emitter points driven by a negative power supply. Ions are generated in the plasma of the corona around the emitter. In the corona region, weakly bound electrons are driven from orbit and attach to a molecular cluster. The resulting negative molecule is repelled from the like-charged emitter. Positive ions are produced in the area around emitter points driven by a positive power supply. The free electron is attracted back to the positive polarity emitter point. In this case, the resulting positive molecular cluster accelerates away from the like-charged electric field of the emitter electrode" [90]. Using the pressured air, the ions that are generated can be directed towards the wafer. This is how the ions can become airborne and

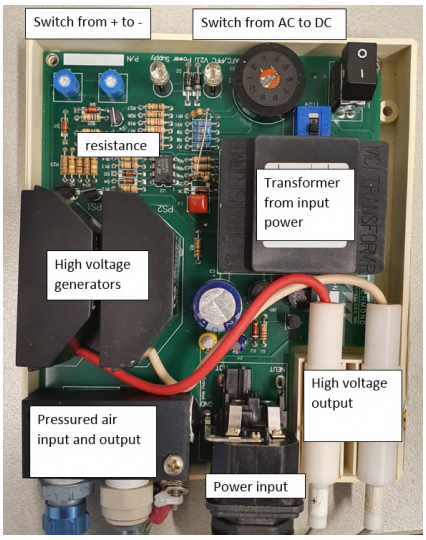

Figure 24: *The inside of the ionizer with labels of the parts.*

used to charge or neutralize a target. A more thorough explanation of the subject can be found in chapter 4.5, where a model is developed to explain the function of the ionizer.

Measurements using a high voltage converter enable the user to measure the amount of kilo-volts on the tip of the emitter. Results show that the highest voltages that can be achieved is 3 kV. The LED light which indicates the amount of voltage passing through is also the brightest at this point. Furthermore, there was always some other output on the other emitter point, which was around 0.5 kV. In this case, the LED light indicating voltage output shined very dim. Noticeable was that the power provided was not a perfect DC voltage, but had some kind of frequency to it. This frequency increased when increasing the voltage. For 0.5 kV the frequency was approximately 50 Hz, for 3 kV this was 275 Hz. Both frequencies however only had amplitudes of 300 V and were therefore always entirely in the positive or negative voltage regime. A picture made of the oscilloscope measurement of a negative emitter point can be seen in figure 79 in the appendix.

3.6 Laser and temperature measurements

Extra experiments included a laser and temperature measurements. The laser was a 5 mW green laser with a wavelength of 532 nm. It shined through the wind tunnel to scatter light of the particles. This light could be caught be a camera (Samsung galaxy S10, 60 Hz, 4k footage). Mirrors were used in some experiments to have more laser beams running through the setup, and therefore increase the likeliness of particles passing through this light. The results were analysed by a Matlab script as well, which is available in appendix 5.

To see if temperature has an effect on the flow in the wind tunnel, plates were heated but not charged. The experiments will be executed in a no wind environment, so the role and significance of free convection can be measured. The plates were heated using both hot water and a hairdryer to heat up the plates to the desired temperature. The plate would then be installed on the same location as the charged plates normally would, to leave all other parameters constant. Different temperatures could be achieved, resulting in different uniformly heated plates. The temperature was measured using a FLIR of the model E6-XT. The FLIR is precise to the 0.06 C°.

4 Simulations

This chapter will discuss the results of the numerical simulation for all the forces. The numerical simulations in COMSOL uses the finite element method (FEM), will be compared with analytical calculations in Matlab, which solely rely on the drag and gravity force or other formulas. Furthermore, a look will be taken to which parameters have a time dependency and how they influence the motion of the particles through the wind tunnel. Finally, particles with different sizes will be inserted in the wind tunnel to see what distance they travel and what their trajectory looks like. All flows are taken to be Newtonian and incompressible, which means that the stress is linearly dependent on the strain and that the temperature fluctuations are small, meaning that the density of all flows is constant.

These simulations will be the basis for the predictions and calculations made in chapter 5. Parameters of the particles such as conductivity, size and density can be adjusted according to the experiment, as well as the flow. Since a lot of simulations need to be run, this chapter will also focus on the difference between turbulent and laminar flows, to see which models have the lowest computation time, while still remaining accurate.

4.1 Horizontal model laminar flow

The first simulations will be run in the horizontal wind tunnel. The dimensions of the wind tunnel are discussed in chapter 3. This chapter will focus on the assumptions made during modeling and how they influence the trajectory. Take notice of the conventions used when labeling the axis of these graphs: the width W=0.59 cm, the length L=2 m and the height H=0.315 cm. These conventions will be used for both the horizontal and vertical setup.

First, the analytical model will be discussed. In this model, the drag force and gravity force play a role (as can be seen in equations 19 and 20), and a constant horizontal velocity is assumed for the particle (given by the flow velocity of 0.4 m/s). The force of the wind and the drag force will be in equilibrium quick (as seen in chapter 2.3.1), meaning a constant velocity in the center of the flow. The Reynolds number of the particle is low causing the flow to be Stokes locally around the particle. Let us assume a particle diameter of 20 µm with a velocity flow of 0.125 m/s for the laminar calculations (so a comparison can be made with earlier research [88]). This means that the drag coefficient will be 121, according to equation 21. Filling this in together with gravity and setting the horizontal velocity constant gives figure 25a. In figure 25b, the trajectory of the particle is plotted for the 3D COMSOL FEM model. In these graphs, only drag force and gravity were taken into account.

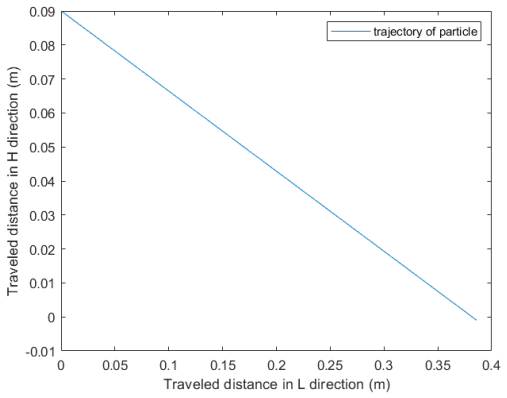

(a) Trajectory expected by analytical simulation

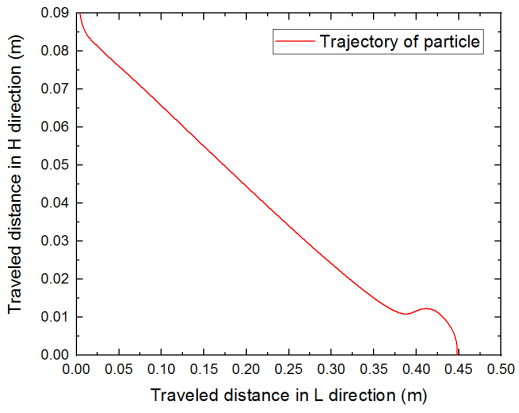

(b) Trajectory expected by FEM simulation

Figure 25: *Left) the trajectory expected for a analytical model in a horizontal simulation in laminar flow. Right) the trajectory expected for a FEM model in a horizontal simulation in laminar flow. Both with u=0.125 m/s, diameter of particle=20 µm and density 2490 kg/m^3*

As can be seen, there is a noticeable difference between the distance a particle travels, which is caused by the development of the flow in the wind tunnel. In the first model, the velocity is given as a parameter and no development or slip condition is taken into account. In the second model, this is not the case, and the velocity profile develops to be zero at the edges (no slip condition) and fastest in the middle of the flow. A visualisation of this is made in figure 26a, where the velocity near the walls is slower (blue) than in the middle of the wind tunnel (red). The main difference in the particle trajectory happens in the boundary layer near the wafer. Particles are accelerated upwards before penetrating the boundary layer due to gravity. This is also why the FEM model predicts that particles travel farther than the analytical model, 45 cm compared to 38 cm for a flow of 0.125 m/s and 20 µm diameter glass particle. The velocity profile of the analytical model is constant and so are the streamlines, so this figure is not sketched. The laminar flow for the FEM simulation can be found in 26a.

To conclude: a laminar flow in this setup can not be modelled with a simple calculation and a uniform velocity profile, and thus FEM simulations need to be used. In the next chapter, a discussion will be made if turbulent models represent the flow better.

4.2 Horizontal model turbulent flow

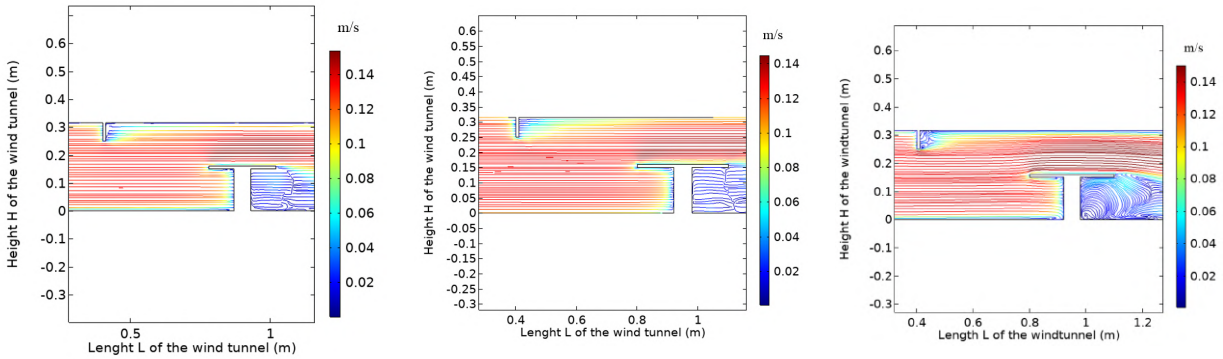

(a) Laminar flow *(b) k-ϵ turbulence* *(c) SST turbulence*

Figure 26: *In all the figures above, the color scheme represents the velocity of the streamline. All lengths are kept constant. Left) the streamlines expected for a laminar flow in a horizontal direction. Middle) the streamlines expected for a k-ϵ turbulence in a horizontal direction. Right) the streamlines expected for a SST turbulence model in a horizontal direction. All with u=0.125 m/s.*

The FEM model visualised in figure 26a still assumes a laminar flow. The Reynolds number of the flow increases with its velocity, and for the current situation in the atmospheric wafer handler, this is 0.4 m/s. This is in the turbulent regime. This is why a comparison needs to be made between models with and without turbulence. Two models are taken into consideration: 1) the k-ϵ turbulence model and the 2) SST model (Menter's Shear Stress Transport). The first model is a two equation model which assumes that the turbulent viscosity is isotropic. The second model is a two-equation eddy-viscosity turbulence model which takes a k-ω turbulence model at the walls and a k-ϵ for the rest of the flow. The results for the streamlines of these turbulent models can be seen in figure 26b for the k-ϵ turbulence model and in figure 26c for the SST model. Both models again assume a no slip condition and the same conditions as the models displayed in figure 25a and 25b to accurately compare them amongst each other.

Noticeable is that all three FEM models (laminar, k-ϵ turbulence and SST) look quite similar. This is logical, turbulence is only a deviation from the mean speed. The models here are stationary, meaning that these deviations are filtered out and a very similar profile occurs for all three models. If turbulence does need to be taken into account, a time dependent study can be used. The wind speeds at which the models are set do not really matter for the eventual profile. In these experiments, a flow of 0.125 m/s was chosen, a similar flow as had been used in the previous research at VDL [88]. The largest difference of these models is

the modeling of the flow near the walls. These differences are discussed in the appendix H, where the wall functions and other important initial values are represented.

At speeds of 0.4 m/s, only the turbulent models accurately converge when choosing a time dependent study, meaning that this is indeed a fully turbulent regime. For a stationary study, the laminar model still converges. At these speeds, the analytical model predicts that particles of 20 μm travel 1.26 m and the FEM model predicts 1.30 m. This is again due to the boundary layer near the wafer and a very similar outcome to the one discussed for smaller velocities (see figure 25a and 25b)

The different turbulent models of the horizontal flow have been discussed in this chapter. There is little difference between the turbulence models in this case, but there is a difference between the turbulence models and the laminar model. The goal now is to do the same for the vertical wind tunnel, as will be discussed in chapter 4.3.

4.3 Vertical model laminar and turbulent flow

In the vertical simulations the flow looks similar for different models as well. To represent the velocities differently, several velocity profiles are sketched in figure 27a, 27b and 27c for a laminar flow, k-ϵ turbulence model and the SST turbulence model. In these figures, a wafer of 30 cm is placed in the center of the flow. Again, the diameter of the particle is 20 μm, the speed of the laminar flow and turbulent flow is 0.4 m/s to compare the three models (this flow is different from previous simulations, but as stated before, the flow profiles look similar). As stated earlier, all models only converge for a stationary study. Nothing really surprising can be seen here when comparing these models to the models used for the horizontal flow simulations, considering the wall functions explained in chapter 4.2 and appendix H. One can see that the laminar and SST model tend to go back to 0 at the walls, while the k-ϵ does not calculate the results near the wall. What is different between the vertical and the horizontal simulation is the way the flow develops under the wafer. There is actually a positive velocity component at the bottom of the wafer (which is also why deposition on the bottom of the wafer occurs) represented by the red line. Furthermore, since the air has less room to move around the wafer, the velocity sharply increases at the borders of the wafer. This is seen in the figures 27a, 27b and 27c at the left and right side, where the velocity increases to 0.8 and 0.9 m/s in the negative z direction. Another conclusion which can be drawn from these figures is that the flow still moves towards the wafer, even 1 cm above the wafer. This gives heavy particles a high probability to deposit on the wafer, since gravity (and thus the inertia of the particle) causes the particles to not follow the streamlines that move away from the wafer at the final cm (just before reaching the wafer). For a visual interpretation of these differences see appendix figure 78a and 78b.

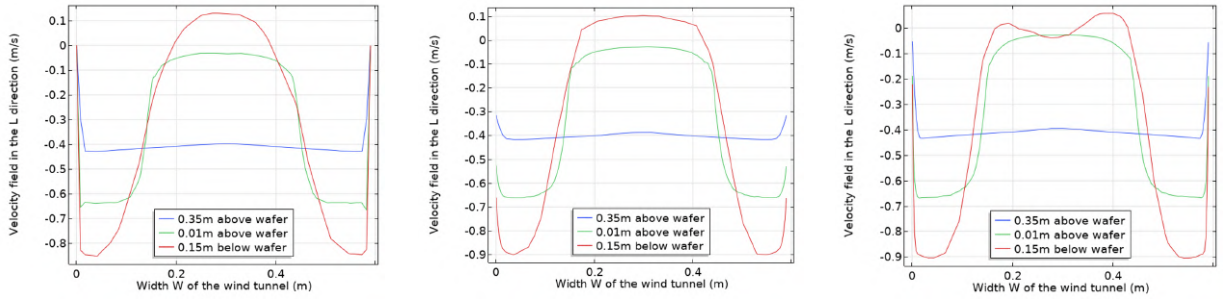

(a) Laminar flow *(b) k-ϵ turbulence* *(c) SST turbulence*

Figure 27: *All lengths are kept constant. Left) the velocity profile expected for a laminar flow in a vertical direction. Middle) the velocity profile expected for a k-ϵ turbulence in a vertical direction. Right) the velocity profile expected for a SST turbulence model in a vertical direction. All with u=0.4 m/s.*

In chapter 4.1, it was already explained what kind of influence the boundary layer might have on the horizontal setup. Now, for the vertical setup the boundary looks different, as could already be seen in plots 27a, 27b and 27c. In these plots it became clear that the wind moves towards the remaining space between the wafer and the wind tunnel, resulting in an area above the wafer where the wind speed approaches zero.

Also, in these plots it became clear that the largest differences of the flow of the different models is present below the wafer. Since this thesis will focus on the deposition on the top of the wafer, a laminar model will be used to limit computational time in the next tests. The wind speed of 0.4 m/s has thus been modelled extensively, but what happens at slower and higher velocities?

To test what effect the wind speed has on the number of particles, a uniformly distributed number of particles were released from the top of the wind tunnel. The inlet thus releases 10000 particles in a matrix like configuration. To put this in other words, the 10000 particles are spread evenly over the entire top of the simulation, causing particles to be found everywhere in the flow. After the simulation has ended, the simulation will tell us how many of these 10000 particles have ended up on the wafer. Knowing that the particles also have a distribution in size, different sizes will be simulated. An overview of the results can be found in table 2, where the wind speed and the particle size is varied, but the amount of falling particles (10000) is kept constant. In this table, it can be seen that the largest differences happen at the beginning, for example when increasing the wind from 0.1 to 0.2 m/s. However, the effect seems to slow down, meaning a smaller difference for the amount of deposited particles can be found between 0.5 m/s and 0.6 m/s. Meaning that the number of particles depositing is exponentially related to the wind speed. At very high wind speeds, an even faster wind speed will not ensure fewer particles depositing on the wafer.

Wind speed m/s	50 μm particles	40 μm particles	30 μm particles	20 μm particles	10 μm particles
0.0	3785	3785	3785	3785	3785
0.1	2639	2233	1706	1033	337
0.2	2105	1655	1153	619	195
0.3	1800	1342	880	460	157
0.4	1611	1158	727	376	143
0.5	1488	1044	636	330	138
0.6	1415	957	577	303	136

Table 2: *Table with different particle sizes and different wind speeds. At faster wind speeds, particle deposition rates for all particles has decreased.*

So, the differences in streamlines between the models are primarily visible at the bottom of the wafer, which is not the focus point of this research. Now that the discussion about the flows has been done, it is time to look at the contribution of charge in these models.

4.4 Vertical and horizontal model with electric field

The final goal of this research is to see if the electrostatic force has an effect on particles and if yes, how to use this to the advantage of the AWH. One possible solution for the horizontal wind tunnel is to try and pull the particles up and away from the wafer (remembering that the top part of the wafer is most important to protect.) This will strengthen the effect of the boundary layer, and thus less particle will deposit on the top of the wafer. One might think that for the vertical wind tunnel, this effect should not matter. Displacing the particles from left to right or vice versa might result in the particles getting more centered. Particles in the center of the wafer are most likely to become contamination on the wafer. When the particle is flying in the center of the wafer, it has to travel 15 cm horizontally in order to evade the wafer, which is a long distance especially when the contaminant is large and thus has a large gravitational component. However, the situation in the atmospheric wafer is more complicated. Contaminants might enter through the openings of the AWH or due to the moving parts of the atmospheric wafer handler (see figure 2), and these locations are known. But particles might also be released by previously contaminated wafers or from the chamber walls, and these locations are more uncertain. However, the wafer will be present on some locations longer than other locations. The fact that the origin of particles can be partly predicted and the position of the wafer is known, one can use this to strategically place the plates which exert the electrostatic force. Finally, when the plates are based on capacitors, they can even be switched on and off based on the position of the wafer in the atmospheric wafer handler. Concluding: having an electric field positioned on the right spot can be beneficial for both setups. Let us start by looking at the charge of the particles and how they influence static charge.

The theory suggests that small particles will receive a lower total charge compared to larger particles. This is because the particle diameter ($\propto r_p$) is directly related to the amount of electric charge an object can hold ($\propto r_p^2$).This however does not mean that because larger particles have a larger charge, they also move the largest distance due to the electric field. The larger particle also has a larger gravitational component ($\propto r_p^3$) which means that this particle will not be in the field for a long time. Since the gravitational force has the largest dependence, this force is expected to be relatively more dominant than the electric force while falling. This means that the smaller particles will be easier to redirect. Furthermore, since the drag force and the electrostatic force are in balance quickly (knowing that the terminal velocity of such particles is low, as shown in equation 22), the trajectory of the particle will be linear. This is confirmed in both the analytical and the FEM model.

However, knowing all this is not enough to calculate the displaced particle distance in the vertical or horizontal setup. One important variable is missing, namely the charge of the particle. As explained in chapter 2.2.2, size, material and even humidity can play a role on the charge of these particles. Our experiments must determine this charge first, before knowing what the input value of the charge will be for different sizes of particles.

4.5 Ionizer model

In chapter 2.2.3, the theory of the ionizer has been discussed. That knowledge is put to use when making a FEM model of the ionizer which is as close to the one in use. This chapter will talk about outcomes of these simulations, as well as difficulties regarding the multi-physics and mesh sizes.

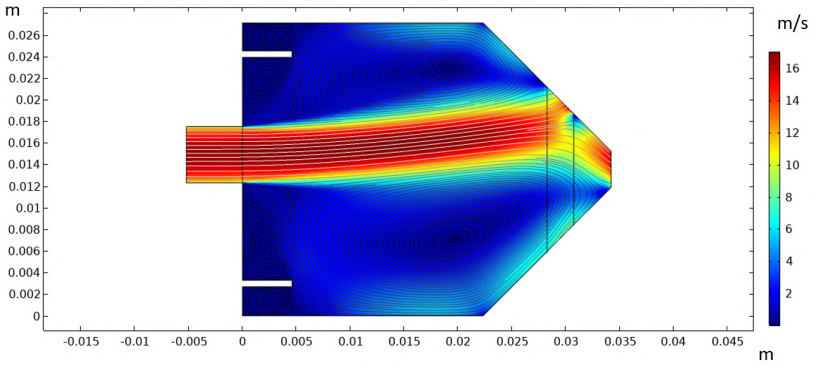

Figure 28: *The 2D flow profile of the ionizer where the electrodes are on the left side of the ionizer.*

The ionizer model will consist of several physical components working together. These components are a 1) a turbulent flow, 2) two electrodes (which are also called emitter points and are visible as notches in figure 28) generating an electric field and therefore generating a space charge and 3) a particle tracing study. The flow of the ionizer enters the ionizer with a diameter of 5 mm, and exits the ionizer with a diameter of 3 mm. This means that the flow will not only speed up, but also create vortexes in the ionisation compartment due to its geometry. The ionizer dimensions are modelled and only the flow is simulated in figure 28 (no other forces taken into account). This figure shows how close the electrodes are to the wall of the ionizer. The flow near the walls is always slower, resulting in a slow flow near the electrodes. The effect of the flow and the realistic flow profile can not be studied, since the cap of the ionizer blocks the view and does not allow any measuring probe. Therefore, no conclusion can be drawn if the slower flow is advantageous (more time for the neutral air molecules to become ions) or disadvantageous (not enough force to push the ions away/lower supply of molecules).

One can also model the electric field for this situation without flow. Since the electric field becomes strongest at the edges, the zoomed in version of the top electrode is visible in figure 29 (this model only converged because no flow has been modelled). In this model, the ground was assumed to be the bottom emitter only (since the rest of the ionizer is made of dielectric material). The reason why the electric field is biggest at the edges is because of the high charge density. To give an example, the top electrode visible in figure

29 was positively charged over the entire area with 3 kV. The charges in the material want to repel each other. Two charges that are present on the flat surface can therefore repel each other with their forces being parallel to the surface. All charges on the flat surface will be evenly spaced, since they feel the same even repellent force (this is why a sphere can be perfectly evenly charged). Now when coming closer to the edges of the electrode, the charges do not only experience a force which is parallel to the surface, but also a force which is perpendicular to the surface. Since the emitter points have very sharp edges (as seen in figure 29, which is a zoomed in emitter point), the parallel force will decrease most in the vicinity of the edge of the cylinder. This parallel force was responsible for moving the electrons away, so more electrons can be near each other since the repellent force becomes smaller. An example of the repellent forces is also shown in figure 29.

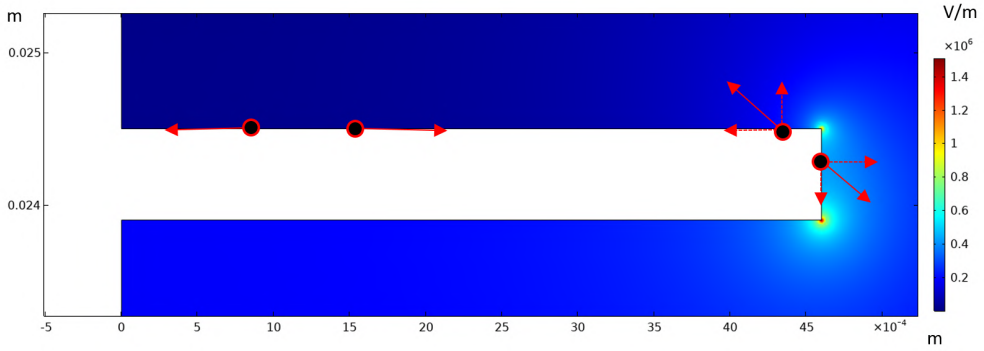

Figure 29: *A simulation on the electric field generated by the electrode in the ionizer with no flow present. The electrode drawn here is the top electrode, and the bottom electrode is considered grounded, resulting in the highest field being present on the bottom sharp edge of the electrode.*

It can be seen how space charge is influenced in figure 30a and 30b due to the speed of the flow. More theory about space charge and what it entails can be found in chapter 2.3.2. The space charge is higher for higher flows, since more new molecules are available for the charge to distribute to. Also, the flow has an effect on the contour of the space charge. At low flows, the charge simply moves towards the grounded plates at the top and bottom. For faster flows however, this is not the case. Ions produced in front of the ionizer will be repelled by the electrode, but the flow is pointed towards the electrode. This means that the ions will stay there for a short period of time. In this time, at high flows, new molecules will be blown towards these ions and also ionize, giving the effect of a high space charge in front of the electrode. This continues until the flow force is bigger than the repelled force from the electrode. At the back of the electrode, ions can also be created. However since the flow and repel force of the electrode are now in the same direction, ions will quickly redistribute someplace else, meaning no space charge is created after the electrode. The space charge is governed by the following set of equations shown in 43, which also shows that the wind speed has a positive effect on the space charge J. Here, b is the mobility of negative or positive ions. [91]

$$\begin{aligned} \nabla \cdot E &= -\rho/\varepsilon \\ \nabla \cdot J &= 0 \\ J &= \rho \cdot (bE + U) \end{aligned} \tag{43}$$

What is known about the flow however is that FEM needs a reasonable flow over the electrodes to make the solution converge (larger than 1 m/s has a converging solution). This is why figure 28 only displays the flow: If the electrodes were to be turned on, a solution to the model could not be found. To still study the effects of the ionizer, the decision was made to stretch out the dimensions of the ionizer (more room for the flow to converge) and remove the inlet tube to make a flow inlet which spans the whole width (to get a decent flow over the electrodes). This model again was hard to converge, and it only did converge at certain flow speeds, geometries and electrode potentials. The model also had difficulties when the test particles (or molecules) came in the vicinities of the electrode. The result of the simulation can be seen in figure 31a and 31b. This model basically resembles an electrostatic precipitator, with only one electrode. Figure 31b also shows a

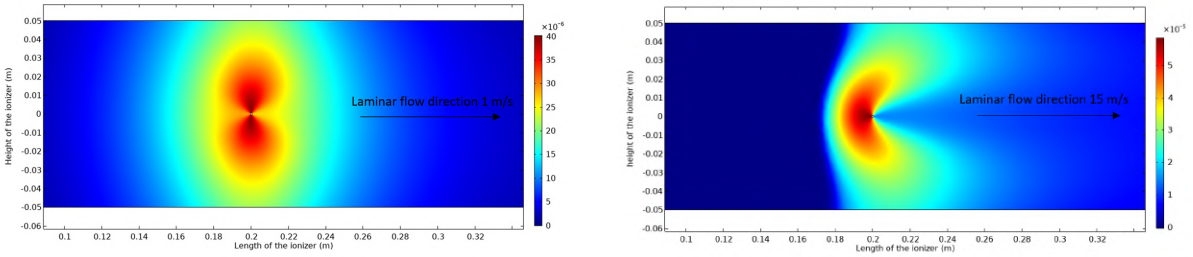

(a) The space charge profile in a 1 m/s laminar flow *(b) The space charge profile in a 15 m/s laminar flow*

Figure 30: *The space charge differences in laminar flows of different velocities with a 20 kV electrode.*

simulation where molecules of 0.15 nm are inserted in the device in a flow of 20 m/s. This is done to see what charge these molecules collect, how many molecules collect a certain amount of charge and how many molecules do not make it to the outlet of the device. Also, different sizes of air molecules can be simulated here. Although an ion does not have a fixed boundary, the ionic radius does assume a hard sphere model. In figure 31b the size of the molecule is 0.15 nm, which is the ionic radius of negative nitrogen. Other ions such as oxygen will have approximately the same ionic radius. Finally, it has to be stressed that this simulation does not give an exact answer to the degree of ionisation by the ionizer used in the experiments. It does give a good idea of how electrodes function and how they affect neutral particles/molecules.

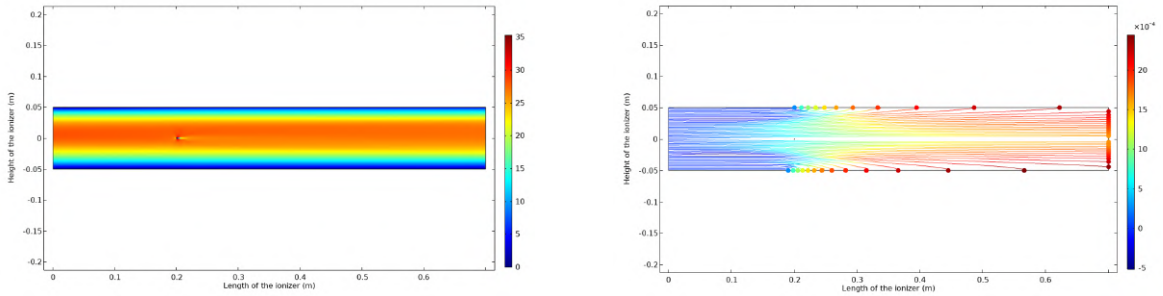

(a) The flow profile of the simplified ionizer at 20 m/s *(b) Charge of 0.15 nm molecules*

Figure 31: *The flow and particle trajectory of a tube with laminar flow and one electrode of 20 kV. The charge of 0.15 nm molecule is measured in elementary units in a flow of 20 m/s.*

The simulations also gave some other interesting results, which are listed below.

1. The space charge deforms at faster flows for positive applied potentials. If the flow is faster, slightly more ions will be present in front of the electrode [92]. However, the faster flow will also decrease the time for molecules to accumulate charge, meaning that in the end, the amount of charge on molecules will be less [93].
2. A turbulent flow with the same wind velocity has a higher velocity near the boundaries, causing faster movement of the molecules near the walls and therefore less molecule charging. This means more molecules will be present at the outlet.
3. A higher electrode potential causes a higher charge on molecules, so also more molecules being lost that collide with the wall.
4. A higher velocity will cause a larger space charge, but since molecules spend less time near the electrode, the charge of the molecules will decrease with increasing flow. Also, at very high velocities, the space charge will not stretch the entire height, resulting in uncharged molecules at the top and bottom of the channel.

5. The smaller the molecules or molecules, the higher the amount of charge gained due to diffusion. This was already seen in previous chapter (figure 12) and again confirmed in this simulation.
6. The ionizer as seen in figure 28 uses a very slow velocity near the electrodes. A molecule with the same charge as the electrode will be easily repelled towards the main flow, a molecule with the opposite charge easily attracted.

4.6 Summary of the simulations

The horizontal wind tunnel can be both computed with an analytical or FEM model. The FEM model however takes into account the boundary layer which develops, and this causes significant changes in particle trajectory. This is why using FEM simulations are better. Different flow models can be chosen from these FEM simulations. It has been shown that near the walls, the laminar model, $\kappa - \epsilon$ model and SST turbulence model differ. This however does not make a large difference, as the particle will mainly travel through the center of the flow, which is almost equal in all simulations.

For the vertical model, the flow is significantly different at the bottom of the wafer. More turbulence causes turbulence models to give better predictions in these areas. Again, this does not really matter, since the focus of the thesis is on the top side of the wafer. Also, the flow of the wind tunnel only matters for particle deposition if the particles are large (>10 µm). For smaller particles, a faster flow than 0.4 m/s does not prevent contamination very effectively anymore.

The simulations with electric fields have shown that particles deviate in a linear manner, because the drag force and electric force are in balance. It has also been shown that smaller particles deviate more because of their mass scales with r^3, while their charging capability scales with r^2. This is both confirmed in the analytical and FEM model.

Finally, the ionizer and space charge are modeled using the FEM model. Different mechanisms of ion generation were found for negative and positive fields. It has been shown that high electric fields are created through the redistribution of charge on the emitter points. Also, space charge can be able to charge particles and make them deviate, as is done in an electrostatic precipitator. This effect might not be large enough in the experimental setup of this thesis, but will be kept as a possible charging mechanism until proven otherwise.

5 Experimental measurements

The result section will explore many different combinations regarding particles, wafers and plates with and without electric fields and even inlets and ionizers are tested to see the effect on particles. To clarify the chapters and the route taken to explore all these possibilities, the tree graph in figure 32 can be used.

First, the results of the horizontal wind tunnel will be discussed. Chapter 5.1 will discuss the clumping behavior and the boundary layer for both glass and copper particles. When the effect of the flow and the configuration of particles are known, chapters 5.2 and 5.3 discuss the behavior of glass and copper particles in the wind tunnel.

Secondly, the vertical wind tunnel will be investigated. Again, in chapter 5.4 the effect of the flow and the spread of the particles due to the inlet will provide an idea to the reader of how the vertical wind tunnel configuration looks and how results are interpreted. Chapters 5.5 and 5.6 will show the results for the electric field for glass and copper particles. Next, the ionizer will be tested using two methods to try and neutralize surfaces and particles if charge on that specific surface is not wanted. Chapter 5.7 and 5.8 will discuss these neutralization methods.

Finally, some extra measurements in the vertical wind tunnel were executed. The first experiment in chapter 5.9 used temperature to visualise how much effect particles deviate if the wafers would not be cooled. In chapter 5.10, an alternate method is used to visualise the deviation of particles. The laser measurements are used on several positions to provide a sense of the particles trajectory.

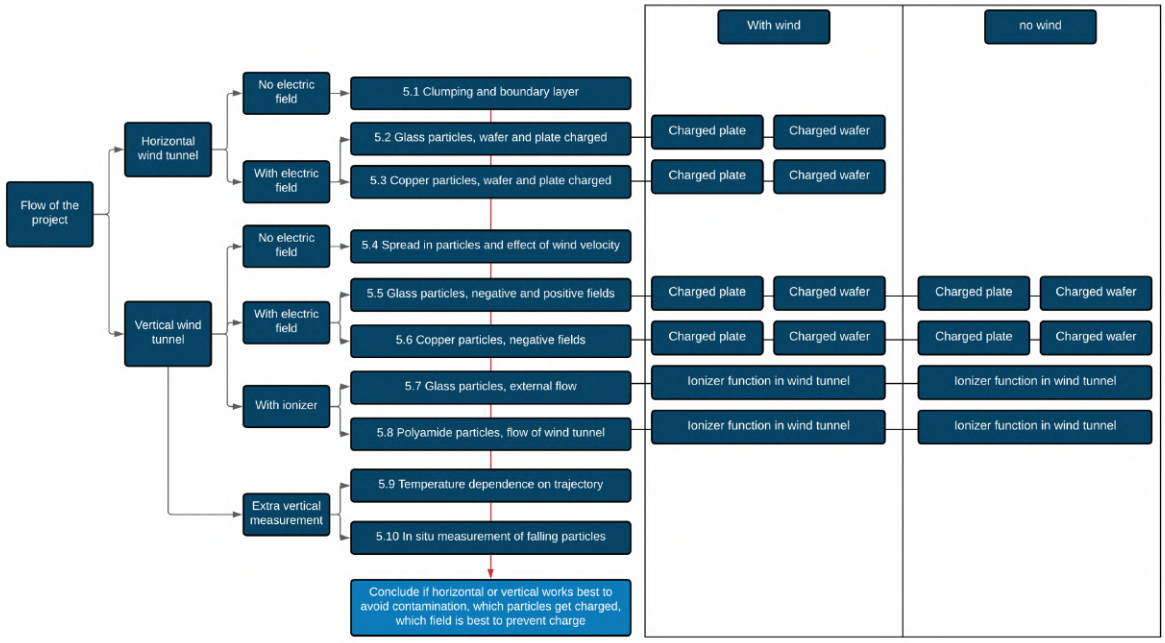

Figure 32: *The workflow of the result chapter. First the horizontal wind tunnel will be discussed, after which the vertical wind tunnel and extra measurements will be discussed.*

The goal of the result section is to provide a basis to answer the research question: "How can the particle trajectories be controlled using static electricity in horizontal and vertical wind flows." Each chapter will start with a short description of the chapter, then the results are discussed and finally a short conclusion or summary is provided. The discussion will provide an overview of these results.

5.1 Horizontal wind tunnel and without electric fields

In this chapter, the result of the particles in the horizontal wind tunnel will be discussed without an electric field. The goal of this chapter is to visualise how these particles behave without an electric field, to make the comparison with a field easier in chapters 5.2 and 5.3. One of the most important results of this chapter is the clumping of particles. This can influence the measurements done by the particles counter.

5.1.1 Trajectory of glass particles

The horizontal setup enables us to do more calibration measurements while already gathering initial results and draw conclusions. This is because the trajectory of these particles can be precisely calculated using COMSOL (as can be seen in figure 25b). This chapter will therefore focus on the results gathered in the horizontal wind tunnel without electric field, how they should be interpreted and how the data is processed. The results will be left as a discussion in chapter 6.

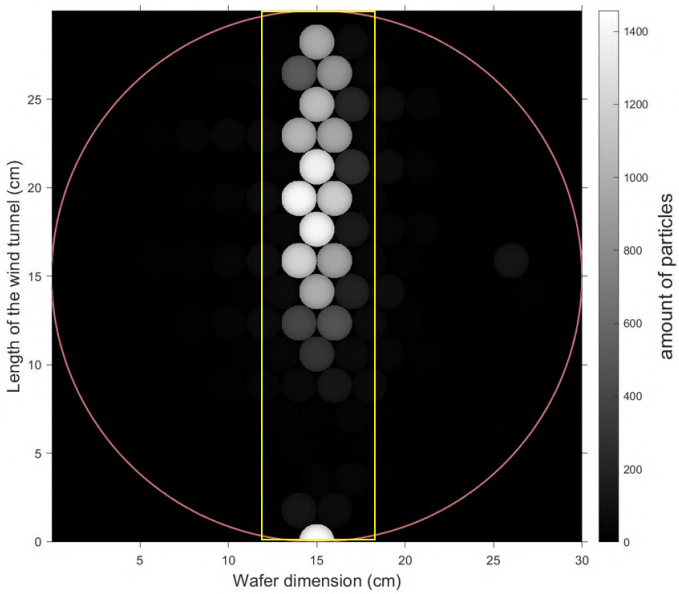

Figure 33: *The number of particles deposited after 20 shakes in the horizontal wind tunnel. The inlet of the particles is taken to be zero, so the front of the wafer is placed directly under the inlet.*

First, let us discuss what the results look like after the particle counter has sucked most of the particles of the wafer. The setup of the particle counter is already described in chapter 3. The particle counter outputs 197 data point which are plotted on the y and x axis as white dots. These dots vary in intensity to visualise the difference in particle count. The brightest rounds visualise the greatest number of particles being present at that certain distance in the wind tunnel (displayed on the y axis as length L). To clarify, in figure 33 the wafer is placed directly under the inlet of particles, which means that the first particles have landed after travelling 10 cm in the wind tunnel. The very first dot (at coordinate [15,0]) is present because the inlet needs to be fixed to the setup, meaning some particles are released during that process. However, the wind is still turned off during the instalment of the inlet, resulting in particles falling straight down and landing at a travelled length of 0 cm. Lastly and very important to point out is the legend on the right of the figure. This legend visualises how many particles are present displayed by the brightest dot, which in figure 33 is 1450 particles.

Furthermore, some other minor things to mention in figure 33 is that the x coordinate of the wafer is placed exactly in the middle in the wind tunnel. This is the reason why the particles are nicely aligned in a vertical line. The red circle gives the dimension of the wafer, which is 30 cm. Finally, the yellow rectangle visualises the interpretation of the data. Since this is the region of interest, these data points will be collected and

linked to the correct travelled length. This means that the data outside the yellow square is often not taken into account in the horizontal measurements unless otherwise stated.

The measurements in the wind tunnel were taken every 15 cm. With the wafer being 30 cm wide, this means that every position was measured multiple times. The raw data of particles that are larger than 5 µm is plotted in figure 34a. 4 Measurements were done, and these are visible by separate colors in figure 34a. There is clearly an increase visible in the number of particles and that the maximum number of particles land after traveling approximately 15 to 20 cm. Also noticeable are the jumps up and down in the data. (especially noticeable in measurement 2, black line, between 30 and 60 cm). This is an artefact of the particle plotter. As can be seen in figure 33, some areas receive two measurements of high particle count, where the next area only receives one high particle count measurement. Since the particle counter has more time to collect particles above the positions with two measurements, it is logical that more particles can be found at this position. Finally, it can also be seen that there are always particles larger than 5 µm depositing on the wafer, even until the very last position at 150 cm. The graph shows a decline of the number of particles deposited on the wafer when the distance grows. To conclude, figure 34a gives the number of particles larger than 5 µm which deposit in the horizontal wind tunnel after a certain distance. This distance can be linked with the size of the particle, as will be discussed in the upcoming sub-chapters. Also, this graph gives the fundamental measurement on which most of the understanding of the horizontal wind tunnel will be based.

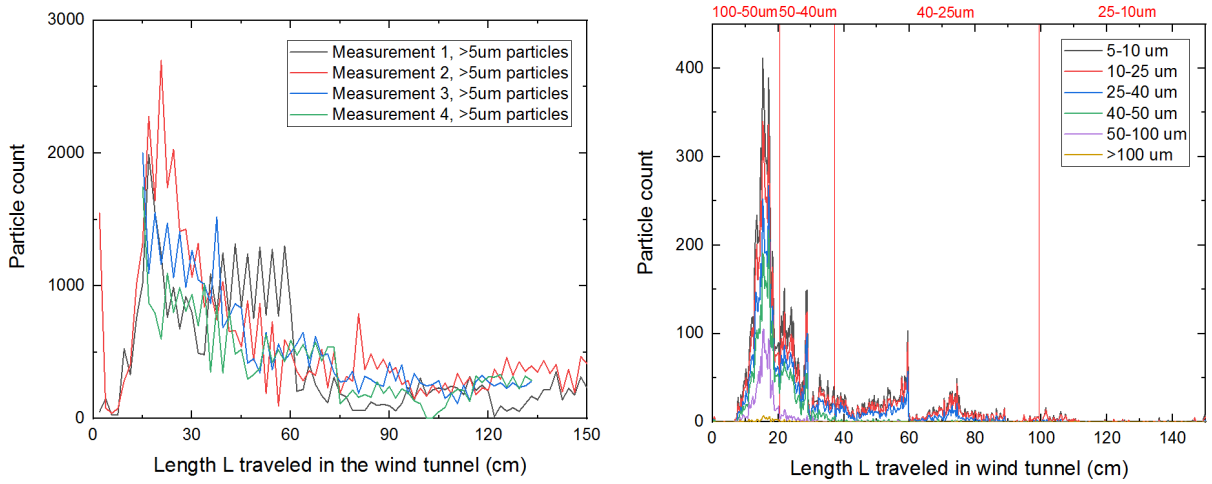

(a) 4 measurements 1100 counter

(b) 1 measurement boulder counter

Figure 34: *Left) the raw data of the horizontal wind tunnel, where the particle count versus the travelled length is visualised. 4 measurements are done with only the largest bin >5 µm visualised. Right) the boulder counter with bins ranging from 5 µm till >100 µm, all bins visualised.*

As the models in chapter 4.2 suggest, the first particles of 44 µm should land after traveling approximately 25 cm in the wind tunnel. The supplier of the particles stated that 44 µm was the maximum size of these particles, but there is already a sharp increase before the 25 cm, as can be seen in figure 34a. The particle size therefore needs to be examined using another particle counter with larger bins, called a boulder counter. The result of the boulder counter can be seen in 34b. It can be seen that the graph has approximately the same peak around 20 cm but is also much more accurate. This is due to the measurement method, as explained in chapter 3.3.5.

Let us explore figure 34b a bit more. First of all, it is noticeable that the bins are active in the correct expected places, marked by the red vertical line. The 100-50 µm bin should only count particles in the first 20 cm of the wind tunnel, which is also what can be seen in figure 34b by the purple line. The green line of 40-50 µm should then take over, and only be active in between 20 and 37 cm. This is indeed the case, since after 37 cm, the line largely disappears. However, it can also be seen that this green line is also active in the first 20 cm of the graph. This is due to clustering of large particles, explained and calculated in chapter 5.1.4. The smaller particles and their clumping is examined in chapter 5.1.3. To draw the red vertical lines

in plot 34b, COMSOL simulations were used. The result of all particle sizes is visible in the appendix in figure 80. As a final note, for the charging of these non-spherical clusters, the results can be extrapolated towards non-spherical particles within a reasonable range. [94]

So to conclude, the particles trajectory and the particle counters do measure the particles in a precise enough manner to determine the maximum trajectory of a large particle. In these experiments, the wafer was moved 30 cm each time. To make sure this position does not matter for the particle count, the effect of the boundary layer must be measured. This will be done in chapter 5.1.2.

5.1.2 Boundary layer effect on different positions

It is important to know that the position of the wafer does not alter the particle trajectories. This chapter will explain more on whether or not the formation of the boundary layer has an effect on the deposition of particles on the wafer.

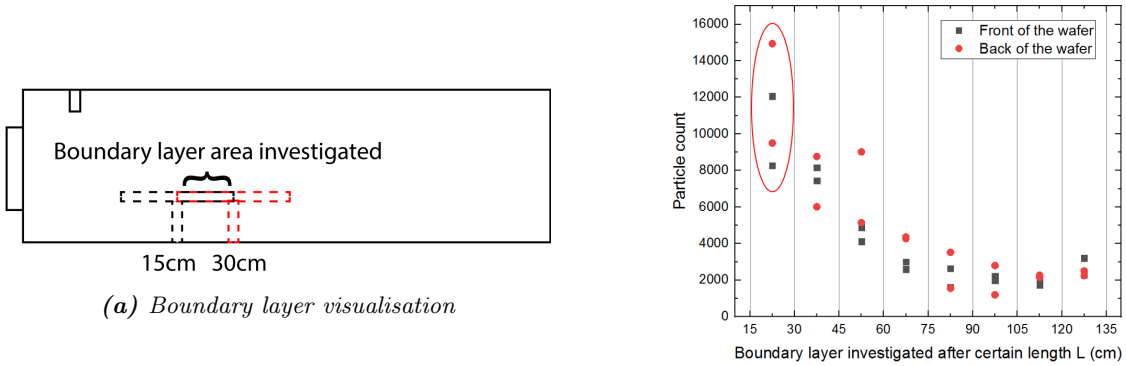

(a) Boundary layer visualisation

(b) Boundary layer measurements

Figure 35: *Left) a schematic drawing of the measurement. Right) the experimental results with an exponential fit through two sets of measurements.*

The boundary effect is visible during simulations. Particles get translated and travel farther due to the boundary layer. However it is not directly visible from the raw data. This is why the wafer is divided into two parts for the next figures (35a and 35b) into a front 15 cm and back 15 cm of the wafer, both on top of the wafer. The front is facing the inlet, and the back is facing the outlet of the wind tunnel. Of these two parts, all particles larger than 5 µm are summed. A visualisation is made in figure 35a. If the boundary layer has no effect on the particles, one would expect that the same number of particles land on the red and black wafer overlap region (noted by boundary layer investigated). The results of these overlap regions are plotted in figure 35b. The red circled area is the overlap area visualised in figure 35a, to make it extra clear which area is meant (so if the data points are between 15 and 30, the overlap is meant when the center of the wafer was at 15 and 30 cm from the particle inlet).

Furthermore, the boulder counter also proves that the development of the boundary layer is not a noticeable effect. The horizontal wind tunnel results as displayed in 34b are is good agreement with the model, which states that the boundary layer does lift particles up and moves them ferther away in the wind tunnel, but it also states that where the boundary layer exactly begins does not matter (at least for the dimensions of the wafer that are discussed in this thesis). It should therefore not matter for the number of particles depositing on the front and the back of the wafer if they are in the same position. An error analysis of figure 35b can be found in appendix N.3.

To conclude, the position of the wafer was determined to be insignificant for the trajectory of the particles. So, the particles that do land sooner than expected do not exert this behavior due to the position of the wafer and the boundary layer. The reason why some particles land on different positions then expected, is discussed in chapters 5.1.3 and 5.1.4.

5.1.3 Clumping of small glass particles

In the COMSOL FEM model, it was expected that only the larger particles make it to the wafer, however one can also see an increase of the smallest particles. The sizes of particles plotted in figure 36 are 0.1-0.15 µm, 0.2-0.25 µm, 0.5-1 µm and again >5 µm. In figure 36 it is noticeable that almost every >5 µm peak is also visible in the 0.1-0.15 µm line. Furthermore, more smaller particles are visible compared to big particles which might be counter intuitive (since smaller particles are harder to remove). Finally, the amount of small particles increases further down the wind tunnel (visible in both the red and black line in figure 36).

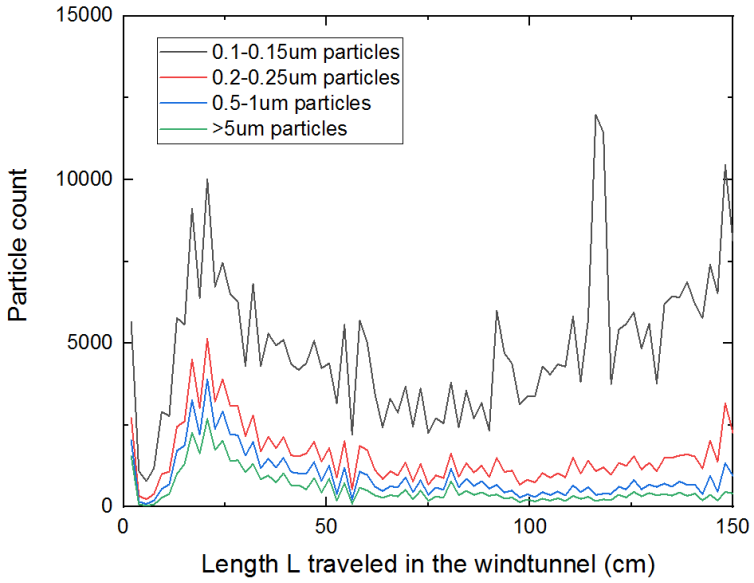

Figure 36: *The raw data of the horizontal wind tunnel, where different sizes of particles at different travelled lengths are visualised. (error analysis in N.3)*

To gain more knowledge about clumping, measurements are done using the electron microscope. The technique and working principal is shortly explained in chapter 3. The results of the electron microscope are visible in figure 37a. In this figure it is visible that the glass beads are not always smaller than 44 µm in diameter, which is an important finding. The particle visible in figure 37a is found after traveling 18 cm in the wind-tunnel. Given that a particle of 54 µm travels a distance of 18.5 cm in the COMSOL FEM model, these are in great agreement. This thus explains the particles found before 25 cm in figure 34a and also confirms that the initial velocity of the particles can be neglected (as already predicted by formula 22).

This is not the only thing which can concluded from this figure. Also noticeable are the clearly spherical particles which stick to this larger glass bead. A particle of 5.4 µm and 1 µm where identified, but there are clearly more even smaller particles present. This is most visible by the bright dots in the middle of the particle or the roughness at the edges of the particle. The observation that particles stick to particles is also important to explain figure 36. As already stated, the peaks at the >5 µm line are also visible in the 0.1-0.15 µm line, which makes sense considering that particles stick to each other. To each 54 µm particle, tens of really small particles of 0.1 µm might stick. Since they are counted separately in the particle counter, this explains why more >5 µm particles also means more 0.1 µm particles.

The size of the particle is not the only thing that can be measured in the electron microscope. It also has the option to measure what element is present on the surface. Take figure 37b for example, where several spots where examined. First spot 1 in the middle of the glass bead. No visible spots can be seen on the wafer, and this is reflected in the analysis of the elementally composition. Spot 1 primarily consists of silicon, which is the primary element in the glass bead. Spot 2 however has high traces of calcium and iron (in combination with silicon). Spot 3 is again put on a bright spot on the bead and also shows a higher concentration of

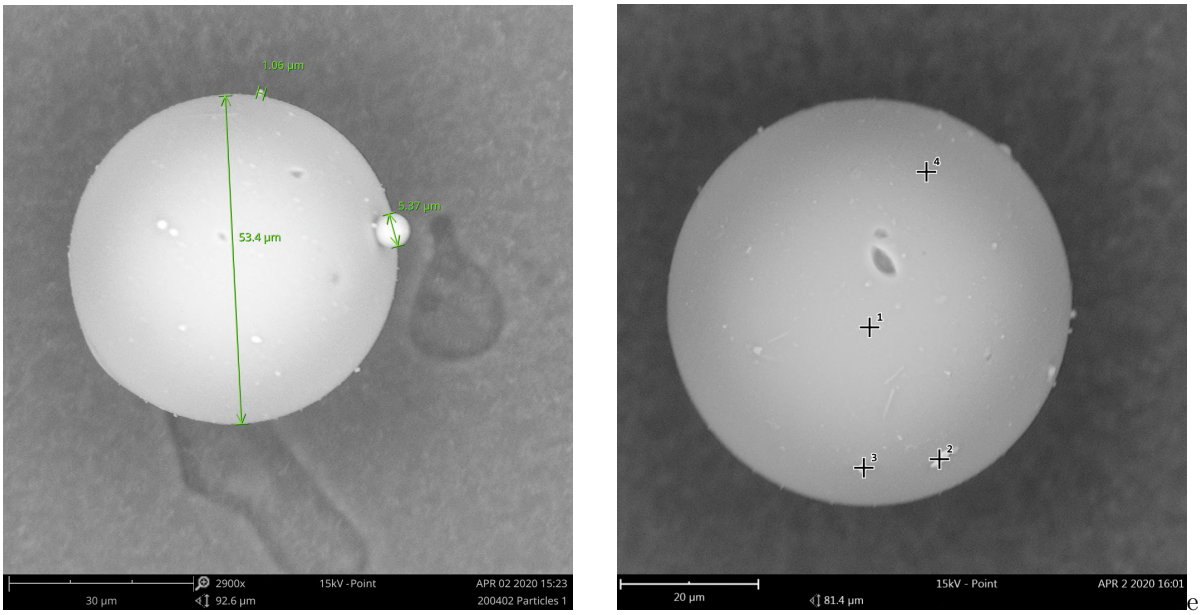

(a) Size visualisation *(b) Element investigation*

Figure 37: *The image retrieved from the electron microscope, showing the particles deposited after 18 cm in the wind tunnel. Left) clearly shows the sizes and particle-particle interaction. Right) shows 4 points of which the elemental composition was investigated.*

calcium, similar to spot 2. Spot 2,3 and 4 all have a higher oxygen concentration compared to spot 1 which is in the middle of the glass bead.

The calcium spot on the particle can be explained using plastics. The glass particles are kept in a plastic bag and more importantly, the syringe used in the particle shaker are both made out of plastics. Calcium carbonate ($CaCO_3$) is one of the most popular materials in plastics, used to give the plastic strength and the surface a nicer finish. Since this material is used at the surface of the plastic and the syringe is heavily interacting with the glass particles, it is not surprising that some of the material may deposit on the glass bead. This might also be a reason why more oxide is found at these locations. The iron found in spot 2 is harder to explain. Since glass beads sometimes contain iron, it could be a small contaminant on the glass bead due to production.

So, using the Solair 1100, it was discovered that smaller particles clump to larger particles and that these particles also have traces of plastic material on the particles. The amount of smaller particles is almost identical to the larger particles with a certain factor of multiplication, as seen in figure 36. Now, the glass particles are larger than 5 µm, which is why the clumping or larger particles using the boulder counter will be investigated in chapter 5.1.4.

5.1.4 Clumping of large glass particles

Let us refer back to figure 34b. In this figure, it was seen that the particles are indeed present in their own bin. Particles of 100-50 µm do not travel further than theoretically expected, and the same goes for the 50-40 µm and 40-25 µm bin. However, it can be seen that the particles ranging from 50 to 5 µm are also present in the first 20 cm. This can be explained using the ratios of particles and the clustering of particles, as will be explained in the rest of this chapter.

The ratios of particles sizes landing on one spot will also tell us something about how likely it is for a particle to stick to another particle. That is shown in table 1 from the 20 shakes measurement. Since not all particles will stick to other particles, it is likely that this ratio will increase. This is because a lot of the 5-10 µm particles will disappear and fly out of the wind tunnel, since the only particles counted in

the experiments are stuck to the larger particles (for every 50-100 µm particles, there will be less 5-10 µm particles). First, graph 34b is split up in different segments displayed by the red line. For each segment, the ratio is determined, taking the 5-10 µm bin as a reference. The distances and the corresponding ratios are visible in table 3. Indeed, the ratios have increased from the reference measurement. Take for example the 0-20 cm travelled length, which has the most counts of the 5-10 µm bin compared to the remainder of the measurements at 20-150 cm. It can be seen that the amount of 50-100 µm particles has been quadrupled compared to the reference 20 shakes 50-100 µm measurement (0.22/0.05=4.4) in the first 20 cm of the wind tunnel. Furthermore, it can be seen that the smallest ratio increases as the travelled length increases, which is logical as well. For larger particles there is more room for smaller particles to attach to. For 50-100 µm diameter particles, five 5-10 µm particles are stuck on average. For 40-50 µm diameter particles, two and half 5-10 µm particles are stuck on average. For 25-40 µm diameter particles, two 5-10 µm particles are stuck on average. Since there is no definite information about the reference measurement and particles being stuck in this measurement, it is hard to state any certain percentages of particles disappearing.

Particle diameter (µm)	20 shakes	0-20 cm	20-37 cm	37-99 cm	99-150 cm
5-10	1	1	1	1	1
10-25	0.75	0.84	0.83	0.88	0.84
25-40	0.37	0.63	0.63	0.49	too small
40-50	0.18	0.49	0.41	too small	too small
50-100	0.05	0.22	too small	too small	too small
>100	0.003	too small	too small	too small	too small

Table 3: *The different ratios of each segment in the horizontal wind tunnel, where the cm corresponds to the travelled length L in the wind tunnel*

To conclude, the ratios of particles increases for smaller particles at larger distances. This is logical, since a longer traveled distance means lighter particles, thus more 5-10 µm particles relatively. This chapter has shown that the primary effects seen are that of the larger particles. The fact that the effect of smaller particles might be covered by the effect of larger particles must be remembered in future experiments with electric fields.

5.1.5 Trajectory of copper particles

Since the effect of electric fields on conductive particles will also be tested in the horizontal wind tunnel, it is necessary to also investigate the trajectory of these particles without field. This chapter will give these results for the copper particles.

For copper particles, the measurement in the horizontal wind tunnel needs to be repeated. One can simulate how far particles of a certain diameter travel in the wind tunnel (as was also done with the glass particles in figure 80). This will determine the size of the particles which deposit on a certain distance from the inlet. A graph of the travelled length measurement can be seen in figure 38a. As can be seen in this graph, there are a lot of large clusters landing near the inlet of the wind tunnel.

These particles were specifically chosen for their smaller diameter (in comparison to the glass particles), and even at the end of the wind tunnel (at 150 cm) the particle clumps are still 9.5 µm in diameter (assuming a solid sphere and assuming the same mass). To research smaller particles easier, it was chosen to lift the stage of the wafer to 22 cm (from 15 cm in all previous experiments) to decrease the height particles have to fall in order to examine the smallest particles. Changing this vertical distance results in copper particles clumps of 8.2 µm till 6.7 µm being examined. An example of this result is shown in figure 38b, where the bin size of 1 till 5 µm is plotted. This bin size was chosen because it had the most counts. Again, the particles that landed on the wafer are clumps, and thus exist of multiple particles (for example 5 particles of 5 µm and 20 particles of 1 µm clumping together)

To conclude, copper particles also clump together, and these large clusters are expected to land in the beginning of the wind tunnel. More information about the clumping of copper particles will be discussed in chapter 5.1.6. The stage of the wafer can be put at a certain height to focus on small particles only, which

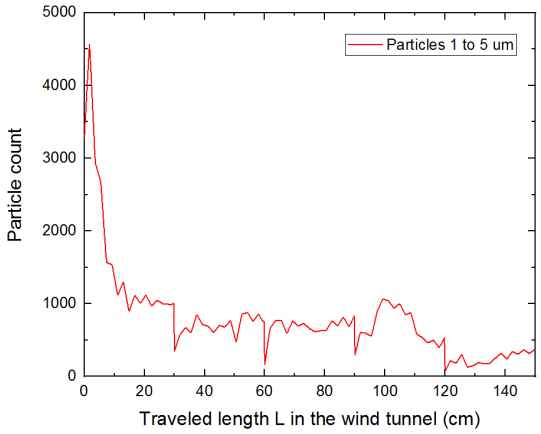

(a) Particles through wind tunnel

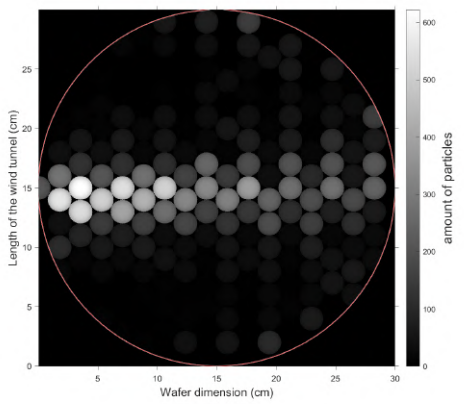

(b) Particles ranging 1-5 µm

Figure 38: *SEM image of the copper particles to investigate their clumping behavior and size distribution. The scale of both images is the same for easier comparison.*

makes these particles certainly not useless. These smaller clumps of particles will then be used in future experiments with the electric fields.

5.1.6 Clumping of copper particles

As previously done in chapter 3.2.3 and 5.1, it is important to get familiar with the particle shaker and the particles which are used in the upcoming experiments. As a first step, the particle counter was used to calculate the average number of particles over a series of 5 measurements. For all copper experiments, particle sizes of 1 to 5 µm are analysed.

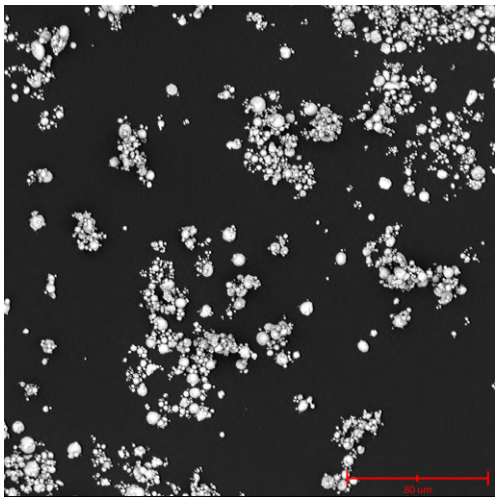

(a) SEM of all particles

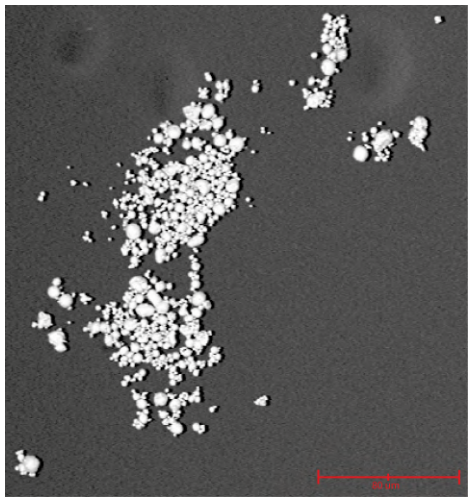

(b) SEM of clumped particles

Figure 39: *SEM image of the copper particles to investigate their clumping behavior and size distribution. The scale of both images is the same for easier comparison.*

The average number of particles released from 20 shakes is 31413 ± 4022 (this calibration was executed by directly dropping 20 shakes of particles on the wafer). Furthermore, electron microscopy images were also taken of the copper particles. This result can be seen in figure 39a. The largest particles as seen on this image are 5 to 6 µm and consist of 100 percent copper, as shown by element analysis in the SEM. Noticeable

from this image is that particles clump even closer together when possible, with more particles of the similar sizes sticking together. This can be explained by Van der Waals forces and capillary forces, which become of bigger influence due to the decreasing diameter (see chapter 2.3.5). For the experiments it is important to use a small inlet opening to prevent a lot of clumping. Furthermore, it is noticeable that more particles have an irregular shape (instead of spherical). This will however only have a minor effect on the accuracy of experiments in the wind tunnel.

To conclude, copper particles also clump together, as was expected from figure 38a. The clumps which were found are calculated to have a certain mass, and this mass coincides with the expected mass of the particle at that position. Again it is confirmed in figure 39a that individual particles are also present.

5.2 Horizontal wind tunnel, with electric fields and glass particles

In the horizontal wind tunnel an electric field might also help with the prevention of contamination. When adding a force upwards (against gravity), it might be possible to hold the contamination in the boundary layer for long enough to pass over the wafer. This will be really hard to do at the start of our horizontal wind tunnel. In the first meter, very heavy particles have the upper hand. Gravity will be a larger force than the electrical charging from the particles. This is why this chapter will only discuss the effect of an electric field at a position in the wind tunnel where smaller particles deposit. The goal of this chapter is to see if electric fields of the opposite polarity have the expected results, and if in this way, contamination can be decreased.

The charged PVC plate is stuck to the top of the wind tunnel to prevent boundary formation from this plate. The plate is charged to -2 kV which is the highest charge that is achievable because the plate (or wafer) first needs to cool to room temperature again. The charged plate will be placed 15 cm above the wafer, resulting in a field of -13 kV/m between the wafer and the plate assuming that the wafer is grounded. However, the particles will spend more duration between the plate and the grounded bottom plate, which results in a field of -6 kV/m. The results of these experiments are compared to the deposition without any electric field, and shown in figure 40.

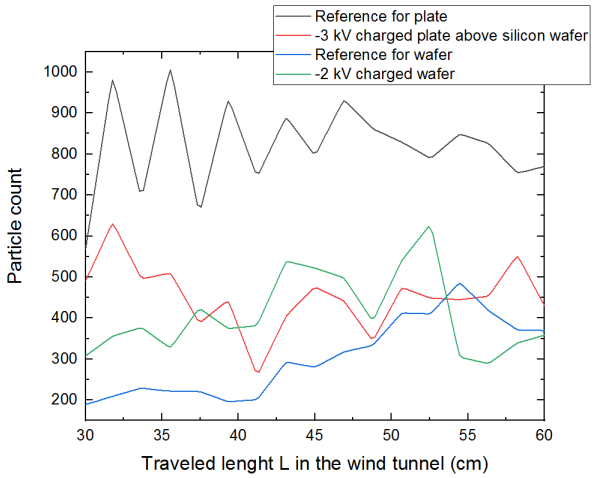

Figure 40: *The influence of the electric field in the horizontal wind tunnel on the deposition of particles.*

As can be seen from figure 40, less particles deposit on the front side of the wafer relatively compared to the neutral wafer scenario (blue and green lines). This is as expected. The glass particles acquire a positive charge due to the inlet and are being attracted to the wafer. Thus the green line must show more contamination compared to the blue line, which it does. The second situation is also as expected: A negatively charged plate will attract the particles away from the wafer, resulting in less deposition. This causes the red line to be below the black line. So, both electric fields show the predicted behavior, and can either decrease or increase deposition of particles on the wafer.

To conclude, in the horizontal wind tunnel electric fields can be used to make particles deviate and prevent contamination if the correct potentials are used. The field must however be carefully chosen, since it can also increase contamination (seen for the wafer measurement). If this would be the case, an ionizer can prevent charge from occurring. This will be discussed in chapters 5.7 and 5.8. The particles are primarily charged by the triboelectric effect, as will also be visible in chapters 5.5.3 and 5.3. First, a look will be taken at the charging and thus deviating properties of copper in chapter 5.3.

5.3 Horizontal wind tunnel, with electric fields and copper particles

To examine if electric fields have an effect on copper particles, several measurements were done. The same method was used as in the glass chapters (charged wafer and plate), but this time inlet materials were changed. Raw particle count plots will be used and they will be analysed using z-tests and correlation tests (which can be found in appendix N). If the result is significant, it will be mentioned in the text.

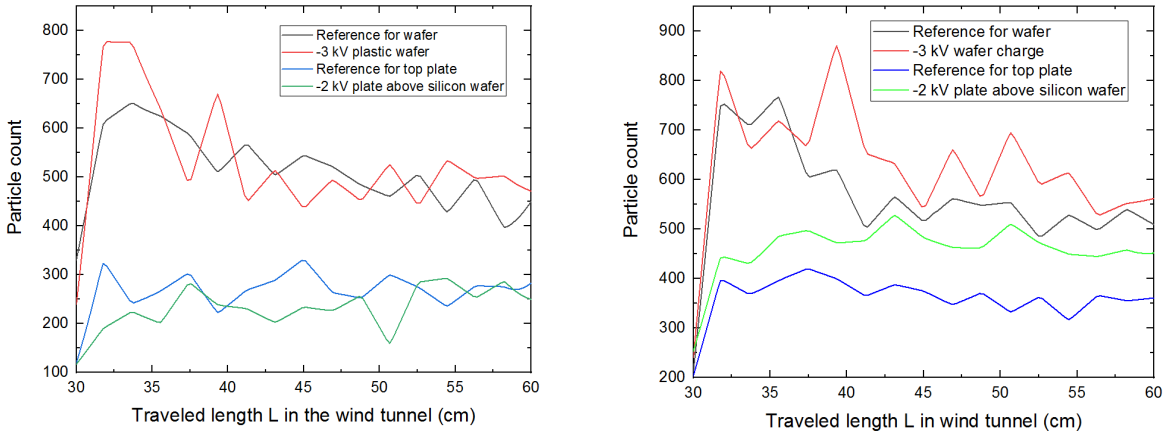

(a) Metal inlet *(b) Plastic inlet*

Figure 41: *The effect of a charged wall or charged wafer in comparison with a reference measurement for both a metal and plastic inlet.*

Firstly, the data with a metal inlet will be analyzed. Due to the conductive properties of both materials, no charge is expected to occur on the particles. This can be seen in figure 41a, where two reference measurements and two charged measurements are displayed. Secondly, the case of a plastic inlet with copper particles is examined. Due to the triboelectric properties of both materials (both negative), a little positive charge is expected to occur on the particles. For figure 41b, only the difference between the two plate measurements is significant (the error calculations can be found in appendix N). Still, it is worth mentioning that the charged wafer measurement does look like expected: A negatively charged wafer would attract a positively charged copper particle, thus the red line would be above the black line. The plate measurement however is counter-intuitive: A negatively charged plate would attract positively charged particles, resulting in less deposition. The opposite effect can be seen in figure 41b, where the green line (representing a charged plate) is above the blue line (reference measurement). A possible explanation could be that the particles that would not have reached the wafer normally, do now because of the electric field. The plate is larger than the wafer and is therefore already placed partly in front of the wafer (see figure 3). The negatively charged plate could attract the positively charged particles to keep them airborne longer. Particles that would have deposited before the wafer, now make it to the wafer and deposit, resulting in extra deposition. This explanation becomes extra likely by looking at figure 38a, where larger quantities of particles could be found towards the inlet.

Noticeable is that the calibration of both wafers (the plastic and silicon wafer) are far apart. This can be because of several reasons: 1) the roughness of the material can cause particles to make more contact with one surface material in comparison with another material, meaning that the adhesion force is lower for the

rough material [95]. 2) The wafer thickness deviates slightly (silicon wafer 1.0 mm and plastic wafer 3.3 mm) which can cause particles sizes that deposit on the wafer to also differ. 3) The roughness of the material causes different eddy flows very close to the wafer, which can cause particles trajectories to differ. This phenomenon (the more particles seem to land or be sucked up from the plastic wafer) was already discussed partly in the theory in chapter 2.3.4.

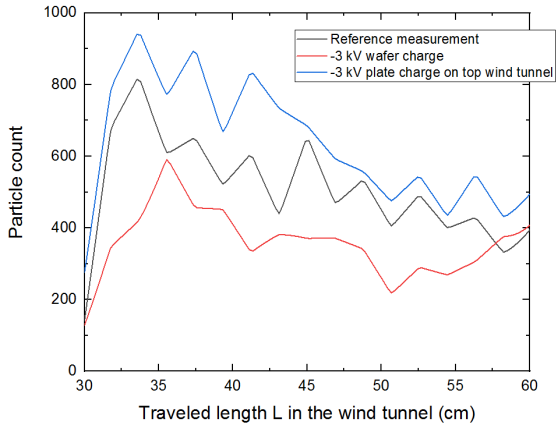

Figure 42: *The effect of a charged wall or charged wafer in comparison with a reference measurement. The wind velocity was 0.4 m/s in this measurement and the inlet made of glass.*

Next, another inlet has been chosen to see if copper particles can acquire charge. This inlet is made from glass which is on the far positive of the triboelectric scale. This would mean that the copper particles acquire a negative charge. Since the copper particles will be negatively charged, they should be repelled from a negatively charged wafer. Furthermore, if the plate is negatively charged, they are again repelled. However, repelling copper particles from the plate would mean an increase in particles depositing on the wafer. The results of the measurements are shown in figure 42 and confirm the hypothesis made above. The charged wafer indeed has less deposited particles and the plate indeed has more deposited particles in comparison to the reference. This would mean that even though the particles are conductive, they can still acquire a charge from certain objects. This charge does not decay as quickly through the air and since the particles are small, there is a relative high area where surface charge can be (relative to the volume of the particle). Meaning that the charge decay is slow enough and particles are able to hold on to their charge long enough to cause a significant effect.

To conclude, copper particles can deviate, if the surface they are released from has insulating properties. This means that in the AWH, especially metallic particles that interact with an insulating surface might cause a problem. This is due to the triboelectric effect, as will also be discussed in chapter 5.5.3. Again it was seen in figure 42 that some electric fields decrease contamination, where other fields increase contamination. An ionizer might neutralize charge where it is not wanted, as can be seen in chapters 5.7 and 5.8.

One now has all the information about electric fields (on both plates and wafers) in the horizontal wind tunnel for both glass and copper. The discussion if a horizontal flow would be beneficial in the wind tunnel will be left for chapter 6. For now, the results from the vertical wind tunnel will be shown to make a good comparison and see if the particles behave the same in a differently oriented flow.

5.4 Vertical wind tunnel and without electric fields

A big difference in the vertical wind tunnel with the horizontal wind tunnel is the symmetry which can be expected. Also, since the flow is (partly) developed, one may expect the same results throughout the whole wind tunnel from simulations (with some error due to eddy currents or Brownian motion of the smallest particles). However, there will always be some spread in the particles depositing. The spread of the particles is going to be explained in chapter 5.4.1. Furthermore, in the horizontal wind tunnel, the wind speed does

not really matter for the largest particles. Even when the wind would be 0.5 m/s, the heaviest particles would still deposit on the wafer, only somewhat further down the wind tunnel. For the vertical setup this is different, since the wind speed is parallel to the gravitational pull. This means that the wind speed might be able to influence the deposition of particles for any wafer position. This is going to be investigated in chapter 5.4.2.

5.4.1 Spread in falling particles

First, a calibration measurement must be done to see how far particles already deviate in the wind tunnel. This will enable us to estimate how far the particles actually deviate due to the electric field. This chapter will provide insight in the standard deviation without an electric field.

There are several reasons why the particles will not fall straight down. First of all, there might be small air flows due to closing the wind tunnel. This may result in small displacements of particles in no wind conditions. These small flows can also be caused by small temperature gradients which cause free convection air flows to occur. Furthermore, the particles might interact which each other. Collisions and electrostatic charge on the particles may result in a spread of these particles before landing on the wafer. The most important reason however is the manner in which the particle shaker is attached. To not damage the filter, the shaker must be attached to the outside of the wind tunnel. This results in a beam going through the wind tunnel, which will cause large shakes. The particle dispenser will thus not be at one exact location all the time, but rather vibrate around this position.

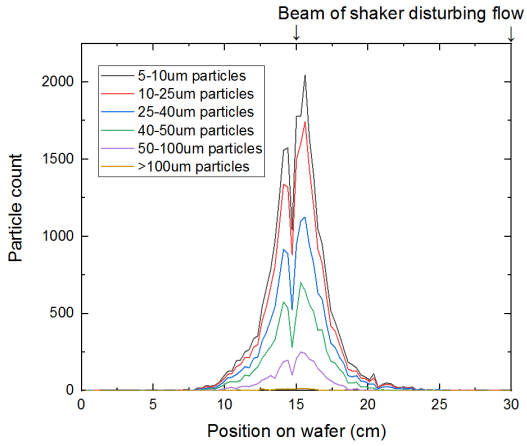

Figure 43: *The glass particle deposition on the wafer when the inlet is 55 cm long and far from the beam. With a wind speed of 0.4 m/s.*

When no wind is present, the presence of the beam is not noticeable. Particles fall straight down and only have a certain spread in them when landing on the wafer. This spread of particles is usually a 4 to 5 cm diameter in the middle of the wafer. However, if the wind is turned on, the presence of the beam becomes very noticeable when releasing the particles close to the vertical beam. The results of these measurement are taken into account in future experiments and these results are displayed in appendix J.

The difference in a velocity profile due to obstacles demonstrates that a non-uniform airflow can cause contamination to behave differently. This in turn can be useful (or unwanted, depending on the field) to steer particles away from the wafer in the atmospheric wafer handler. The practicability of applying this technique in the atmospheric wafer handler and the advantages and disadvantages will be discussed in the discussion (chapter 6). To conclude, the setup should be adapted to make sure the particles land in the middle when a flow is present. This can be done by extending the inlet. The glass particles deviation is approximately 5 cm radially outwards from the center of the wafer.

5.4.2 Wind speed and boundary layer

As previously stated, the wind speed in the vertical wind tunnel can have an effect on the number of particles depositing. This effect will be investigated in this chapter using glass particles.

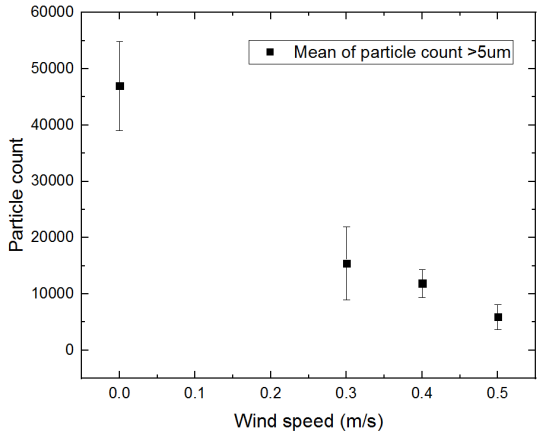

Figure 44: *The effect of wind speed on the particle deposition on the wafer. A faster wind speed will ensure fewer particles being deposited on the wafer.*

The wind speed can strengthen the effect of the boundary layer, and thus decrease the number of particles depositing. Three wind speeds are achievable in the wind tunnel without changing any conditions, which are 0.3 m/s, 0.4 m/s and 0.5 m/s. Of course 0 m/s is also measured as a witness sample, to see how the particles behave when no flow is present. The results of the different wind speeds can be seen in figure 44. In the theory, it was already discussed how a faster wind speed would ensure fewer particles depositing on the wafer (see table 2). This simulation was run with one particle size specifically, and in these experiments, a range of particle sizes will be present. In figure 21, this decrease can be seen clearly. All particles above 5 µm were considered and summed. All experiments were performed 4 times to determine the 68 percent reliability interval. This interval is also visualised in the figure. The experiments performed at 0.5 m/s have fewer deposited particles than 0.3 m/s in the mean as expected for these large particles. The reason why the wind speed does not exceed 0.4 m/s is firstly due to the temperature of the wafer, which needs to be controlled precisely and this becomes harder when the flow increases. Secondly, a faster wind flow will also increase any vortex formation in the wind tunnel. These vortexes were not taken into account in this experiment, but are important in the AWH.

To conclude, a faster flow indeed decreases contamination for larger particles on the vertical wafer. Some disadvantages where however discussed based on the AWH why it might be counter-effective to increase this wind velocity. Also, for smaller particles the effect of a faster flow will decrease (see table 2). These smaller particles are the largest problem in the AWH. Thus, increasing the airflow would not have a very beneficial effect on the particle deposition, meaning the remaining experiments will be executed at a flow velocity of 0.4 m/s.

5.5 Vertical wind tunnel, with electric fields and glass particles

In the previous chapter, the first calibration measurements were executed to visualise the spread in the vertical wind tunnel. This was measured with the flow on. However, the advantage of the vertical wind tunnel is that a flow is not necessary to carry particles to the wafer. Meaning that without the flow, the electrostatic force can be exaggerated. This chapter will consist of several chapters where the flow was not present. First, in chapter 5.5.1, the effect of a negative field without a flow will be investigated. The average charge of a particle will be calculated in this chapter. Chapter 5.5.2 will do the same for positive fields. The percentage of charged particles and the cause of this charge is explained in chapter 5.5.3. All these experiments were executed without a flow. In chapter 5.5.4, the flow is present. Finally, in chapter 5.5.5 the

wafer is charged instead of the plate.

5.5.1 Charge on particles: The boulder counter in negative fields

The boulder counter makes is easier to distinguish the size of the particles, enabling the user to investigate the change in trajectory and thus the effect of charge and size. Be aware that the charge is not measured directly, as is also the case in previous chapters. A particle of 100 µm might be lightly charged, but since it is so heavy, it will not alter its trajectory that easily. That is why it is hard to say whether fairly large particles >50 µm are charged or not. For smaller particles however, there is a noticeable change in the trajectory. Let us explore these measurements without any wind and for two scenarios; 0 kV/m and -12 kV/m.

The first measurement is used as a reference measurement for the different particle sizes. Since there are no horizontal forces acting on the particles, one would expect all particles to fall straight down. This is visible in figure 45a with a certain spread. Now applying the field on the left again, one expects the particles to deviate to the left. This is visible in figure 45b for different particle sizes. According to expectations: the smaller particles deviate more due to the field than the larger particles. This can be seen by the red and black lines which have the largest deviation to the left. In both graphs there are little particles larger than 100 µm particles, which is why the yellow line has more noise than the other bins. The different amounts of deviation are calculated using the full width at half maximum, since all graphs look the same on the right side of the graph. The percentage of charged particles deviating in the field is calculated by integrating the total area under the curve.

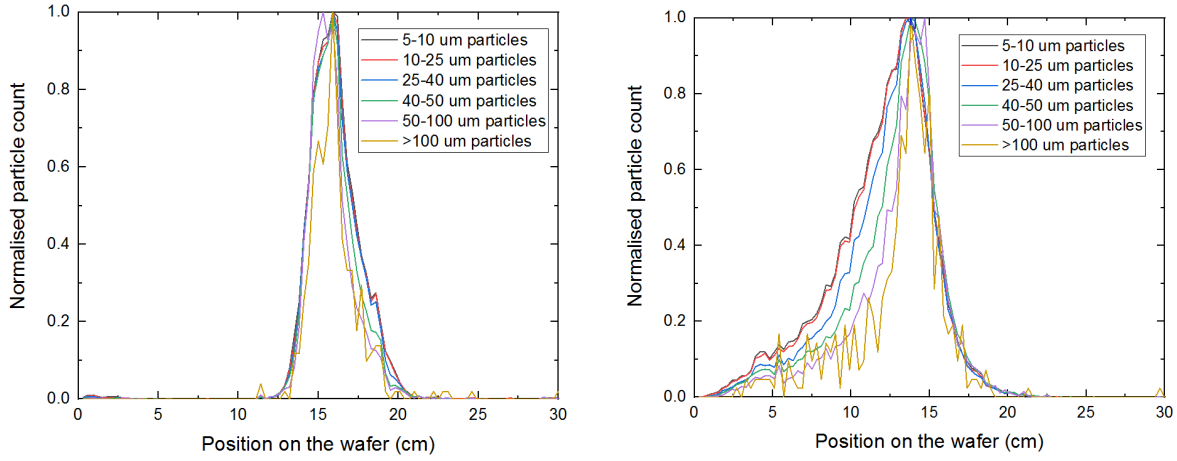

(a) *0 kV/m particle position*

(b) *-12 kV/m particle position*

Figure 45: *Left) the position of particles without an electric field. Right) the position of particles with a -12 kV/m electric field. Both plots were made with the help of the boulder counter in no wind conditions.*

The full width half maximum (FWHM) change tells us the distance particles of each category have moved. It gives the displacement if a particle was charged in the first place, assuming that the FWHM stays constant on one side of the graph. The -if a particle was charged- is an important remark. As can be seen in the field with the electric field in figure 45b, the maximum number of particles still end up near the center of the wafer. Also, the FWHM increases for smaller particles. In the next paragraph, a calculation will be made about each particle that is charged and caused by the triboelectric effect only. In other words, the neutral particles will not be taken into account.

Taking the change in FWHM enables us to calculate the charge each bin of particle sizes approximately has. This is done by taking the lower and upper limit of the particle size, so a spread of charge can be calculated. This can be seen in the last column of table 4. The number on the left is the smallest particle diameter in that bin. The right number in the final column represents the largest particle diameter in that bin. This means that the first bin (ranging from 5 to 10 µm) can have particles ranging from 36 eV (for the

5 µm particle) to 288 eV (for the 10 µm particle). It can be noted that the charge keeps increasing as the particle size increases, even though less horizontal distance is covered. This is because of the scaling: The triboelectric effect works on the surface ($\propto r_p^2$) and gravity ($\propto r_p^3$). Having said this, what can also be noted from figure 45b is that there are also particles of 5 µm which travel even further than 2.41 cm. The charge of each individual particle can differ a lot, ranging from no charge to traveling left 10 cm horizontally. The fact that the size of the particle is not exactly known and the fact that the same particle can possess different quantities of charge, makes it hard to apply a model or formula with a reasonable confidence. However, all particle charge examined, even the most deviating particles fall within the maximum charge which could be caused by triboelectric charging of 100 e/μm^2 and are comparable to other studies with similar particle size. [52] [53]

Particle diameter (um)	FWHM 0 kV/m	FWHM -12 kV/m	FWHM change	charge on particle (e)
5-10	2.99	5.13	2.14	36 - 288
10-25	2.91	5.01	2.1	288 - 4360
25-40	2.84	4.27	1.43	4360 - 11200
40-50	2.58	3.52	0.94	11200 - 15600
50-100	2.23	2.64	0.41	15600 - 54500
>100	1.82	2.22	0.4	>54500

Table 4: *The FWHM with no field applied and an electric field of -12 kV/m, the change of this FWHM due to this field and the charge on that particle diameter bin.*

Next, one can calculate the percentage of particles landing on a different place on the wafer. If the curves would be exactly the same, the percentage of charged particles would of course be zero. It is also important to normalise the curves, since this ensures that the number of particles released is not a variable anymore. Furthermore, it is important to note that the curve has not been translated to the right or left. Since this is not the case (both maximums of 0 kV/m and -12 kV/m are at the center of the wafer at 15 cm), the extra area under the curve that has been created due to the changing trajectory of particles can be used to calculate the percentage of charged particles. The percentage and area change are given in table 5. To calculate the final total charge percentage, this area percentage change needs to be multiplied with the percentage of each bin in the particle distribution. This distribution is determined from table 1, and goes as follows: 5-10 µm bin = $\frac{222}{534}$, 10-25 µm bin = $\frac{166}{534}$, 25-40 µm bin = $\frac{83}{534}$, 40-50 µm bin = $\frac{40}{534}$, 50-100 µm bin = $\frac{19}{534}$, >100 µm bin = $\frac{4}{534}$. This gives a final percentage of 43.2 percent of particles which have a noticeable amount of charge.

Particle diameter (um)	Area 0 kV/m	Area -12 kV/m	Area percentage change
5-10	3.39	6.1	44.4
10-25	3.31	5.98	44.6
25-40	3.22	5.43	40.7
40-50	2.96	4.96	40.3
50-100	2.72	4.25	36
>100	2.19	3.44	36.3

Table 5: *The area under the curve with no field applied and an electric field of -12 kV/m and the increase of this area in percentage due to this field.*

To conclude, particles of 5 µm are charged with approximately 36 e. This is the average amount of charge, meaning that some particles will have less to no charge at all, while other particles have way larger charges present on the particle. This chapter shows that it is possible to deviate particles in electric fields and that triboelectric charging seems the main mechanism. This will be discussed in greater length in chapter 5.5.3.

5.5.2 Charge on particles: The Solair 3100 in positive fields

In appendix chapter K and 5.5.1 negative fields were used to measure the deviation of particles. In this chapter the unexpected results when measuring with a positive field created by charge induced charge separation are discussed. Furthermore, models that calculate the contribution of space charge will be discussed and an explanation will be provided why space charge gives the values it does and if these results are reliable.

It has been discovered that the glass particles are primarily positively charged, which is why the hypothesis would be for particles to move away from the positively charged plate. However, as can be seen in figure 46a, this is not the case. 3 Averaged measurements of both an uncharged and positively charge plate can be compared here, and the results show that there is less deviation of the particles compared to the experiment with a negatively charged plate. Furthermore, due to the mobility difference of ions and electrons, one would expect the same space charge with both a negative and positive electric field present in the wind tunnel. Positive ions which are being created near the plate get repelled from the positively charged plate and have to travel towards the grounded plate at the other side of the wind tunnel. Electrons that are created due to collisions get attracted to the positively charged plate, but travel much quicker than ions. The effect of the space charge can also be seen in figure 46b. This figure will again be plotted for a negative field in figure 47b and looks very similar, only deviating towards the other side. Furthermore, space charge could not have been a large effect in all plate measurements. If there is an effect, all particles would deviate under the influence of the field. This can not be seen in figure 46a. More reasons why space charge does not have a contribution will be discussed in chapter 5.5.3

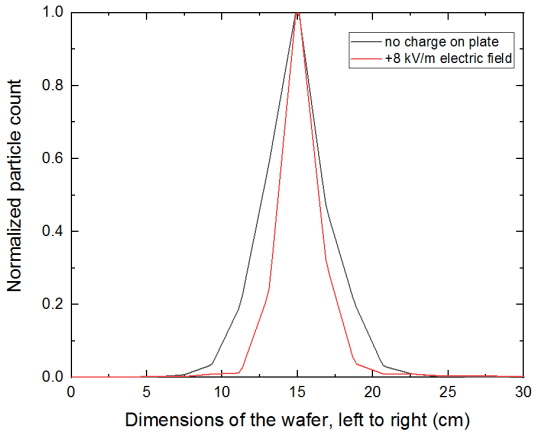

(a) Positive field

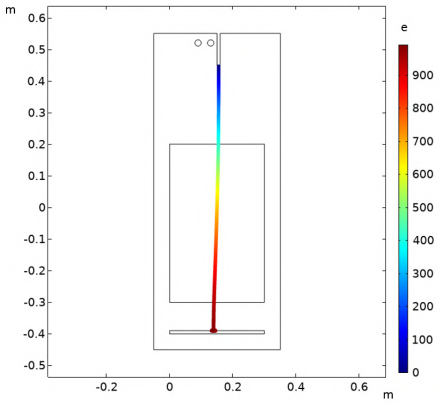

(b) Charge accumulation of positive field

Figure 46: *Left) particle counter measurements in a positive field. Right) charge accumulation of initially uncharged particles and the deviation of these particles in a positive field for a 17.5 µm glass particle.*

The question remains why particles do not deviate that much in a positive field. Not much changes, except for the direction of the field. Some minor changes must explain the difference. Hypothesis following from these changes for this phenomenon will be discussed here.

- The positive field is generated using a different method than the negative field. Instead of contact induced charge separation, the positive field is created using charge induced charge separation. The electrostatic field meter measures a positive field around the entire plate, but it could be a reason why particles do not deviate.
- The positive field is harder to generate and decays faster. A glass plate was used to check the experiments, and the results showed that the particles 1) did not deviate again and 2) charge decayed fast on this plate, leading to smaller fields compared to the negative field testing.
- Due to the smaller fields, the plates were installed as fast as possible. This left little time for the plate to cool, causing convection to have an effect. This effect is opposite to that of the positive field and

glass particles.

- The field interferes with the particles before they have left the inlet. The charged plates are relatively close to the particle inlet, and this field might influence the particles.
- The wafer interferes with the electric field.
- The field is not homogeneous, causing unwanted phenomena to occur.

Since the last three items are also occurring in a negative field, it seems very likely that the lack of deviating particles occurs because of the charging mechanism which is being used. It therefore remains a discussion point why this statically positively charged plate does not exert the same but opposite behavior force compared to the negatively charged plate. This will be discussed in chapter 6. For now, let us combine the knowledge of the positive fields and negative fields and reason why the calculated percentage of particles which is charged is a reasonable estimate in chapter 5.5.3.

5.5.3 Percentage of charged particles and cause of charge

As seen in paragraph 5.5.1 and in appendix K, approximately 30 to 43 percent of the particles are charged. In this paragraph it is explained why this number is reasonable. First of all, the charge that is acquired by the particles is probably caused by the contact induced static energy that the glass particles and the plastic cone have. Looking at the triboelectric effect, plastic likes to be negatively charged and glass positively charged, so these two materials can charge each other easily. Glass-glass interaction however can also cause triboelectric effect, caused by the difference in size of these particles. Source [96] states: "smaller particles tend to charge negatively and larger particles tend to charge positively." Thus this would result in positively and negatively charged particles. If these particles would not clump together, there should be particles of both polarities. In a certain field, this would mean that particles deviate in both directions. However, as can be seen in figure 47a (and other figures using vertical electric fields as well), there is only a noticeable deviation of particles in one direction. To conclude, the glass-glass interaction causing charge as well is insignificant compared to the glass-plastic interaction.

This raises the question: what percentage of the glass particles actually comes in contact with the plastic? To start answering the question, it will be calculated how many particles fit in the final outlet of the syringe, which has a cone like diameter of 190 µm. The theoretical result can be seen in the appendix in table 9. This table however only states one specific size, and the glass beads used in the experiments have a size distribution. With the particle distribution approximately known (due to the boulder counter), it can be calculated how many particles touch the outer diameter of the syringe. The middle value of the bin (for the 5-10 µm bin, this is 7.5 µm) is multiplied with the percentage of particles in this bin (seen in the previous chapter) and the percentage which would touch the outer radius. This calculation results in the approximation that 36.6 percent of the particles touch the plastic inlet at the final part of the inlet. If it is assumed that all particles which come in contact with the inlet get charged, 36.6 percent of the particles should get charged. This is in the middle of the two previously calculated results of 30 percent and 43.2 percent. Thus theoretically the plastic inlet and the triboelectric effect between the inlet and the glass particles can cause some or even all of the charge which can be found on the particles. This hypothesis is confirmed by testing with a metal inlet where the glass particles have rested in for days, making sure that the charge partially decayed (the glass particles rest in an plastic container which could provide extra charge, which is why the particles were left for a long duration). The comparison is visualised by averaging three measurement in figure 47a and interpolating. However, the effect on the trajectory with a metal inlet has not completely gone, particles still tend to move towards the plate with the electric field. This can be explained by the triboelectric series again. Glass (positive) and plastic (negative) boost the charge exchange, while glass and metal (neutral) exchange charge to a lower degree. This means that some charge can still be present, although not the same amount as could be seen from glass-plastic interactions.

This is also why field charging and diffusion charging will not have a large contribution. This can also be seen in figure 47b, where a glass particle of 17.5 µm (middle of 10-25 µm bin which deviates the most according to figure 45b) has been modelled. It can be seen that all particles should deviate from their trajectory, which is not the case. Furthermore, if space charge would be the most dominant charging mechanism, the

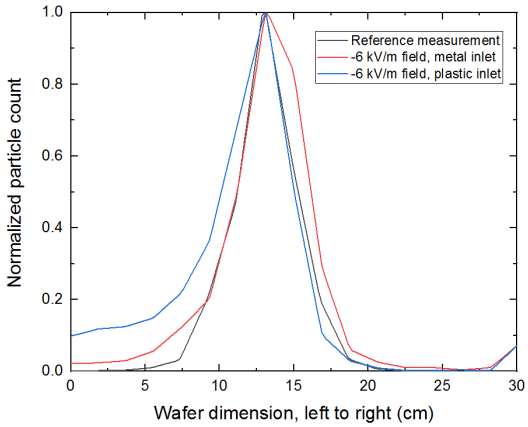

(a) -6 kV/m field

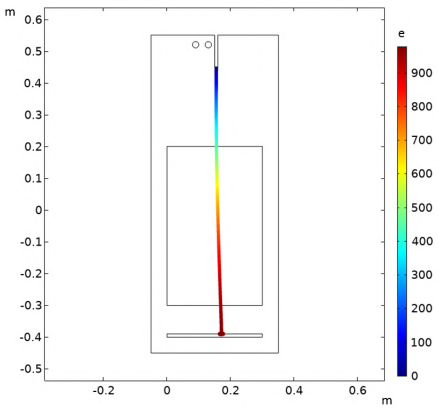

(b) Charge accumulation of negative field

Figure 47: *The difference in travelled distance for a metal and plastic inlet in a -6 kV/m field, visualising the contribution of the triboelectric effect and electric field effect. The contribution of the electric field charge accumulation is modelled on the right for a 17.5 µm glass particle.*

inlet material would not matter that much. All particles could leave the inlet uncharged and charge while falling through the wind tunnel. This is why the effect as seen in COMSOL is probably exaggerated. It is known that air is a poor conductor, and without the ionizer there will not be many ions generated. If ions are created, their path length in atmospheric pressure is in the 100 nm range, giving ions little chance to speed up and possibly ionize another surface. Finally, the plates that are used in these experiments are statically charged, meaning that the electric field will be fairly distributed over the surface (charge can not move towards the outermost corners of the material, as it would for conductive plates or emitter points, as can be seen in figure 29). This is reason to believe that space charge does not have a significant effect in a no wind condition. As will be seen in figure 58a and 58b, this is the same for the situations with a flow present. The space charge even significantly drops (from 10^{-8} to 10^{-17} C/m^3).

A distinction between triboelectric and electric field charging can not readily be made, since the particles are insulating. More clarity about this subject and the effect of charging in the field can be gained with conducting particles, as can be seen in chapter 5.6.

5.5.4 The effect of charged particles with a uniform airflow

As stated several times before, the largest particles determine the behavior of the other particles. This is due to clumping of the particles. This means that there are only a few particles of 5-10 µm which are free to move and experience sufficient effect of the electric field. Evidence for this can be seen in the horizontal wind tunnel, few particles land far away (figure 34b). The same effect can be seen in the vertical wind tunnel with electric field, where the lines of 5-10 µm and 10-25 µm are close together (figure 45b). Remember that doubling the diameter of the particle, reduces the horizontal translation by a factor 2^3. Because the airflow reduces the amount of time which particles spend in the electric field and because a very small number of particles under 10 µm remain unclustered, it is concluded that the effect of the electric field is negligible once the wind is switched on. Only small particles of 1 µm start to display a noticeable effect in simulations at flows of 0.4 m/s according to the models.

5.5.5 Glass particles, the charge on the wafer and adhesion forces

Another charged surface which can be investigated is a charged wafer.[58] This chapter will compare the expected deviation due to the electric field with the experimentally measured values.

To see if the particles indeed behave as expected, COMSOL FEM simulations were executed with both wind

and no wind conditions. The simulations were executed with a 17.5 µm particle of glass with electric charges of 0 e, 2000 e and 4000 e, where the wafer had a charge of -3 kV. Also worth mentioning is that the inlet is moved 1 cm from the center (as can be seen in table 6 in the second column). In real experiments the particles also deviated slightly, and since COMSOL only uses ideal situations, the inlet must be out of center to not get the same answer for each particle charge. Moving the inlet slightly off-center will cause particles to experience a radial outwards force due to the electric field as well (next to the z-force opposite to the gravity). These charges are based on the range calculated in table 4 to pick realistic values. The resulting deviations are given in table 6. As can be seen in the table, only small deviations are expected for no wind conditions. Only 1 mm of deviation can be seen for the 17.5 µm particles with a charge of 4000e compared to the uncharged particles. In simulations with wind, the effect increased to 9 mm. As can also been seen, the wind itself has an even larger effect on the particles, making them deviate 9.7 cm. The wind combined with the radial force of the field strengthens the deviation of the glass particles from the wafer.

Glass particle (17.5 µm) charge (e)	deviation center no wind (cm)	deviation center wind (cm)
0	1	10.737
2000	1.052	11.218
4000	1.098	11.637

Table 6: *The deviation of a 17.5 µm glass particle with a -3 kV charged wafer and an inlet which is 1 cm off-center from the middle of the wafer. The velocity of the wind in the simulations was set to 0.4 m/s*

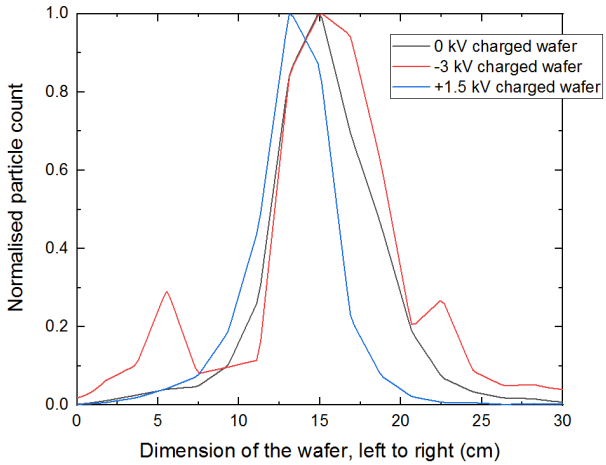

Figure 48: *The influence of the charge of the wafer on the deposition of particles, each situation averaged over 3 measurements and no external flow.*

A charged plastic wafer is used to examine which effects the charge of a wafer has on the particle trajectory of glass. Again, approximately 60 percent of the particles will be neutral, and 40 percent of the particles will have some form of positive charge. All experiments were also averaged over 3 measurements containing 20 shakes of particles in a vertical wind tunnel with no flow.

As seen in plot 48, the negatively charged particles land mostly in the middle of the wafer, while neutral particles deviate the most from the center. This confirms what was expected from theory: 1) the negative wafer attracts particles and the particles will therefore fall near the center of the wafer. 2) a neutral wafer will not attract any particles and therefore particles keep the minimal sidewards trajectory they might have. This increases the number of particles landing away from the center of the wafer, as can be seen in figure 48. It is noteworthy that the positive wafer does not deviate from the negative wafer. One would expect a positive wafer to repel particles, making their sidewards movement even more pronounced. Chapter 5.5.2 gives hypotheses why the positive field does not repel particles to the same degree as a negative field. A reason why this could be the case, is that the measurements as seen in figure 48 are not significant as

determined by the error analysis in appendix N.3. It was already hypothesized that the differences would be small indeed (see table 6), and the error measurements confirm this hypothesis. To conclude, no significant difference can be found between a neutral and a charged wafer, but slight differences (visually and in figure 48) can be seen. Meaning that the effect is not totally unnoticeable, but just small, as was expected by models.

To conclude the vertical wind tunnel setup for glass particles, it was shown that negative fields can cause particles to deviate. This can be beneficial in preventing contamination, knowing that streamlines can carry the particles away more easily if they are situated at the sides of the wafer. The experiments with no flow present showed significant results. However, smaller particles should be used to investigate if this is true, which is why the copper particles with a smaller diameter in combination with a glass inlet will be used again in chapter 5.6.

5.6 Vertical wind tunnel, with electric fields and copper particles

Since glass particles did not always give significant results, smaller particles are used in this chapter. This will be advantageous when researching the small electrical effects when a flow is present.

One important remark is that to not overload the particle counter, a sticker is being used in the exact center of the wafer. This sticker is 4.5 cm in diameter. This means that the area from the center of the wafer moving radially out until 2.25 cm are covered and no particles are detected here. This can be seen in figure 49, where a clear decrease in particles can be seen near the center (while the maximum number of particles is expected and can normally be seen here). This sticker thus covers the largest clumps of copper particles, which is not worth investigating. The focus will be on the smaller copper particles, which will be more easily diverted and can therefore be found farther from the center. The sticker has no influence on the particles that are far from the center. Also noticeable is that in figure 49 the wind speed does not make a large difference based on the number of particles which can be found there. This could also be seen in table 2.

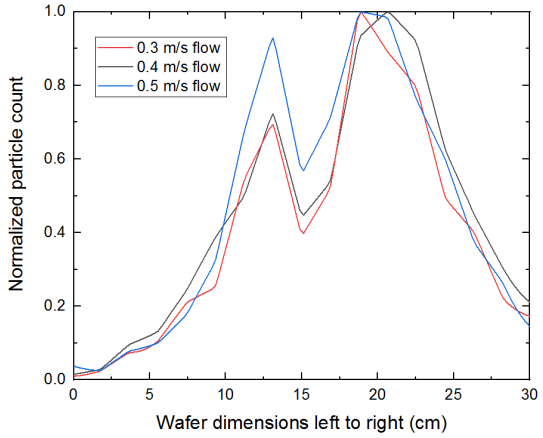

Figure 49: *The deposition of copper particles with a sticker in the middle to limit count. Wind speeds of 0.3, 0.4 and 0.5 m/s were used.*

Next, let us compare the results gathered from two different kind of inlets, namely plastic and glass. As seen in chapter 5.3, the plastic inlet does not show any particle charging and therefore no deviations. This was again confirmed in the vertical wind tunnel experiments. These results can be seen in figure 83a and 83b in the appendix. The particles behave the same as the calibration measurements and therefore these graphs will not be discussed in great detail in this chapter. However, the glass inlet did show some changes in particle count in chapter 5.3, which is why the discussion will be mainly focused on this inlet. The results of the glass inlet are visible in figure 50a and 50b for the charged plate and charged wafer respectively with a flow of 0.4 m/s present. Both graphs do not show a significant deviation from the calibration measurement (as calculated in appendix N). The measurement where there is no flow, did also not provide any significant

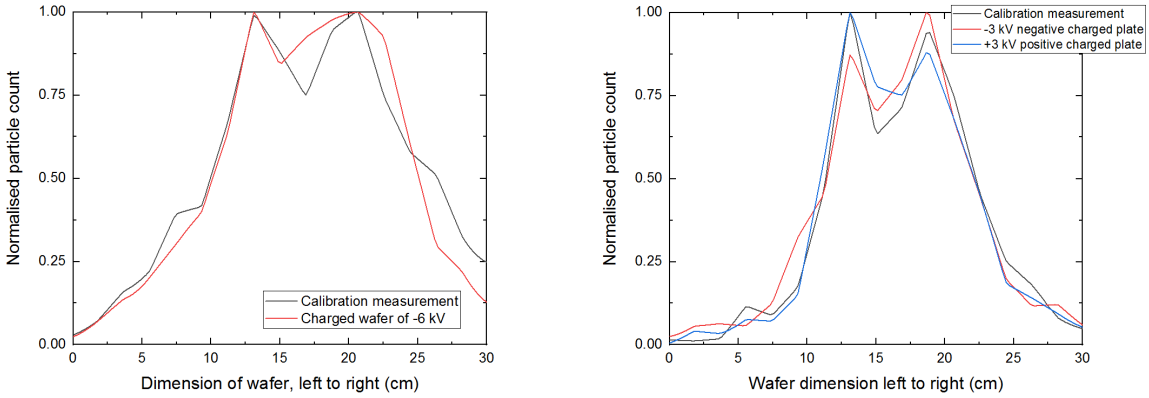

(a) *Copper deviation in field by plate*

(b) *Copper deviation in field by wafer*

Figure 50: *The deviation caused by electric fields of both a plate (positioned on the right, 50 cm apart) and a charged wafer with a glass inlet with a flow of 0.4 m/s present.*

differences between the measurements. This would mean that the copper particles do not hold any charge. Due to their conductive properties, a dipole can exist in the particle, neutralizing the outside electric field. A simple calculation shows that this is easily realisable (Filling in formula 12). For a particle of 5 µm and a perfect dipole (point charges on the outer edges of the particle), 26 elementary charges are needed. However, this would mean that the particle is neutral to begin with. A charge Q on a metal sphere will not disappear, and also experience a net force. This means that there is little to no charge on the particle to start with. The hypothesis is that the copper particle will almost always touch another copper particle, which in its turn will be in contact with millions of other copper particles (or even the ground). Only when the copper particle moves along the inlet and not touch any other conductive particle, will it be able to pick up a charge. The chances of this happening are small and not visible in the measurements as shown in figure 50a and 50b. The difference between this vertical and horizontal measurement still needs to be explained in chapter 6.3. However, there is a slight chance for these copper particles to get charged due to the inlet. This has been

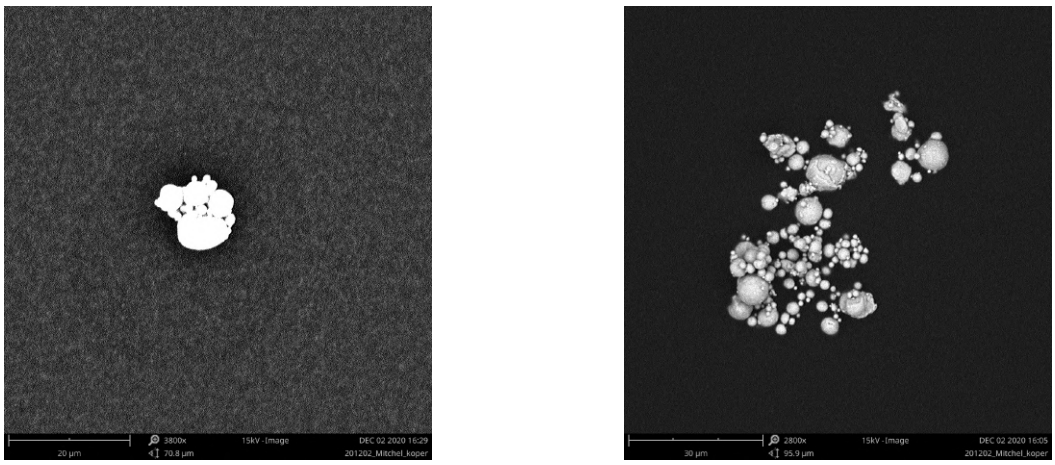

(a) *Copper deviation calibration*

(b) *Copper deviation in field by plate*

Figure 51: *The difference in particle clumping size landing at 10 cm from the center of the wafer due to an electric field. Many shakes were needed to have any particles deposit on this place.*

shown in the SEM using the following method: A SEM sticker was placed at 10 cm from the center of the wafer when there was no field present. In another measurement, this sticker was placed in the same position, this time in a field caused by a plate that was charged to a potential of -3 kV (giving a field of -6 kV/m). By

shaking the inlet many times, a lot of particles were released in the wind tunnel in the situation where no flow was present. The results are shown in the SEM images below. For the control measurement, a couple of 5 µm single sphere particles and small clumps were present on the sticker (figure 51a). For the measurement with a field, larger clumps of particles could be seen (figure 51b). These particles are of course somewhat heavier. In this case the clump would be the same as a single spherical particle of 13 µm in diameter if the behavior of both the clump and a perfectly spherical particle is assumed the same. It must be stated however that very few particles could be found on both stickers, stressing that this effect is minimal. Because only a few particles could be found, this result should be considered more as an indication then a significant result.

To conclude, the fact that copper particles are smaller could not be used to the advantage of the research. The charging of the copper particles is too small in all experiments to draw significant conclusions of particles deviating in a flow.

As seen in almost all previous experiments, an electrostatic force (or electric field) can be used to deviate particles. This effect is hypothesized to become even bigger for smaller particles. As discussed several times before, the field can decrease but also increase contamination. This is why, in the instances that the contamination would increase, an ionizer can be used. This will be discussed in chapters 5.7 and 5.8.

5.7 Ionizer, Charging and neutralization of surfaces

This chapter will first provide the functioning of the ionizer in normal conditions. The ionizer normally functions with fast flows and close to the surface. This will confirm if the ionizer is able to charge or neutralize surfaces. In chapter 5.8, the ionizer will be applied in experiments with particles in the wind tunnel.

As can be seen throughout this thesis, the charge on static plates or on the wafer can have effects on the trajectory and adhesion forces of particles. In previous experiments, the charge was applied using contact induced electricity. The focus of this subsection will be investigating the different methods of charging surfaces, how an ionizer might be able to charge and neutralize the surface and what possible explanations of these charging and uncharging phenomena are.

The working principle of the ionizer is explained in chapter 3.5. The ionizer has different settings and can handle different polarities of charge. This means one can test many different situations. The ionizer is for example capable to not only neutralize a surface, but also charge it slightly. This can be seen in appendix L. More importantly however is how long the charge can be held by the wafer or plate as a calibration measurement. The following experiment was done, to investigate if these surfaces also retain this charge. The substrates were charged by the ionizer, after which measurements of their static charge were done. These measurements were done with both a positive and negative ionisation of the ionizer, since some materials have the tendency to be charged positive (silicon for example), were others have the tendency to be charged negatively (PVC for example). The results can be seen in figure 52a and 52b. For both figures, two measurements were done per material.

As can be seen in both figures, PVC has the ability to hold more charge. After 70 seconds for the positively charged wafer and after 100 seconds for the negatively charged wafer, no change in the charge is present anymore. It is known that PVC likes to be negatively charged, and this is also visible in these figures. The positively charged PVC wafer holds 0.2 kV, while the negatively charge PVC wafer holds -0.7 kV approximately. For both ionizations, the charge of the silicon oxide wafer almost decreases to 0 kV and no clear difference can be seen for a positive or negative ionization. The silicon oxide and aluminum wafer were also tested and showed very similar results compared to the silicon wafer. Grounding the wafers also resulted in charge developing, except for the PVC wafer, because of its high resistivity no real difference could be found when grounding the wafer or not. To conclude, an ionizer can charge a surface, but in case of conductive surfaces this charge will decay quickly.

Next, the charged surface will be neutralized. This can be done in three settings; only negative, only positive and positive and negative ions combined. The plastic wafer will be charged negatively using contact induced charging before the experiments to acquire much charge, and since it is the only wafer which can hold

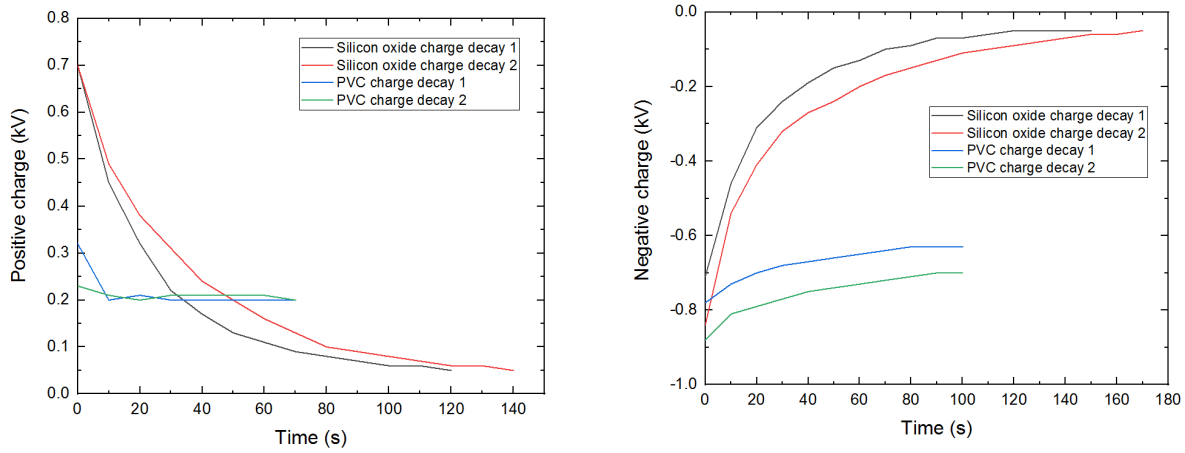

(a) *Positively ionized* ***(b)*** *Negatively ionized*

Figure 52: *The charge decay of a positively and negatively charged silicon and PVC wafer. The voltage of the emitter points are ±3 kV and the wafers were ionized with the ionizer for a full minute.*

charge for a longer duration of time. This wafer can be charged up to -6 kV, after which the measurement immediately begins. First one must know how fast the charge on the wafer decays without any external factors such as flow or extra ionization. This exponential decay was previously proven for glass, as can be seen in appendix 81. The same kind of measurement is done for the plastic wafer, resulting in a resistivity of $1.1 * 10^{-13}$. If the ionizer manages to speed up this decay of charge, it will be useful to use in order to neutralize the surface faster. The results of this experiment are presented in graph 53. In this graph, the ionizer will be applied all over the wafer for a set time. Also to test if the ions indeed make a difference, an airflow without any ionizer is also applied to the wafer in the same positions (see appendix 82). It is clear that the ionizer, with the correct settings, helps to neutralize the plastic wafer faster than it would with natural charge decay only. One thing to note in figure 53 is that even negative ions can help neutralize the wafer, and this is because of two reasons; 1) the negative ionization in the flow can, partly because of its velocity, create positive ions. These are then attracted to the wafer 2) the positive electrode could not be completely switched of, resulting in some positive ions (after recombination reactions) as well. These ions easily react with the negatively charged PVC wafer.

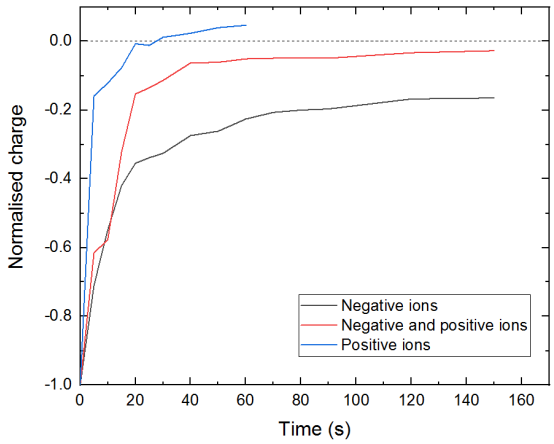

Figure 53: *A negatively charged PVC wafer with a normalised charge being neutralized by the ionizer in three different settings: only negative, positive and negative and only positive.*

So, the ionizer functions well in these conditions to neutralize surfaces. In chapter 5.8 it will be investigated

if these properties can also be used in the wind tunnel.

5.8 Ionizer, Charging and neutralization of particles

This chapter will continue where the previous chapter left of. It is known that the ionizer functions and can neutralize surfaces. In these experiments, the influence on trajectories will be investigated when the ionizer is present in the wind tunnel. This ionizer will be installed at the top of the wind tunnel, in order to not disturb the flow or particle trajectories caused by the electric fields which are exerted by the ionizer. Chapter 5.8.1 will research the effect for glass particles using an external flow and chapter 5.8.2 will research the effect for polyamide seeding particles using the emitter points and the flow of the wind tunnel.

5.8.1 Ionizer effects with glass particles

From the previous chapter it has become clear that an ionizer can be used to neutralize negatively charged surfaces such as wafers. That can be beneficial if the wafer and the particles are attracted to each other due to the charge. This is why the ionizer has been further investigated in the wind tunnel. Two methods were investigated: 1) The ionizer requires some flow over the emitter points, and thus it was chosen to use the pressurized air gun of the ionizer and blow this ionized air into a channel with small holes. These small holes distributed the ionized air in the wind tunnel, as can be seen in figure 54a. 2) The ionizer is placed in the wind tunnel without an external source of flow. This method uses polyamide particles in chapter 5.8.2. In this chapter method 1 will be discussed in more detail.

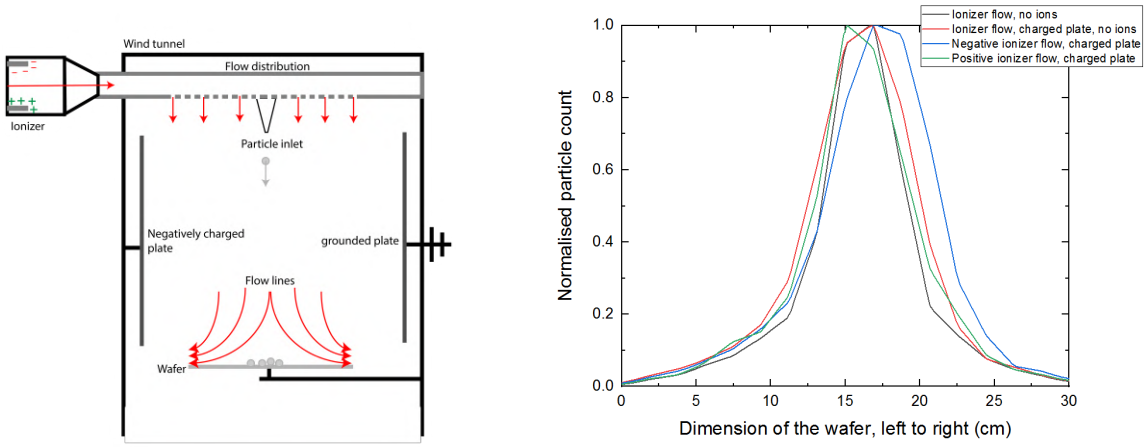

(a) Schematic drawing of ionizer experiment

(b) Different ionizer polarization's

Figure 54: *The schematic drawing of the ionizer used in the experiments, and the results gathered from this experiment. All lines represent 3 measurements averaged, no external fan flow but an air gun pressurised flow.*

Particles were released from the inlet with no wind present (except for the external flow to make the ionizer function). These particles travelled through a negative electric field before ending up on the wafer. When measuring the difference between positive, negative and neutral ionization in this field, no clear distinction could be found. This could be because the influence of the (ionized) flow overruled the force from the negatively charged plate. Also, since the flow of the ionizer was parallel to the plate and parallel to the trajectory of the particles, it could be the case that using an ionizer does not gain any results. Firstly the particles are dragged along with the ionized flow and therefore do not encounter many ions, secondly the charged plate does not have a velocity component near its surface, especially when the flow is weak and parallel to this plate. The results of the ionizer experiments can be seen in figure 54b. Other experiments, where both the flow from the fan and the flow from the pressured air gun were taken into account, did also not show any deviation caused by the polarity of the ionizer. As can be seen in figure 58a and 58b, the field created due to these emitter points had little effect on the particles.

To conclude, using this setup did not provide any significant neutralizing results. This is why two changes will be made in chapter 5.8.2: The polyamide particles will be smaller than glass particles but also insulating, resulting in charge on the particles and large effects due to the electric fields. Secondly, the ionizer emitter points are put directly in the wind tunnel with no external flow.

5.8.2 Ionizer effects with polyamide particles

Since the glass particles are too large for the Solair 1100 and the change of trajectory for copper particles is minimal, a final and third kind of particle is used. More details about these particles can be found in chapter 3.3.1. This chapter will thus show if another neutralization method with smaller particles does give significant results of neutralized surfaces. Neutralizing surfaces or particles can be advantageous if these particles would otherwise be attracted to the wafer.

As in previous chapters, the particles will first be put under a SEM to get an idea of particle size distribution and clumping of the particles. These results can be seen in figure 55. What is noticeable about this figure is the amount of spacing between each particle when the particles clump. This has not been seen in either the glass of copper particles SEM images (figure 37a or 39b). This is a clue that the capacity of the particles to hold static charge is large. Particles do not necessarily have to touch in order to be bound together by this electric effect. In the rest of this chapter, it will become evident that these particles are indeed very likely to charge statically. As an example, the charge of a 28 μm particle is calculated to be 5500 e. The particle here is calculated to be this big using the approximate mass of the particle as seen in figure 55 and the known deviation at which this particle was found. This is similar to glass when looking at the table 4 in a similar size bin, but the polyamide particles are lighter, meaning they spend more time airborne.

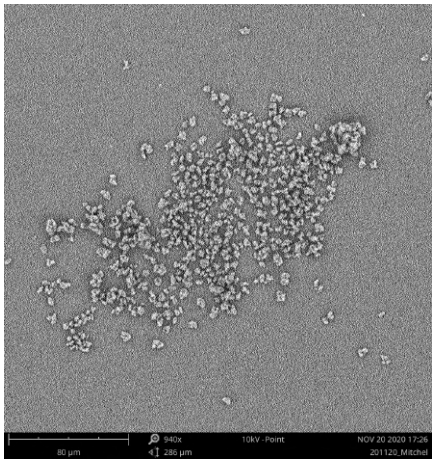

Figure 55: *The SEM image of polyamide seeding particles when put directly under the SEM at a known deviation from the center.*

The effect of the ionizer was again researched in two separate situations, in a no-wind environment and with a flow of 0.4 m/s present. For all situations, a calibration was done (so without the ionizer turned on) to compare the results. In all experiments, the ionizer was set so both emitter points emit ions. Differently stated, both negative and positive ions are created when the ionizer is switched on. These results are plotted in the same graph as the measurements with the ionizer turned on. Let us first take a look at the results that were gathered with no flow present. One would expect little effect on the calibration measurement. If the particle would get charged or neutralized due to the ions present, there is no field present to actually deviate the particles. Furthermore, in a no-wind scenario, the hypothesis would be that ions do not distribute over the whole wind tunnel. This would increase the likeliness for particles to get neutralized or the plate (which is relatively close to the ionizer compared to the wafer) to get more neutral in the process (charge decay due to ions). This would mean that the deviation caused in the charged plate scenario would decrease. Since ions might not be able to neutralize the wafer, the effect would only be noticeable if particles are neutralized. Let us compare these hypothesis with the data gathered in figures 56a, 56b and 56c.

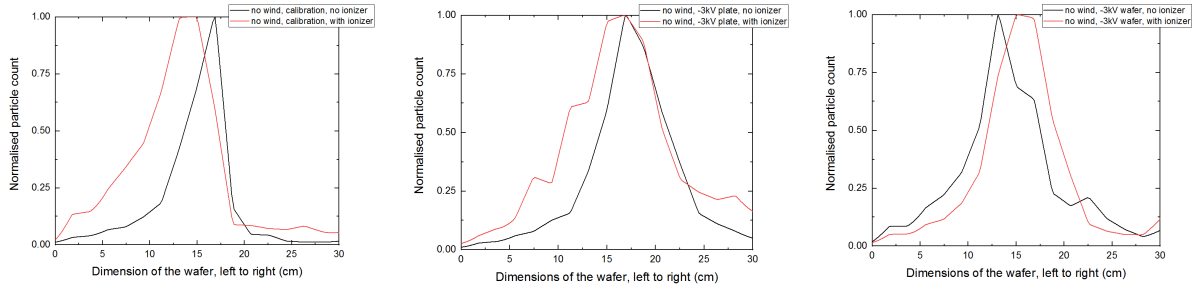

(a) *Calibration* ***(b)*** *Negatively charged plate* ***(c)*** *Negatively charged wafer*

Figure 56: *No wind measurements and comparisons if the ionizer was turned on or off. For the plate measurements, the ground was located on the left and the charged plate on the right with a distance of 50 cm in between.*

Firstly, the calibration data. As can be seen in figure 56a, the data with ionizer turned on deviates more to the left than the measurement with the ionizer off. A hypothesis should be developed why this happens. The emitter points might create a field near the inlet which attracts particles. However, this seems unlikely, since the particle inlet is far away (10 cm) from the ionizer compared to other objects and the other emitter point (1.5 cm apart). The results as shown in this paragraph did suffer from the fact that the polyamide particles are small and likely to charge. This resulted in contamination in the tubes towards the particle counter and the particle counter itself. Due to the contamination in unwanted places, more noise was detected compared to the measurements in glass and copper and a correction was done to eliminate this noise.

This calibration could have an effect on the second graph (figure 56b) , namely the negatively charged plate measurements. A second cause of particles not deviating that much could be based on the hypothesis stated above: either the particles or the plate gets (partly) neutralized, causing static charge to be less dominant, decreasing deviation and making particles land more towards the center of the wafer again. Another and final explanation might be the neutralization of the inlet. Each material has a certain capacitance (the maximum amount of static charge it can hold). If this level is reached, it is easier to charge a material using charge induced charge separation. When the ionizer is present near the inlet, it might be able to neutralize the inlet (partly). This will in its turn create a neutral inlet again, which could have an effect on the charging of glass particles.

For the third graph (figure 56c) the particles would normally deviate radially outwards because of the wafer field (which is shaped like a long point charge, where the e-field lines move away from the wafer and bent outwards towards the wall of the wind tunnel). This is indeed seen in the first calibration measurement with no ionizer. The particles which would normally land somewhat out of center are pushed even more out of center. The ionizer balances this phenomenon. This time, it does not seem if the same effect as in the calibration (figure 56a) played a role; the particle would deviate even more towards the left if the particles were already pulled towards the left slightly when leaving the inlet. However, when doing the error analysis, it has been shown that all three figures are not significantly different from each other (as can be seen in appendix N.3). This would mean that at no wind conditions, the ionizer does not have a large effect on the neutralization of particles.

For the scenario with wind, the results are expected to be different. The flow of air ensures particles are not airborne for a long duration, resulting in a lower chance to be neutralized by ions. Furthermore, since the flow works parallel to the plate, one would expect less ions to reach the plate and neutralize the plate. The neutralization of the wafer however could be increased, since the flow with ions is moving perpendicular to the wafer. In short, no deviations are expected in the calibration measurement, smaller deviations are expected in the plate and wafer measurements. Since the no wind graphs were already insignificant, it might be logical to conclude that the graphs as shown in figures 57a, 57b and 57c are also not significant. This has also been shown in appendix N.3. The hypothesis that the ionizer would have less effect seems to be true for these graphs. Comparing figure 56b with 57b and figure 56c with 57c, it can be seen that the deviation

from the calibration (black line) is indeed less for both cases with the ionizer (red line). One does have to consider how significant this result is, and if this can be stated as a definite proof.

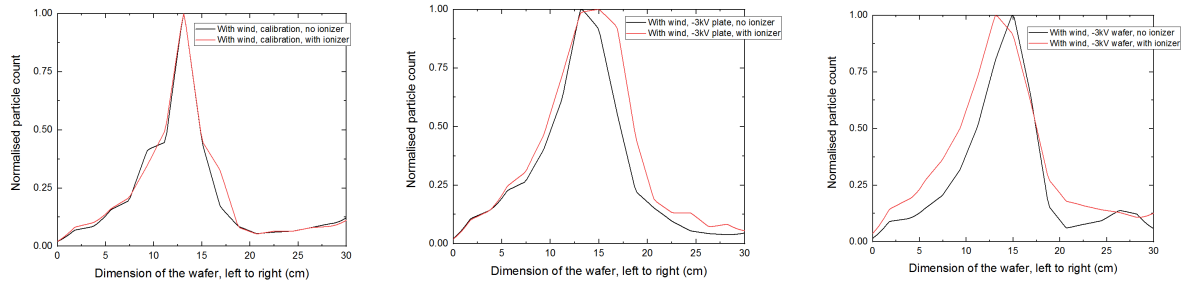

(a) *Calibration* ***(b)*** *Negatively charged plate* ***(c)*** *Negatively charged wafer*

Figure 57: *With wind measurements and comparisons if the ionizer was turned on or off. For the plate measurements, the ground was located on the left and the negatively charged plate on the right with a distance of 50 cm in between.*

A reasoning why the ionizer does not work can be found by doing simulations. The space charge significantly drops when introducing some kind of flow to the setup. Furthermore, this flow is not fast enough to force ions towards a certain surface or particle. A fast flow applied directly to a material does neutralize a statically charged surface, as seen in chapter 5.7. The time present between the time of ion generation and the surface which needs to be neutralized is too large. Another reason why the neutralization does not work is because of turbulence. The ionizer will create a lot of eddies, causing a lot of ions to also follow streamlines which never hit the wafer or particles. This results in a lot of ionization being wasted.

An example of a field with the corresponding space charge can be seen in figure 58a and 58b. In figure 58a the charged plate and the corresponding electric field can be seen on the left, as well as two rounds with one charged positively and one negatively (at the top of the setup). These rounds resemble the ionizer with a bipolar setting. In figure 58b, the space charge throughout the setup can be seen with a flow of 0.4 m/s present. The electric field looks homogeneous and no sudden changes happen. This is different for the space charge, where some deviation can be seen in the figure near the ionizer. Notice however must be paid to the legend showing the difference between the bright red and blue areas: the difference is only $2 * 10^{19}$ C/m^3. As can also be seen in this figure that, due to the wind, all ions distribute over the whole wind tunnel (after some startup time, the simulation is stationary and simulates the final stable situation)

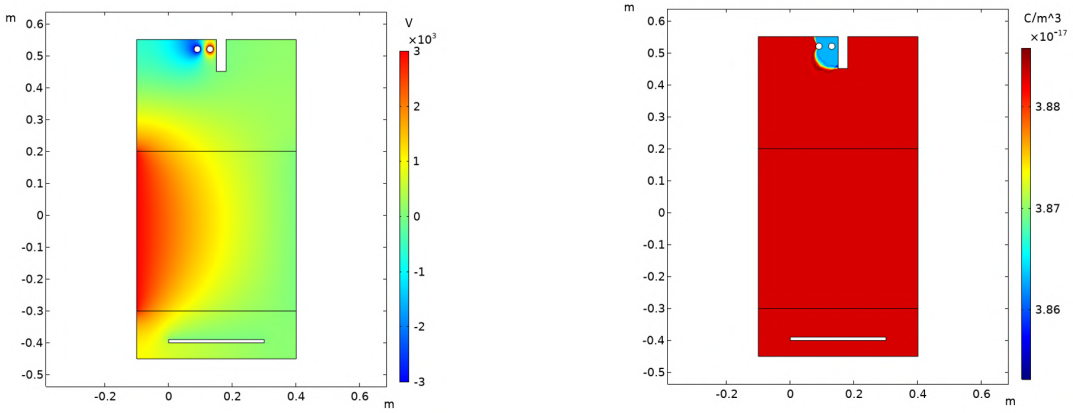

(a) *Field in the wind tunnel with ionizer* ***(b)*** *Space charge with ionizer*

Figure 58: *The field and the corresponding space charge of the setup with the ionizer installed in the wind tunnel directly (thus without external pressurised flow) but with a flow of 0.4 m/s.*

To conclude, no neutralization method with the ionizer worked so-far. It is recommended that this study is continued, as will be explained in chapter 7. For now, all particles, with and without flow and in a horizontal and vertical wind tunnel are measured. This was done using a particle counter which did not provide any information about the trajectory of the particle in the wind tunnel itself. This is why a laser will be used to execute in situ measurements in chapter 5.9.

5.9 Vertical wind tunnel, laser measurements of trajectories and particle diameters

To validate the measurements done in chapter 5.8.2, a laser and a camera have been used to visualise particle trajectories. The particles used in this chapter are polyamide seeding particles. More details about the setup and the method used can be found in chapter 3. Using the laser measurement: the position during travel, the velocity and diameter of the particle can be determined. First, a look will be taken to the particle position in a situation where there is no electric field to compare this situation to an situation with an electric field (both with no flow present). Secondly, the velocity will be determined of the smallest particles visible to calculate the minimum mass and diameter of the particles using two methods. Finally, a discussion will be given on the advantages and disadvantages of this method.

To discover the particle deviation at different positions in the wind tunnel. The laser was positioned on different locations. Every 8 cm from the inlet (starting at 8 cm, since at 0 cm the particle location is known) the laser was positioned in such a way that the particles fell through the lasers beam, scattering light at 90 degrees, which in turn was captured with a camera. To get reliable measurements, a lot of particles were dropped in a small time-frame to get as many bright spots as possible. One such a bright spot is depicted in figure 59b. Stripes were used in the wind tunnel as a reference to convert from pixels to cm, and in this way, the deviation as shown in figure 59b could be calculated. Adding up all those bright spots using a Matlab script (appendix chapter P) and averaging gave us the result as shown in figure 59a. This experiment was executed as a calibration (shown by the black line) and once again with a negative field of -6 kV/m, shown by the red line (the plate was charged with -3 kV with a distance of 0.5 m between plate and ground). As can also be seen in this figure, the method of measuring is not very accurate. The expectation for the black line would be an average of 0, while the red line should be linearly increasing (drag force and electric force reach equilibrium fast because of terminal horizontal velocity). But the end outcome for the red line is close to what has been found in chapter 5.8.2, namely a 0.71 cm deviation. The 0.71 cm was calculated by comparing a reference measurement with a measurement including a -6 kV/m electric field. Figure 59a predicts this average deviation to be around 0.83 cm (the final two data points of the red line averaged to increase accuracy).

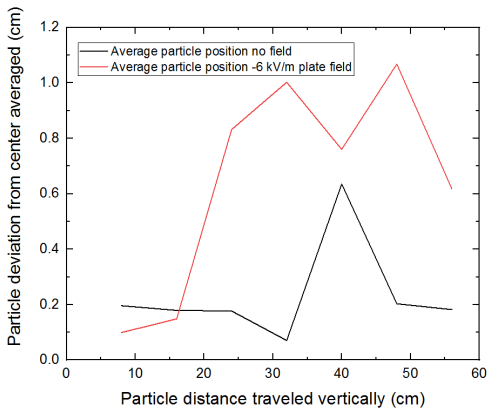

(a) Deviation from center in electric field

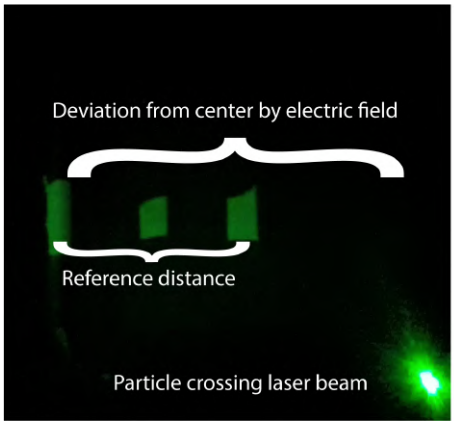

(b) Particles deviating from center

Figure 59: *The deviation caused by electric fields measured by a laser and a camera. Several flashes of light as displayed in the right figure are analysed to give the average deviation*

Next, by visualising the particles for a longer duration of time, the particle velocity can be determined. Assuming a perfect sphere and knowing the particles density, one can calculate the diameter from the velocity of the particle (since the terminal velocity is reached after tenths of milliseconds). To start with calculating the velocity, two methods can be used. In the first method, the laser light is shined on a slightly reflective surface to increase ambient light. This enables the camera to capture a longer path of the particle. Using the distance the particle travelled, the frame-rate and the difference in frames between two pictures, one can easily calculate the velocity. The smallest particle which was visible on the film for a long duration of time travelled at 0.021 m/s, which means a diameter of 26 µm (averaged over 100 frames). The method and the particles that were followed are shown in figure 60a. This figure consists of two pictures and the details of the footage. Even smaller particles can be seen, but these measurements are not very reliable. Looking at a particle traveling through the laser beam and knowing the width of the beam, one can calculate how many frames the particle is visible. In some footage (60 frames per second), particles are visible for 16 frames in the 3 mm wide beam. This would mean a velocity of 0.011 m/s, which translates to a particle that is 19 µm in diameter. Smaller particles can thus be identified, but with less confidence in the velocity

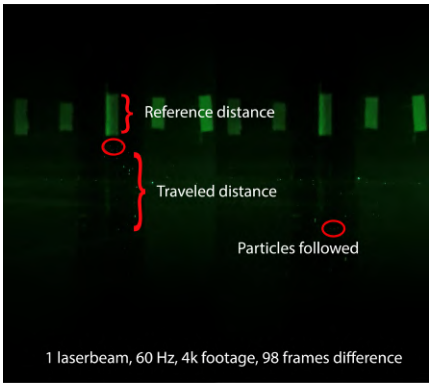

(a) Method 1 of analysing particle velocity

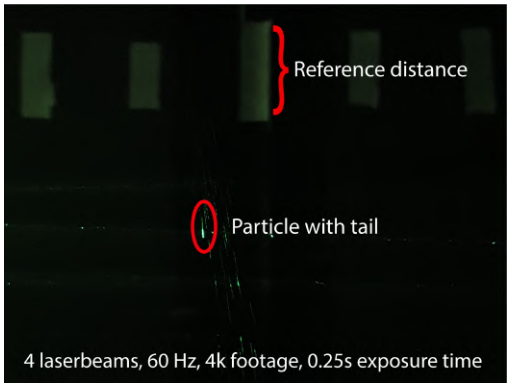

(b) Method 2 of analysing particle velocity

Figure 60: *Two methods of measuring particle velocity. 1) a video where the time between frames is taken to calculate travelled distance. 2) a picture with a long exposure time and the tail distance is taken as distance reference.*

Another method to calculate the velocity of particles is to use photos with a long exposure time. For this method, more light is needed. To achieve this, mirrors were placed in the wind tunnel to be able to reflect the laser, giving a total of 4 laser beams going across the wind tunnel. This enables the camera to capture a lot of light and visualise a part of the particle trajectory. The exposure time is known and by measuring the tail of light of the particle in one such an image, the particle velocity can be determined. Using this method, the velocity of the smallest particle was 0.018 m/s. This in turn means a diameter of approximately 24 µm. As shown by these calculations, both methods can visualise the same class particles, that is particles of approximately 25 µm and up. An example of such a measurement is shown in figure 60b.

This chapter thus gives a proof of concept: larger particles can be visualised by a 5 mW laser and a camera due to scattering, and the deviation of these particles can be measured as well. There are only some small advantages to this method, namely one does not have to touch the wafer or wind tunnel to do the measurements. Furthermore, this method is cheaper to execute (no particle counter is required). But the method has more disadvantages such as:

- A lot of particles need to be dropped. Only a small fraction of the particles will travel through the laser beam.
- The method is a lot more time intensive. The laser has to be relocated a lot, requiring calibration every time. The video footage also needs to be analysed, and a 1 minute 4k resolution video is easily 0.5 gb in size.
- Since the laser has to be relocated often, the plate needs to be recharged often as well.

- The method is not very accurate, as only a few large flashes of light occur.
- It is hard to visualise smaller particles. To be able to visualise particles of 5 µm, stronger lasers and lenses are necessary. This goes against the advantage of cost effectiveness and the laser would shine with such a high intensity that it would become unsafe to handle.
- It is hard to visualise particles with more velocity, making it almost impossible to capture any flashes of light when the wind of the wind tunnel is turned on.
- The laser can not be used to close to the wafer (causing reflection in the camera), which makes it hard to visualise particles close to the wafer.

As made clear by this summation of disadvantages, it is easier to use the particle counter for more reliable and fast results. This is why, in this whole thesis, the particle counter has been used as the default research method. This result did however prove that it is possible to use a laser to visualise part of the trajectory.

5.10 Vertical wind tunnel, temperature effects on particles

This chapter is an extra chapter, which explains why it is important to let the charged plates and wafers cool down to the ambient temperature before starting experiments. It was discovered in all no-wind experiments that the temperature did influence the measurements if no cool down time was taken. This chapter will discuss the measurements that were done, the simulations that were made based upon these results and at which convective flows the particles deviation is noticeable. The effect of temperature is only noticeable at low enough speeds, so this would be at only a few places in the AWH.

In the vertical wind tunnel experiment, effects of the temperature were already noticeable at 1 degree Celsius difference. When statically charging the wafer by contact, the temperature would also rise with 1-1.5 degree Celsius. To gain understanding about this effect, different temperature differences and the particle deposition position were measured. These results are visible in figure 61a, were the largest influence on the particles is visible for the highest temperature. Noticeable is how at larger temperature differences, the particles do not fall near the center of the wafer anymore. Even the heaviest particles are affected and have a change in trajectory. This phenomenon was not seen in the electrical studies of previous chapters.

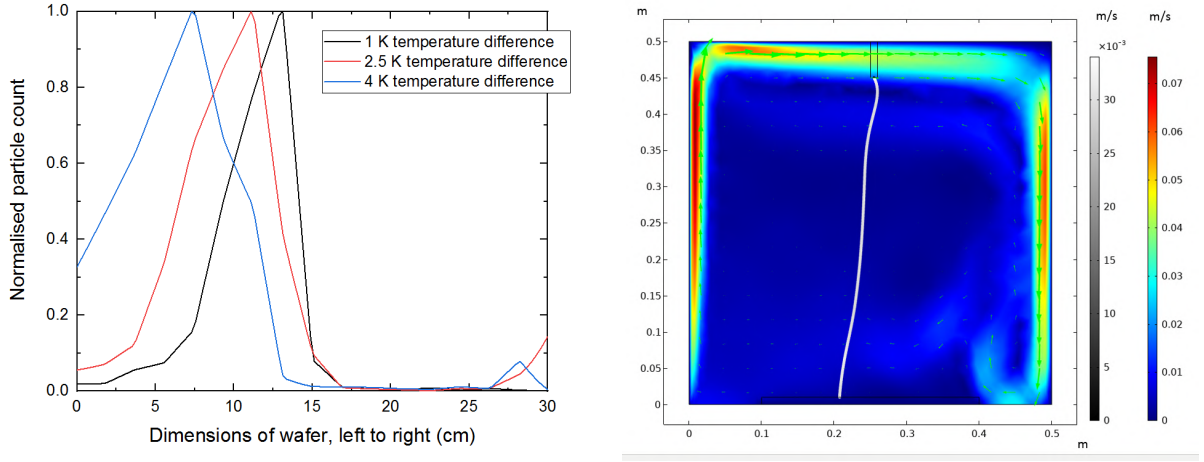

(a) Experimental temperature difference *(b) Simulated temperature difference*

Figure 61: *The experimental results of different temperatures on the particle deposition position on the wafer. The simulation shows that 20 µm glass particles and plates with a 2.5 C° difference have the same deviation*

The cause of these particles deviating is the flow that is created from convection. The simulation as seen in figure 61b is the convective flow that is created by a 2.5 C° difference. The flow goes up, bounces against

the filter and flows down on the other side of the wind tunnel. Here, part of the flow will be lost since the wafer does not fill the whole area. In figure 61b the flow can leave via an outlet in the bottom right corner. However, some flow will also bounce from the wafer and result in a flow the left. This flow eventually causes the particle to land out of center. As can be seen in the simulation as well, the speed of the flow does not have to be big at all. The flow in the middle of the simulation (dark blue) is somewhere around 0.01 m/s, but since the particles are suspended in the wind tunnel for a longer duration (14.9 seconds for a 20 µm glass particle diameter), this slow wind can have a large effect.

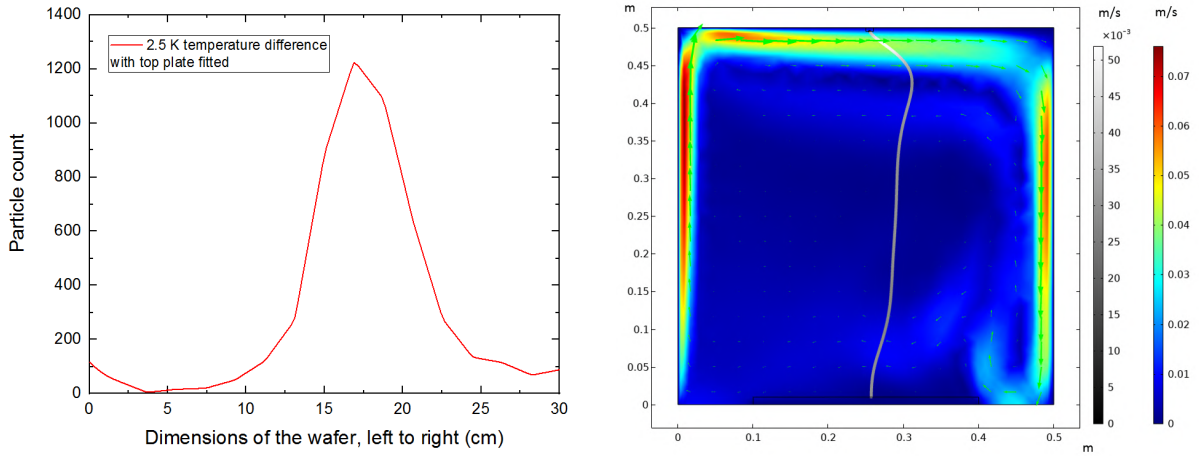

(a) Experimental temperature difference *(b) Simulated temperature difference*

Figure 62: *The experimental results of a top plate being added to the setup making the outlet at the same level as the top of the wind tunnel. The simulation shows that 20 µm glass particles and plates with a 2.5 C ° difference have the same deviation*

In the previous paragraph the particle inlet was extended 5 cm from the filter. In the following experiment, this inlet was reduced to 0 cm. The addition of an extra ceiling plate resulted in the same functioning of the outlet, but only the farthest end of the cone outlet being visible and poking through the plate. This time, the results with the same temperature difference of 2.5 degrees showed that particles do fall in the middle of the wafer. The flow caused by temperature has to be largely conserved, so any flow to the right must be compensated by a flow to the left. The problem in previous experiment was that the particles could not travel with the flow going to the right side on the top of the wind tunnel, since the outlet extended in the wind tunnel. Figures 62a and 62b show these results. To conclude, one must pay attention when doing experiments in the wind tunnel with no flow and temperature differences present. A top plate can partly solve the problem, but even better is to let the statically charged plates cool down to room temperature after charging.

To conclude and as done throughout this thesis, it is important to let the plates and wafers cool if the charge remains on the wafer for long enough. This effect is also a good explanation of what happened during the experiments with the positive plates (as seen in chapter 46a)

5.11 Summary of the measurements

It has been found that particles clump together in the horizontal wind experiments, meaning smaller particles will deposit on places where they are not expected. This is true for glass and copper particles. SEM images show how these particles clump. When adding an electric field to the setup, the glass particles (positively charged) deviate according to the applied field (negatively charged plate or wafer). So, contamination can be increased or decreased using electric fields. For copper particles, this effect was also seen, but only when using a glass inlet. The glass inlet maximizes triboelectric charging. For other inlets such as plastic and metal, no significant deviation from the starting trajectory was found.

In the vertical wind tunnel, particles spread out about 5 cm. Also, the inlet position has to be taken into account in order to not disturb the flow. It has been shown that increasing the wind speed minimizes particle contamination for glass particles because of their large size. In the vertical wind tunnel with no flow present experiments can be executed to maximize the deviation of particles. This shows significant effects for glass particles and enables us to calculate the charge on the particles according to their size. This charging is caused by triboelectric charging. For copper particles, this charging was minimal, causing no deviation to occur for copper particles in the horizontal wind tunnel. The glass and copper particles were too large (also due to clumping) to show a significant effect in negative fields applied to the wafer or when the flow was turned on. Furthermore, positive fields did not show the expected result, and possible causes should be hypothesized.

An ionizer can be used to neutralize surfaces. Faster neutralization occurs when the ionizer is used at small distances with a large flow and is directly applied to the charged material. This was not the case in the wind tunnel, since the distance between the ionizer and charged surfaces are large and the flow is weak for both tested scenarios. This caused no significant changes in trajectory of the particles when the ionizer was present.

The trajectories of the particles can be investigated using a laser. By calculating the velocity of the particle it has been concluded that 25 µm particles could be easily visualised. This technique however has many disadvantages compared to the particle counter setup. Finally, temperature measurements have shown that if not taken into account, convection can play a role in the deviation of particles from their calibration trajectory. This is why it is important to let all the components in the wind tunnel cool down to room temperature, especially if experiments without a flow are executed.

6 Discussion

The discussion will be split into several parts. These parts consist of the major findings of the study, the limitations of the findings and an explanation for any surprising or inconclusive results. The discussion will provide a larger overview of what has been done, what could have gone better and which results are not yet fully clear.

6.1 Relation between theory, simulations and measurements

Each theory section and force will be discussed to see the influence it has on the setup and results (chapter 5) and if the influence is the same as would be expected by theory (chapter 2.3). Also, models that were discussed in the theory (chapter 2) will be considered when discussing and comparing the theory with the results. Some results were already briefly discussed in the results section. This section will provide an overview of that discussion in one chapter.

6.1.1 Flow in the wind tunnel

As can be seen in the contour plots 22b, approximately 30 cm in the wind tunnel, deviation in the center of the wind tunnel are hard to find (thus creating an uniform flow). The flow is measured to be 0.4 ± 0.02 m/s. Furthermore, wind measurements with smoke and a laser have confirmed the eddy's and turbulence that are expected in the wind tunnel. Also the no-slip condition and boundary layers were verified. For the boundary layer, the position of the wafer does not matter, as seen by comparing figure 80 in the appendix with the results (in figures 35b and 34b).

6.1.2 Charging and neutralization of particles

Triboelectric charging is the largest charging mechanism in the wind tunnel. This was seen in chapter 5.5.3, where the calculated amount of charged particles coincided with the expected amount of particles receiving some kind of charge. The triboelectric series can be seen in figure 8. As was expected from theory, the metal inlet had less effect compared to a plastic inlet using glass particles, as can be seen in figure 47a. The charge that was calculated during these measurement fell within the current maximum amount of charge (100 e/μm^2) per surface area, as shown in table 4 and source [52]. Also, the chapter of triboelectric charging (chapter 2.2.2) shows methods of charge induced and contact induced charging. Both mechanisms were used throughout this thesis, and it was indeed confirmed that contact induced charging of metals is not easy to do (as seen in figure 8). It is also stated that the static charge is especially active in the first 30 nm of the surface. The wafers supplied by VDL do not have a native oxide layer, explaining why there is no silicon oxide layer to hold the charge. Finally, formula 14 proposed that there is an exponential decay of static charge. This was also seen in figure 81 in the appendix. In the experiment, a glass substrate was charged and the resistivity calculated. This results matched the found value of resistivity for glass in literature.

The airflow over the ionizer emitter points is not that large, as can be seen in 28. This flow will even be slower if no external flow is used and the emitter points are placed directly in the wind tunnel. This is why, during our study, no significant results could be found for the ionizer. Also, the space charge as proposed is only veracious for lower pressures, and this might result in errors in the final result of the simulations. The space charge as expected from the model (in a no wind scenario) is to high, compared to the results. Furthermore, chapter 2.2.3 proposed that particles should have some kind of charge which is Gaussian distributed. Due to other effects (such as minor flows in the wind tunnel or particle-particle interactions) this was however to hard to measure with the current equipment. Finally, figure 9 shows that the ionizer has an ideal ion balance for a charged insulator. The measurement shown in figure 53 indeed confirm the functioning of the ionizer and the difference between ions and neutralization times.

6.1.3 Forces on the particles

Gravity and drag force

As can be seen in figure 34b, the red lines show the calculated behavior in this flow (with a boundary layer, but this effect would be minimal for the largest particles of 50 µm). The purple line in figure 34b stops exactly where the force of gravity, drag and a flow combined would expect the particle to land. This in turn concludes that for these simple experiments including drag, flow and gravity behave as expected by theory.

Electrophoresis

As suggested in the theory already, the diffusion and electric field charging mechanisms only occur in high field (20 kV/m). The fields and ions per cubic cm are not met in the wind tunnel, and so table 12 shows a result which is to large compared to the results. The same goes for formulas 30 and 31, where 1 second in the wind tunnel with given constants gives a charge of 38 e for diffusion charging and 47 e for electric field charging. This would not compare nicely with the calculated charge of 36 e on a 5 µm glass particle. During the thesis then, these formulas could not be verified and were not used when interpreting the results.

Another result which was tested and is correct are the results as presented in figures 13a and 13b. Starting with the horizontal wind tunnel as visualised in figure 13b, it shows deviation even for larger particle sizes. This was also seen in the executed experiments (such as figure 40 or figure 77a in the appendix). For the vertical wind tunnel, no deviation should be found for the flows with the downward flow. This was shown in figure 48 and figure 77b in the appendix (although sometimes, small deviations were visible) for both fields on the wafer and plate. Simulations confirm the lack of deviation from trajectory for charged wafers as well, visible in table 6. These results were thus also predicted by previous literature, and even smaller particles should be investigated to see the classic v shape from figures 13a and 13b. In no wind scenarios, theory did give the expected results, as will be discussed in the next paragraph.

To conclude, all particles in negative fields behave as expected when knowing the charge of the particle. This charge could not be precisely calculated at the start of the experiments. So, the experiment was executed first, the charge calculated and simulations with this calculated charge were done. This connected the theory with the simulations and measurements.

Thermophoresis

Convection does play a role when heating up certain surfaces in no wind conditions. This convection could perfectly explain why particles deviate in the wind tunnel, as explained in chapter 5.10. In chapter 5.10, models and results are compared side to side to be able to explain the deviation. The thermophoresis force is to weak to cause deviations, as expected from theory.

Adhesion forces

As stated in chapter 2.3.5, the adhesion force of the sphere with the wafer can be described by the DMR model. The models do assume however that the contact between the bodies is elastic, and this assumption may not be fully true. The exact forces were not measured during the experiments, but the assumption that smaller particles are harder to remove was however confirmed in experiments. This can be seen in table 8, where the wafer was scanned multiple times. After the first measurement, the >5 µm particles decrease with 95.5 percent while the 0.1-0.15 µm bin decreases with 74 percent (meaning relatively, more small particles are left behind).

Another clue that the roughness and surface energy can make a difference, can be found by looking at the measurements in figures 41a and 41b. In these figures the reference lines for both wafers are significantly far apart. This could be caused by the increased turbulence that is created by a rougher surface (thus increasing lift forces and turbophoresis) and the difference in thickness of the wafer. Another reason might be that in one wafer measurement the particle counter was closer to the wafer, resulting in more particles. Finally,

and also a probable explanation, is that the adhesion and roughness causes another pull-off force which can increase or decrease particle count.

6.2 Limitations of the findings

As in all studies, this study also has its limitations. One of the largest limitations was the choice of particle counter. The Solair 1100 is fabricated to measure particles smaller than 5 µm, but a lot of particles were larger than that. This would also limit the number of particles which could be sucked up and analysed by the particle counter. The largest clusters would contaminate the particle counter itself. When this happened, the particle counter would need to be cleaned, taking up part of the budget and time for the project. Furthermore, the tubes connecting the particle counter to the plotter could become contaminated due to the size of the particles. The glass and polyamide particles were chosen because of their availability at VDL and the quantities at which these particles were available.

Another limitation was the clumping of particles. This made it harder to visualize single particles. One particle would be insignificant when placed near a clump of a couple 100 particles. This problem could be solved using a direct measurement, as done with the laser. However to visualise smaller particles, stronger lasers or better camera equipment with lenses would be necessary. This equipment was not readily available and a stronger laser would require more severe safety measurements. The same argumentation can be used for the insulating plates used in these experiments, since conductive plates would be more dangerous under high voltage and a high voltage source was not available.

A limitation due to time constraint is the method at which the particle counter and plotter is used. each position is counted for 12 seconds at 197 positions. These points are discrete. A better method would involve some kind of overlap between the positions, but this would increase the time a wafer needs to be analysed. Due to the amount of experiments which were done this was not a possibility.

6.3 Explaining unexpected or inconclusive results

There are only three unexpected or inconclusive results based on theory and the predictions. The first results which needs more discussion is the deviation of particles in positive fields. The second issue has to do with the COMSOL space charge simulations, which suggest that in no wind conditions, the particles would always deviate. The third unexpected result were the copper particles, which did deviate under the influence of electric fields in the horizontal wind tunnel, but did not deviate in the vertical wind tunnel

First, the positive fields. In all experiments with all kind of particles, the particles did not deviate in the same manner as they would in a negative field. This could be because of several reasons. Firstly, the charging mechanism is different. To create a positive field, charge induced charging is used instead of contact induced charging. However, even after this charging process, the electrostatic field meter does give a positive readout. In another experiment where a glass plate was used and charged with contact induced charging (similar to the creation of negative fields), the particles did not seem to deviate as well. The reason therefore is not totally clear, but a hypothesis can be created. A list of reasons was already given in the results section, but some of the reasons are: 1) the positive field is harder to create, making the field weaker. 2) The charge decay of positive fields is faster than those of negative fields, again making the field weaker. 3) Because of this quicker decay, the positively charged plates were not always fully cooled down to room temperature. The effect of temperature is in the opposite direction then that of the positive field, cancelling each other out.

Another inconclusive result is given by the COMSOL simulations. These simulations concluded that the space charge generated by the plates and the ionizer in no wind conditions is sufficient to make all particles deviate. In almost all experiments it has been found that the largest amount of particles is still centered, meaning that only the smaller particles deviate. Furthermore, it has been seen that the change of the inlet material can drastically affect the particles charge and therefore trajectory. Therefore, the space charge could have had a minor effect, but concluding from the experiments with different inlets it is evident that the triboelectric effect is a larger charging mechanism. Furthermore, simulations pointed out that COMSOL is indeed a black box model. The results regarding space charge were not always consistent and convergence was

hard to achieve in some models. A final answer to see if the space charge is indeed a significant phenomenon could be explored by doing more laser measurements to see if the particle trajectory is linear or exponential. These laser measurements must however be more accurate than measured before in chapter 5.9.

Finally, the copper particles deviation. There was a difference visible between the vertical and horizontal measurement of the copper particles with electric fields present. The horizontal experiments did show a significant deviation in particle trajectory and deposition, where the vertical experiments did not. The hypothesis is that the difference in the results are caused by two differences in the setup: 1) for the vertical setup, the wafer charge experiments oppose gravity. However, the particles do not have a horizontal pointing vector in their trajectory. Meaning that even if these forces were the exact opposite, gravity would still win and particles would not be moved sideways enough. For the horizontal wafer, the force also opposes gravity, but this time the flow causes a large velocity towards the side of the wafer. This combined with the boundary effect causes particles to deposit less frequently. 2) The amount of contact between particles might have been larger in the vertical setup. In the vertical wind tunnel, the flow is disturbed by the inlet. This could mean that copper particles interact more before starting their free-fall. When they do make contact, they will not gain any charge. Also, the inlet of the horizontal wind tunnel experienced more rough shakes compared to the vertical wind tunnel (because of the construction).

7 Conclusion and Recommendations

This conclusion will be a briefer summary of the results gathered and already discussed in the discussion. In this chapter, simplifications are made to visualise which particles do deviate in electric fields. Also, the applicability of the study is discussed and recommendations for future studies are made.

7.1 Overview of the results

The research question at the start of the study was as follows: How can the particle trajectories be controlled using static electricity in horizontal and vertical wind flows? There seem to be multiple answers to this single question, since it depends on each situation (particle material, inlet material, plate/wafer/ionizer charge). Let us first take a look at the horizontal wind tunnel. A summary of these results are shown in figure 63. As can be seen, insulating particles such as glass show changes in their trajectories for both a charged plate and charged wafer in the horizontal wind tunnel. For copper particles, this change in trajectory was inlet dependent: A glass inlet could significantly alter the copper particles trajectory. For the vertical wind tunnel, glass and polyamide particles only showed significant deviation when no wind was present. Copper particles never showed any significant deviation in the vertical wind tunnel. For all non-significant scenarios, it is expected that smaller particles will be significant. For both setups, the ionizer did not function in the current setup, and different methods have to be used in order to neutralize specific surfaces or particles. This is caused by the distance between the ionizer and the flow velocity.

In figure 63, the green color displays a significant result. The orange color displays a result which is not significant, but small deviations could be seen visually or by using the SEM. Also, the orange color is used when certain inlets did create a change in trajectory, where others did not. The red color shows no significant effect at all.

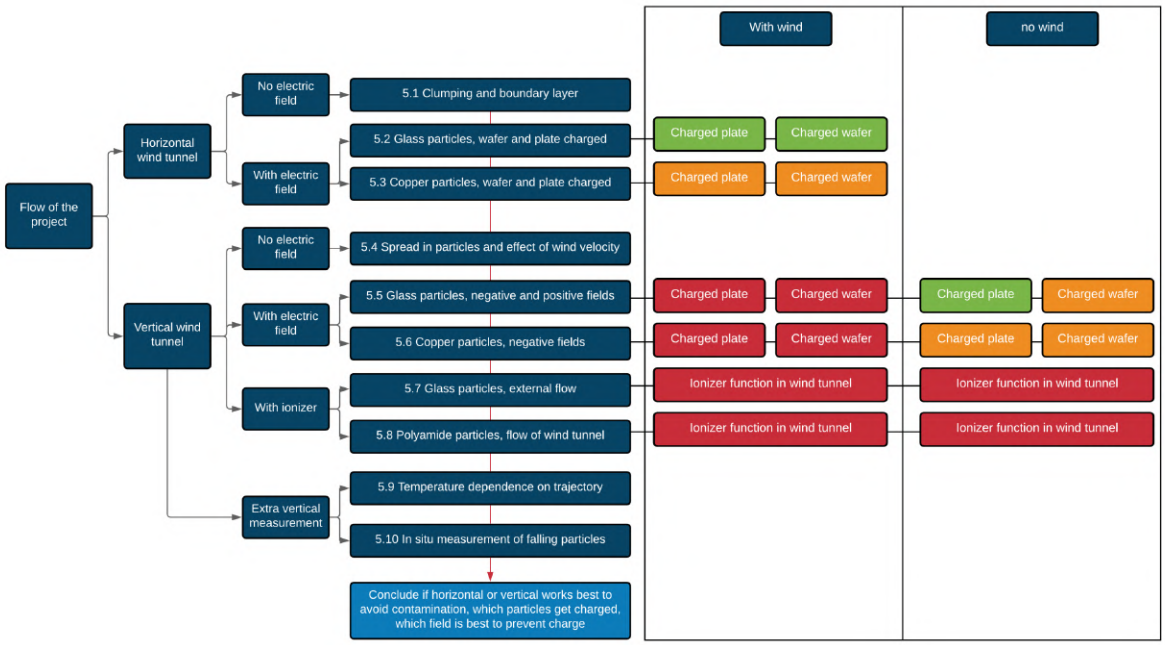

Figure 63: *All possible configurations being researched in the horizontal and vertical wind tunnel, with different particles, with or without wind. The graph shows in which experiments a significant deviation could be found.*

This would mean that the hypothesis could be answered as follows: Particle trajectories can be controlled and altered using electric fields using different directions of electric fields, different inlet materials and different particles. Let us make the translation from these results to the AWH to see how contamination can be prevented in the AWH itself. The summation below will provide the conclusions as stated earlier, and how they can be applied to the AWH:

- Identify where fields are present: as seen in this thesis, knowing the direction and polarity of the electric field can decrease or increase contamination. Keep the fields which decrease contamination.
- Neutralize fields which increase contamination: this thesis has shown that it is possible to neutralize surfaces with the ionizer if the ionizer is used correctly.
- Choose materials which are unlikely to charge: if particle contamination is increased due to the field on the wafer (for example a negative field and a lot of glass particles in the AWH), pick a different building material which is unlikely to charge.
- Or choose materials which are more likely to charge: if particle contamination is decreased due to the field on the wafer (for example a positive field and a lot of glass particles in the AWH), use this material in places where it is not yet used.

To put it in other words: VDL should research which particles and which fields are present in the AWH. Only then can be determined if using or keeping these electric fields would be beneficial or negative. If it does provide a negative result, a neutralization method should be used. It is therefore, and this can not be stressed enough, situation dependent if an electric field can prevent contamination of particles on the wafer.

7.2 Applicability and contribution

This thesis was started by mentioning why it is important for chips not to get contaminated. That will namely result in defects of the chips and cause chips to not function properly. The consequence being that chips have to be thrown away and less chips can be produced per minute, which causes losses for the manufacturer. This research has tried to prevent this contamination using electric fields. Also, this research uses real particles to examine the deposition, whereas VDL has often only used flow and streamlines to look at particle deposition. This research has shown that this is not always reliable, since streamlines would never touch the wafer whereas particles do. Furthermore, one knows that there are electric fields present on the wafer and other surfaces, so using them to our advantage can be useful. This will cause less deposition of particles, less defaults in chips and therefore a higher profit per wafer.

Knowing this, the design of the AWH can be altered to have the following options:

- Have an ionizer present which has a separate and faster flow than the AWH itself. This will ensure the neutralization of specific surfaces. By neutralizing surfaces, particles are not attracted to the surface and follow the field lines more closely.
- Be aware of areas in the AWH where different kind of materials touch and interact which each other. This could lead to triboelectric charging of these particles.
- Take into account the different kinds of particles in the AWH, and understand that conducting and insulating particles do not follow the same electrostatic and electrodynamics laws.
- In areas where the flow is slow, electric fields can be used to attract particles. The flow reaches a minimal near the boundaries of the AWH, where large vortexes lift the air back up. Since most particles develop near the moving parts (such as the gripper arm), this could be an ideal place to catch (insulating) particles.
- Understand that different sizes of particles can cause more or less changes in trajectory due to electric field. Smaller particles will be (according to simulations) easier to attract with electric fields. This is also why electrets are used in HEPA filters.

These are some of the measures which could be taken to use the electric field to the advantage of the user and prevent contamination. Furthermore, this thesis can be used in future experiments to approximate the effect of electrostatic charge on particles. This will not only create more understanding of the researched phenomenon, but it will also ensure more precise results in future experiments.

7.3 Suggestions for further research

This research was a simplification of the setup which needed to be improved, namely the AWH. A logical next step in this research would be the translation of this project to the AWH. This thesis could include where the static charge causes most deviation of particles and how this can be used to the advantage of the user to prevent contamination. When these locations are known, different flow profiles or ionizer setups could be used to neutralize the charge in unwanted areas, reducing the risk of particles moving towards the wafer because of electrophoresis. This ionizer setup should be capable of producing a higher ion concentration compared to the ionizer used in this thesis.

Another part of the research that needs to be completed is the simulation and experimental validation of contamination on a moving wafer. In all experiments in this thesis, the wafer remained stationary. In the AWH however, the wafer moves rapidly, causing particles trajectory to change. This complex flow profile would also bring with it the chance of particles to deposit more easily on the wafer. In all experiments in this thesis, either a horizontal or vertical flow was being used. When moving a wafer, a combination of flow directions might be the best option. This would again complicate the situation, but ensure that when the wafer is moving, a boundary layer is present at all times.

Another thing which can be improved in this research is accuracy. Firstly, this could be done by ordering particles of one unique size. This would reduce particle clumping and ensure that each particle that is counted, is of that specific size. This would improve estimations of particle charge. Secondly, applying plates that are conductive and can withstand high voltages would ensure a more even profile. This would also ensure that the particle inlet is at a potential of zero, taking away the possible electrostatic effects at play in the inlet due to the electric field. Thirdly, an in situ measurement technique would ensure that the particle trajectories can be better visualised and understood. It also reduces the amount of assumptions necessary, which is always an improvement on the current thesis.

References

[1] *Vision and mission of ASML*. https://www.asml.com/en/company/about-asml/vision-and-mission. [Online; accessed 05-02-2021].

[2] Karen Reinhardt and Werner Kern. *Handbook of silicon wafer cleaning technology*. William Andrew, 2018.

[3] *Entrance length (fluid dynamics)*. https://en.wikipedia.org/wiki/Entrance_length_(fluid_dynamics). [Online; accessed 13-01-2021]. 2014.

[4] William C Hinds. *Aerosol technology: properties, behavior, and measurement of airborne particles*. John Wiley & Sons, 1999.

[5] JV Sengers et al. "Kinetic theory of drag on objects in nearly free molecular flow". In: *Physica A: Statistical Mechanics and its Applications* 413 (2014), pp. 409–425.

[6] Richard Häfeli. "Fluid dynamic characterization of single-and multiphase flow in structured porous media". MA thesis. ETH-Zürich, 2010.

[7] Tuncer Cebeci. *Analysis of Turbulent Flows with Computer Programs*. Elsevier, 2004.

[8] aokomoriuta. *Law of the wall*. https://en.wikipedia.org/wiki/Law_of_the_wall. [Online; accessed 13-01-2021]. 2011.

[9] Hermann Schlichting and Klaus Gersten. *Boundary-layer theory*. Springer, 2016.

[10] Ivan Marusic et al. "On the logarithmic region in wall turbulence". In: *Journal of Fluid Mechanics* 716 (2013).

[11] Shinhao Yang et al. "Aerosol penetration properties of an electret filter with submicron aerosols with various operating factors". In: *Journal of Environmental Science and Health Part A* 42.1 (2007), pp. 51–57.

[12] Rashmi Thakur, Dipayan Das, and Apurba Das. "Electret air filters". In: *Separation & Purification Reviews* 42.2 (2013), pp. 87–129.

[13] Kwang-Chul Noh et al. "Filtration of submicron aerosol particles using a carbon fiber ionizer-assisted electret filter". In: *Aerosol and Air Quality Research* 11.7 (2011), pp. 811–821.

[14] Benjamin YH Liu and Kang-ho Ahn. "Particle deposition on semiconductor wafers". In: *Aerosol Science and Technology* 6.3 (1987), pp. 215–224.

[15] David J Griffiths. *Introduction to electrodynamics*. 2005.

[16] AM Seyam, W Oxenham, and T Theyson. "Antistatic and electrically conductive finishes for textiles". In: *Functional finishes for textiles*. Elsevier, 2015, pp. 513–553.

[17] Yeon Joo Kim et al. "Effect of the relative permittivity of oxides on the performance of triboelectric nanogenerators". In: *RSC advances* 7.78 (2017), pp. 49368–49373.

[18] Herbert B Michaelson. "The work function of the elements and its periodicity". In: *Journal of applied physics* 48.11 (1977), pp. 4729–4733.

[19] AF Labadz and J Lowell. "Contact charge density and penetration depth". In: *Journal of electrostatics* 26.3 (1991), pp. 251–260.

[20] Niels Jonassen. *Electrostatics*. Springer Science & Business Media, 2013.

[21] Albert E Seaver. "An equation for charge decay valid in both conductors and insulators". In: *arXiv preprint arXiv:0801.4182* (2008).

[22] Anne Marie Helmenstine. "Table of electrical resistivity and conductivity". In: *ThoughtCo. Sep* 24 (2018), p. 2018.

[23] Jie Zhao. "Study of the Effect of Rubbing Materials on the Tribo-electrification of Textile Materials". In: (2003).

[24] Kashmiri Lal Mittal. *Particles on Surfaces: Detection: Adhesion, and Removal*. CRC Press, 1994.

[25] Arnold J Steinman. "Preventing Electrostatic Problems in Semiconductor Manufacturing". In: *Compliance Engineering* 21 (2004), pp. 89–93.

[26] Christian Bohling and Wolfgang Sigmund. "Self-limitation of native oxides explained". In: *Silicon* 8.3 (2016), pp. 339–343.

[27] Abhishek Rathi and Bjoern Martin. "Surface charging of Silicon dioxide & Aluminum oxide structures". In: *16th International Workshop on Physics of Semiconductor Devices*. Vol. 8549. International Society for Optics and Photonics. 2012, 85491Y.
[28] Wouter Olthuis and Piet Bergveld. "On the charge storage and decay mechanism in silicon dioxide electrets". In: *IEEE Transactions on Electrical Insulation* 27.4 (1992), pp. 691–697.
[29] Anatolii D Zimon. *Adhesion of dust and powder*. Springer Science & Business Media, 2012.
[30] A Revil. "On charge accumulation in heterogeneous porous rocks under the influence of an external electric field". In: *Geophysics* 78.4 (2013), pp. D271–D291.
[31] Tadahiro Ohmi, Seiji Sudoh, and Hiroyuki Mishima. "Static charge removal with IPA solution". In: *IEEE Transactions on semiconductor manufacturing* 7.4 (1994), pp. 440–446.
[32] Boy van Minderhout et al. "Charge neutralisation of microparticles by pulsing a low-pressure shielded spatial plasma afterglow". In: *Plasma Sources Science and Technology* (2021).
[33] Arnold Steinman. "Reducing electrostatic related defects in photolithography". In: *International Symposium on Semiconductor Manufacturing, Extended Abstracts of ISSM*. IEEE. 1994, pp. 179–182.
[34] Katsuyuki Takahashi et al. "Development of a Corona Discharge Ionizer Utilizing High-Voltage AC Power Supply Driven by PWM Inverter for Highly Efficient Electrostatic Elimination". In: *Electrostatics-Applications in Physics, Chemistry, Biology and Others*. IntechOpen, 2019.
[35] Joseph M Crowley et al. "Equivalent circuits for air ionizers used in static control". In: *Journal of electrostatics* 61.2 (2004), pp. 71–83.
[36] Bangwoo Han et al. "Unipolar charging of fine and ultra-fine particles using carbon fiber ionizers". In: *Aerosol Science and Technology* 42.10 (2008), pp. 793–800.
[37] Aurora Hernandez-Sierra, Francisco José Alguacil, and M Alonso. "Unipolar charging of nanometer aerosol particles in a corona ionizer". In: *Journal of Aerosol Science* 34.6 (2003), pp. 733–745.
[38] A Ohsawa. "Efficient charge neutralization with an ac corona ionizer". In: *Journal of electrostatics* 65.9 (2007), pp. 598–606.
[39] Toru Ikeuchi et al. "Neutralization by a corona discharge ionizer in nitrogen atmosphere". In: *Electrical Engineering in Japan* 177.3 (2011), pp. 1–8.
[40] Motoaki Adachi, David YH Pui, and Benjamin YH Liu. "Aerosol charge neutralization by a corona ionizer". In: *Aerosol science and technology* 18.1 (1993), pp. 48–58.
[41] Kenkichi Nagato et al. "An analysis of the evolution of negative ions produced by a corona ionizer in air". In: *International Journal of Mass Spectrometry* 248.3 (2006), pp. 142–147.
[42] Daniel J Rader and Anthony S Geller. "Particle transport modelling in semiconductor process environments". In: *Plasma Sources Science and Technology* 3.3 (1994), p. 426.
[43] Subhasish Dey, Sk Zeeshan Ali, and Ellora Padhi. "Terminal fall velocity: the legacy of Stokes from the perspective of fluvial hydraulics". In: *Proceedings of the Royal Society A* 475.2228 (2019), p. 20190277.
[44] SAJ Morsi and AJ Alexander. "An investigation of particle trajectories in two-phase flow systems". In: *Journal of Fluid mechanics* 55.2 (1972), pp. 193–208.
[45] Daniele Pugliesi. *Law of the wall*. https://en.wikipedia.org/wiki/Law_of_the_wall. [Online; accessed 13-01-2021]. 2012.
[46] Denis Keefe, Philip J Nolan, and Theodor Alfred Rich. "Charge equilibrium in aerosols according to the Boltzmann law". In: *Proceedings of the Royal Irish Academy. Section A: Mathematical and Physical Sciences*. Vol. 60. JSTOR. 1959, pp. 27–45.
[47] Chunhong He and Goodarz Ahmadi. "Particle deposition in a nearly developed turbulent duct flow with electrophoresis". In: *Journal of Aerosol Science* 30.6 (1999), pp. 739–758.
[48] ASML. *specifications of TWINSCAN NXE:3400B*. https://www.asml.com/en/products/euv-lithography-systems/twinscan-nxe3400b. [Online; accessed 07-02-2020]. 2020.
[49] Marcos Vinícius Rodrigues et al. "Measurement of the electrostatic charge in airborne particles: II-particle charge distribution of different aerosols". In: *Brazilian Journal of Chemical Engineering* 23.1 (2006), pp. 125–133.
[50] LV Deputatova et al. "Measurement of the charge of a single dust particle". In: *Journal of Physics: Conference Series*. Vol. 653. 1. IOP Publishing. 2015, p. 012129.
[51] CN Davies. "Definitive equations for the fluid resistance of spheres". In: *Proceedings of the Physical Society* 57.4 (1945), p. 259.

[52] Stefano Alois et al. "Quantifying the contact electrification of aerosolized insulating particles". In: *Powder Technology* 332 (2018), pp. 106–113.
[53] Boy van Minderhout et al. "The charge of micro-particles in a low pressure spatial plasma afterglow". In: *Journal of Physics D: Applied Physics* 52.32 (2019), 32LT03.
[54] WD Marra Jr and JR Coury. "Measurement of the electrostatic charge in airborne particles: I-development of the equipment and preliminary results". In: *Brazilian Journal of Chemical Engineering* 17.1 (2000), pp. 39–50.
[55] David B. O'Hara et al. "Aerosol particle charging by free electrons". In: *Journal of Aerosol Science* 20.3 (1989), pp. 313 –330. ISSN: 0021-8502. DOI: https://doi.org/10.1016/0021-8502(89)90007-4. URL: http://www.sciencedirect.com/science/article/pii/0021850289900074.
[56] RH McKnight. "The measurement of net space charge density using air filtration methods". In: *IEEE transactions on power apparatus and systems* 4 (1985), pp. 971–976.
[57] Win Labuda Lodevicus Hermans. "Electrostatic Charges in the Production Environment of the Semiconductor Industry". In: *ReinRaumTechnik* 1,2,3 (2005), pp. 1–31.
[58] Takeshi Hattori et al. *Ultraclean surface processing of silicon wafers: secrets of VLSI manufacturing*. Springer Science & Business Media, 2013.
[59] Phil A Lawless. "Particle charging bounds, symmetry relations, and an analytic charging rate model for the continuum regime". In: *Journal of Aerosol Science* 27.2 (1996), pp. 191–215.
[60] S Opiolka, F Schmidt, and H Fissan. "Combined effects of electrophoresis and thermophoresis on particle deposition onto flat surfaces". In: *Journal of Aerosol Science* 25.4 (1994), pp. 665–671.
[61] Job Beckers et al. "Particle contamination control by application of plasma". In: *Extreme Ultraviolet (EUV) Lithography XI*. Vol. 11323. International Society for Optics and Photonics. 2020, p. 113232L.
[62] Handol Lee and Se-Jin Yook. "Deposition velocity of particles in charge equilibrium onto a flat plate in parallel airflow under the influence of simultaneous electrophoresis and thermophoresis". In: *Journal of aerosol science* 67 (2014), pp. 166–176.
[63] Alison J Buckley, Matthew D Wright, and Denis L Henshaw. "A technique for rapid estimation of the charge distribution of submicron aerosols under atmospheric conditions". In: *Aerosol Science and Technology* 42.12 (2008), pp. 1042–1051.
[64] Indra Adhiwidjaja et al. "Simultaneous phenomenon of particle deposition and reentrainment in charged aerosol flow—effects of particle charge and external electric field on the deposition layer". In: *Advanced Powder Technology* 11.2 (2000), pp. 221–233.
[65] Frank Stratmann, Heinz Fissan, and Thomas Peterson. "Particle deposition onto a flat surface from a point particle source". In: *The Journal of Environmental Sciences* 31.6 (1988), pp. 39–41.
[66] Gwi-Nam Bae, Chun Sik Lee, and Seung O Park. "Measurements and control of particle deposition velocity on a horizontal wafer with thermophoretic effect". In: *Aerosol science and technology* 23.3 (1995), pp. 321–330.
[67] Zhao-Qin Yin et al. "Thermophoresis and Brownian motion effects on nanoparticle deposition inside a 90 square bend tube". In: *Aerosol Air Qual Res* 18.7 (2018), pp. 1746–1755.
[68] Chuen-Jinn Tsai et al. "Thermophoretic deposition of particles in laminar and turbulent tube flows". In: *Aerosol Science and Technology* 38.2 (2004), pp. 131–139.
[69] Francisco J Romay et al. "Thermophoretic deposition of aerosol particles in turbulent pipe flow". In: *Journal of Aerosol Science* 29.8 (1998), pp. 943–959.
[70] Frank P Incropera et al. *Fundamentals of heat and mass transfer*. Wiley, 2007.
[71] Jun Zhang et al. "Fundamentals and applications of inertial microfluidics: a review". In: *Lab on a Chip* 16.1 (2016), pp. 10–34.
[72] J Halbritter. "Torque on a rotating ellipsoid in a rarefied gas". In: *Zeitschrift für Naturforschung A* 29.12 (1974), pp. 1717–1722.
[73] Karl I Borg, Lars H Söderholm, and Hanno Essén. "Force on a spinning sphere moving in a rarefied gas". In: *Physics of Fluids* 15.3 (2003), pp. 736–741.
[74] Dino Di Carlo et al. "Particle segregation and dynamics in confined flows". In: *Physical review letters* 102.9 (2009), p. 094503.
[75] Xue-Yong Zou et al. "Effects of the Magnus and Saffman forces on the saltation trajectories of sand grain". In: *Geomorphology* 90.1-2 (2007), pp. 11–22.

[76] Abhijit Guha. "A unified Eulerian theory of turbulent deposition to smooth and rough surfaces". In: *Journal of Aerosol Science* 28.8 (1997), pp. 1517–1537.
[77] Abhijit Guha. "Transport and deposition of particles in turbulent and laminar flow". In: *Annu. Rev. Fluid Mech.* 40 (2008), pp. 311–341.
[78] John Young and Angus Leeming. "A theory of particle deposition in turbulent pipe flow". In: *Journal of Fluid Mechanics* 340 (1997), pp. 129–159.
[79] Mehdi Soltani and Goodarz Ahmadi. "On particle adhesion and removal mechanisms in turbulent flows". In: *Journal of Adhesion Science and Technology* 8.7 (1994), pp. 763–785.
[80] Lieng-Huang Lee. *Fundamentals of adhesion*. Springer Science & Business Media, 2013.
[81] Lars-Oliver Heim et al. "Adhesion and friction forces between spherical micrometer-sized particles". In: *Physical Review Letters* 83.16 (1999), p. 3328.
[82] Robert Jones et al. "Adhesion forces between glass and silicon surfaces in air studied by AFM: Effects of relative humidity, particle size, roughness, and surface treatment". In: *Langmuir* 18.21 (2002), pp. 8045–8055.
[83] RJ Jaccodine. "Surface energy of germanium and silicon". In: *Journal of the electrochemical society* 110.6 (1963), p. 524.
[84] MB Ranade. "Adhesion and removal of fine particles on surfaces". In: *Aerosol Science and Technology* 7.2 (1987), pp. 161–176.
[85] Hyojin Kweon, Sotira Yiacoumi, and Costas Tsouris. "The role of electrostatic charge in the adhesion of spherical particles onto planar surfaces in atmospheric systems". In: *Colloids and Surfaces A: Physicochemical and Engineering Aspects* 481 (2015), pp. 583–590.
[86] François Gensdarmes. "Chapter 1.3 - Methods of Detection and Characterization". In: *Nanoengineering*. Ed. by Patricia I. Dolez. Amsterdam: Elsevier, 2015, pp. 55 –84. ISBN: 978-0-444-62747-6. DOI: https://doi.org/10.1016/B978-0-444-62747-6.00003-8. URL: http://www.sciencedirect.com/science/article/pii/B9780444627476000038.
[87] Mehrzad Shams, Goodarz Ahmadi, and Hasan Rahimzadeh. "A sublayer model for deposition of nano- and micro-particles in turbulent flows". In: *Chemical engineering science* 55.24 (2000), pp. 6097–6107.
[88] L.E.A.Janssen. "Particle Deposition in a Horizontal Channel Flow". In: (2019).
[89] Qiang Yuan et al. "Mechanical and thermal properties of high-density polyethylene toughened with glass beads". In: *Journal of applied polymer science* 89.8 (2003), pp. 2102–2107.
[90] Jim Curtis and Howard Siegerman. "Ionizer pin cleaning maintains performance Avoiding contaminant build-up is critical for controlling electrostatic charge". In: *ITW Simco and Texwipe* (October 2006).
[91] Chenghang Zheng et al. "Numerical simulation of corona discharge and particle transport behavior with the particle space charge effect". In: *Journal of Aerosol Science* 118 (2018), pp. 22–33.
[92] H Ait Said, H Nouri, and Y Zebboudj. "Effect of air flow on corona discharge in wire-to-plate electrostatic precipitator". In: *Journal of Electrostatics* 73 (2015), pp. 19–25.
[93] SH Kim and KW Lee. "Experimental study of electrostatic precipitator performance and comparison with existing theoretical prediction models". In: *Journal of Electrostatics* 48.1 (1999), pp. 3–25.
[94] JCA van Huijstee et al. "Plasma assisted particle contamination control: plasma charging dependence on particle morphology". In: *Metrology, Inspection, and Process Control for Semiconductor Manufacturing XXXV*. Vol. 11611. International Society for Optics and Photonics. 2021, 116113A.
[95] Yakov I Rabinovich et al. "Adhesion between nanoscale rough surfaces: II. Measurement and comparison with theory". In: *Journal of colloid and interface science* 232.1 (2000), pp. 17–24.
[96] Daniel J Lacks and Artem Levandovsky. "Effect of particle size distribution on the polarity of triboelectric charging in granular insulator systems". In: *Journal of Electrostatics* 65.2 (2007), pp. 107–112.
[97] Silicon Valley Microelectronics. *Silicon Wafer Manufacturing Process*. https://www.svmi.com/silicon-wafer-manufacturing-semiconductor-process/. [Online; accessed 09-April-2020]. 2018.
[98] Borivoje Nikolic. *Chapter 2 The manufacturing Process*. http://bwrcs.eecs.berkeley.edu/Classes/icdesign/ee141_f01/Notes/chapter2.pdf. [Online; accessed 09-April-2020]. 2000.
[99] *CMOS*. https://en.wikipedia.org/wiki/CMOS. [Online; accessed 13-01-2021]. 2014.
[100] Haifeng Zhang and Goodarz Ahmadi. "Aerosol particle transport and deposition in vertical and horizontal turbulent duct flows". In: *Journal of Fluid Mechanics* 406 (2000), pp. 55–80.
[101] M Bahrami. "Forced convection heat transfer". In: *Simon Fraser University* (2009).

[102] Bahman Zohuri. "Forced Convection Heat Transfer". In: May 2017, pp. 323–345. ISBN: 978-3-319-53828-0. DOI: 10.1007/978-3-319-53829-7_9.

[103] W. Thielicke and Stamhuis. "PIVlab – Towards User-friendly, Affordable and Accurate Digital Particle Image Velocimetry in MATLAB". In: *Journal of Open Research Software* 2.30 (2014).

[104] Thi Quynh Nguyen et al. "Identification and quantification of FOUP molecular contaminants inducing defects in integrated circuits manufacturing". In: *Microelectronic Engineering* 105 (2013), pp. 124–129.

Appendices

A Table of constants

Name	Symbol	Value
C_d	Drag coefficient sphere	0.47
d_w	Wafer diameter	0.3 m
e	Elementary charge	$1.602 * 10^{-19}$
g	Gravitational constant	9.81
k	Thermal conductivity air at 293K	0.024 W m^{-1} K
L	Length of the wind tunnel	2 m
W	Width of the wind tunnel	0.59 m
H	Height of the wind tunnel	0.315 m
μ	Dynamic viscosity at room temperature	$1.81 * 10^{-5}$ kg $m^{-1}s^{-1}$
ν	Kinematic viscosity at room temperature	$1.48 * 10^{-5}m^2s^{-1}$
Pr	Prandtl number at room temperature	0.707
ρ	Density air	1.225 kg m$^-3$
V_{bv}	breakdown voltage air	$3 * 10^6$ V m^{-1}
m_e	mass electron	$9.11 * 10^{-31}$ kg
q	charge electron	$1.602 * 10^{-19}$ C
ϵ_0	vacuum permittivity	$8.854 * 10^{-12}$ C V^{-1} m
μ_0	vacuum permeability	$4\pi * 10^{-7}$ N A^{-2}
K_b	Boltzmann constant	$1.38 * 10^{-23}$ J K^{-1}
p	atmospheric pressure	101.325 Pa
λ	Mean free path in air	68 nm
h	heat transfer coefficient air	50 W m^{-2} K

Table 7: *Table of all physical constants used in this thesis*

B Scope, Constraints, requirements and assumptions

B.1 Scope

The main question of this research will be: How can the particle trajectories be controlled using static electricity in horizontal and vertical wind flows. The sub-questions of this research will thus be: How are the trajectories of microscopic particles influenced by an electric field in an uniform flow? How does the trajectory change if either the wafer, wall or particles are charged? Is there a difference between different particle materials? Can we predict the behavior of these particles? Which flow velocity is the best to prevent contamination on the wafer and why? And can we use an electric field in our advantage to prevent contamination on the wafer? How would such a setup look like and would it be applicable to build in the atmospheric wafer handler?

B.2 Constraints

Constraints are limitations or restrictions imposed on the project. These constraints are often subdivided in three parts (called the triple constraints): time, scope and costs. These three subjects will be split up in this paragraph and discussed.

- The time to complete the project is limited to one year. Tasks that include electric fields and the deviation of particles will be prioritized, subjects and research topics such as temperature, using turbulence or exploring different research methods will be focused on later in the project if time allows to.
- Scope: the scope of the project will be limited to the wind tunnel and not explore any measurements in the AWH itself. It will only include two to three kinds of particles, of which one is conductive and

one is insulating. The measurements will be executed both in no wind and 0.4 m/s wind conditions. Finally, the ionizer will be used to research if it has an effect on the static electric fields. The claims made in the result or conclusion must be backed up by literature or simulations.

- Costs: Cost is also defined as resources. There is no hard budget for the project, but the costs must be kept to a minimum. This is done using the existing setup with a particle counter and moving stage, as well as by using the existing wind tunnel. All materials used in the study (except for the particles) will be made by the researcher himself with the tools and materials which are available at VDL ETG.

B.3 Requirements

Requirements are conditions or tasks which must be completed in order to guarantee the success of the project. Again, the requirements can be split into several parts. The 6 classifications are described by the PMBOK 6th edition and are listed below.

- Business requirements – describe why the project is being undertaken.
- Stakeholder requirements – describe the needs of a stakeholder or stakeholder group.
- Solution requirements – describes features, functions, and characteristics of the product, research, or result that will meet the business and stakeholder requirements.
- Functional requirements – describes the behaviors of the product or research.
- Non-Functional requirements – describes the environmental conditions or qualities required for the product or research to be effective.
- Transition requirements – describes the temporary capabilities needed to transition from the current as-is state to the desired future state.
- Project requirements – describes the actions, processes, or other conditions the project needs to meet.
- Quality requirements – describes any condition or criteria to validate the successful completion of a project deliverable or fulfillment of other project requirements.

Now not all requirements are applicable or that important to this project. The transition requirements will be briefly discussed (how can the acquired knowledge be used in the AWH) but no requirements will be coupled to this. Furthermore, the quality requirement is often used to visualize a new product. Since VDL will not be designing a new AWH, this requirement will also be left out. The remaining requirements will be applied to the project and discussed here:

Business requirements

- The project should give insight to and provide evidence for the change of trajectory of particles in electric fields.
- The project should include a full overview of different kind of particles and different conditions.
- The project should test and validate a solution to the existing problem in the form of an ionizer.

Stakeholder requirements

- The project must be useful in transitioning from the setup to the AWH where the results can be used to prevent contamination
- The particles used as contamination differentiate from the flow. Simulations and results must be gathered to visualize the importance of this effect.

Solution requirements: Functional requirements

- The wind tunnel must be fully enclosed with no outward flow
- The flow should be uniform (with a certain variance which is acceptable), since this causes spread of the deposition.

- The flow with an average velocity of the flow of 0.4 m/s. This velocity can have an error of 5 percent in order for particles to still exert the same behavior.
- The wind tunnel must be stable and rigid so no movements take place when doing the measurements.
- The plates must be uniformly charged within a certain percentage of error and an average of 3 kV.
- The plate with charge must be floating while the charge of the ground plate must be zero.
- The wind tunnel must be stable and rigid so no movements take place when doing the measurements
- Both plates must be of the same length and they will be placed in between the particle inlet and wafer with some room below and above the plates.
- The plates must be of the same temperature which will in all experiments be room temperature.
- The particle counter must be in the range of the falling particles.
- The particle counter must have stopped counting when moving to the next position in order for all available particles to be collected.
- The particle counter must not interfere with the wafer and therefore not touch the wafer during the measurement.
- The particle counter must be attached to a stable setup and at a consistent height to exert the same force for each measurement.
- The particle counter does not collect particles from another position on the wafer, it only collects particle from the given position of the plotter.
- The plotter must move in the same direction and in the same manner in each measurement in order to acquire consistent results.
- The ionizer must exert the same voltage (and therefore create the same amount of ions) in each measurement within a certain margin of error.
- The particles used in the experiment must be of a size 1-10 μm or contain this size of particles.
- The particles in these experiments must have a known distribution in mass and it must be known of what elements the particles are made of. Furthermore, they must be spherical in shape.
- The inlet in which the particles rest must be one material of which the properties are known.
- The inlet must give the same number of particles falling after each shake within a certain margin of error.

Solution requirements: Non-Functional requirements

- The temperature and humidity in the air must be as constant as possible during the measurements.
- The wafer must be handled with great care (using gloves and clothes to not disturb the measurement).
- The charge applied to the wafers will be done using the same method each time.
- The measurement must be within reasonable agreement with the other measurements in the series in order for the measurement to be taken into account.
- The measurements must be validated using error analysis in order to acquire a significant result.

Project requirements

- The measurement will be executed several times and statistically tested. These results will be compared with existing literature and computer simulations.

B.4 Assumptions

An assumption is a thing that is accepted as true or as certain to happen without further proof. However, for research, these assumptions must have some ground and logical thinking in order for them to be used. The assumptions made in this research are listed below.

- The transition to the wind tunnel to the particle plotter does not have a significant effect on the contamination or particles which are on the wafer. The transition is also consistent each time.
- The conducting particles are perfectly conducting (resistance is 0) while the insulating particles are perfectly insulating (resistance is infinity).
- The particles within the bin of the particle counter will be taken to be in the middle of that bin. For example: if the particle bin of 5-10 μm collects particles, the particles will be assumed to be 7.5 μm in diameter.
- The same percentage of particles will be collected each time a wafer is examined for each specific kind of particles.
- The wafer is placed in the same position in the wind tunnel and on the particle plotter each measurement
- The number of particles in the inlet deviates slowly over time, so a certain volume of particles must be present at the inlet to minimize fluctuations.

C Information on chips and wafers

C.1 The making of a chip

The first thing one must know about any kind of transistor is what a n-type and p-type transistors are. The n-type transistor is doped with extra electrons, meaning there are electrons free to move around in the bulk of the material. If one wishes to dope silicon with n-type, phosphorus can be used. Since phosphorus has 5 electrons in its outer shell and silicon only has four, there is one electron left that does not fit in the structure. This extra electron is the electron which is free to move. The opposite goes for p-type transistors, where a hole is free to move. A hole means that one electron is missing, thus a hole can be seen as a positive charge. To dope silicon to get a p-type transistor, boron can be used.

The first step in the process is the fabrication of the silicon wafer itself. This silicon wafer is sliced from a silicon ingot, which is a large cylinder with the correct diameter for the process (in modern production, this is 300 mm). To avoid contamination of the wafer already, the wafer ingot is heated to its melting temperature. As a high temperature coil moves down towards the bottom of the ingot, all contaminants that were on the surface are taken up by the melting silicon. When the heated coil reaches the end of the ingot, it has removed any contamination, and a silicon wafer can be cut from the ingot. This wafer often has a thickness smaller than 1mm. The surface is lapped, etched and polished. A possibility is to put the wafer into a super-heated steam oven at 1000 C° that can even control the thickness of silicon oxide that is formed. After inspection and confirmation that indeed all contaminants are removed and the surface is flat enough, the wafer is ready for further processing. [97]

The next step is to apply a photoresist coating. As the name already suggests, this layer is sensitive to light, which will be useful during the next step. The photoresist is applied by spinning the wafer while a small droplet of photoresist is applied to the center of the wafer. The spinning of the wafer will enable an even distribution of the photoresist over the wafer. After this processing step, UV light irradiates the surface. A certain pattern is used, called a mask, which enables the UV-light to only shine through the mask at certain places. This means that the surface with photoresist now has areas which are treated and not treated. The next step in the process is to remove portions of the photoresist. Important to note is that there are two kinds of photoresist, a negative and positive photoresist. In a negative photoresist, the area that is irradiated by the UV light will remain. In a positive photoresist, the area that is irradiated will dissolve. One can remove the wanted portion of the oxide layer which is now exposed using acid etching (chemical), or plasma etching. Based on which method is used, the wafer also needs to be dried. This can be done using a spin drying technique with water and nitrogen. The process is contamination sensitive, so it

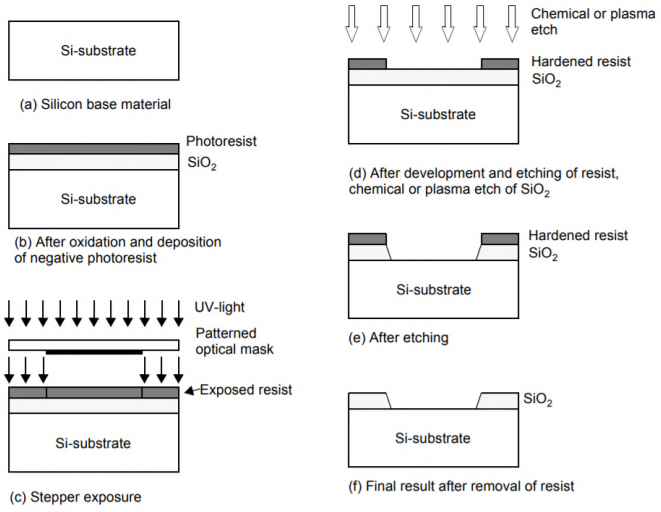

Figure 64: *The typical process a wafer goes through [98].*

is very important that this process takes place in a very clean environment. Now the material consists of an oxide and photoresist layer on one position, and just the bare material on another. In figure 64, this is step (e). After this step, several other processes can take place. Some common examples are atomic diffusion and ion implantation. In atomic diffusion, the wafer is inserted into a hot furnace. The dopants and an inert gas are introduced, and as they pass over the wafer, they will be deposited on the exposed surface. The dopants will enter the surface and create a well. The second method is ion implantation, where a beam of ions is aimed at a specific part of the surface. The ion penetration depth and dosages can be controlled by selecting the beam energy or the amount of dopants. The ion implantation technique takes longer but is more precise than the atomic diffusion technique, where the whole wafer is treated in one go. After this process, a dopant well is formed, and the photoresist layer which remained can be removed using a high temperature plasma. The remaining CMOS process (Complementary metal–oxide–semiconductor) can now start. One is now in step 3 in figure 65 of the CMOS process. The figure itself is pretty self-explanatory, but it is worth mentioning some highlights of the CMOS chip.

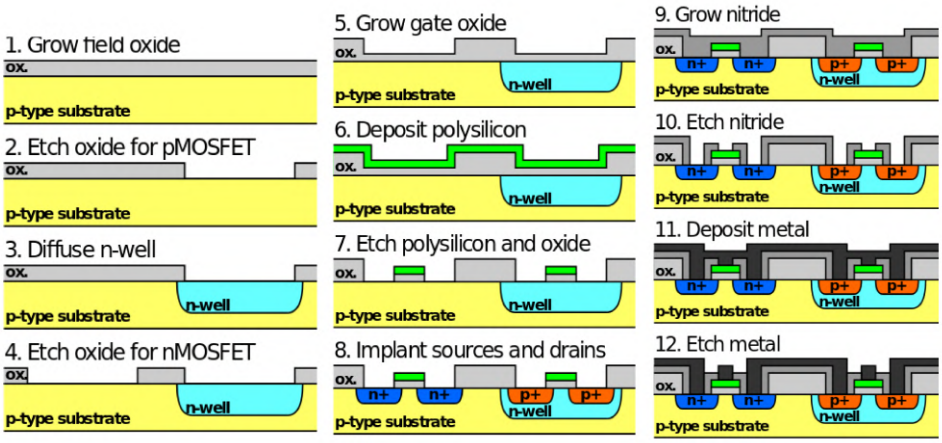

Figure 65: *The production process of a CMOS device given in 12 simplified steps. The sketch is not to scale and often not performed in the same plane [99].*

A CMOS uses both n-type and p-type doped areas. Actually, a CMOS consists out of two type of transistors, a PMOS with holes available to move and a NMOS with electrons available to move. Important to know

is that the PMOS reacts opposite to the signal given to it. In other words, if the PMOS input voltage is high, the output voltage will be low. If the input voltage it low, the output voltage will be high. A NMOS transistor reacts with a signal which is the same as the input because of the free electrons of the n-type material. So if the input voltage is high, the output voltage is high and if the input voltage is low, the output voltage will be low. Combining these two will result in a CMOS, which is thus basically an invertor. A CMOS will react opposingly to the input voltage as well. A positive input results in a negative output and a negative input results in a positive output. It does this by applying the voltage source (VDD) to the PMOS and the ground (VSS) to the NMOS. This is visualised in figure 66. The CMOS is so popular because of its inverting properties. It uses only little power when switched off (negative input becomes positive output). A great example of the application of a CMOS is the small battery which can be found in your computer to hold your bios settings. The CMOS only uses power when switching between transistors, which the bios hardly does. To conclude: the CMOS uses the switches PMOS and NMOS to invert the signal, thus becoming very energy efficient.

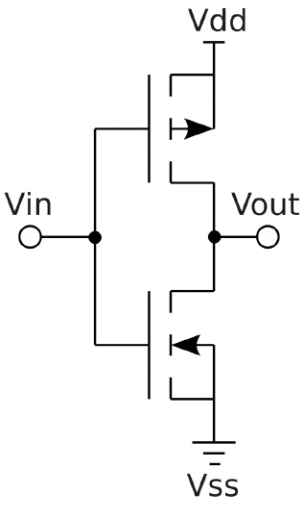

Figure 66: *The typical circuit of a CMOS transistor, the most commonly used transistor in industry because of its energy effectiveness. [99]*

The wafer now consists out of all these transistors but is not done yet. The back end of the line process just started. This process connects different transistors and parts of the wafer through wiring and extra interconnecting metal layers. These layers are made of metal with a dielectric between each metal layer, and a connection between these metal layers is made. When all metal layers are applied, one final passivation layer is used to protect the chip. After this process it is time to test the wafer, mount and dice the wafer (often called die separation) and finally IC package the wafer to avoid any damage. After these steps, the chip is a finalized product and can be used in a variety of applications.

C.2 Classification of contamination

This research will partly focus on subdividing the particles and classifying them by size and force of adhesion. This is done because of several reasons. The test method by yield and reliability can not be used: the wafer which is being used in the experiments is not a functioning one, making it impossible to test the reliability of the wafer. The research of contamination by material is useless: The material of the contamination will be differed, but it will also be known at the start of the experiment, making it unnecessary to actually research. And finally, the classification by detection method is hard to use: the detection methods are limited by the materials which are available during the course of this research, making it hard to distinguish contamination based on this method. So, two classifications will be used to investigate the properties of the contamination: the size, which can be measured by a particle counter, and the force of adhesion, which will differ due to Van der Waals forces or electrostatic forces. A more thorough analyses of all forces acting on the particle

will be discussed in chapter 2.3.

C.3 The process of the AWH

The wafer starts in a carrier handler unit with a FOUP. This FOUP can be locked to prevent contamination and can store 25 wafers with 300 mm in diameter. Attaching the FOUP to the machine is a challenge on its own, since the wafers should not be exposed to the air of the environment. Using hatches and latch keys the FOUP can be opened, exposing the wafer to the inside of the AWH. The unload robot picks up the wafer using a gripper. This gripper works using vacuum pads, so during each loading and unloading stage, the backside of the wafer contacts the gripper. The unload robot has a lower and an upper arm, which enables it to move in many directions. With this freedom to move, the wafer will be placed on the store unit or pre-aligner. The store unit stores the wafer to dry (in immersion systems) and already does part of the temperature conditioning. After the store unit or immediately from the unload robot, the wafer is transported to the pre-aligner. It is here where the wafer receives its uniform temperature. The wafer arrives at the pre-aligner with a temperature difference of ± 1 K. Once it has left the pre-aligner, it will have a uniform temperature with a difference of ± 3 mK. Not only does the pre-aligner ensure a uniform temperature distribution, it also aligns the wafer to the correct position. The wafer has a small nudge, which can be seen using the edge sensor. By rotating and scanning the wafer the nudge will be at a predetermined location, ensuring that all wafers enter the wafer stage in the same configuration. Also, continuously rotating the wafer will ensure an even more uniform temperature distribution. Once both the temperature and alignment are done, the wafer is picked up again using another arm, which is named the load robot in figure 1. The wafer is now transported to the wafer stage or to the vacuum wafer handler. This vacuum wafer handler can be added in the machine to ensure that the wafer is already at the right pressure before entering the wafer stage. In this case the wafer travels from the atmospheric wafer handler to a loadlock to the vacuum wafer handler. The vacuum wafer handler also has a pre-aligner, which ensures that the wafer is conditioned before entering the final stage of the process. If the processing of the wafer is done, the wafer will travel back from the wafer stage to the vacuum wafer handler, to the loadlock to eventually end up in the atmospheric wafer handler again. The atmospheric wafer handler is controlled by the electronic rack, the only device not yet mentioned in this explanation. It takes care of the correct power being supplied to the moving arms. It also controls the heaters, fans and it has a CPU system to control the movement of the loading and unloading arms. A visual impression of the FOUP, the pre-aligner and the store unit can be seen in figure 1.3. This also gives a visual clue of how close the filters will be to the wafer, since the top of the machine (given by the blue frame) is already visible in this figure.

D Deposition velocity and dimensionless relaxation time

The deposition velocity is defined as the ratio of particle flux towards a surface to aerosol concentration above the surface, and it is used to estimate the level of particulate contamination. Following the examples of other research [100] [87], let us express the particles equation of motion, including the drag and gravitational force, as can be seen in equation 44

$$\frac{\mathrm{d}\boldsymbol{v}^{+p}}{\mathrm{d}t^{+}} = \left(1 + 0.15\mathrm{Re_p}^{0.687}\right)\left(\frac{\boldsymbol{v}^{+f}}{\tau_p^{+}} - \frac{\boldsymbol{v}^{+p}}{\tau_p^{+}}\right)\left(t^{+}\right) + \boldsymbol{g}^{+} \tag{44}$$

Where

$$x^{+} = \frac{xu^{*}}{v}, \quad v^{+p} = \frac{v^{p}}{u^{*}}, \quad v^{+f} = \frac{v^{f}}{u^{*}}, \quad t^{+} = \frac{tu^{*2}}{v} \tag{45}$$

represent all the dimensionless time scales. The superscript f denotes the flow, and superscript p the particle. u^{*} represent the flow shear velocity. In equation 44 the particle relaxation time is given by

$$\tau_p^{+} = \frac{1}{18} C_c \frac{\rho^p}{\rho^f} d^{+2} \tag{46}$$

and is thus quadratically related to the dimensionless particle diameter $d^{+} = \frac{du^{*}}{v}$. Also, C_c is the stokes-Cunningham slip correction factor, which is related to the molecular free path. This slip factor is displayed in formula 29.

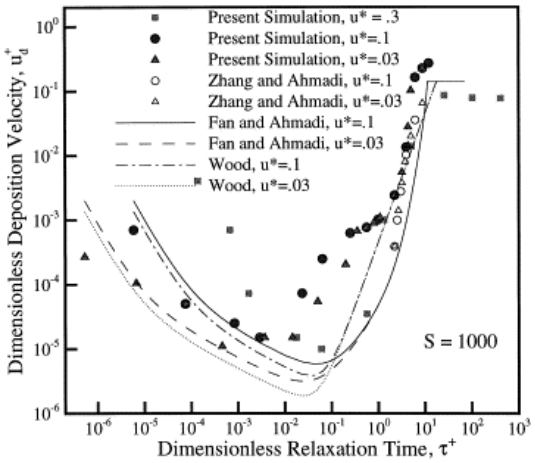

Figure 67: *The dimensionless relaxation time related to the dimensionless deposition velocity. [87]*

Plotting the dimensionless relaxation time and the dimensionless velocity for particles gives figure 67. It is important to discuss this figure since it tells us something about the amount of particles which are reaching the wafer. A higher deposition velocity means more particles are reaching the wafer, which means more contamination. It also states that particles with a relaxation time in the order of 10^{-2} deposit least frequently. The effect of these range of particle sizes is often easy to influence, as can be seen in chapter 2.3.2 and 2.3.3. A relaxation time of the order 10^{-2} resembles a particle with diameter 0.5 µm.

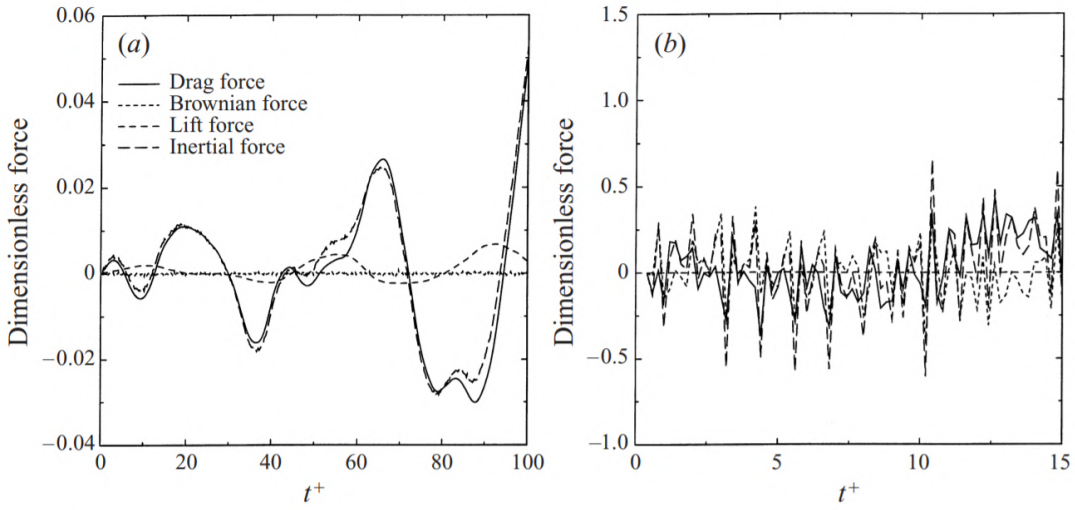

Figure 68: *The variation of several forces over a dimensionless unit of time for a) 15 µm and b) 0.1 µm particles. Visualising that it is hard to describe the motion of small particles because of the larger variations [100].*

Figure 67 however only states the deposition velocity, while this research also focuses on the trajectory of the particles and the forces it experiences during its time airborne. It is therefore important to realize which forces are playing a role when, and the variation of these forces. The variation of the forces and their magnitude is visualised in figure 68. In dimensionless time, forces can vary quite significantly, especially for smaller particles (at which more forces play a considerable role)

E Free convection

Convection can be described more easily using some dimensionless numbers, such as the Nusselt number, the Prandtl number and the Grashof number. The Nusselt number gives the ratio between convective and conductive heat transfer and is defined as $\mathrm{Nu} = \frac{hL}{k}$. The Prandtl number is a dimensionless constant which explains the ratio between the momentum and thermal diffusivity. The Prandtl number is defined as $\mathrm{Pr} = \frac{\nu}{\alpha} = \frac{c_p \mu}{k}$ where c_p is the specific heat and α is the thermal diffusivity. Finally, the Grashof number is the dimensionless number which gives the ratio between the force caused by density changes and viscous forces. It is given by $\mathrm{Gr} = \frac{g\beta\Delta T L^3}{\nu^2}$. [101] [102] However, the most important dimensionless number is the Rayleigh number, which gives the relation between the thermal transport via diffusion and convection. The Rayleigh number is given by: $\mathrm{Ra} = \frac{\Delta\rho V g}{\eta\alpha} = GrPr$ (where η is the dynamic viscosity and α the thermal diffusivity) With these numbers, it can be seen that in a flow of 0.4 m/s, the free convection (or forced convection caused by the flow) is not noticeable. In situations without the flow however, it is predicted that natural convection can play a role in particle transport.

F Confirmation of uniform flow

To validate the velocity results in the wind tunnel, smoke was used to determine the velocity profile. The smoke was analyzed using PIVlab [103]. First, the Matlab script as described in appendix chapter P was used to reduce background noise and form 120 images from a video. These 120 images are then inserted into PIVlab and analysed using this Matlab based program. The desired region of interest is selected and a pixel is transformed to a real distance using several markers in the wind tunnel. These markers in the wind tunnel have a pre-measured distance, so one can translate one pixel to a certain distance. The velocity component of all 120 images is calculated, after which the mean is taken over these 120 images. This mean velocity in the L direction can be saved. This means one ends up with one image (which is the mean of 120 images) that has ± 300 vectors which indicate the velocity of the wind at that certain place in the wind tunnel. These vectors are then plotted in a histogram, as can be seen in figure 69a (close to the filter) and figure 69b (1 meter from the filter). Taking the average value of this histogram will therefore results in the average value of the wind speed over all 120 images.

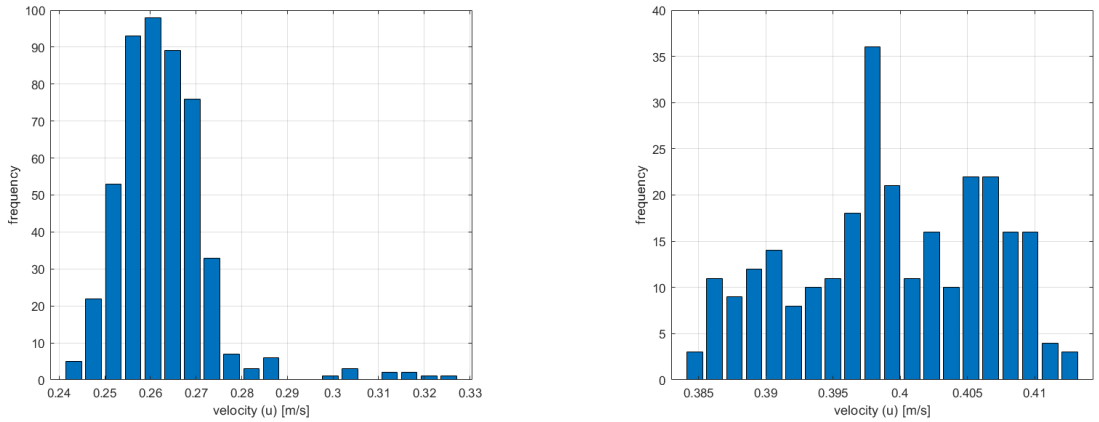

(a) *Velocity of smoke near wafer*

(b) *Velocity of smoke middle wind tunnel*

Figure 69: *Left) velocity of smoke near the filter with mean 0.26 m/s. Right) velocity of smoke in the middle of the wind tunnel with mean 0.4 m/s. Velocity of the wind is 0.4 m/s and the smoke was inserted in the center of the wind tunnel at different positions L.*

A very good agreement with the air velocity meter was found. The smoke again showed velocities ranging from 0.2 to 0.7 m/s when it was blown L=2 cm from the filter. Since the contour plots shown in figure 22b have also shown deviations near the filter, this could have also been expected for the smoke. The result of the measurement close to the filter can be seen in figure 69a where the mean velocity in the L direction is

0.26 m/s. This is thus an example of the smoke being released right after the material, thus slowing down the velocity of the wind and therefore the smoke. The filter also explains the outliers at 0.33 m/s in this graph. The smoke might have blown slightly to the left or right, encountering wind that had not interacted with the material of the filter, and thus the smoke speeds up. As stated before, the frequency in figure 69a gives the amount of vectors that have a certain velocity in the L direction when the mean is taken from the 120 images. This means that from the final mean image, approximately 600 vectors with velocity u in the L direction were plotted in figure 69a and 300 vectors for 69b. The amount of vectors available depends on the density of the smoke, a faster wind speed means that the smoke is more likely to distribute over the wind tunnel faster. Furthermore, the smoke was also blown into the wind tunnel at L=1 m. This resulted in a mean of 0.40 m/s, and the distribution of the velocity magnitude can be found in figure 69b. These two measurements combined have ensured that the wind tunnel flow is uniform and predictable.

G Amount of particles left after the first measurement

Particle diameter (µm)	1st measurement	2nd measurement	3rd measurement	4th measurement
0.1-0.15	130272	34192	11060	4318
0.15-0.2	92348	23066	5331	1925
0.2-0.25	48178	10249	1963	804
0.25-0.3	44795	7809	1225	498
0.3-0.5	42299	5867	809	333
0.5-1	37086	3059	424	169
1-5	34064	2223	308	122
>5	29311	1319	202	70

Table 8: *The difference in particle measurements when measuring one wafer multiple times*

The following experiment was executed to see how many particles would be left after the first, second and third measurement. A certain amount of particles were deposited on the wafer and measured for the first time. These particles were evenly spread over the wafer. After the first measurement was finished, the second measurement was immediately started without interfering with the wafer. This was done for a total of 4 times. The results were summed over the whole wafer and can be seen in table 8. One can see that it is indeed harder to remove small particles from the wafer as suggested by theory (chapter 2.3.5). This can be seen by dividing the second, third or fourth measurement by the first measurement. For example, the ratio of 0.1-0.15 µm particles still being present on the wafer is $\frac{34192}{130272} = 0.265$, while for the >5 µm particles this is $\frac{1319}{29311} = 0.045$. A bigger ratio means that more particles are left compared to the initial amount of particles. This again shows that it is most accurate to measure the >5 µm particles only one time, since there is only a 5 percent error in the measurement. This can be calculated using the first measurement, and dividing this by the amount of particles found in the 2nd, 3rd and 4th measurement summed up. For the smallest particles ranging from 01-0.15 µm, this percentage can exceed 38 percent. So to conclude, it is important to remember that there are still particles present after the first measurement on the wafer. The particles that are present after one measurement are predominantly smaller particles, since they are harder to remove. After the 4 measurements in table 8, SEM measurements were done to determine the particles which were left on the wafer. For the largest of particles (>5 µm), approximately 15 percent is analysed by the particle counter in the first measurement. Using the previously mentioned SEM, an average amount of particles was determined from 5 images to calculate the amount of particles that were left. Important to note is that this 15 percent is measurement dependent. As stated before, smaller particles are harder to remove and the distribution of particles can also play a role. If a lot of particles are centered in the middle (like in the vertical wind tunnel measurements), then it might be harder for the particle counter to collect them all.

H Wall functions and turbulence parameters

The k-ϵ turbulence model assumes that the turbulent viscosity can be modelled using two extra parameters: the turbulent kinetic energy k and the turbulent dissipation rate ϵ. The equation than reads

$$\mu_T = \rho C_\mu \frac{k^2}{\varepsilon} \tag{47}$$

where C_μ is a constant (often 0.09). To solve these parameters, two transport equations have to be solved, given for k by

$$\rho \frac{\partial k}{\partial t} + \rho \mathbf{U} \cdot \nabla k = \nabla \cdot \left(\left(\mu + \frac{\mu_\mathrm{T}}{\sigma_k} \right) \nabla k \right) + P_k - \rho\varepsilon \tag{48}$$

Where P_k is the production term and given by

$$P_k = \mu_\mathrm{T} \left(\nabla \mathbf{U} : \left(\nabla \mathbf{U} + (\nabla \mathbf{U})^T \right) - \frac{2}{3} (\nabla \cdot \mathbf{U})^2 \right) - \frac{2}{3} \rho k \nabla \cdot \mathbf{U} \tag{49}$$

The transport equation for ϵ is given by

$$\rho \frac{\partial \varepsilon}{\partial t} + \rho \mathbf{U} \cdot \nabla \varepsilon = \nabla \cdot \left(\left(\mu + \frac{\mu_\mathrm{T}}{\sigma_\varepsilon} \right) \nabla \varepsilon \right) + C_{\varepsilon 1} \frac{\varepsilon}{k} P_k - C_{\varepsilon 2} \rho \frac{\varepsilon^2}{k} \tag{50}$$

In these set of equations, C_μ, $C_{\epsilon 1}$, $C_{\epsilon 2}$, σ_k and σ_ϵ are all constants determined by literature. To model these functions and thus the flow in COMSOL, initial parameters or start values need to be inserted. These start values are given by the following set of equations. From top to bottom, the equations are calculating the initial values for the turbulent kinetic energy k, the turbulent dissipation rate ϵ, the initial turbulence intensity I and the turbulence length scale l.

$$k = \frac{3}{2}(UI)^2 \tag{51}$$

$$\varepsilon = c_\mu^{\frac{3}{4}} k^{\frac{3}{2}} l^{-1} \tag{52}$$

$$I = 0.16 \mathrm{Re}^{-\frac{1}{8}} \tag{53}$$

$$l = 0.07 \frac{2WH}{W+H} \tag{54}$$

Now, as stated earlier, there is a difference in how these models behave close to the wall. The k-ϵ model uses a wall lift off function. This means that the flow near the wall is not solved in the model. To determine the width of this wall lift off, equation 55 is used in COMSOL.

$$\delta_w = \frac{\delta_w^+ \mu}{\rho u^+} \tag{55}$$

Where δ_w^+ is given by equation 56 and u^+ was given by equation 7. Here, m_m is the height of each mesh cell.

$$\delta_w^+ = \max \left(\frac{m_m}{2} \frac{\rho C_\mu^{1/4} \sqrt{k}}{\mu}, 11.06 \right) \tag{56}$$

To conclude for the k-ϵ model, there are two extra sets of equations which have to be solved, given 4 initial parameters. The flow near the wall is not solved, and therefore the velocity profile near the wall does not go to zero, even though there is a no slip condition. This is an important conclusion for particle deposition.

The SST model uses the previously discussed k-ϵ model in the center of the flow, but combines it with the k-ω model near the walls to retrieve a full picture of the flow. The k-ω model is given by the following set of equations given in 57.

$$\begin{aligned} \rho \frac{\partial k}{\partial t} + \rho \mathbf{U} \cdot \nabla k &= P_k - \rho\beta k\omega + \nabla \cdot \left((\mu + \sigma\mu_\mathrm{T}) \nabla k \right) \\ \rho \frac{\partial \omega}{\partial t} + \rho \mathbf{U} \cdot \nabla \omega &= \alpha \frac{\omega}{k} P_k - \rho\beta\omega^2 + \nabla \cdot \left((\mu + \sigma\mu_\mathrm{T}) \nabla \omega \right) \end{aligned} \tag{57}$$

Where, α, β and σ are constants and $u_T = \rho\frac{k}{\omega}$. The SST model thus solves this equation near the walls. Because the velocity at the walls is zero, so is k. This means that the boundary condition for ω becomes

$$\lim_{D_w \to 0} \omega = \frac{6\mu}{\rho\beta D_w^2} \tag{58}$$

Where D_w is the distance to the wall. Since the mesh wants to avoid singularities at the wall, ω is not solved for the single mesh element at the wall. Instead, COMSOL uses the following approximation given in equation 59 to get accurate results near the wall boundary. In this equation, τ_w is the wall shear stress.

$$l_w^+ = \rho\sqrt{\tau_w/\rho}l_w/\mu \approx 1 \tag{59}$$

To conclude for the SST model, the wall function is solved using the k-ω model. The rest of the flow is solved using the k-ϵ model. The SST model uses various difficult equations to ensure that both equations have a nice transition. These transition equations are outside the scope of this research, and these are not discussed here.

I Advantage and disadvantages of the particle counter Solair 1100

The particle counter has the advantage that it can do a whole wafer measurement within an hour. It does this without touching or interfering with the wafer, which is advantageous because 1) the particle counter itself does not leave behind contaminants on the wafer in this manner, 2) the influence on the static charge which can be found on the wafer is kept to a minimal and 3) it does not deform, shake or move the wafer when the particle counter is on. However, keeping the particle counter hoovering above the wafer also has two disadvantages, namely 1) particles which might be just inside of the particle counters suction range can experience some force and therefore release themselves to early (when the particle counter has not yet hovered above that specific position) and 2) there is a certain percentage of particles left after the particle counter has treated the whole wafer. There are also particles left if the particle plotter would touch the wafer, just a smaller percentage of the total is left. This chapter will mainly focus on the two disadvantages by asking two questions. Firstly, is the particle counter sucking up particles which were not directly beneath the particle counter and if yes, how large of an area is being affected by this phenomenon. Secondly, how many particles are left after the treatment, and is this constant and predictable.

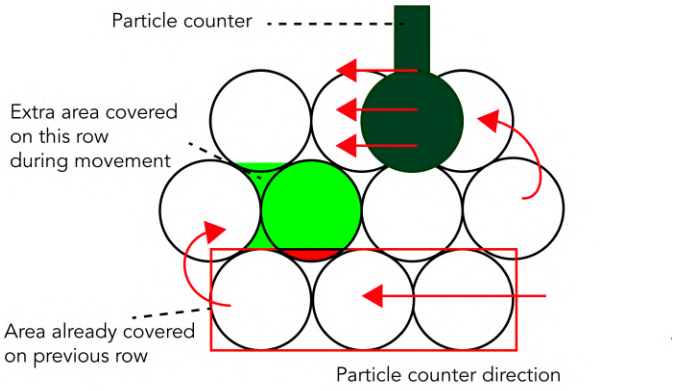

Figure 70: *An illustration to represent the area that the particle counter covers during one measurement. Light green displays the extra area and red is the area which is already treated.*

Let us start with the first disadvantage: determining the error of the suction diameter in our particle counter. The position of the particle counter can be very precisely controlled, up to 0.003 mm. So the problem has more to do with the height of the particle counter above the wafer. At a height of 3 mm, the suction diameter is determined to be approximately 2.12 ± 0.27 cm. In the figures of the particles on the wafer (as displayed in figure 23) the white rounds are displayed with a diameter of 2 cm. So when the particle counter is at rest, the suction is accurately described. When the particle counter moves however, it partially moves over

an area which is not yet covered by the particle counter. An illustration of this can be seen in figure 70. In this figure, the red area displays which part of the circle that it is supposed to measure is not taken into account, and the green area visualises which area is measured when the particle counter hovers and moves to the next position. These areas almost cancel each other. Concluding: the error of the particle counter due to position or movement is neglectable.

Secondly, the particles remaining on the wafer after the first measurement is done. This disadvantage will always exist, even when the particle counter does contact the wafer. Furthermore, measurements can be done to determine how many particles are actually analysed, to provide a comparison between the real amount of particles and the measured amount of particles. This has been done thoroughly in appendix chapter G.

J The influence of a beam through the vertical wind tunnel

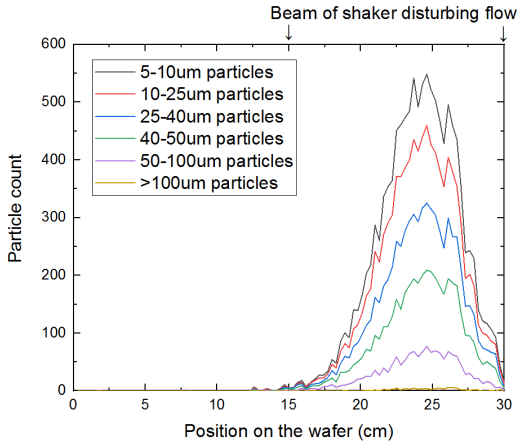

Figure 71: *The particle deposition on the wafer when the inlet is 5 cm long and close to the beam.*

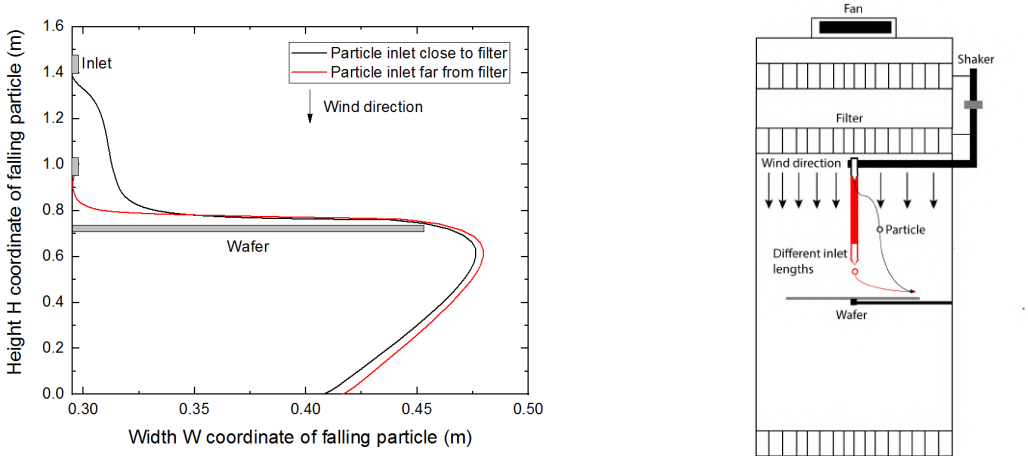

(a) *Particle trajectory close and far from filter* ***(b)*** *Sketch experiment*

Figure 72: *Left) The trajectory of particles when the inlet is close to the extending beam or far from the extending beam. Right) a sketch to clarify the release position of the particles.*

First of all when no wind is present, the presence of the beam is not noticeable. Particles fall straight down and only have a certain spread in them when landing on the wafer. This spread of particles is usually a 4 to 5 cm diameter in the middle of the wafer. However, if the wind is turned on, the presence of the beam becomes

very noticeable when releasing the particles close to the vertical beam. The results of these measurement are taken into account in future experiments and these results are displayed in appendix J.

Using the boulder counter, this can be seen in graph 71 for a wind velocity of 0.4 m/s, where the particles have a clear preference to go to the right hand side. On this side, the rod was also placed to hold the shaker in place, thus the wind speed was slower. To validate this preference of moving right, the theoretical trajectory of a simulation can be seen in the appendix 72a. To solve this problem, the inlet was extended down by 50 cm to ensure that the wind velocity profile could become uniform again. This resulted in a distribution which was centered, as can be seen in graph 43. Again, the theoretical result of extending the inlet can be seen in appendix 72a, where the particle starts to fall later. To clarify how the setup looks like, a sketch in similar colors is made in figure 72b.

K Calculating the charge of a glass particle in a vertical wind tunnel

The velocity and trajectory of particles were discussed with and without flow. Now that one has a better understanding of how the particle behave without an electric field, experiments with an electric field can be executed. In this chapter, the charge in relation to the particle size will be discussed. The hypothesis is that smaller particles are more easily affected by the electric field than larger particles. This would mean that a sufficiently high field would start to alter the trajectory of 5 µm particles, while 50 µm particles would experience relatively little change in their trajectory.

Knowing the strength of the field and the dimensions of the wind tunnel, will allow us to calculate the charge of particles based on their size. However, there is a challenge involved in this measurement, since our primary particle counter can not distinguish particle sizes above 5 µm. This means that knowledge of the horizontal measurements are needed to have an idea of the particles distribution in size. Also, knowing that the smallest particles deviate the most, one can use this boundary of 5 µm particles to spot the smallest particles. Finally, scanning electron microscope measurements are used to confirm the predictions.

First, let us look at the raw data. This example contains the vertical measurements with no wind and a field of -12 kV/m applied to the particles (further details of the setup can be found in chapter 3). Again, the particle counter is used to plot the position of particles larger than 5 µm. This figure can be seen in 73a. A few things stand out in this figure. First of all, most particles are still present near the center, meaning that these particles have no charge or are the heavier particles which fall almost straight down. The second thing that is noticeable is that the particles which do deviate from their normal trajectory, all deviate to the left. Since the negative electric field is present on the left side of figure 73a, the particles must possess a positive charge. The triboelectric series indeed shows that the glass particles would like to be positively charged and the plastic inlet gets negatively charged, making this result as expected. The third noticeable thing is that the particles deposition is stretched out to the left side completely, or stated otherwise, there is no area on the left that is black anymore. This could mean that some particular particle sizes might have already deviated so much that they exceeded the wafer dimensions and therefore did not deposit on the wafer. This is why smaller fields must also be investigated as will be done later on in this chapter.

The second way to interpret the data is to visualise figure 73a in a graph. This is done by linearly interpolating the data using Matlab script P as can be seen in the appendix. The linear interpolation provides extra data-points between the peaks without altering the image itself. With the extra data-points, some constants can be calculated more precisely. The linear interpolation can be done because of the assumption that particles are continuously distributed, while the measurement itself is discrete. In electric fields, particles will deviate corresponding to their polarization. For figure 73b this means that on the left side there should be particles present, while on the right side of the wafer almost no particles are present. Graph 73b shows exactly this behavior. Take into account that the graph is normalised for the particle count. It does not matter how many particles were actually detected, rather the change of the particle deposition profile matters.

One extra step can be taken in the analysis of charge of particles, which is finding the approximate number of particles that are charged. This next figure will be based partly upon figure 73b. Starting at the center (at 15 cm), the area below the graph will be analysed until a certain percentage of particles is achieved. 50 Percent of the particles are within a range of 2.5 cm of the center. This also means that the remaining 50 percent of the particles land outside this 2.5 cm radius. Since most particles still land in the middle

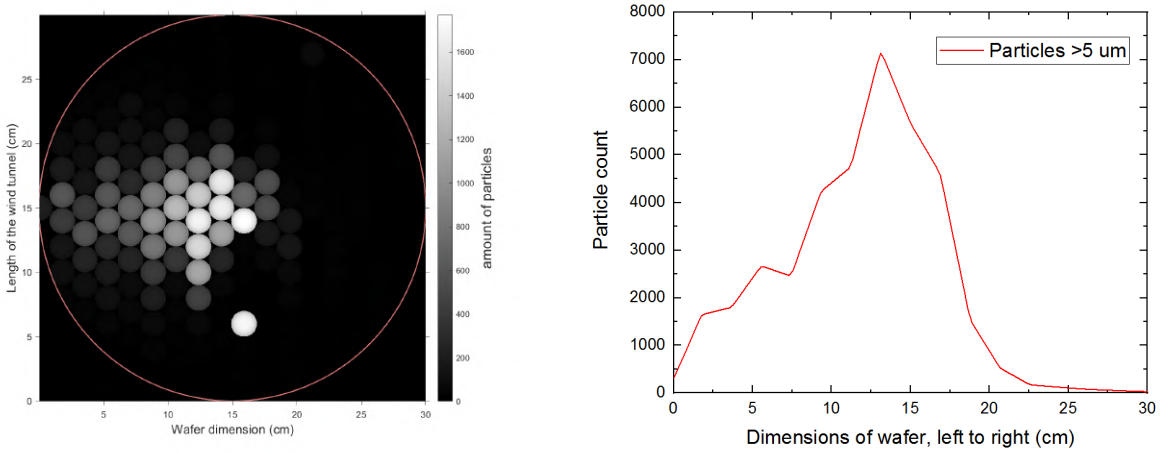

(a) *The particles deposition position on the wafer*

(b) *Particle count interpolation integrated*

Figure 73: *Left) raw particle count visualisation of glass particles under the influence of a -12 kV/m field on the left side. Right) summation of the deposited particles, with most particles being near the center of the wafer and particles density decreasing near the edge of the wafer.*

of the wafer, it can be assumed that for a large fraction of particles the charge is unaltered or not easily measurable. Only at the larger deviations a difference will be noticeable between 0 kV (which does not show any deviations to the left or right) and a figure such as 73b which has particles depositing on the left side of the wafer and displays a field of 12 kV/m.

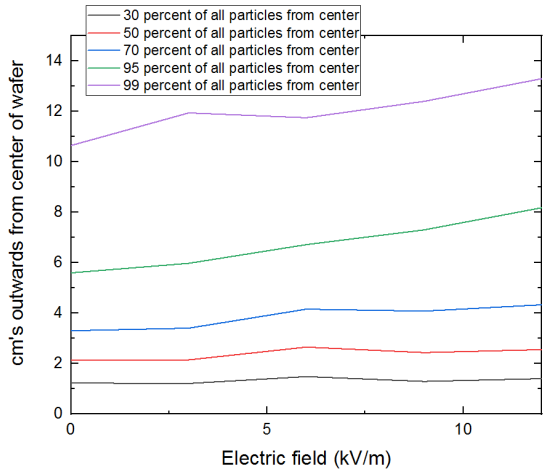

Figure 74: *The percentage of the total number of particles landing at a certain position, starting from center = 0 cm outwards. The graph represents how the displacement of the particles can be compared to the kV/m that is applied.*

The procedure as just described is how figure 74 is made. The first 30 and 50 percent of particles, starting at the center at 15 cm and moving outwards on both sides, are similar for all fields. Only at 70 percent of the total amount of particles a clear linear upwards slope can be seen. This means that at 0 kV/m, 70 percent of the particles have landed between 8.9 cm and 21.1 cm. For -12 kV/m, 70 percent of the particles have landed between 7 and 23 cm, a 1.9 cm increase on both sides. This increase means that enough particles have moved due to the electric field so that it is actually measurable. So in these experiments, certainly

more than 30 percent of the particles are charged and can be influenced by an electric field. Note that this is not an exact method, but it does give an impression of what percentage of the particles might be charged. Other particles may also possess charge, but their charge was not large enough (or the mass of the particle was to large) to show any deviation.

To compare the calculated amount of particles being charged with theory, it is assumed that all particles that touch the outer diameter of the particle inlet get charged. This is calculated for each individual particle size. If these sizes are known, the total percentage of charged particles can be calculated, as also discussed in chapter 5.5.3.

Particle diameter (µm)	Particles in syringe diameter (190 µm)	Particles touching outer diameter
5	1123	117
10	277	56
15	122	36
20	68	26
30	29	16
40	16	11
50	9	8

Table 9: *Amount of particles fitting in the diameter of the syringe and the amount of particles making contact with the outer diameter.*

L Charging using an ionizer

Charging method	Silicon (kV)	Silicon Oxide (kV)	PVC (kV)	Aluminum (kV)
Contact induced	0	0	3	0
Charge induced	0.1	0.1	0.1	0.2
Ionizer boundary charging negative	-0.2	-0.1	-0.3	-0.2
Ionizer center charging negative	-0.4	-0.2	-0.5	-0.4
Ionizer boundary charging positive	0.8	0.8	0.2	0.6
Ionizer center charging positive	1.4	1.3	1	1

Table 10: *Different charging methods with different wafer materials and whether they charge using a certain method.*

Trying to charge all materials will be done both with a solely positive output and solely negative output and a neutral surface. The ionizer will both be applied to the center of the wafer and the boundary, to see what effect the ionizer has on the entire wafer. The ability to charge the surface using the ionizer can be seen in table 10. All surfaces were treated with the ionizer for 60 seconds, uniformly distributed over the wafer, with the same flow velocity and the same potential on the emitter points. These results were measured immediately after the ionizer was removed.

M Particle generation and deposition in the AWH

M.1 Particle generation in the AWH

The particles that deposit on the wafer in the AWH must come from somewhere, and this chapter will be used to explain the parts in the AWH that generate the particles and the processes which occur to make it more likely for particles to actually deposit. Processes such as electrophoresis and thermophoresis will be left out of this chapter since they are already discussed in more length in other chapters.

Let us first find out where these particles come from. There are a couple of sources which might contribute to particles in the AWH and look at these reasons one by one. These could be:

1. Particles entering through the HEPA filter
2. Particles entering with the wafer itself
3. Particles entering the AWH during service
4. Particles being generated due to friction.

Let us first start with number 1) Particles entering through the HEPA filters. As already discussed in chapter 2.1.3, it is most probable for particles in the order of 0.1 µm to enter the setup. Since the AWH setup consist of two HEPA filters, it is very unlikely to see large number of particles entering the AWH in this way. As an example, one HEPA filters will reduce the air value from ISO4 class to ISO-1 class, reducing the number of particles with 100000. If two HEPA filters are place in series, only 1 in 10^{10} particles will make it in the AWH. To conclude, the airflow is not a source of contamination.

This is not the only place in the AWH that is opened. Another place which gets opened more frequently is where the wafers first enter the setup. The FOUP is attached to the AWH in such a way that contamination is minimized. However, cross contamination still occurs, as stated in [104]: "Results confirm the molecular cross-contamination chain: contaminants from air are transferred to FOUP and subsequently from FOUP to wafers. If no volatile acid is detected in FOUP atmosphere, no defect will be present on wafer." All other literature on the material stated approximately the same, that molecular contamination is a problem, however none mention (larger) aerosols as being part of the problem. Furthermore, literature states that this molecular contamination can be solved by purging with inert gasses.

Thirdly, particles can also enter the setup during service or the lack of service. Both the HEPA filters and the FOUPs must remain clean at all times and should be replaced from time to time. These HEPA filters can lose the properties of the electrets or become polluted after some time. Replacing them is necessary to ensure their particle stopping properties. When this is not done on time, more particles may enter the setup as described before, and contamination can occur. Also, when replacing these wafers, the AWH has to remain clean or be cleaned after the service. An example of how to clean the wafer afterwards is to first run the AWH several times using dummy wafers (wafers which purpose it is to pick up contamination and leave the AWH without further processing). No real information however can be found of ASML's service records, and this part of controlling contamination is outside VDL's control.

Finally, another source of particles might exist in the AWH. The arm of the AWH consists out of several parts which can cause friction. This friction can cause contamination in the form of aerosols. The amount of contamination coming from this process in not known exactly, but oils and metal contamination particles are most probable. To prevent contamination from escaping from the robot arm, plasma seals are currently developed. These seals charge the particles and make them deviate in the influence of external fields. This is the most probable particle generating mechanism, which is why it is important to have a flow present at all times and that this flow does not have any vortexes. This will prevent particles which are released due to friction from the arms to travel upwards with a vortex and eventually land on the wafer.

M.2 Particle deposition in the AWH

There are also some reasons why particles might be more likely to land on the wafer. Some of these reasons are listed her below.

1. Non-uniform airflow at certain places in the AWH.
2. Moving and stopping motion of the wafer because of transport.
3. Gripping of the wafer by the arm or store unit.

The first reason becomes apparent when looking at the AWH design. To ensure a sturdy design, the AWH consists out of two downward stream channels with a beam in the middle. This beam can also be seen in figure 2. This causes the down-flow of air to be disturbed in the area below this beam. The wafer is not

positioned for a long duration below the beam. However, the particles that are positioned below the beam will not follow the ideal streamlines out of the AWH, but instead be trapped in a vortex. This means that if particles end up in the vortex, they will stay in the AWH for a much longer duration as usual, which can cause contamination eventually.

Another reason why contamination can deposit on the wafer is the motion of the arms. When the arm moves with a constant velocity, the volume of air being moved stays approximately constant as well. This means that a boundary layer is created in the same manner as the horizontal wind tunnel. It has been shown in simulations and experiments that particles get lifted up by this boundary layer, but heavy particles may penetrate through the boundary layer. This will not be a very big problem however since the wafer has already moved away from this position. The wafer also moves with a higher velocity (3 m/s) than the vertical wind flow (0.4 m/s). Even when the vertical flow hits the wafer and becomes mostly horizontal, the motion of the wafer (caused by the arm) will still outweigh the vertical air speed. The hypothesis therefore is that the biggest problem is the abrupt stop and starting motion of the wafer. Take the stopping motion for example. The wafer has been traveling at a constant velocity, moving through a constant volume of air. This volume of air is displaced causing a boundary layer which points in the opposite direction as the movement of the wafer. When the wafer comes to a stop, the air movement will still continue due to inertia. Since the wafer is now at a standstill however, the vertical airflow will become dominant again. There is a point on the wafer where the wind speeds (vertical flow hitting the wafer and the horizontal inertia volume flow) cancel each other, making the wind zero. To illustrate this, a wafer was moved manually with a speed of approximately 2 m/s and brought to a sudden stop. The effect of this sudden stop is partly visible in figure 75, where 6 frames shot at 60 fps are shown. The middle of the wafer (white triangle) is marked with a black line, meaning that from this point, the vertical wind would be split in the directions shown by the red arrows (as also shown in figure 75). There is also a wind of 0.4 m/s present at all times (also shown by the vertical red arrows). Most noticeable is the vortexes which are created around the middle of the wafer (highlighted by the red rounds drawn around them). Several spots of smoke are visible that do not move and become vortexes. These vortexes could contain small particles which could than, because there are no clear streamlines present, deposit on the wafer. This measurement is not very accurate (done manually with a smaller wafer and only one direction of translation), but does display that the fast motion of the wafer can cause extra contamination.

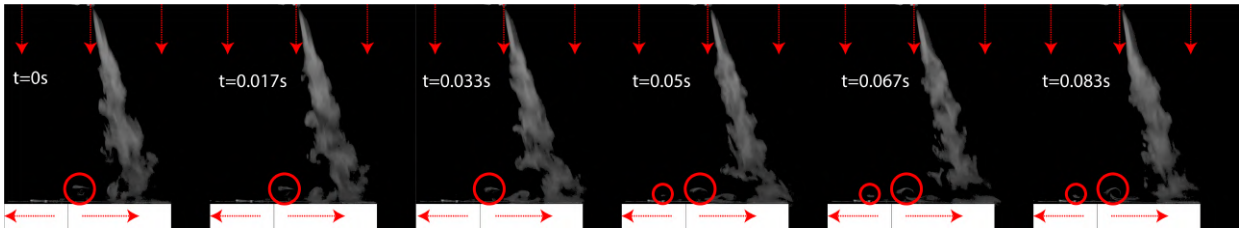

Figure 75: *The sudden stop of the wafer movement displayed in 6 frames visualised with smoke. The vertical wind speed is 0.4 m/s, the velocity of the wafer approximately 2 m/s and the recordings are 60fps.*

Thirdly, every contact point can cause particles to be released. Since the gripper has to firmly hold the wafer in place at high moving velocities, it needs some force to do this. This is done by sucking down the wafer on the gripper. This however also causes the wafer to be in firm contact with gripper, which can therefore deposit contamination on the back side of the wafer. When the gripper or the wafer moves at higher velocities (or the wafer gets charged due to processing), the particles that were deposited could become airborne. Another point of contact is the store unit, where wafers are placed before or after the procedure. This contact could again lead to deposition of particles on the back side of the wafer, which get released by the motion of the wafer or the gripping of the wafer. The contribution of these processes to the total particle count is not known, but it is known that more particles can be found on the backside of the wafer where the gripper has been.

N Error analysis

This error analysis is vital to the research, since it concludes whether or not the results gathered in the figures is significant. For both the horizontal and vertical wind tunnel, different tests will be used to examine if the results are significant. This chapter must however begin with a disclaimer: A non-significant result does not mean that no effect is exerted on the particles. It does mean that according to the standard deviation calculated, no effect can be proven. Furthermore, a significant result does not mean that the effect is relevant for the final application in the AWH. A couple of millimeters deviation might be significant, but not relevant.

N.1 Error analysis of the horizontal wind tunnel

For the horizontal wind tunnel, a z-test will be used to examine if the raw particle counts are different in one data set compared to another data set. The z-test must have a normal distribution and a known standard deviation (σ). The first normality distribution is tested by doing the exact same measurement 25 times and examining if the data is indeed normally distributed. With an H0: the data set is normally distributed, the result of the Shapiro Wilko test of normality results in a p value of p-value=0.5816 and a W value of W = 0.96746. This means that there is no evidence to assume the experiments in the horizontal wind tunnel are not normally distributed. Furthermore, the standard deviation of these 25 measurements results in 2037 $\pm$ 204 particles, or 10.1 percent of the total particle count. The assumption will be made that this standard deviation is the same for all measurements for a couple of reasons: 1) the particle counter has stopped counting before going to the next position, ensuring that it has sucked up all the particles it could have, 2) The particle inlets also have a normal distribution, as shown in chapter 3.3.5. 3) The particle sizes are approximately the same in all experiments when measuring on the same position. Knowing this, and the fact that the same mean ($\delta = 0$) will be tested over 3 measurements ($n = 3$), formula 60 can be used to calculate the z value of each two data sets. The p-value can be derived from this z-value by taking a one tailed normal distribution with the negative z-value, and multiplying this by 2 to get a two tailed test. In all experiments, alpha will be taken to be $\alpha < 0.05$. Furthermore, the null hypothesis (or H0 for short) will be stated before the table.

$$z = \frac{\bar{x}_1 - \bar{x}_2 - \Delta}{\sqrt{\frac{\sigma_1^2}{n_1} + \frac{\sigma_2^2}{n_2}}} \tag{60}$$

Furthermore the Pearson correlation matrices will be given and the adjusted p-values of several figures will be calculated. The Pearson correlation matrix shows how the best fit line and the data are correlated. Using a matrix, multiple data sets can be compared with one another. Furthermore, the adjusted p-value indicates which factor level comparisons within a family of comparisons (hypothesis tests) are significantly different. If the adjusted p-value is less than alpha, then you reject the null hypothesis. So, the Pearson correlation matrix is used to calculate the correlation of data

QQ-plots will be used to show how the data follows a certain distribution. This distribution can be normal but also exponential. Any outliers or patterns show if the data is indeed distributed in a way.

T-tests test if the data of one data set deviates from the mean of another data set. The T-test uses the mean, standard deviation and data points to assess if there is a significant difference in the means of both data and if they can be compared. A single sample t-test assesses if the mean significantly deviates from 0. Tables can be used to recalculate this t-value with the degrees of freedom to a p-value, which will again assume an $\alpha < 0.05$ to be significant. If the p-value is below 0.05, the results are significantly different from each other. The T-test will be used in experiments where the standard deviation from the Z-test can not be used.

Linear regression models can be used to see how the data fits a linear line. This test also shows if there is a significant linear regression visible at all, or if the data has not got enough slope. This test can be used in experiments were the amount of charged particles was examined, and to see at which percentage a significant slope can be found, and thus statistical prove that indeed a certain percentage of the particles is charged.

N.2 Error analysis of the vertical wind tunnel

A chi square test can be executed to see if two data sets are independent, comparing one expected data set (the calibration measurements without any external fields) with the observed data set (the measurement with an external field). Furthermore, both data sets have to be normalized to 1, since this test is used to examine the change of position, not the raw particle count. These tests will thus show if the data sets have a significant deviation from the calibration measurement. In order to execute these measurements, the wafer can be divided into certain segments. Knowing that the measurements methods used in these experiments are not always as precise, it has been chosen to pick intervals of 1cm. This means that the region of interest from 10 to 20cm is divided into 10 sections, where all counts in that 1cm are summed. There are two reasons to take 1cm intervals. Firstly, each sample should be large enough so that there is a reasonable chance of observing outcomes in every category. If the expected counts are too low, the p-value test is not accurate. Secondly, the relevant deviation is also approximately 1cm. In other words, in the experiments performed in this thesis, one can be sure to see a relevant deviation of the trajectory if this deviation is 1cm or greater. The emphasis is on the word relevant: A chi square test can point out if the deviation is significant, it is the task of the analyser to conclude if the test also shows a relevant deviation.

N.3 Error analysis of all relevant figures

figure 40

Figure 40: The raw data of the horizontal wind tunnel, where different sizes of particles at different travelled lengths are visualised

H0: The data in graph 40 in not significantly dependent on each other.

Pearson correlation matrix	0.1-0.15um	0.2-0.25um	0.5-1um	>5um
0.1-0.15um	1	0.994	0.986	0.962
0.2-0.25um	0.994	1	0.997	0.979
0.5-1um	0.986	0.997	1	0.990
>5um	0.962	0.979	0.990	1

Table 11: *Pearson correlation matrix of figure 39.*

Adjusted p-values	0.1-0.15um	0.2-0.25um	0.5-1um	>5um
0.1-0.15um		<.0001	<.0001	<.0001
0.2-0.25um	<.0001		<.0001	<.0001
0.5-1um	<.0001	<.0001		<.0001
>5um	<.0001	<.0001	<.0001	

Table 12: *Adjusted p value figure 39.*

conclusion: the H0 hypothesis must be rejected since all p-values are smaller than 0.05, meaning there is a very strong relationship between the data sets. For figure 39, this means that the small and large particles are significantly correlated and thus that the hypothesis of smaller particles sticking to larger particles is true based on a statistical standpoint.

Error figure 42

Figure 42: The particle diameter distribution of the glass beads of both the Solair and boulder counter

QQ-plot hypothesis: The data set of figure 41 must follow and exponential decay distribution

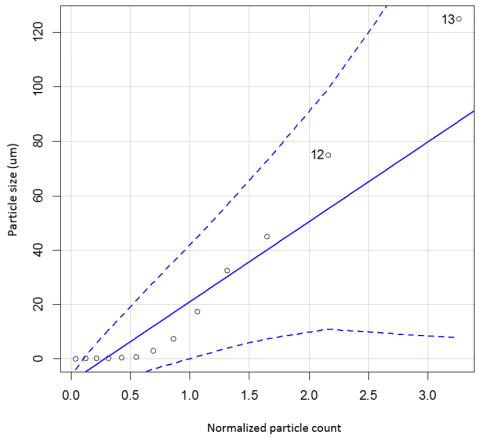

Figure 76: *QQplot showing if an exponential distribution fits the data.*

Conclusion: The hypothesis must be rejected since there is a clear deviation from the line visible in the data. The data first lacks behind the exponential qq-line, after which is recovers and becomes too steep for the qq-line. The deviation here therefore suggests that the glass particles used in the experiments can not be assumed to be exponentially distributed.

Error figure 43

Figure 43:Left) COMSOL simulation showing the relation between particle size and the travelled length in the wind tunnel Right) The experimental results with an exponential fit through two sets of measurements H0 adjusted p-value: The data in graph 43 in not significantly dependent on each other.

Pearson correlation matrix	front wafer meas 1	front wafer meas 2	back wafer meas 1	back wafer meas 2
front wafer meas 1	1	0.958	0.852	0.940
front wafer meas 2	0.958	1	0.877	0.842
back wafer meas 1	0.852	0.0.877	1	0.744
back wafer meas 2	0.940	0.842	0.744	1

Table 13: *Pearson correlation matrix of figure 42.*

Adjusted p-values	front wafer meas 1	front wafer meas 2	back wafer meas 1	back wafer meas 2
front wafer meas 1		0.0002	0.0073	0.0005
front wafer meas 2	0.0002		0.0042	0.0087
back wafer meas 1	0.0073	0.0042		0.0341
back wafer meas 2	0.0005	0.0087	0.0341	

Table 14: *Adjusted p value figure 42.*

H0 t-test: The data of the front and back wafer does not deviate from a mean of 0 when subtracting the data from each other.

One Sample t-test data: differences of back and front boundary layer t = 1.8684, df = 7, p-value = 0.1039 95 percent confidence interval: -201.2401 to 1716.7401 mean of boundary layer data set: 757.75

Conclusion: The H0 hypothesis of the adjusted p-value must be rejected on both accounts of the adjusted p value and t-test p-value. The adjusted p value shows that the data is significantly dependent on each other, which might already suggest that the development of the boundary layer has no significant influence on the boundary of the particles. ’

To make sure this is indeed correct, both the mean from the two front wafer and the two back wafer measurements were subtracted from each other. If the data would be entirely the same, the subtraction of the two data sets would result in 0. This was not the case since there is a spread in the data, meaning a one sample t-test can conclude if the data is indeed similar. The p-value has a value of 0.1, meaning that the H0 hypothesis must be accepted, and that indeed the data does not deviate from the mean 0. This can also be seen in the 95 percent confidence interval, where the value 0 is included in the interval. This all means that there is no statistical reason to assume that the development of the boundary layer has any effect on the number of particles depositing on the wafer in this experiment.

figure 44

Figure 44: The influence of the electric field in the horizontal wind tunnel

H0: the influence of the plate on top of the wind tunnel has no effect on the amounts of particles depositing

p value of the calibration and wafer: 8.8036e-12 p value of the calibration and charged plate: 2.7182e-04.

For both p-values, the H0 must be rejected and the alternative hypothesis accepted. The data does show a significant difference, meaning that applying charge on either the wafer or on the walls of the horizontal wind tunnel has a noticeable effect on particle trajectory.

figure 48

Figure 48: The percentage of the total number of particles landing at a certain position, starting from center=0cm outwards. The graph represents how the displacement of the particles can be compared to the kV/m that is applied

H0 hypothesis: A linear trend can not be found in the data of figure 46

Percentage of particles	p-value linear regression model
30 percent	0.303
50 percent	0.137
70 percent	0.025
95 percent	<.0001
99 percent	0.0167

Conclusion: for the first two data lines (30 and 50 percent), the H0 hypothesis must be accepted. Indeed no linear regression can be assumed here. For the other three lines (70,95 and 99 percent), the H0 hypothesis must be rejected, meaning linear regression is visible. This also means that based on these results its statistically true that if not taking into account the first 70 percent of data point from r=0, the rest of the data shows a linear increase and is thus charged. Or in other words, 30 percent of the particles show visible charge effects.

figure 46

Since the z-test is valid only if a clear sigma could be established, it was chosen to do a t-test for this measurement. This means that the sigma test does not have to be executed for 0.3 and 0.5 m/s, saving a lot of experimenting.

Doing a t-test for this amount of data does not bring with it a lot of power. To decrease the error in the 0.5 m/s from 2000 to 1000, 12 extra measurements must be executed minimally. Since this would result in a total of 48 extra experiments (also for 0.0 m/s, 0.3 m/s and 0.4 m/s), it is assumed with reasonable accuracy that these means are indeed different. For 0.3 m/s and 0.5 m/s, the difference of the means not being 0 (thus the same mean) is 93.5 percent (so there is a 6.5 percent change that the means of 0.3 m/s and 0.5 m/s are in reality the same).

figure 50

Figure 50: Left) Particle counter measurements in a positive field. Right) charge accumulation of initially uncharged particles and the deviation of these particles in a positive field for a 17.5um glass particle

H0: The data as shown in figure 50 is statistically the same.

chi square test 4 intervals of 3 cm. 3 values smaller than 5, namely 1, 1 and 4 for expected value. The P Value of 0.706, The result is not significant at $p < 0.05$.

This means that there is no reason to reject the H0 hypothesis and that indeed figure 50 can be described as one dataset. This would mean that the positive field is hardly noticeable by the particles, as shown and discussed earlier.

figure 51

Figure 51: The difference in travelled distance for a metal and plastic inlet in a -6 kV/m field, visualising the contribution of the triboelectric effect and electric field effect. The contribution of the electric field charge accumulation is modelled on the right for a 17.5um glass particle.

H0: The data as shown in figure 50 is statistically the same.

Pearson correlations: ...1 ...2 ...3 ...1 1.0000 0.9494 0.9400 ...2 0.9494 1.0000 0.7961 ...3 0.9400 0.7961 1.0000

For the metal and reference: chi square 6 intervals of 3cm at the left side (side at which particles deviate in field), DF=5. The P-Value is 0.001. The result is significant at $p < 0.05$.

For the plastic and reference: chi square 6 intervals of 3cm at the left side (side at which particles deviate in field), DF=5. The P-Value is < 0.00001. The result is significant at $p < 0.05$.

Both results are therefore significant and there is reason to reject the H0 hypothesis. The data in figure 51 is statistically unlikely to of the same dataset, meaning that the negative field indeed changes particle trajectories noticeably for both inlets.

figure 52

Figure 52:The influence of the charge of the wafer on the deposition of particles, each situation averaged over 3 measurements and no external flow

H0: The data as shown in figure 52 is statistically the same.

negative wafer and reference: p of wafer 0.21 positive wafer and reference: p of wafer 0.56

Both p values with references to the calibration do not show a significant result, so the H0 hypothesis must be accepted. The effect of charging a wafer with no flow does not alter particle trajectory significantly

figure 55

Figure 55: The schematic drawing of the ionizer used in the experiments, and the results gathered from this experiment. all lines represent 3 measurements averaged, no external fan flow but an air gun pressurised flow

H0: The data as shown in figure 52 is statistically the same.

Pearson correlations: ...2 ...3 ...4 ...5 ...2 1.0000 0.9943 0.9984 0.9941 ...3 0.9943 1.0000 0.9919 0.9927 ...4 0.9984 0.9919 1.0000 0.9953 ...5 0.9941 0.9927 0.9953 1.0000

chi squared of not charged and negatively charged plate: 1.7748, DF 9, The P-Value is 0.994549. The result is not significant at $p < 0.05$. chi squared of not charged and negative ionisation: 1.0715 , DF 9, The P-Value is 0.999256. The result is not significant at $p < 0.05$. chi squared of not charged and positive ionisation: 1.1972 , DF 9, The P-Value is 0.998832. The result is not significant at $p < 0.05$.

As also shown in the figure, the graphs are really close together, expecting no significant deviation. This can also be seen in the p values, suggesting that the H0 hypothesis must be accepted. There is no clear difference between situations with or without the ionizer.

figure 58

Figure 58: The effect of a charged wall or charged wafer in comparison with a reference measurement for both a metal and plastic inlet. Both figures were made with no wind.

H0: The data as shown in figure 58a is statistically the same.

metal inlet, plates, blue and green: 0.0842 p value metal inlet, wafer, red and black: 0.71 p value

For both p values there is no significant result that could be found, meaning that with a metal inlet the copper particles do not charge enough to have a significant change in particle deposition.

H0: The data as shown in figure 58b is statistically the same.

plastic inlet, plates, blue and green: 0.0041 p value plastic inlet, wafer, red and black: 0.179 p value

The H0 statement is partly true. It can be seen that for the measurements where the plates were charged that the result is significant, but for the wafer measurement that the results do not statically vary enough. This is in line with the first metal measurement, where the p value of the plates was also smaller than that of the wafer.

figure 59

Figure 59: The effect of a charged wall or charged wafer in comparison with a reference measurement. The wind velocity was 0 m/s in this measurement and the inlet made of glass.

H0: The data as shown in figure 59 is statistically the same.

ref and wafer: 2.1662e-05 p value ref and plate: 0.01 p value

Both results are significant in comparison to the reference measurement, meaning that a glass inlet charges particles significantly enough to measure a difference in particle deposition

figure 60

Figure 60: The deposition of copper particles with a sticker in the middle to limit count. Wind speeds of 0.3, 0.4 and 0.5 m/s were used

H0: The data as shown in figure 60 is statistically the same.

0.4 and 0.3 The P-Value is 0.999995. The result is not significant at $p < 0.05$. DF=9 0.4 and 0.5 The P-Value is 0.995546. The result is not significant at $p < 0.05$. DF=9

Both p values are larger than 0.05, meaning that the wind speed does not alter particle deposition for these sizes of particles. The H0 must therefore be accepted

figure 61

Figure 61: The deviation caused by electric fields of both a plate (positioned on the right, 50 cm apart) and a charged wafer with a glass inlet

H0: The data as shown in figure 61 is statistically the same.

plates: The P-Value is 0.980613. The result is not significant at $p < 0.05$. DF=9 wafer: The P-Value is 0.99178. The result is not significant at $p < 0.05$. DF=9

Both p values are larger than 0.05, meaning that the electric fields present do not alter particle deposition for these particles and their properties. The H0 must therefore be accepted.

figure 64

Figure 64: No wind measurements and comparisons if the ionizer was turned on or off. For the plate measurements, the ground was located on the left and the charged plate on the right with a distance of 50 cm.

H0: The data as shown in figure 64 is statistically the same.

Cal: The P-Value is 0.049346. The result is significant at $p < 0.05$. Plates: The P-Value is 0.284024. The result is not significant at $p < 0.05$. Wafer: The P-Value is 0.613187. The result is not significant at $p < 0.05$.

The only significant difference is that of the calibration measurement. But since it is very close to our alpha level (of 0.05) and no real deviation is expected from this measurement, the question is whether it is also relevant. Looking at the other p-values of the graphs, the calibration measurement probably has some kind of error in the measurement. To conclude, it is safe to say that the effect of the ionizer does not have a significant effect on the particle trajectory in similar conditions with no wind.

figure 65

Figure 65: With wind measurements and comparisons if the ionizer was turned on or off. For the plate measurements, the ground was located on the left and the negatively charged plate on the right with a distance of 50 cm

H0: The data as shown in figure 65 is statistically the same.

Cal: The P-Value is 0.999992. The result is not significant at $p < 0.05$. plates: The P-Value is 0.99472. The result is not significant at $p < 0.05$ wafer: The P-Value is 0.976266. The result is not significant at $p < 0.05$.

All p values are large, meaning there is a reason to believe the H0 hypothesis is true. This means that the ionizer does not have a significant effect on the particle trajectory in the wind tunnel with the wind on

figure 68

Figure 68:The experimental results of different temperatures on the particle deposition position on the wafer. The simulation shows that 20 µm particles and plates with a 2.5 K difference also have the same deviation

H0: The data as shown in figure 65 is statistically the same.

1K and 2.5K: The P-Value is 0.001565. The result is significant at $p < 0.05$. 2.5K and 4K: The P-Value is 0.000063. The result is significant at $p < 0.05$.

Since both p values are well below 0.05, there is reason to assume that the H0 hypothesis is not true and that a temperature difference in no wind conditions have a significant effect on the particles trajectory. This means that time must be given for the plates and wafers to reach room temperature, which takes a couple of minutes.

figure polyamide appendix

H0: The data as shown in figure 65 is statistically the same.

no wind, ref and plate: The P-Value is $< .00001$. The result is significant at $p < 0.05$. DF=4 no wind, ref and wafer: The P-Value is .032169. The result is significant at $p < 0.05$. DF=4

wind, ref and plate: The P-Value is .221057. The result is not significant at $p < 0.05$. DF=4 Wind, ref and wafer: The P-Value is .141268. The result is not significant at $p < 0.05$. DF=4

Since the expected values were low at the borders of the graph (resulting in a non-precise result), it was chosen to pick 5 intervals in the middle of the wafer, each 3cm. This raised the expected value, enabling the

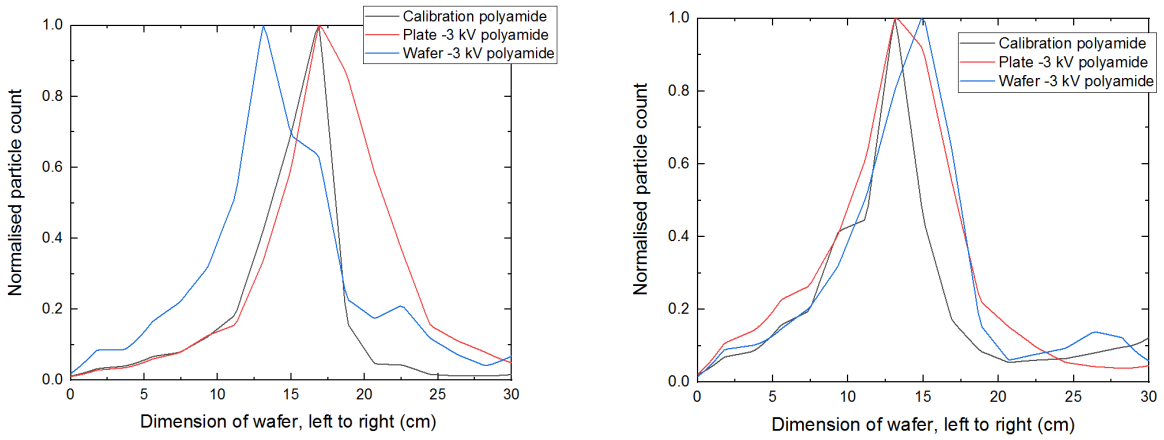

(a) No wind *(b) With wind*

Figure 77: *Visualising the differences between different scenarios of a charged wafer and a charged plate in both a no wind and 0.4 m/s wind condition with polyamide particles.*

chi-squared test. The no-wind measurements have shown clear deviation from the center of the wafer for both cases, meaning that the field does have an effect on particle trajectories. For the wind measurements, it was not successfully shown that the field indeed causes a significant result. However, visually there is a result present. Chapter 5.8.2 will go into more detail about this result. However, the chi squared test does state that the electric field in the setup with wind is not significant and that the H0 hypothesis will be accepted.

O Remaining figures

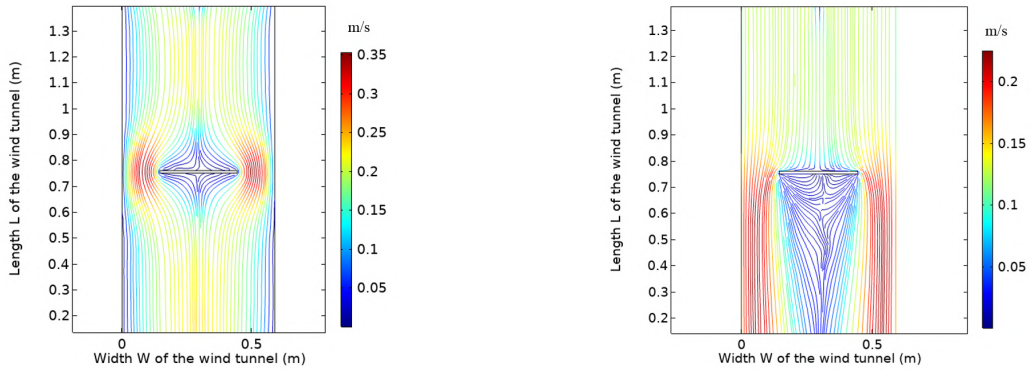

(a) Laminar flow *(b) Turbulent flow*

Figure 78: *A visual interpretation of both a laminar and turbulent flow. As can be seen in these figures, the largest difference can be found below the wafer.*

Figure 79: *The frequency and voltage of a negative emitter point.*

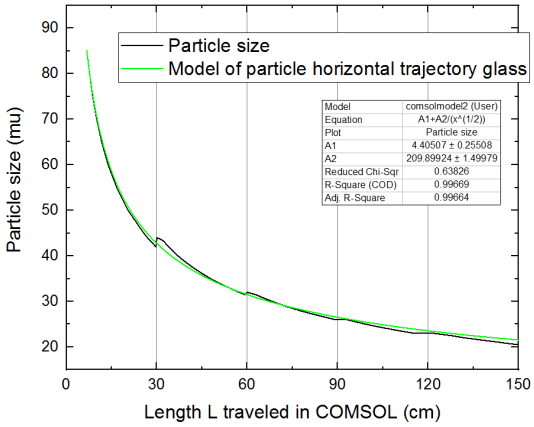

Figure 80: *The expected travelled trajectory for different particle sizes (glass particles). This figure was used to determine the red lines in plot 34b which show the expected bin size of particles landing in the wind tunnel.*

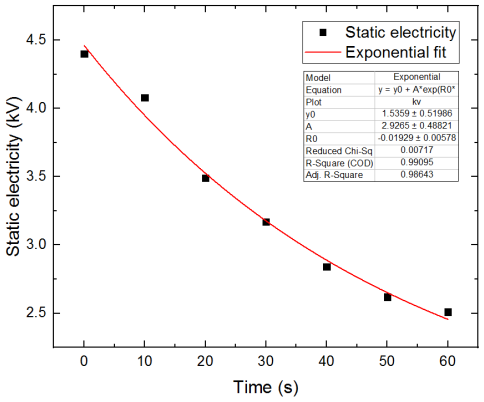

Figure 81: *The exponential curve as stated by formula 14 measured experimentally by rubbing a cloth and a glass together, insulating the glass and doing a measurement of the electrostatic field.*

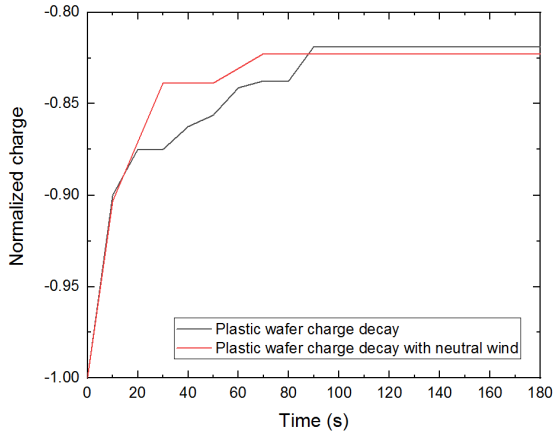

Figure 82: *The exponential curve as stated by formula 14 measured experimentally by rubbing a cloth and the plastic wafer together. This electrostatic field measurement is capable of calculating the approximate resistivity of the material.*

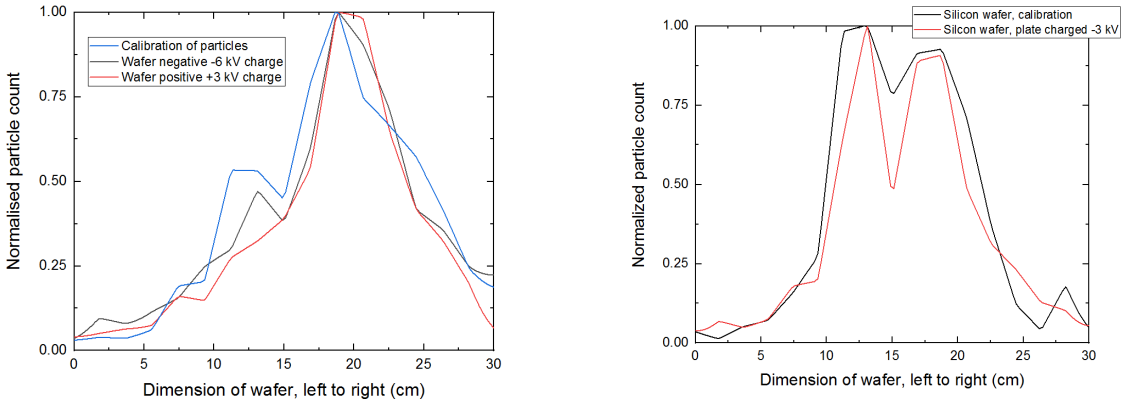

(a) *Copper trajectory with charged plate* ***(b)*** *Copper trajectory with charged wafer*

Figure 83: *The measurement results in no wind conditions in a vertical wind tunnel. Both fields did not show a significant deviation from the calibration measurement.*

$$
\begin{aligned}
n_{\mathrm{p}}/n_{\mathrm{t}} &= \prod_{p=1}^{+\infty} A_p^+/\Sigma \quad p>0 \\
n_{\mathrm{p}}/n_{\mathrm{t}} &= \prod_{p=-1}^{-\infty} A_p^-\Sigma \quad p<0 \\
n_0/n_{\mathrm{t}} &= 1/\Sigma \\
\Sigma &= 1+\sum_{p=1}^{+\infty}\prod_{p=1}^{+\infty} A_p^+ + \sum_{p=-1}^{-\infty}\prod_{p=-1}^{-\infty} A_p^- \\
A_p^+ &= \frac{N^+}{N^-}\frac{\eta_{p-1}^+}{\eta_p^- + (N^+/N^-)\,\eta_p^+ - \eta_{p+1}^- A_{p+1}^+} \\
A_p^- &= \frac{N^-}{N^+}\frac{\eta_{p-1}^-}{\eta_p^+ + (N^-/N^+)\,\eta_p^- - \eta_{p-1}^+ A_{p-1}^-}
\end{aligned}
\tag{61}
$$

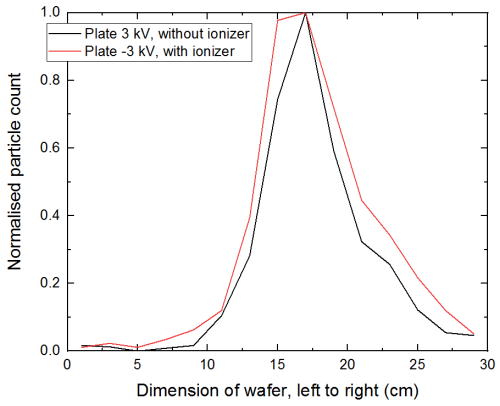

Figure 84: *Alternative method to measure the amount of particles on the wafer in a no wind condition wind tunnel with a -3kV plate.*

P Matlab scripts

Listing 1: *Script used for controlling the arm where the particle counter is attached to*

```
% port='LPT1';
% s=serial(port);
% fopen(s);
PU='echo PU > LPT1';
PD='echo PD > LPT1';
PA='echo PA > LPT1';

%positions
CENTER='echo 7500,6000 > LPT1';
AWAY='echo 1000,11600 > LPT1';
CORNER='echo 1000,11600 > LPT1';
%corners
C1='echo 13100,400 >LPT1';
C2='echo 1800,400 >LPT1';
C3='echo 1800,11600 >LPT1';
C4='echo 13100,11600 >LPT1';
CI1000='echo CI1000 > LPT1';

%radial
dos(C1);
xcenter=7500;
ycenter=6000;
effmaxradius=5600;
roffset=600;
maxradius=effmaxradius-roffset;
xsteps=18; %was 18
ysteps=16;
ttest=zeros([xsteps*ysteps,2]);
x=zeros(1,xsteps);
y=zeros(ysteps,xsteps);
j=1;
kvar=0.25;
for i=1:xsteps
    x(i)=xcenter-effmaxradius+(i-1)/(xsteps-1)*(2*effmaxradius);
    for k=1:ysteps
        yc=ycenter-effmaxradius+(k+kvar-1.25)/(ysteps-1)*(2*effmaxradius);
        if (x(i)-xcenter)^2+(yc-ycenter)^2<=(effmaxradius)^2
```

```
            y(j,i)=yc;
            j=j+1;
        end
    end
    kvar=-kvar;
    j=1;
end
disp('calc done')

waittime=0; %Don't change
surfacetime=11; %was 11
correctiontime=0.7; %Also don't change
totaltime=waittime+surfacetime+correctiontime+0.3;
tic
pause(correctiontime);
i=1;
revpar=-1;
for j=1:xsteps
    for k=1:ysteps
       % i=phisteps*(r-1)+phi;
       if y((ysteps+1)*sign(-revpar+1)+sign(revpar)*k,j)>0
        dos(['echo ',num2str(x(xsteps+1-j)),', ',num2str(y((ysteps+1)*...
            sign(-revpar+1)+sign(revpar)*k,j)),' > LPT1']);
        %pause(waittime);
        %dos(PD);
        pause(surfacetime);
        dos(PU);
        ttest(i,[1,2])=[toc/i-totaltime,totaltime*i];
        pause(correctiontime-i*ttest(i,1))
        i=i+1;

       end
    end
    revpar=-revpar;
    disp([num2str(i-1),' out of ', num2str(length(y(y>0)))]);
end
dos(CENTER);
tetetttest=ttest(:,1)+totaltime;
tonk(:,[1,2,3])=[tetetttest(:,1).*ttest(:,2)/totaltime,ttest(:,2),...
    tetetttest(:,1).*ttest(:,2)/totaltime-ttest(:,2)];
```

Listing 2: *Script used for plotting the results of the particle counter and the script used in 1*

```
A=readmatrix('C:\Users\s153308\Downloads\stage VDL\horizontaal.xlsx');
%A(246,:)=0;
column=14; % 7<=integer<=14
selectcolumn=A(:,column);
xsteps=18;
ysteps=16;
B=zeros(ysteps,xsteps);
psize=1200;
xcenter=7500;
ycenter=6000;
effmaxradius=5600;
roffset=600;
q=2;
j=1;
kvar=0.25;
x=zeros(1,xsteps);
```

```
y=zeros(ysteps,xsteps);
for i=1:xsteps
    x(i)=xcenter-effmaxradius+(i-1)/(xsteps-1)*(2*effmaxradius);
    for k=1:ysteps
        yc=ycenter-effmaxradius+(k+kvar-1.25)/(ysteps-1)*(2*effmaxradius);
        if (x(i)-xcenter)^2+(yc-ycenter)^2<=(effmaxradius)^2
            B(j,i)=sum(A(q,column));
            y(j,i)=yc;
            j=j+1;
            q=q+1;
        end
    end
    kvar=-kvar;
    j=1;
end


C=zeros(psize);
D=C;
for k=1:xsteps
    for j=1:ysteps
        xmeas=round(psize/2+(x(k)-xcenter)/effmaxradius*psize/2);
        ymeas=round(psize/2+(y(j,k)-ycenter)/effmaxradius*psize/2);
        if ymeas>0
        for measurex=-psize/30:psize/30
            for measurey=-psize/30:psize/30
                if measurex^2+measurey^2<=(psize/30)^2 && (measurex+...
                        xmeas-psize/2)^2+(measurey+ymeas-psize/2)^2<=(psize/2)^2
                   D(xmeas+measurex,ymeas+measurey)=1;
                    if C(xmeas+measurex,ymeas+measurey)==0
                        C(xmeas+measurex,ymeas+measurey)=...
                            C(xmeas+measurex,ymeas+measurey)+...
                            0.7*normpdf(measurex^2+measurey^2,0,2000)*B(j,k);
                    else
                        C(xmeas+measurex,ymeas+measurey)=C(xmeas+measurex...
                            ,ymeas+measurey)+0.3*normpdf(measurex^2...
                        +measurey^2,0,2000)*B(j,k);
                    end
                    %C(xmeas+measurex,ymeas+measurey)=C(xmeas+measurex...
                    %,ymeas+measurey)+normpdf(measurex^2+measurey^2,0,2000)*B(k,j);
                end
            end
        end
        end
    end
    disp([num2str(k), ' out of ', num2str(xsteps)])
end
centers=psize/2*[1 1]; %show red rings on plot
radii=psize/30*[15]; %show red rings on plot
Cblur=imgaussfilt(10*C,20);
CC=max(C);
CCC=max(CC);
CCCC=C.*1/CCC; %to highlight contrast
Cend=CCCC.*max(selectcolumn);
Cendr=imrotate(Cend,180);

img=imshow(Cend,[]), colorbar;%cblur voor met gaussian filter
%img=surf(Cblur), colorbar %3d plot met kleurtjes
%img.EdgeColor='none' %3d plot met kleurtjes
```

```
viscircles(centers,radii,'linewidth',0.1)
axis on

conversion=30/1200; % in cm/pixel
addMMx=@(x) sprintf('%1d',x*conversion);
addMMy=@(y) sprintf('%1d',(y-1200)*-conversion);
xticklabels(cellfun(addMMx,num2cell(xticks'),'UniformOutput',false));
yticklabels(cellfun(addMMy,num2cell(yticks'),'UniformOutput',false));
xlabel('Wafer dimension (cm)', 'fontsize', 14)
ylabel('Length of the wind tunnel (cm)', 'fontsize', 14)
h = colorbar;
ylabel(h, 'amount of particles', 'fontsize', 16);
figure(1)
print -clipboard -dbitmap
saveas(1,'30cm.jpeg');
```

Listing 3: *Script used for pre-processing the movie before inserting in PIVlab*

```
%Prepare images for PIV analyis

showMovie=0;
createSumImage=1;
makeImagesPIV=1;

BaseDir='C:\Users\s153308\Downloads';
FileName='aprilvideo2';
startTime=0;
nImages=120;

FileNumber=FileName(5:end);
FileNamePIV=[FileName,'.piv'];

FileNameIn=[BaseDir,'\',FileName,'.mp4'];
FileNameOut=[BaseDir,'\',FileNumber,'\',FileName];
disp(['Input file: ',FileNameIn])
disp(['Output file: ',FileNameOut])

if ~exist([BaseDir,'\',FileNumber],'dir')
   mkdir(BaseDir,FileNumber);
end

readerobj = VideoReader(FileNameIn);
frameRate = readerobj.FrameRate

readerobj.CurrentTime = 0;

vidFrame = readFrame(readerobj);
[m,n]=size(vidFrame(:,:,1));
yPixels=[1:m];
xPixels=[1:n];

frameTime=startTime;
if showMovie==1
    currAxes = axes;
    i=1;
    while hasFrame(readerobj)
        readerobj.CurrentTime = frameTime;
        vidFrame = readFrame(readerobj);
        imagesc(vidFrame(:,:,:), 'Parent', currAxes);
```

```
        title(['left mouse: forward, right mouse: back, space: stop,...
            frame time: ', num2str(frameTime)],'HorizontalAlignment','left')
        [x,y,c]=ginput(1);
        if c==1
            frameTime=frameTime+(1/frameRate);
        end
        if c==3
            frameTime=frameTime-(1/frameRate);
            if frameTime<0
                frameTime=0;
            end
        end
        if c==32
            break
        end
        disp(num2str(frameTime))
    end
end

if createSumImage==1

    %Sm=[0 0 1 0 0;0 1 2 1 0; 1 2 3 2 1; 0 1 2 1 0;  0 0 1 0 0]/19;

    readerobj.CurrentTime = startTime;
    nImage=0;

    SmokeSum=zeros(m,n,1);
    while hasFrame(readerobj) && nImage<=nImages
       vidFrame = readFrame(readerobj);
       nImage=nImage+1;

       SmokeGray=rgb2gray(vidFrame(yPixels,xPixels,:));
       %%Remove low level signal
       %%SmokeGray=wiener2(SmokeGray,[10,10]);
       %%SmokeGray=conv2(SmokeGray,Sm,'same');
       SmokeSum=SmokeSum+double(SmokeGray);
    end

    figure(3),imagesc(log(SmokeSum))
    saveas(3,[BaseDir,'\',FileNumber,'\',FileName],'jpg')
    save([BaseDir,'\',FileNumber,'\SmokeSum.mat'],'SmokeSum')
if makeImagesPIV==1  %line 5

    load([BaseDir,'\',FileNumber,'\SmokeSum.mat'])
    iMask=(SmokeSum<1000);

    readerobj.CurrentTime = startTime;
    nImage=0;

    SmokeSum=zeros(m,n,1);
    while hasFrame(readerobj) && nImage<=nImages
       vidFrame = readFrame(readerobj);
       nImage=nImage+1;
       SmokeGray=rgb2gray(vidFrame(yPixels,xPixels,:));
       %Remove low level signal
%      SmokeGray=wiener2(SmokeGray,[10,10]);
%      SmokeGray=conv2(SmokeGray,Sm,'same');

       SmokeLevel=40;
```

```
        I=SmokeGray<SmokeLevel;
        SmokeGray(I)=0;

        SmokeGray(iMask)=0;

        figure(2),imagesc(SmokeGray);
        imwrite(SmokeGray,[BaseDir,'\',FileNumber,'\',FileNamePIV,'.',...
            sprintf('%04d',nImage),'.jpg'],'BitDepth',8);
        title([num2str(nImage),'/',num2str(nImages)]);
    end
end
```

Listing 4: *Script used for the interpolation of data.*

```
%clear all
data=1;
A=readmatrix('C:\Users\s153308\Downloads\stage VDL\metingen\....xlsx');
column=12; % 7<=integer<=14
selectcolumn=A(2:198,column)-min(A(2:198,column));
xsteps=18;
ysteps=16;
B=zeros(ysteps,xsteps);
psize=1200;
xcenter=7500;
ycenter=6000;
effmaxradius=5600;
roffset=600;
q=2;
j=1;
kvar=0.25;
x=zeros(1,xsteps);
y=zeros(ysteps,xsteps);

for i=1:xsteps
    x(i)=xcenter-effmaxradius+(i-1)/(xsteps-1)*(2*effmaxradius);
    for k=1:ysteps
        yc=ycenter-effmaxradius+(k+kvar-1.25)/(ysteps-1)*(2*effmaxradius);
        if (x(i)-xcenter)^2+(yc-ycenter)^2<=(effmaxradius)^2
            B(j,i)=sum(A(q,column));
            y(j,i)=yc;
            j=j+1;
            q=q+1;
        end
    end
    kvar=-kvar;
    j=1;
end

psummed(:,data)=flip(sum(B));
psummednor(:,data)=psummed(:,data)/max(psummed(:,data));
psummedmax(:,data)=max(psummed(:,data));

%% plot scatter
X=(y>0.5).*x;
Y=y;
X(X==0)=NaN;
Y(Y==0)=NaN;
%mesh(X,Y,B);
plot3(X,Y,B)
```

```
%% plot contour
coordinatesy2=nonzeros(y(:));
coordinatesx=(y>0.5).*x;
coordinatesx2=nonzeros(coordinatesx);
coordinates=[coordinatesx2,coordinatesy2,selectcolumn];
X=coordinatesx2;
Y=coordinatesy2;
Z=selectcolumn;

xmin=min(coordinatesx2);
xmax=max(coordinatesx2);
ymin=min(coordinatesy2);
ymax=max(coordinatesy2);
zmin=0;
zmax=1000;

X(198:225)=[xmin xmax xmin xmax xmax xmax xmin xmin xmax xmax 3218 3218 ...
    3876 3876 4535 4535 5194 5194 10460 10460 11120 11120 11780 11780 ...
    12440 12440 xmax xmax];
Y(198:225)=[ymin ymin ymax ymax 7493 4507 9000 3000 5253 6747 10110 1893 ...
    10480 1520 10850 1147 ymax ymin ymin ymax 10850 1147 9733 2267 ...
    9360 2640 8240 3760];
Z(198:225)=[0 0 0 0 0 0 0 0 0 0 0 0 0 0 0 0 0 0 0 0 0 0 0 0 0 0];
T = table(X,Y,Z);
f = fit([T.X, T.Y],T.Z,'linearinterp');
plot( f, [T.X, T.Y], T.Z )
%% calculate intergral
clear q q2 q3
q = quad2d(f,xmin,xmax,ymin,ymax,'AbsTol',1e-4,'reltol',1e-4);
step=(xmax-xmin)/120;
for i=xmin:step:xmax-step
    q2(round(i),:)=quad2d(f,i,i+step,ymin,ymax,'AbsTol',1e-4,'reltol',1e-4);
end
q3=nonzeros(q2);
norq3(:,data)=flip(q3/max(q3));
parq3(:,data)= norq3(:,data)*psummedmax(:,data);
```

Listing 5: *Script used for the analysis of particle position using a laser.*

```
%clear all
vidObj    = VideoReader('particlevisveld8cm.mp4') ;
nFrames   = vidObj.NumberOfFrames;
tFrame    = (1:nFrames) / vidObj.FrameRate ;
ghostCom  = zeros( nFrames, 1 ) ;
%%
   for fId = 1 : nFrames
      grayImage = rgb2gray( read( vidObj, fId )) ;
      ghostCom(fId) = sum( grayImage(:) );
      %ghostCom3=ghostCom2.*ghostCom
      %positionCom(1:m,1:n)= ghostcom2.*sum(grayImage(1:m,1:n));
   end
Framewidth=size(grayImage,2);
Framelength=size(grayImage,1);
ghostCom2=max(ghostCom)*0.75<ghostCom;
ghostCom3=nonzeros(ghostCom2.*[1:nFrames]');
for i=1:length(ghostCom3)
grayImage2 = rgb2gray( read( vidObj, ghostCom3(i) ));
flash(i)=sum(grayImage2(:));
%position(i,1:Framewidth)=sum(grayImage2(1:Framewidth,1:Framelength));
```

```
position(i,1:Framewidth)=sum(grayImage2(1:Framelength,1:Framewidth));
sumposition=sum(position)';
end

%%
%positionCom(1:Framewidth)= sum( grayImage(400:Framelength,1:Framewidth));
figure(1) ;  clf ;
set( gcf, 'Color', 'White', 'Units', 'Normalized','OuterPosition', [0, 0.1, 1, 0.6] ) ;
plot( tFrame, ghostCom/max(ghostCom), 'b' ) ;
set( gca, 'YTick', [0, 1] ) ;
xlabel( 'Time [s]' ) ;
[r]=risetime(ghostCom);
FREQUENCY=numel(r)/60;
figure(2)
plot(sumposition)
```